**Univerzita Hradec Králové**

**Přírodovědecká fakulta**

**Katedra fyziky**

# Calculation of Sensitivity to Neutrinoless Double Beta-Decay for COBRA Demonstrator

Diploma Thesis

| | |
|---|---|
| Autor: | Maroš Petro |
| Studijní program: | N0553A110001 - Fyzikální měření a modelování |
| Studijní obor: | Fyzika, Navazující magisterský, Kombinovaná |
| Vedoucí práce: | Mgr. Miroslav Macko, Ph.D. |
| Odborný konzultant: | RNDr. Jiří Lipovský, Ph.D. |

Hradec Králové 2021

**Prohlášení:**

Prohlašuji, že jsem diplomovou práci vypracoval samostatně a že jsem v seznamu použité literatury uvedl všechny prameny, z kterých jsem vycházel.

V Hradci Králové dne

26.7.2021

Maroš Petro

## Annotation

PETRO, M. *Calculation of Sensitivity to Neutrinoless Double Beta Decay for COBRA Demonstrator*. Hradec Kralové, 2021. Diploma Thesis at Faculty of Science University of Hradec Kralové. Thesis Supervisor Miroslav Macko.

The goal of this diploma thesis is to calculate half-life sensitivities ($T_{1/2}$) of the COBRA experiment to neutrino-less double-beta decay for four different isotopes (ground state to ground state transitions): $^{128}$Te (Q = 865.9 keV), $^{70}$Zn (Q = 998.5 keV), $^{130}$Te (Q = 2527.0 keV), and $^{116}$Cd (Q = 2813.5 keV). COBRA experiment is an experiment searching for neutrino-less double-beta decay using array of 64 cubic CdZnTe semiconductor detectors of 1 cm$^3$ volume each. Analysis is based on the data from the first phase of the project, so-called COBRA Demonstrator, collected between 2013 and 2019 (total exposure of 1.252 kg.yr). The Dataset was split into subsets called partitions and, in order to obtain the optimal regions of interest for each individual partition, optimized window counting method was employed. The detector signal count sensitivities were calculated using the author´s own implementation of Feldman and Cousins method.

In comparison to Bayesian analysis from 2016 ([1]), we received improved half-life sensitivities for $^{130}$Te ($T_{1/2} \geq 6.9 \cdot 10^{21}$ yr) and $^{116}$Cd ($T_{1/2} \geq 1.8 \cdot 10^{21}$ yr). Worse limits were obtained for $^{128}$Te ($T_{1/2} \geq 1.8 \cdot 10^{21}$ yr) and $^{70}$Zn ($T_{1/2} \geq 4.9 \cdot 10^{18}$ yr). The worse limits for $^{128}$Te and $^{70}$Zn can be accounted for the different values of isotope abundances used in the article and the presented thesis as well as the oversimplified background model. The uncertainties of the experimental parameters were omitted and should be included in future work in order to obtain more robust results.

**Keywords**

Neutrinoless Double Beta-Decay, Feldman and Cousins, Optimized Window Counting, Sensitivity, Half-Life, Te-128, Zn-70, Te-130, Cd-116

## Anotace

PETRO, M. *Výpočet citlivosti na bezneutrínový dvojný beta rozpad pro COBRA demonštrátor*. Diplomová práce na Přírodovědecké fakultě Univerzity Hradec Králové. Vedoucí diplomové práce Miroslav Macko.

Cílem diplomové práce je vypočítat citlivosti poločasu rozpadu ($T_{1/2}$) experimentu COBRA na bezneutrinový dvojný beta rozpad ($0\nu\beta\beta$) ze základního stavu do základního stavu pro čtyři různé izotopy: $^{128}$Te (Q = 865,9 keV), $^{70}$Zn (Q = 998,5 keV), $^{130}$Te (Q = 2527,0 keV) a $^{116}$Cd (Q = 2813,5 keV). Experiment COBRA je detektor, který hledá $0\nu\beta\beta$ pomocí seskupení 64 kubických CdZnTe polovodičových detektorů s objemem 1 cm$^3$. Analýza je založená na údajích z první fáze projektu, takzvaného COBRA demonstrátora, shromážděných v letech 2013 až 2019 (celková expozice 1,252 kg.yr). Data byla rozdělena na jednotlivé oddíly. Na získání optimálních energetických oken pro každý jednotlivý oddíl byla použita speciální metoda optimalizace oken. Citlivost detektoru na počet signálů byla vypočítána pomocí vlastní implementace metody Feldmana a Cousinse.

V porovnání s analýzou z roku 2016 ([1]) jsme dostali vylepšenou citlivost na poločas rozpadu pro $^{130}$Te ($T_{1/2} \geq 6,9 \cdot 10^{21}$ r) a $^{116}$Cd ($T_{1/2} \geq 1,8 \cdot 10^{21}$ r). Horších limitů bylo dosaženo pro $^{128}$Te ($T_{1/2} \geq 1,8 \cdot 10^{21}$ r) a $^{70}$Zn ($T_{1/2} \geq 4.9 \cdot 10^{18}$ r.). Horší limity pro $^{128}$Te a $^{70}$Zn se dají připsat rozdílným hodnotám relativního zastoupení izotopů použitých v článku a v prezentované práci, jako i příliš zjednodušenému modelu pozadí. Nejistoty experimentálních parametrů byly zanedbány a měly by být zahrnuty do budoucí práce.

**Klíčová slova**

bezneutrinový dvojný beta rozpad, Feldman a Cousins, metoda optimalizovaného počítání oken, citlivost, poločas rozpadu, Te-128, Zn-70, Te-130, Cd-116

# Contents

# List of Figures

# List of Tables

# INTRODUCTION

One of the fastest growing fields in particle physics today is the field of neutrino physics. The sm of Particle Physics [2, 3, 4] is the most precise theory of fundamental particles currently available. Its precision was proved by hundreds of independent experiments. However, the model has its own limitations. There is already an experimental proof of a particle property which the SM does not describe satisfactorily. Based on the proof of the existence of neutrino oscillations [5, 6] neutrinos should not be massless. This conflicts with the SM assumption of massless neutrinos. While we know neutrinos should have mass, we were not able to measure it yet. We do not know what the nature of neutrinos is – whether they behave as Dirac or Majorana particles [7]. It is unclear whether sterile neutrinos exist.

The presence of so many unanswered questions about neutrinos makes it more important to develop methods to study these elusive particles. The study of double beta-decay shows a promise in answering some of the questions regarding neutrino physics. Double beta-decay is an incredibly rare process – a typical half-life of the so-called two-neutrino double beta ($2\nu\beta\beta$) process is approximately $10^{18}$ years – it has only been measured in 12 different isotopes. Its lepton conservation violating mode, the so-called neutrino-less double beta ($0\nu\beta\beta$)-decay, has never been observed. Discovery of $0\nu\beta\beta$ is the only known experimental possibility which could prove that neutrinos are so-called Majorana particles (the neutrinos and antineutrinos would be the same). It can also provide information on the neutrino mass. By studying the half-life ($T_{1/2}$) of the decay, it is possible to extract the effective mass of a neutrino. There are many double beta-decay experiments in different phases of development.

One such experiment is the COBRA experiment. It is a semiconductor CdZnTe detector located in an underground laboratory in Italian Appenines, in the LNGS laboratory. The subject of this thesis is the analysis of the data measured with the COBRA detector regarding the search for a rare process – $0\nu\beta\beta$-decay.

In the Chapter 1, I first describe the historical background of particles, and especially, neutrino physics. The SM is first introduced from a historical viewpoint. The discoveries of the fundamental particles are summarized and the forces that are incorporated in the SM are outlined. Next, the history of the postulation and the discovery of the neutrino, along with relevant physics is detailed. In here, the unanswered questions about neutrinos are formulated. Furthermore, the mechanism of ordinary and double beta-decay is described, the spectral shape is explained. The reasoning of how the study of $0\nu\beta\beta$-decay can provide information on the effective neutrino mass is given. At the end of the first chapter, examples of the contemporary double beta-decay experiments are provided.

The Chapter 2 is dedicated to the COBRA experiment itself. Here, the structure, composition and design of the detector is discussed. The principles of semiconductor detectors are described.

In the Chapter 3, one can find brief description of well-known Feldman and Cousins method [8]. Feldman and Cousins method is a statistical method used for the estimation of sensitivities of detectors searching for rare processes. It is a method based on the frequentist probabilistic approach. Motivation, detailed procedure and the challenges of applying this method are described. Furthermore, an analysis of some limitations of this method are presented and resolved. The implementation of the method in a form of C++ class is briefly described.

Finally, in the Chapter 4, the results of the calculation of $T_{1/2}$ sensitivity to $0\nu\beta\beta$-decay are provided. In this chapter, the structure of the data is outlined and the relevant data cuts are explained. The optimized window counting method is introduced and the results are presented. The results are discussed at the end of the chapter.

CHAPTER 1

# THE STANDARD MODEL AND THE NEUTRINO PHYSICS

## 1.1 Standard Model of Particle Physics

The $20^{th}$ century has seen an abundance of high-energy physics experiments studying elementary particles. Most of these experiments profited from particle accelerator technology, where the researchers could control the conditions of the experiment. They have discovered many new particles which were, at the time, considered elementary (i.e. they are not divisible). Today, we distinguish 12 elementary fermions and 5 elementary bosons. The fermions are further divided into leptons and quarks based on the interactions they undergo. The bosons provide interactions between leptons and quarks: Electromagnetic (photon), Strong (gluon), Weak (W and Z). The fifth boson – the Higgs boson – is not directly linked to any of the four forces of nature we know, nevertheless, it is crucial to explain how particles get their masses. The aforementioned particles are all part of the Standard Model (SM), which is currently the most precise and widely accepted model of fundamental particle physics. The success of the SM is confirmed by hundreds of experiments. All particles of the SM can be found in Figure 1.1. Let us now briefly talk about each sector in a bit more detail.

The electron was discovered in 1897 by J.J. Thomson [10], being the first known subatomic particle. Muons were discovered in 1936 by C. D. Anderson and S. Neddermeyer. They observed that the muons curved in the same direction as electrons in a magnetic field, therefore, they must have the same charge. However, the curvature was not as pronounced, suggesting muons to be more massive than electrons. This was later confirmed in 1937 by J.C. Street in a cloud chamber experiment [11]. Tau particle, an even more massive cousin of electron was discovered in 1975 by M. L. Perl et al. [12]. Together these formed the particle species known as charged leptons. The neutral lepton – neutrino – was postulated in 1930 by W. Pauli (more on this in Section 1.2).

Protons were the first baryons, discovered by E. Rutherford in 1911 [13]. $\pi$ mesons were the first mesons to be discovered in 1947 by Lattes et. al. [14]. The list of discovered mesons and baryons was growing very fast during those years. Each seemingly elementary. There was an urgent need for categorization of all these new particle species into a system. It has been noticed that many of these newly discovered particles have much in common with other particles, while being different from others. In late 1960s, the list of newly discovered particles became so long that the particle physicists were colloquially calling this list a "particle zoo" [15]. It was only after the theoretical introduction of quarks in 1964 (and their experimental observation) that it became clear hadrons and mesons were not elementary, but are

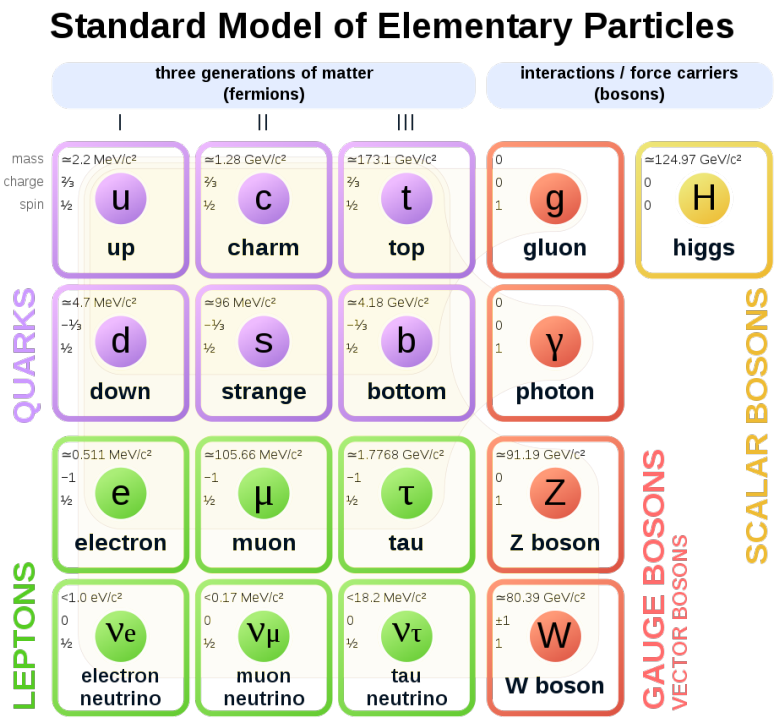


Figure 1.1: Current form of the Standard Model of Particle Physics. The symbols for each particle are depicted in the Figure. From [9].

composed of quarks.

A clue as to how the categorization was to be made was by looking at how each newly discovered particle interacts with the four fundamental forces. The forces are Strong nuclear interaction, Weak interaction, Electromagnetism (EM) and Gravity. Some particles interact via four interactions, such as quarks. Others interact via Weak interaction, electromagnetism and gravity, for example electrons and muons. On the other hand, neutrinos discovered in 1956 [16], seemed to interact only via the Weak interaction. The SM which satisfied this need for unification, is attributed mainly to three particle physicists. In 1961 S. Glashow combined Electromagnetism and Weak interactions [2]. Later in 1967, S. Weinberg managed to incorporate the Higgs Mechanism (named after P. Higgs [17, 18, 19]) into the Electroweak theory [4]. Independently, A. Salam developed a similar theory to Weinberg's in 1968 [3]. Today this is also referred to as the Glashow-Weinberg-Salam model [20]. Subsequently, the SM was finalized in the 1970s with the experimental discovery of quarks and incorporation of the theory of strong interactions (Quantum ChromoDynamics – QCD) into the model. And thus it was possible to have one theory describing the properties of matter particles with the relevant interactions.

The SM, however, includes only three out of four forces of nature, excluding gravity. It should be understood that the SM is only valid to a certain extent and it will necessarily need to be extended despite its current success. There are limitations to the SM. First, the aforementioned fact is that only three of the four fundamental forces are incorporated (the Strong interaction, the Weak interaction and the EM). It is also only an approximation of more general physics within a relatively low energy boundary. It is not possible to make a theory that would be viable for $E \to \infty$,

| Quark | Symbol | Charge | Mass | Spin |
|---|---|---|---|---|
| Up | u ($\bar{\text{u}}$) | 2/3 | 2.2 MeV/$c^2$ | 1/2 |
| Down | d ($\bar{\text{d}}$) | $-1/3$ | 4.7 MeV/$c^2$ | 1/2 |
| Charm | c ($\bar{\text{c}}$) | 2/3 | 1.28 GeV/c$^2$ | 1/2 |
| Strange | s ($\bar{\text{s}}$) | $-1/3$ | 96 MeV/$c^2$ | 1/2 |
| Top | t ($\bar{\text{t}}$) | 2/3 | 173.1 GeV/c$^2$ | 1/2 |
| Bottom | b ($\bar{\text{b}}$) | $-1/3$ | 4.18 GeV/c$^2$ | 1/2 |

Table 1.1: Table presenting the three generations of quarks, distinguished by a horizontal line. In the symbols column, the anti-quark symbol is presented in the parentheses – it is marked by a bar over the symbol.

there must always be a cutoff at some finite energy. An extension, the so-called physics beyond the SM (BSM), will be necessary. In fact, already now, there is an experimental proof of BSM physics (e.g., neutrino oscillations discussed in Section 1.2).

In the following sections, the individual building blocks of SM will be described in more detail. First, the three forces included in the SM and their associated particles will be presented in short. Fermions will be detailed next and then the two main components of the SM will be presented together, forming the current version of the Standard Model.

### 1.1.1 Fermions

Fermions in the SM are the particles which account for the matter in the universe. Fermions within the SM, are divided into two main groups – quarks and leptons. There are three so-called generations of fermions for both quarks and leptons. Each fermion has its corresponding anti-particle, which arises as a consequence of the Dirac equation. Anti-particles are same as their matter counterpart but their electromagnetic charge is opposite. There are altogether 12 fermions (and 12 anti-fermions) in the SM. All fermions have 1/2 spin angular momentum by definition. This is different from bosons, which have integer spin angular momentum.

**Quarks** interact via all four fundamental forces. There are six quarks (and six anti-quarks), divided into three generations. Each generation of quarks has two members, one with EM charge of $+2/3$ and one with $-1/3$. The quarks are presented in Table 1.1. Quarks have non-zero effective mass, with up and down quarks being the lightest. One of the unexplained puzzles theoretical physicists are trying to understand is the so called Fermion Mass Hierarchy problem [21]. Table 1.1 shows the masses of each quark in the SM. One can notice that up quark (charge $+2/3$) is lighter than down quark (charge $-1/3$), while the opposite pattern is present for the other quarks. Charm and Top quarks, both with charge $+2/3$ are heavier than their $-1/3$ charge counter parts – strange and bottom quarks.

As seen in Table 1.1 there is a sizeable difference in the magnitude of masses for the first generation quarks – u,d, and the others. Up and down quarks' masses are in the order of few MeV/$c^2$, whilst c,s,t, and d are much heavier. This is one of the reasons why only the up and down quarks are stable and the others decay. Quarks have color charge, a quantum number which arises from the quantum chromodynamics (QCD – theory of strong interactions). This allows quarks to

interact with gluons and consequently with the strong nuclear force. Quarks also interact with the electromagnetic force (they have EM charge), weak nuclear force (through decay) and with gravity.

Second group of fermions composing the SM is the group of **leptons**. Once again, there are three generations of leptons. Charged leptons interact via Weak interaction, EM and Gravity. They have EM charge of $-1$. Neutral leptons – neutrinos – have no EM charge. They interact only via Weak interactions (within the SM they are considered massless and therefore do not interact via Gravity). As leptons do not participate in the strong interaction, they do not carry color charge. The charged and the neutral leptons always come in pairs, there is an associated neutrino to each of the three charged leptons. We recognize three *flavours* of neutrinos, there are electron-neutrinos, muon-neutrinos and tau-neutrinos.

The three charged leptons have associated masses within the SM. Electron is the lightest of the three, with mass of $\simeq 0.511$ MeV/$c^2$. Muon has mass of $\simeq 105.66$ MeV/$c^2$ and tau $\simeq 1.777$ GeV/$c^2$. The electron is the only stable charged lepton. As mentioned earlier, neutrinos are considered massless within the SM. This, however, has been proven to be wrong [22] experimentally and suggests that there is the so-called physics beyond the Standard Model, which will be discussed in 1.2.

### 1.1.2 Forces and Gauge Bosons

The SM is currently the best working theory combining three of the four known fundamental forces. The SM has been successful in putting together the interactions of EM, Strong nuclear force, and Weak nuclear force. Despite much effort, gravity has not been incorporated into the SM. The three forces included in the SM have each their corresponding force carrier particles – gauge bosons. All the gauge bosons have integer spin angular momentum, by which they are defined. Gluons, photons, $W$ and $Z$ bosons have spin of 1. Higgs boson is (so far) the only known particle with zero spin angular momentum. In order to explain the concept of bosons being the force carriers, a very fitting analogy is commonly used. Two people, person A and person B, are standing in separate small boats floating on a lake . They are opposite to each other. Person A throws a basketball at person B. After person A throws the basketball, he/she is pushed backwards to preserve its momentum. Person B catches the basketball and is, therefore pushed away from person A. In this analogy, the basketball represents the gauge bosons, while the people represent the matter particles. As a result of the exchange of the basketball, two people are pushed away from each other – repulsive force.

So far, only half of the problem has been analogously explained, the repulsion effect of forces can be thought of as two people throwing a basketball. A slight modification in the analogy is used to describe attraction. The only difference in analogy is now the exchange item. Instead of throwing a basketball, a boomerang is now used. The person A is facing away from person B and throws the boomerang, the motion pushes him toward person B. The boomerang flies around the two people and comes back toward person B. Person B catches the boomerang and is pushed towards the person A. Hence the two are closer to each other, the boomerang attracted them. And so, the exchange of force-carriers can affect the state (motion) of matter particles, without ever actually touching.

The introduction of exchange forces was made by W. Heisenberg in 1932 [23] and

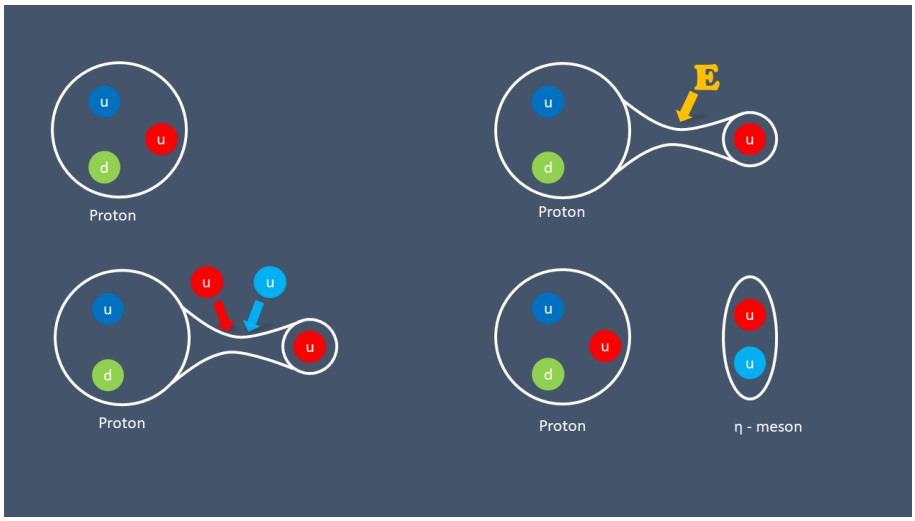


Figure 1.2: Illustration of the color confinement. Four stages of are depicted. First, the neutral baryon (proton in this case) is depicted. Second, energy is added into the system as the up quark is being pulled away. Third, enough energy has been added so that a new pair of up and anti-up quarks is created. Fourth, two neutral hadrons are formed – a proton and an $\eta$ – meson. Inspired by [24].

E. Majorana in 1933 [7].

**Electromagnetic force**, is carried by photons. It is the Coulomb Electromagnetic force that holds together atoms, attracting electrons to protons inside a nucleus. Electromagnetic force acts in a long range, virtually infinite.

**Strong nuclear force** is responsible for holding together quarks inside baryons and mesons [25]. The Strong nuclear force is responsible for holding atomic nuclei together by binding neutrons and protons close to each other. As the name suggests, it is the strongest of all the known forces. It is so strong, that it is capable to overcome electromagnetic repulsion between the protons in nucleus. Strong nuclear force is short-ranged at about 1 fm ($10^{-15}$ m). This is why one can observe its effect almost exclusively on the scale of nuclei. The force carriers of the strong force are eight gluons. Gluons are associated with the quantum property of quarks called color charge. In contrast to the well-known EM charge which comes in two states (positive and negative), the color charge can come in three states: red, green, and blue. The name "color" charge is derived from the fact that the mixing of the color states is governed by the same mathematical principles as the mixing of the colors of the actual visible electromagnetic spectrum. In the strong interaction between quarks, this color is carried by said gluons.

While photons are the interaction particles responsible for EM interaction, they do not actually carry any charge, therefore, they do not interact among themselves. However, with gluons it is opposite. Gluons carry a color charge and can interact with quarks and with other gluons. This makes QCD particularly complicated. In nature, the asymptotic (i.e. with negligible influence from interactions with other particles) particle states are only color-neutral. Only such combinations are allowed, which have the net color charge of zero. For example, mesons are particles composed of a quark and an anti-quark pair of opposite color charges. Another way of creating neutral color charge particles is to combine three quarks of different colors, creating baryons (e.g. protons or neutrons) [25]. Mesons and baryons can be jointly named

| **Force** | **Carrier** | **Phenomenon** | **Spin** | **Mass** | Range |
|---|---|---|---|---|---|
| Electromagnetic Force | Photon | Electromagnetism | 1 | 0 GeV/c$^2$ | $\infty$ |
| Strong Nuclear Force | Gluon | Quark "glue" | 1 | 0 GeV/c$^2$ | $10^{-15}$m |
| Weak Nuclear Force | $W^{\pm}, Z$ bosons | Nuclear Decay | 1 | Finite Mass | $10^{-18}$m |

Table 1.2: Table presenting a short summary of the forces included in the SM. Some of the interesting features mentioned in the text are included in the table.

hadrons. The requirement of allowing only for color-neutral states is called the color confinement. Quarks (and other color charged objects) cannot be separated from one another. When they are close to each other inside of a hadron, quarks which are essentially free particles. Potential energy due to the presence of quarks being in proximity is very small. To pull quarks apart, energy must be added. As quarks are separated further from each other, the potential increases. Eventually, enough energy is added that a new pair of quark and an anti-quark can be created neutralizing the system into zero color charge.

The origin of the color confinement has been, among others, studied by Gross, Wilczek and Politzer. They were awarded a Nobel prize for "for the discovery of asymptotic freedom in the theory of the strong interaction." in 2004 [26, 27, 28, 29]. The strength of the strong interaction is smaller at short distances (higher energies) and larger at longer distances (smaller energies).

Finally, the SM incorporates **Weak interaction** and its associated $W^+$, $W^-$ and $Z^0$ bosons. The Weak interaction is the cause of nuclear decay. The processes based on the exchange of the charged Weak bosons, $W^+$ and $W^-$ are capable of altering the EM charge of the particles in the final state compared to the ones in the initial state. It is also possible for the weak interaction to not change the charge by exchanging the neutral weak boson $Z^0$ (the so-called neutral current processes). Similarly to the Strong nuclear force, Weak interaction is short ranged. In fact, it is even shorter ranged [30]. In processes undergoing Weak interaction, the so-called lepton number is assigned to the leptons. The lepton number of +1 is associated with matter, whereas lepton number of -1 is associated with antimatter. In the SM, only processes where this quantity is conserved are allowed. To demonstrate this law, let us consider the decay of a neutron, depicted in equation (1.1). This is a process governed by Weak interaction.

$$n \longrightarrow p^+ + e^- + \bar{\nu_e} \tag{1.1}$$

On the left hand side of equation (1.1), neutron has lepton number 0, since it does not contain any leptons. This means, that the right hand side of the equation must also have a total lepton number equal to zero. Proton, again, has no leptons so its lepton number is zero for the lepton number to be conserved. However, an electron has an electron lepton number of +1, this means that it must be accompanied by an electron anti-neutrino, which has an electron lepton number of −1. There are no muons or tau leptons on either side of the equation so $L_\mu = L_\tau = 0$. Therefore, the equation (1.1) can be represented in lepton numbers as in :

$$\begin{aligned} L_e: &\quad 0 \longrightarrow 0 + 1 - 1 \\ L_\mu: &\quad 0 \longrightarrow 0 \\ L_\tau: &\quad 0 \longrightarrow 0\ . \end{aligned} \tag{1.2}$$

The last gauge boson added to SM is the Higgs boson, experimentally confirmed in 2012 [31, 31], which conveys the **Higgs mechanism**. While gluons and photons are massless, $W^+$, $W^-$ and $Z^0$ bosons together with Higgs boson have non-zero mass.

Table 1.2 provides a short summary of the three fundamental forces included in SM and their associated gauge bosons. Gravity is not present in the table as it is not included in SM.

## 1.2 Neutrino Physics

### 1.2.1 History

#### 1.2.1.1 Discovery of Radioactivity

In 1896, French physicist H. Bequerel discovered the spontaneous radioactivity in uranium. He was studying the fluorescence properties of uranium salts. In his experiment, he wrapped a photographic plate in black paper, so that no light would be able to get through. Then he placed uranium salt on top of the black paper. He expected that if he exposed the uranium salt to sunlight, it would emit X-rays through fluorescence and darken the photographic plate below. After some time, he noticed dark spots that appeared on the plate. These spots, however, could not have originated from any visible fluorescence, the uranium was not glowing visibly. He realized that there must have been some kind of invisible radiation originating from the uranium salt itself, capable of penetrating through the black paper and reaching the photographic plate [25].

Later on, in 1899, E. Rutherford, discovered that there are in fact two distinct types of radiation emitted from the uranium salt. Based on their abilities to penetrate materials, he named the less penetrating radiation as $\alpha$-radiation, while the more penetrating type he named $\beta$-radiation [32]. Finally, in 1900, P. Villard discovered an even more penetrating type of radiation, $\gamma$-radiation [33]. Around the same time, in 1901, E. Rutherford together with F. Soddy realized that the origin of the radiation was due to the decay of radioactive elements. The atoms undergo a transmutation into other elements accompanied by emitting $\alpha$- or $\beta$-radiation.

Naturally, these discoveries lead to a great deal of research and effort being put into studying each. Especially the studies of spontaneous decays are interesting in the scope of this thesis. In order to study the different decays, one can look at the spectra produced by radioactive elements. From the nature of the decay (an atom splits into two parts), it can be assumed that both $\alpha$- and $\beta$-decays would obey kinematics of a two-body system. This, curiously, turns out to not be the case for the $\beta$-decay spectrum.

#### 1.2.1.2 Problem of the Continuous Spectrum

The unexpected shape of the beta-decay spectrum plays an important role in the discovery of the neutrino and neutrino physics as a whole. To better understand the importance of the $\beta$-decay spectrum, and its importance for neutrino physics, it is desirable to first look at the spectrum of a two-body decay, such as an $\alpha$-decay.

When a parent nucleus X undergoes $\alpha$-decay, it splits into a daughter nucleus Y and an $\alpha$-particle:

$$ {}^{A}_{Z}X \longrightarrow {}^{A-4}_{Z-2}Y + {}^{4}_{2}\mathrm{He} \ . \tag{1.3} $$

$A$, the nucleon number of parent nucleus drops by 4 units and, $Z$, the proton number, drops by 2 units. The emitted alpha particle is the ${}^{4}_{2}$He nucleus. Let us write down the relations of conservation of energy:

$$ M_p c^2 + T_p = M_d c^2 + T_d + M_\alpha c^2 + T_\alpha \tag{1.4} $$

Here, $M$, stands for the rest mass and the $T$ for the kinetic energy. Indices $p$, $d$ and $\alpha$ stand for parent nucleus, daughter nucleus and the $\alpha$ particle, respectively. Finally, $c$ is the speed of light. Typically, an alpha particle emitted in alpha-decay has a kinetic energy around $4 - 10.5$ MeV [34]. If we take into account its mass around 3727 MeV we can state that the alpha particle originating in the decay is non-relativistic within a good approximation. The same holds for the parent and daughter nuclei. Therefore, we can express the conservation of momenta and the relations for kinetic energies using simple, non-relativistic relations:

$$ M_d v_d = M_\alpha v_\alpha, \quad T_p = 0, \quad T_d = \frac{1}{2} M_d {v_d}^2, \quad T_\alpha = \frac{1}{2} M_\alpha {v_\alpha}^2 \ . \tag{1.5} $$

Here, we take into account the fact that we describe the decay in the reference frame of parent nucleus, therefore $T_p$ is zero. If we put all the kinetic energies in equation (1.4) to one side, and all the rest-mass energy components to the other side, we obtain:

$$ T_d + T_\alpha = (M_p - M_d - M_\alpha)c^2 \equiv Q \ . \tag{1.6} $$

Here, Q is defined as the disintegration energy of the decay (it is also called Q-value). In order for the decay to take place spontaneously, the **Q-value must be positive** [25]. If we now substitute $T_d$ and $T_\alpha$ using equations (1.5) we get:

$$ \begin{aligned} T_d + T_\alpha &= \frac{1}{2}\left( M_d {v_d}^2 + M_\alpha {v_\alpha}^2 \right) = \frac{1}{2}\left[ M_d \left( \frac{M_\alpha}{M_d} v_\alpha \right)^2 + M_\alpha {v_\alpha}^2 \right] \\ &= \frac{1}{2} M_\alpha v_\alpha^2 \left( \frac{M_\alpha}{M_d} + 1 \right) = T_\alpha \left( \frac{M_\alpha}{M_d} + 1 \right) \ . \end{aligned} $$

And since $T_d + T_\alpha = Q$, we finally obtain:

$$ T_\alpha = \frac{M_d}{M_d + M_\alpha} Q \ . \tag{1.7} $$

It is evident that the kinetic energy of the alpha particle depends only on the masses of the daughter nucleus and the alpha particle, and the Q-value. The daughter nucleus is typically much heavier, composed of more than hundred nucleons while the alpha consists of only four. This fact makes the ratio $M_d/(M_d + M_\alpha) \approx 1$, therefore, $T_\alpha \approx Q$. The heavy daughter nucleus carries a negligible amount of decay energy $Q$, while $\alpha$-particle carries almost all of it. For a given parent nucleus, the kinetic energy of the alpha particle is always the same, which results in a discrete spectrum. An example of experimental $\alpha$-decay spectrum of ${}^{218}$Po is shown in Fig-

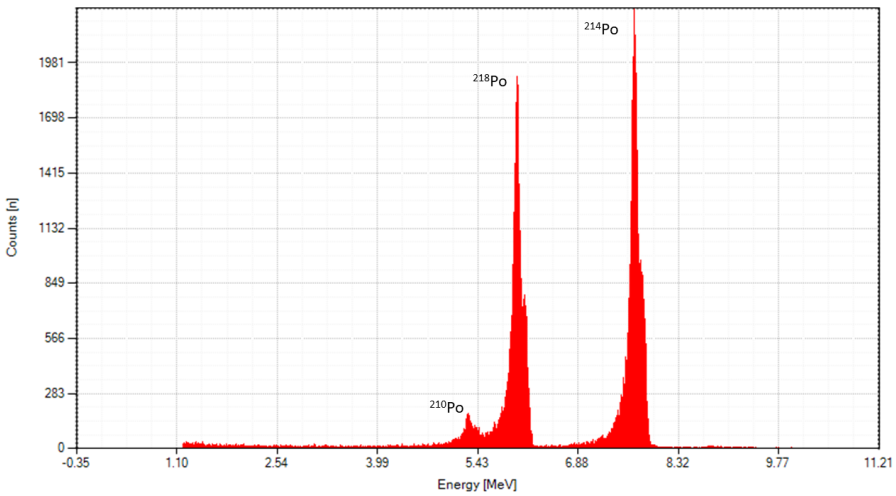


Figure 1.3: An example of alpha spectrum from $^{222}$Rn decay measured in LSM Modane laboratory. The three $\alpha$-peaks of Polonium daughter elements are depicted in the figure. For the decay chain see 1.4.

ure 1.3. In the spectrum, except for $\alpha$-peak originating directly from $^{218}$Po decay, one can also recognize separate $\alpha$-peaks from $^{210}$Po and $^{214}$Po. These peaks are the consequence of $\alpha$-decays down the uranium decay chain whose partial scheme is shown in Figure 1.4. The lines are clearly separated and discrete as expected. They represent the individual Q-values of respective $\alpha$-decays.

As stated in the beginning of this section, the $\beta$-decay spectrum is different. In 1902, W. Kaufmann performed experiments using a radium source as a $\beta$-emitter. In the experiment, he managed to calculate the mass of the $\beta$ radiation particles and found that it is actually the same (*"within observational error"* [36]) as the mass of an electron. He concluded that the $\beta$-rays are electrons, which was not known back then.

Since $\beta$-radiation is composed of electrons, it stands to reason that the $\beta$-decay *should* follow similar behaviour as $\alpha$-decay. It *should* be a two-body decay following (1.8). The same notion for calculating the Q-values as in $\alpha$-decay case *should* hold. The electrons emitted *should* be mono-energetic. And finally, the spectrum *should* be discrete.

$$ {}^{A}_{Z}X \rightarrow {}^{A}_{Z+1}Y + e^{-} \tag{1.8} $$

Surprisingly, W. Kaufmann and others studying the $\beta$-decay saw something that did not resemble the $\alpha$-decay spectrum. They did not see any obvious discrete features (characteristic lines) in the spectrum, but rather a continuous distribution of energy. Furthermore, the apparent broad distribution of electron energies has a maximum at the Q-value for the given $\beta$-decay. An example of a theoretical $\beta$-decay spectrum is shown in Figure 1.5. There were various hypotheses, trying to explain why the $\beta$-spectrum appeared to be continuous. The physicists were questioning the experimental setup. There were suggestions that the $\beta$-sources had been contaminated by other emitters which would disturb the spectrum. Another hypothesis speculated that the $\beta$-rays might have lost some of the energy along the way to the detector. An era of experiments trying to explain the problem of the

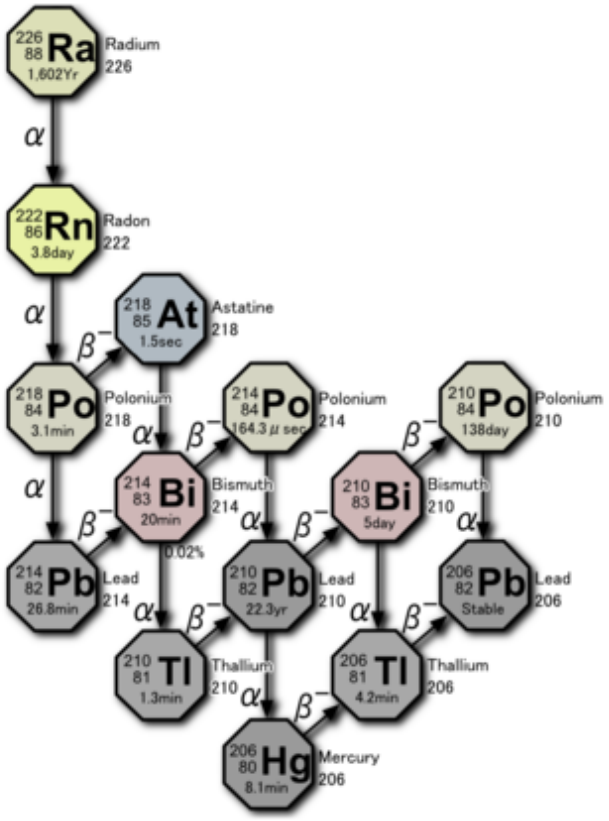


Figure 1.4: Uranium decay chain. Adapted from [35].

continuous $\beta$-spectrum has begun [36]. None, however, managed to convincingly show that the spectrum is discrete.

In 1927 C. D. Ellis and W. A. Wooster finally presented definitive evidence that the spectrum of $\beta$-decay is, in fact, continuous [37]. This discovery threatened two very well established conservation laws. The law of conservation of energy was endangered by the fact that the equation (1.4) would seemingly not hold for $\beta$-decay. The law of conservation of angular momentum seemed to be violated in the experiments studying the nuclear spin of $^{14}$N. According to the knowledge at the time (i.e., the nucleus was thought to be composed of electrons and protons), the calculated nuclear spin of $^{14}$N should have been equal to $-1/2$. However, measurements showed the spin to be an integer [38]. The question remained opened until 1930.

#### 1.2.1.3 Neutrino Postulate

Once it became clear that the $\beta$-decay spectrum really was continuous, a new question needed to be answered. Why is the spectrum continuous?

Most notably, two solutions presented themselves. The first, an undesirable one, was to alter the conservation laws, which were violated in $\beta$-decay. It was suggested that the energy is not conserved for each decay separately, but only statistically. This approach would help explain why the electrons emitted from a $\beta$-source could have various energies from the same decay. However, it did not help explaining the conservation of angular momentum violation. Anyway, this turned out to be incorrect by the findings of C. D. Ellis and W. A. Wooster in 1927 [37]. In fact, if the energy was to be conserved only statistically, there would be no reason to observe

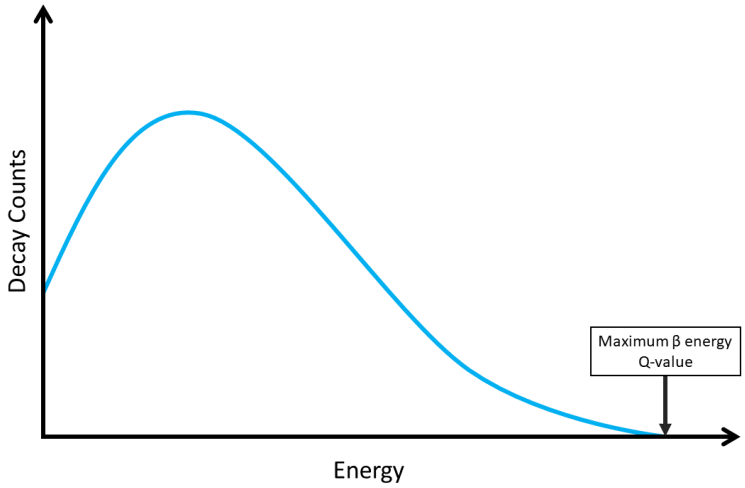


Figure 1.5: Example of typical shape of the $\beta$-decay spectrum. The units are arbitrary for the purposes of illustration.

maximum at the decay's Q-value. The second solution was proposed by W. Pauli in 1930. He proposed an existence of a new particle – a neutrino. Originally, he named this particle *neutron*, however, this name was 2 years later given to newly observed neutral nucleon discovered by J. Chadwick [39]. In a famous letter, which he addressed to the *Physical Institute of the Federal Institute of Technology, Zürich* on December 4th 1930, starting with the words "*Dear* ***radioactive*** *ladies and gentlemen,...*" he stated: "*I have done a terrible thing, I have postulated a particle that cannot be detected.*"

Thanks to the introduction of this *undetectable* particle, Pauli was able to explain the continuity of the $\beta$-spectrum. While the total released energy in the decay is constant, only part of it is carried away by the electron. The rest of the energy is carried away by the neutrino. This "saved" the conservation of energy. In order to preserve the momentum, Pauli proposed that the neutrino has mass of the same order of magnitude as the electron, but no larger than 0.01 times the mass of a proton and spin $-1/2$. Since the neutrino was undetectable, he predicted that it should also have zero EM charge.

In 1934, an Italian physicist Enrico Fermi proposed a quantitative theory of $\beta$-decay [40] (translated in: [41]). He profitted from Pauli's idea of an existence of the neutrino and modified it. He proposed, that in the process of $\beta$-decay, a neutron turns into a proton by emission of an electron and a neutral particle – neutrino: equation (1.9). Moreover, he offered a prediction of the $\beta$-decay half-life along with quantitative description of the shape of the $\beta$-spectrum. He even concluded that "*...the rest mass of the neutrino is either zero, or, in any case, very small in comparison to the mass of the electron.*" [41].

$$ {}^{A}_{Z}X \rightarrow {}^{A}_{Z+1}Y + e^{-} + \nu \tag{1.9} $$

Fermi's theory still held true when positron was discovered by C. D. Anderson in 1933 [42]. The $\beta$-decay, where a proton changes into a neutron and emits positron ("positively charged electron") along with a neutrino, was easily incorporated. And later still, on the basis of his paper, the inverse process has been proposed and

discovered. It was the so-called inverse $\beta$-decay, where a neutrino interacts with a proton (neutron), changing it into a neutron (proton) by the emission of a positron (electron). Enrico Fermi was also the inventor of the first nuclear reactor [43]. This, coincidentally, allowed for the discovery of the neutrino.

#### 1.2.1.4 The First Neutrino Detection

Since the postulate, it took more than twenty years for neutrinos to be detected for the first time. It was achieved by **Frederick Reines and Clyde Cowan**. They designed an experiment using a nuclear reactor as a source of intense neutrino flux. The flux of neutrinos arises from the fission fragments undergoing $\beta$-decay. In order to detect the neutrinos, they profited from a process called inverse beta-decay (predicted by E. Fermi):

$$\bar{\nu_e} + p \longrightarrow n + e^+ \tag{1.10}$$

In their experiment, they filled a large tank with water and placed layers of scintillators on the sides (in a sandwich arrangement). The scintillators are detectors that flash with visible light when a gamma particle interacts with the scintillator material. The tank was then placed in proximity of the nuclear reactor, so that the neutrino flux would reach it in high intensities. The scheme of the detector is shown in Figure 1.6. As the positron, created in inverse beta-decay, initiated by the incoming neutrino, collides with an electron inside the water tank, the two particles annihilate and produce two $\gamma$-particles. These two $\gamma$-particles travel in opposite directions and each carry energy equal to 511 keV [16]. The two gammas were detected in coincidence. Shortly after, the neutron from the decay was captured on the cadmium nucleus. In order to capture the neutrons, Cadmium Chloride (contained in a common household detergent) was added to the water tank. Cadmium is also a strong neutron absorber (used in reactors as a moderator of the chain reaction). Equation (1.11) describes the reaction.

$$n + {}^{108}Cd \longrightarrow {}^{109}Cd* \longrightarrow {}^{109}Cd + \gamma \tag{1.11}$$

A $\gamma$-particle is emitted as the cadmium de-excites into the ground state. This $\gamma$ has been measured in the scintillator and it is often called a delayed signal. These two signals, together detected as the "delayed pulse pair" [16], compared with the dependence of the signal on the reactor power, resulted in the discovery of the neutrino.

### 1.2.2 Solar Neutrino Problem

The Sun obtains most of its energy from the reactions in the so-called proton-proton chain. The chain describes the conversion of hydrogen atoms into helium within the Sun's core. Neutrinos are released as the consequence of the nuclear reactions inside the core [45]. The Sun acts as a neutrino generator, emitting neutrinos into the Space. A fraction of neutrinos reach the Earth completely undisturbed along the way. In 1960's R. Davis and J. Bahcall performed a neutrino experiment inside the Homestake Gold Mine. The experiment was designed to measure the flux of neutrinos arriving on the Earth, generated in the Sun's core. To determine the flux of neutrinos, Davis proposed to use a tank filled with $3.8 \cdot 10^5$ $l$ of perchloroethylene

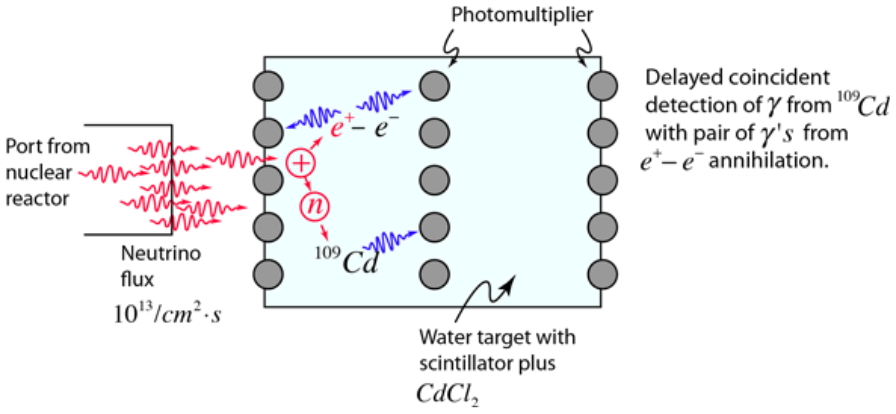


Figure 1.6: Scheme of the Cowan and Reines Neutrino Experiment. The red wavy arrows represent the neutrinos, whereas the blue wavy arrows represent the $\gamma$s. From [44].

($C_2Cl_4$) as a medium with which the neutrinos would interact. The tank contained estimated $2.2 \cdot 10^{30}$ atoms of $^{37}Cl$ [46]. The experiment was designed to take advantage of the reaction:

$$\nu_e + {}^{37}Cl \rightarrow {}^{37}Ar + e^- \ . \tag{1.12}$$

A neutrino, originating in the Sun, reacts with $^{37}Cl$ transforming it to $^{37}Ar$ while an electron is emitted. The argon was periodically extracted from the tank and its decay was then observed. The number of decayed argon nuclei were counted. This provided a method for determination of the number of neutrinos interacting in the tank. Based on this measurement, the neutrino flux from the Sun has been estimated. The Comparison of this estimation to the calculation performed by J. Bahcall showed a discrepancy. The flux measured in the experiment was significantly smaller than what the model predicted. Repeated measurements, even in other experiments, found similar discrepancies. These results gave rise to what is known today as the "Solar Neutrino Problem".

Three possible explanations were discussed. First, maybe the experiments were conducted incorrectly. However, after much refinement of the experimental techniques, this explanation was not valid anymore. Second, the theoretical calculations were considered to be wrong. Two decades of refinement and checking for errors ruled out this explanation as well. Third, the understanding of neutrino physics was insufficient.

One explanation proposed by Bruno Pontecorvo in 1958, considered a previously unknown behaviour of neutrinos – neutrino oscillations [47]. Neutrino oscillations are a phenomenon in which the neutrinos are capable of changing their flavour as they propagate through space. Furthermore, if neutrinos would oscillate, it would suggest that not only do they can change their flavour, but it would also mean that neutrinos cannot be massless. Neutrino oscillations were confirmed by Super-Kamiokande Observatory (discovery announced in 1998 [48]) and the Sudbury Neutrino Observatories (2001 [49]) and were awarded a Nobel prize in 2015. This was the solution to the Solar Neutrino Problem.

To understand how the neutrino oscillations prove neutrinos have non-zero

masses, an assumption about neutrino flavour and mass eigenstates must be made. The assumption is that the neutrino **flavour** eigenstates ($\nu_e$, $\nu_\mu$, $\nu_\tau$) – neutrino interaction states – are different from the neutrino **mass** eigenstates ($\nu_1$, $\nu_2$, $\nu_3$) – neutrino propagation states. The transformation between the two bases is provided via the unitary matrix, the so-called PMNS matrix (Pontecorvo – Maki – Nakagawa – Sakata) [50, 51]. The transformation is given by:

$$|\nu_\alpha\rangle = \sum_i U_{\alpha i}|\nu_i\rangle \tag{1.13}$$

$$|\nu_i\rangle = \sum_\alpha U^*_{\alpha i}|\nu_\alpha\rangle \tag{1.14}$$

Here, $\alpha$ denotes flavour eigenstate and $i$ denotes the mass eigenstate. $U_{\alpha i}$ are the matrix elements of the PMNS matrix. The flavour eigenstates are a superposition of the mass eigenstates and vice versa. As a simplification, a two-neutrino mixing can be assumed. Then the transition would be given by:

$$\begin{pmatrix}|\nu_\alpha\rangle\\|\nu_\beta\rangle\end{pmatrix} = \begin{pmatrix}cos(\theta) & sin(\theta)\\-sin(\theta) & cos(\theta)\end{pmatrix}\begin{pmatrix}|\nu_1\rangle\\|\nu_2\rangle\end{pmatrix} \tag{1.15}$$

Here, the 2×2 unitary PMNS matrix is expressed as a function of $\theta$, is the so-called mixing angle. This form fulfills the conditions of unitarity ($UU^\dagger = U^\dagger U = I$) and reduces the number of parameters to one. It can be shown that the probability for a relativistic neutrino to change flavour from $\nu_\alpha$ to $\nu_\beta$ is then given by:

$$P(\nu_\alpha \to \nu_\beta) = sin^2(2\theta)sin^2\left(\frac{\Delta m^2_{ij}\mathrm{L}}{4\mathrm{E}}\right) . \tag{1.16}$$

Here, E is the energy of the neutrino, L is the distance which neutrino travelled and $\Delta m^2_{ij} \equiv m^2_i - m^2_j$ is the mass square difference. The probability is zero only if $\Delta m^2_{ij} = 0$ (or $\theta = 0$, which was measured not to be the case). Since oscillations *were* observed, the probability is not zero and $\Delta m^2_{ij} \neq 0$. Thus, at least one neutrino mass eigenstate has non-zero mass. However, the fact that $\Delta m^2_{ij} \neq 0$, does not provide information on the actual values of $m_i$ nor $m_j$. Furthermore, it is not known which neutrino mass eigenstate is the lightest (or heaviest). This imposes the *Neutrino Mass Hierarchy* problem. So far, the experiments measured the square mass differences of neutrino mass eigenstates as $|\Delta m^2_{31}| = |\Delta m^2_3 - \Delta m^2_1| \approx 2.5 \cdot 10^{-3}\mathrm{eV}^2$ and $\Delta m^2_{21} = m^2_2 - m^2_1 \approx 7.39 \cdot 10^{-5}\mathrm{eV}^2$ [52]. Conventionally, it is considered that $m_1 < m_2$. Thus, there are two alternatives for a possible mass ordering (or hierarchy). Either $m_1 < m_2 < m_3$ (the so-called normal ordering) or $m_3 < m_1 < m_2$ (the so-called inverted ordering). Figure 1.7 depicts the two hierarchies. One way of determining whether the neutrinos follow the Normal or Inverted hierarchy is by studying the beta-decay processes.

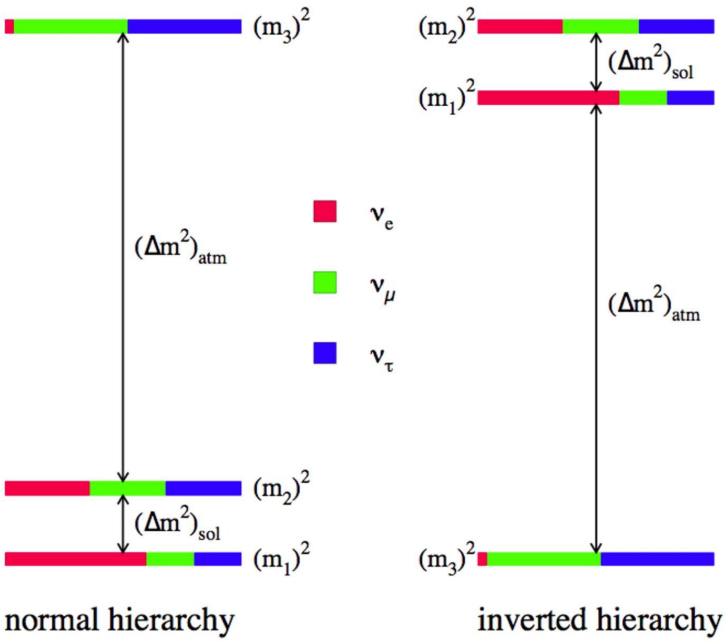


Figure 1.7: Illustration of the two possible neutrino mass orderings (hierarchies). The three different colors represent the neutrino flavour eigenstates. The horizontal bars represent the neutrino mass eigenstates. Normal hierarchy is considered if $m_1 < m_2 < m_3$. Inverted hierarchy is considered if $m_3 < m_1 < m_2$. From [53].

## 1.3 Beta-Decay

### 1.3.1 Ordinary Beta-Decay

There are three known basic $\beta$-decay modes: $\beta^-$, $\beta^+$ and Electron Capture (EC). Their formulas can be found in the Equations (1.17) – (1.19). $\beta^-$ ($\beta^+$) is a process where a neutron (proton) bounded inside a nucleus turns into a proton (neutron) accompanied by emission of an electron (positron) and an electron antineutrino (neutrino). In EC, an electron from the K-shell (the closest shell to the nucleus) of an atom is captured by the nucleus and excites the nucleus [25]. The nucleus de-excites by undergoing a beta-decay. There are other ways for the excited nucleus to de-excite, however, they are not the subject of this thesis.

$$\beta^- : \quad {}^A_Z X \longrightarrow {}^A_{Z+1} Y + e^- + \bar{\nu}_e \tag{1.17}$$

$$\beta^+ : \quad {}^A_Z X \longrightarrow {}^A_{Z-1} Y + e^+ + \nu_e \tag{1.18}$$

$$EC : \quad e^- + \; {}^A_Z X \longrightarrow {}^A_{Z-1} Y \qquad + \nu_e \tag{1.19}$$

There are multiple features to be addressed. The first is that the beta-decay is not a two-body final state process (in comparison to $\alpha$-decay described in Section 1.2), but a three-body final state process (excluding EC). This fact gives rise to the continuous spectrum of $\beta$-decay. A typical spectrum is depicted in Figure 1.5.

#### 1.3.1.1 $\beta$-Decay Q-value

Theoretical beta-decay electron energy spectrum has a sharp end, marked in Figure 1.5. It is a point where electron carries away almost the whole energy of the decay – the Q-value. This is slightly different for each $\beta$-decay mode. Since Q-value is defined as subtraction of the rest-mass energies of the reaction products from the parent nucleus, it can be calculated following way:

$$Q_{\beta^-} = [m_p(Z,N) - m_d(Z+1,N-1) - m_{\nu_e}]c^2 \quad (1.20)$$
$$Q_{\beta^+} = [m_p(Z,N) - m_d(Z-1,N+1) - 2m_e - m_{\nu_e}]c^2 \quad (1.21)$$
$$Q_{EC} = [m_p(Z,N) - m_d(Z-1,N+1) - m_{\nu_e}]c^2 - B_e \quad (1.22)$$

Here, $m_p, m_d$ are the masses of atoms with Z protons and N neutrons, $m_e$ is the mass of an electron, $B_e$ is the binding energy of the captured electron [54].

Let us now discuss the nuclear mass terms $m(Z,N)$. To estimate the mass of the nucleus properly, one needs not only to sum the masses of the nucleons as if they were free but also to account for the energy of the bond between nucleons $E_B$(Z,N) in the following way:

$$m(Z,N) = Zm_p + Nm_n - E_B(Z,N) \quad (1.23)$$

Based on the liquid drop nuclear model, the binding energy $E_B$(Z,N) can be estimated relatively precisely by a semi-empirical Bethe-Weizsäcker formula [55]. The model treats the nucleus composed of Z protons and N neutrons as if it were a drop of an incompressible fluid. The nucleons inside are bound by the nuclear force. The strength of the binding energy $E_B(Z,N)$ is modeled by equation (1.24).

$$E_B(Z,N) = a_V A - a_S A^{2/3} - a_C \frac{Z(Z-1)}{A^{1/3}} - a_A \frac{(A-2Z)^2}{A} + \delta(N,Z) \quad (1.24)$$
$$\delta(N,Z) = \begin{cases} a_p \frac{1}{\sqrt{A}} & \text{even-even nuclei} \\ 0 & \text{odd-even or even-odd nuclei} \\ -a_p \frac{1}{\sqrt{A}} & \text{odd-odd nuclei} \end{cases}$$

There are five components of this formula.

- $\boldsymbol{a_V A}$ represents the *volume* component of the binding energy. The radius of the drop is proportional to $r_0 A^{1/3}$ (where $r_0$ is the radius of a nucleon and A = Z+N) and since volume grows as the third power of the radius, the volume factor is hence $a_V A$.
- $\boldsymbol{a_S A^{2/3}}$ represents the *surface* component of the binding energy. This is analogous to the surface tension of the liquid drop. Hence, the energy is proportional to the surface area growing as $A^{2/3}$. The negative sign represents the decrease in binding energy, it is a correction for the surface nucleons which are less bound due to the lower number of nucleons in their vicinity (as opposed to the nucleons inside the bulk).
- $\boldsymbol{a_C \frac{Z(Z-1)}{A^{1/3}}}$ represents the *Coulomb energy*. There are $Z(Z-1)/2$ pairs of

protons interacting via Coulomb force. Since potential energy of a sphere is proportional to $1/r_0$, this results in $1/A^{1/3}$. As protons have the same charge, the force is repulsive and the binding energy is decreased.

- $\boldsymbol{a_A \frac{(A-2Z)^2}{A}}$ represents the *symmetry* of the nucleus. It is preferential to have $Z = N$ as this results in equal number of energy states occupied by each proton and neutron. This is due to Pauli Exclusion principle, which states that no two identical particles can occupy the same state.

- $\boldsymbol{\delta(N, Z)}$ represents the *pairing* of the spins of the nucleons. There are three possibilities of pairing.

  1. Both N and Z are even ⇒ A is even. In such case for every proton (neutron) with spin up, there is a paired proton (neutron) with spin down. The binding energy is increased by $a_p \frac{1}{\sqrt{A}}$.
  2. Either N or Z are odd ⇒ A is odd. In this case, $\delta(N, Z) = 0$.
  3. Both N and Z are odd ⇒ A is even. There is one proton and one neutron without a pair, which decreases the binding energy by $-a_p \frac{1}{\sqrt{A}}$.

The values of the model parameters $a_V$, $a_S$, $a_C$, $a_A$ and $a_p$ were obtained by fitting the measured data. Due to the presence of the $\delta(N, Z)$ pairing term, one distinguishes three different cases of what mass distribution looks like as a function of Z for a given value of A. If we consider a case with an odd A (e.g., $A = 107$ in Figure 1.8) the resulting nuclei can be either odd-even or even-odd.

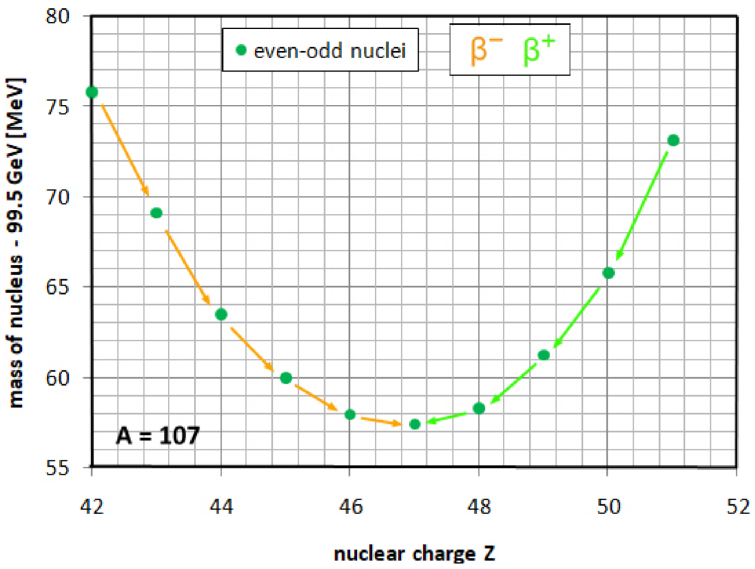


Figure 1.8: Mass of nucleus for an odd A = 107. The decay modes are presented by orange and green arrows for $\beta^-$ and $\beta^+$-decays respectively. From [56] .

In this case, the term $\delta(N, Z)$ is zero and the function follows a single parabola. Thanks to Figure 1.8 it is possible to see that the most stable nucleus at the bottom of the parabola is the one with Z = 47. Depending, whether the nucleus has a relative deficit of protons ($Z < 47$) or excess ($Z > 47$) it tends to increase it or decrease, respectively. This transmutation is, of course, driven by $\beta$-decay as this is

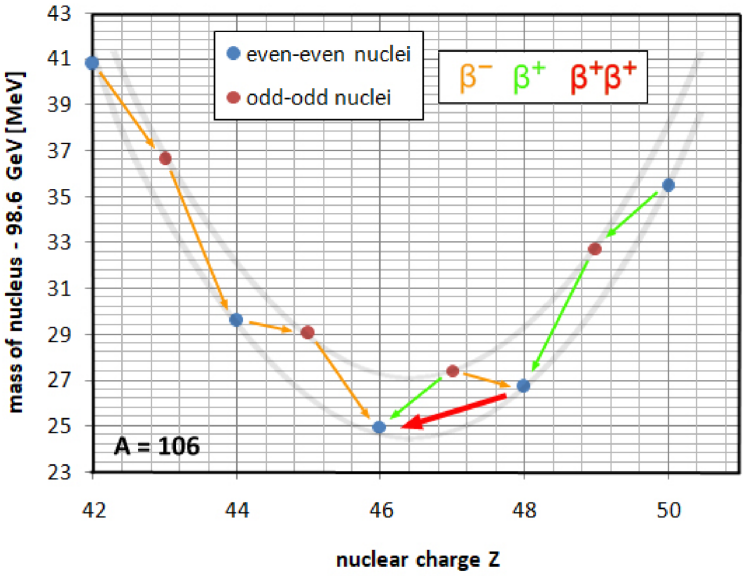


Figure 1.9: Mass of nucleus for an even A = 106. The ordinary beta-decay modes are presented by orange and green arrows for $\beta^-$ and $\beta^+$-decays respectively. The allowed double-beta-decay is marked by red arrow. From [56].

the only decay channel which is capable to change the proton number of the nucleus by one unit while preserving the total mass number A. The decays are represented in Figure 1.8 by orange and green arrows. Orange arrows point from left to right and represent $\beta^-$-decay – number of protons (Z) increases. The green arrows point right to left and represent $\beta^+$-decay – number of protons decreases. Naturally, the decay can only proceed towards the nucleus with lower binding energy.

On the other hand, there are two possibilities when constructing a nucleus with an even number A. Either both Z and N are even, or both are odd simultaneously. The pairing term of the binding energy function causes the function of binding energy to split into two individual parabolas, as shown in Figure 1.9. Both these parabolas are shifted by the value of $2a_p$. The odd-odd nuclei contain one proton and one neutron without a pair which decreases its binding energy (increases its mass) with respect to the even-even nuclei in which all nucleons are paired up. This is the reason we find all odd-odd nuclei in the top parabola and all even-even nuclei in the lower one. Orange and green arrows represent again $\beta^-$ and $\beta^+$, respectively. However, in case of the nucleus with $Z = 48$ (Cd), the $\beta^+$-decay is forbidden because the nucleus $Z = 47$ (Ag) is energetically inaccessible (larger mass). Nevertheless, the nucleus with $Z = 46$ (Pd) is reachable and a process changing the number of protons Z by two units is possible. This process is called the double beta-decay. The process is indicated by a red arrow in Figure 1.9. The double beta-decay is the main interest of the presented thesis.

### 1.3.2 Double Beta-Decay

Double beta-decay is the rarest process known to mankind. There are only 35 candidate isotopes which can theoretically undergo double-beta-decay [57]. Its existence was proposed by M. Goeppert-Mayer already in 1935 [58]. In the decay which M. Goeppert-Mayer proposed, two neutrons bound in the nucleus simultaneously trans-

form into two protons while two electrons and two antineutrinos are emitted. This is the most basic double beta-decay mode called two-neutrino double beta-decay ($2\nu\beta\beta$). In 1939, Furry proposed the existence of lepton number violating version of this process, called neutrinoless double beta-decay ($0\nu\beta\beta$). This process has been observed for the first time in 1987 in a time-projection chamber experiment by Elliott et al. [59]. $0\nu\beta\beta$ was not yet observed.

#### 1.3.2.1 Two-Neutrino Double Beta-Decay

There are four basic $2\nu\beta\beta$-decay modes. They are summarized in equations (1.25) through (1.28). Double beta-decay was already observed for 11 isotopes for $2\nu\beta\beta$ mode and 3 isotopes for EC/EC capture mode [60].

$$2\nu\beta^-\beta^- : \quad {}^A_Z X \longrightarrow {}^A_{Z+2}Y + 2e^- + 2\bar{\nu}_e \tag{1.25}$$

$$2\nu\beta^+\beta^+ : \quad {}^A_Z X \longrightarrow {}^A_{Z-2}Y + 2e^+ + 2\nu_e \tag{1.26}$$

$$2\nu\beta^+/EC : \quad e^- + {}^A_Z X \longrightarrow {}^A_{Z-2}Y + e^+ + 2\nu_e \tag{1.27}$$

$$2\nu EC/EC : \quad 2e^- + {}^A_Z X \longrightarrow {}^A_{Z-2}Y + 2\nu_e \tag{1.28}$$

The typical half life of this decay is of the order of $10^{18}$ years and longer. In comparison, the age of the universe is approximately $1.38 \times 10^{10}$ years, making the double beta-decay incredibly rare in comparison. The half-life can be expressed as:

$$[T^{2\nu\beta\beta}_{1/2}]^{-1} = \frac{\Gamma_{2\nu\beta\beta}}{\ln(2)} = G^{2\nu\beta\beta}|M^{2\nu\beta\beta}|^2. \tag{1.29}$$

Here, $\Gamma_{2\nu\beta\beta}$ stands for the decay rate, $G^{2\nu\beta\beta}$ is the phase space factor and $M^{2\nu\beta\beta}$ is the nuclear matrix element [61]. The phase space factor can be calculated exactly and it represents the kinematics of the decay. However, the nuclear matrix elements are very complicated to be calculated.

As stated previously, there are only 35 isotope candidates for double-beta-decay. The double beta-decay is several orders of magnitude rarer than single beta-decay, therefore, it is necessary to search for this process in isotopes where the single beta-decay is either completely forbidden due to the conservation of energy or strongly suppressed by spin rules. Examples of such an isotope can be seen in Figure 1.9. As explained above, the single $\beta^+$ from nucleus Z=48 to Z=47 is energetically forbidden, nevertheless, the $2\nu\beta^+\beta^+$ to Z = 46 is still possible. The first time double-beta-decay was observed was in 1987, using $^{82}$Se. The isotopes observed for $2\nu\beta\beta$-decay, along with years of discovery and half-lives are presented in Table 1.3.

#### 1.3.2.2 Neutrinoless Double Beta-Decay

In 1937 E. Majorana published an article in which he showed that, if one were to consider a situation where a neutrino would be its own antiparticle ($\nu = \bar{\nu}$), the $\beta$-decay processes would not be changed. The same principles would hold regardless of whether a neutrino (or an antineutrino) is involved. Such neutrinos are then called Majorana neutrinos ($\nu_M$) [62]. Two years later, in 1939, W. Furry published an article in which he proposed a double beta-decay without the emission of neutrinos. This would only be possible if the neutrinos were, in fact, Majorana particles. The

| Isotope | Average $T_{1/2}^{2\nu\beta\beta}$ [yr] | Discovered [yr] |
|---|---|---|
| $^{48}Ca$ | $5.3^{+1.2}_{-0.8} \cdot 10^{19}$ | 1996 |
| $^{76}Ge$ | $(1.88 \pm 0.08) \cdot 10^{21}$ | 1990 |
| $^{82}Se$ | $0.87^{+0.02}_{-0.01} \cdot 10^{20}$ | 1987 |
| $^{96}Zr$ | $(2.3 \pm 0.2) \cdot 10^{19}$ | 1993 |
| $^{100}Mo$ | $7.06^{+0.15}_{-0.13} \cdot 10^{18}$ | 1991 |
| $^{116}Cd$ | $(2.69 \pm 0.09) \cdot 10^{19}$ | 1995 |
| $^{128}Te$ | $(2.25 \pm 0.09) \cdot 10^{24}$ | 1991 |
| $^{130}Te$ | $(7.91 \pm 0.21) \cdot 10^{20}$ | 1991 |
| $^{136}Xe$ | $(2.18 \pm 0.05) \cdot 10^{21}$ | 2014 |
| $^{150}Nd$ | $(8.4 \pm 1.1) \cdot 10^{18}$ | 1995 |
| $^{238}U$ | $(2.0 \pm 0.6) \cdot 10^{21}$ | 1991 |
| $^{78}Kr$ | $1.9^{+1.3}_{-0.8} \cdot 10^{22}$ | 2017 |
| $^{124}Xe$ | $(1.8 \pm 0.5) \cdot 10^{22}$ | 2019 |
| $^{130}Ba$ | $(2.2 \pm 0.5) \cdot 10^{21}$ | 1996 |

Table 1.3: Table of observed $2\nu\beta\beta$-decay isotopes. The recommended (average) $T_{1/2}^{2\nu\beta\beta}$ is included. The third column represents the year the decay was first observed. The isotopes above the horizontal line between $^{238}U$ and $^{78}Kr$-decay in $2\nu\beta\beta$ mode, the three isotopes below decay in ECEC mode. The values are taken from [60].

proposed $0\nu\beta\beta$-decay modes are listed in equations (1.30) - (1.33).

$$0\nu\beta^-\beta^- : \quad {}^A_Z X \longrightarrow {}^A Y^{Z+2} + 2e^- \tag{1.30}$$

$$0\nu\beta^+\beta^+ : \quad {}^A_Z X \longrightarrow {}^A Y^{Z-2} + 2e^+ \tag{1.31}$$

$$0\nu\beta^+/EC : \quad e^- + {}^A_Z X \longrightarrow {}^A Y^{Z-2} + e^+ \tag{1.32}$$

$$0\nu EC/EC : \quad 2e^- + {}^A_Z X \longrightarrow {}^A Y^{Z-2} \tag{1.33}$$

In its simplified form, the neutrinoless double beta-decay can be understood in the following way: a neutron undergoes an ordinary beta-decay with the emission of an electron and an anti-neutrino ($\bar{\nu_e}$). This anti-neutrino, being a Majorana particle, would instantaneously get reabsorbed as a neutrino in an inverse beta-decay (IBD). Previous description has its impressions, nevertheless, it serves good enough to help visualizing the idea of neutrinoless double beta-decay. However, neutrinos being identical to their anti-particles is not enough to justify this process. Another issue is the neutrino's chirality. The antineutrino emitted in the first decay – of the described example – is right-handed. However, the neutrino absorbed in the IBD is left-handed. The neutrino must have switched its chirality in the process. This is because in weak interactions (such as this one) only the left-handed particles or right-handed anti-particles are allowed to interact with the $W^\pm$ bosons. In order for a particle to switch its chirality, it must have non-zero mass. Within the SM, neutrinos are massless, so they cannot change chirality [63]. Thus, the process of neutrinoless double beta-decay can only occur if neutrinos are Majorana particles **and** have non-zero mass. The $0\nu\beta\beta$ involves BSM physics.

It is obvious from the equations (1.30) - (1.33) that the $0\nu\beta\beta$ violates the lepton number conservation. This can be interpreted as a production of the matter or

antimatter depending on which of the mechanisms of the $0\nu\beta\beta$ we consider. Such a process might shed light on the problem of the abundance of matter over antimatter. While the exact mechanism of the $0\nu\beta\beta$-decay is still unknown, the decay rate for the process can be calculated analogously to the $2\nu\beta\beta$ rate in (1.29). The equation (1.34) for $0\nu\beta\beta$-decay rate is as follows [64]:

$$[T_{1/2}^{0\nu\beta\beta}]^{-1} = \frac{\Gamma_{0\nu\beta\beta}}{\ln(2)} = G^{0\nu\beta\beta}|M^{0\nu\beta\beta}|^2 \left(\frac{|\langle m_{\beta\beta}\rangle|}{m_e}\right)^2 \tag{1.34}$$

Here, $\Gamma_{0\nu\beta\beta}$ is the decay rate, $G^{0\nu\beta\beta}$ is the phase space factor (related to the electron energy) and $M^{0\nu\beta\beta}$ is the nuclear matrix element (containing the information of the nuclear structure). In comparison to the $2\nu\beta\beta$, a new factor $\langle m_{\beta\beta}\rangle$ appeared in the equation in comparison to equation (1.29). This factor is called "the effective neutrino mass". It is calculated as the superposition of the neutrino mass eigenstates $m_i$ and nuclear matrix elements $U_{ei}$ of the PMNS mixing matrix [65]:

$$\langle m_{\beta\beta}\rangle = \sum_{i=1}^{3} m_i U_{ei}^2 \tag{1.35}$$

The fact that the $T_{1/2}^{0\nu\beta\beta}$ of the decay is dependent on neutrino mass provides for a powerful tool in determination of neutrino masses and neutrino mass ordering. If one were to measure decay $T_{1/2}^{0\nu\beta\beta}$ for a specific decay (isotope) along with the correct $G^{0\nu\beta\beta}$ and $M^{0\nu\beta\beta}$, one could determine the neutrino effective mass! This is not possible with $2\nu\beta\beta$ because the half-life does not depend on the neutrino masses. However, $0\nu\beta\beta$-decay was never measured. It is an incredibly rare process. The current best $\langle m_{\beta\beta}\rangle$ limit and recommended by [66], was obtained by KamLAND-Zen experiment by observation of $^{136}$Xe. The values cited are:

$$T \quad > 0.25 \cdot 10^{26} \text{ yr} \Rightarrow \langle m_{\beta\beta}\rangle \quad < (0.09 - 0.24)\text{eV}.$$

The list of the best current limits on the $0\nu\beta\beta$ half-life for different isotopes can be found in Table 1.4).

Improving the $0\nu\beta\beta$ experimental limits has a direct influence on the Neutrino Mass Hierarchy problem. Figure 1.10 shows the relationship between $|\langle m_{\beta\beta}\rangle|$ and the smallest neutrino mass $m_{min}$ (it is unknown whether this is $m_1$ or $m_3$).

Currently, the experimental results for $|\langle m_{\beta\beta}\rangle|$ do not provide an answer to the mass ordering problem. However, as the experimental techniques improve, the effective mass limit is expected to be lowered. If the calculated limit reaches $|\langle m_{\beta\beta}\rangle| < 15$ meV (below the blue shaded area), it would mean that the neutrino masses follow the Normal Ordering principle. Thus, $m_1$ would be the lightest neutrino mass $m_1 = m_{min}$. This conclusion assumes that $0\nu\beta\beta$ exists. Since it has not been measured yet and the calculated values are only given as limits, it may not be conclusive.

#### 1.3.2.3 Spectrum of $0\nu\beta\beta$-Decay

Typical experimental signature for both the $2\nu\beta\beta$ and $0\nu\beta\beta$ is the sum of the kinetic energies of the emitted electrons. The (anti)neutrinos in case of $2\nu\beta\beta$ are not detectable, they leave the detector undetected. The difference between $2\nu\beta\beta$ and

| Isotope | $Q_{2\beta}$, keV | $T_{1/2}$, yr | $\langle m_{\beta\beta}\rangle$, eV | Experiment |
|---|---|---|---|---|
| $^{48}$Ca | 4267.98 | $> 5.8 \cdot 10^{22}$ | $< 3.1 - 15.4$ | CANDLES |
| $^{76}$Ge | 2039.00 | $> \mathbf{3.5 \cdot 10^{25}}$ | $< \mathbf{0.18 - 0.48}$ | GERDA-I+GERDA-II |
| | | $(> 5.2 \cdot 10^{25})$ | $(< 0.15 - 0.39)$ | |
| $^{82}$Se | 2997.9 | $> 3.6 \cdot 10^{23}$ | $< 1 - 2.4$ | NEMO- 3 |
| $^{96}$Zr | 3355.85 | $> 9.2 \cdot 10^{21}$ | $< 3.6 - 10.4$ | NEMO-3 |
| $^{100}$Mo | 3034.40 | $> 1.1 \cdot 10^{24}$ | $< 0.33 - 0.62$ | NEMO- 3 |
| $^{116}$Cd | 2813.50 | $> 1.9 \cdot 10^{23}$ | $< 1 - 1.8$ | AURORA |
| $^{128}$Te | 866.6 | $> 1.5 \cdot 10^{24}$ | $2.3 - 4.6$ | Geochem. exp. |
| $^{130}$Te | 2527.52 | $> 4 \cdot 10^{24}$ | $< 0.26 - 0.97$ | CUORICINO + CUORE0 |
| $^{136}$Xe | 2457.83 | $> \mathbf{0.5 \cdot 10^{26}}$ | $< \mathbf{0.09 - 0.24}$ | KamLAND-Zen |
| | | $(> 1.07 \cdot 10^{26})$ | $(< 0.06 - 0.16)$ | |
| $^{150}$Nd | 3371.38 | $> 2 \cdot 10^{22}$ | $< 1.6 - 5.3$ | NEMO-3 |

Table 1.4: Table of limits on $0\nu\beta\beta$ for $T_{1/2}^{0\nu\beta\beta}$ and $\langle m_{\beta\beta}\rangle$. Confidence level used for the results was 90%. From [66].

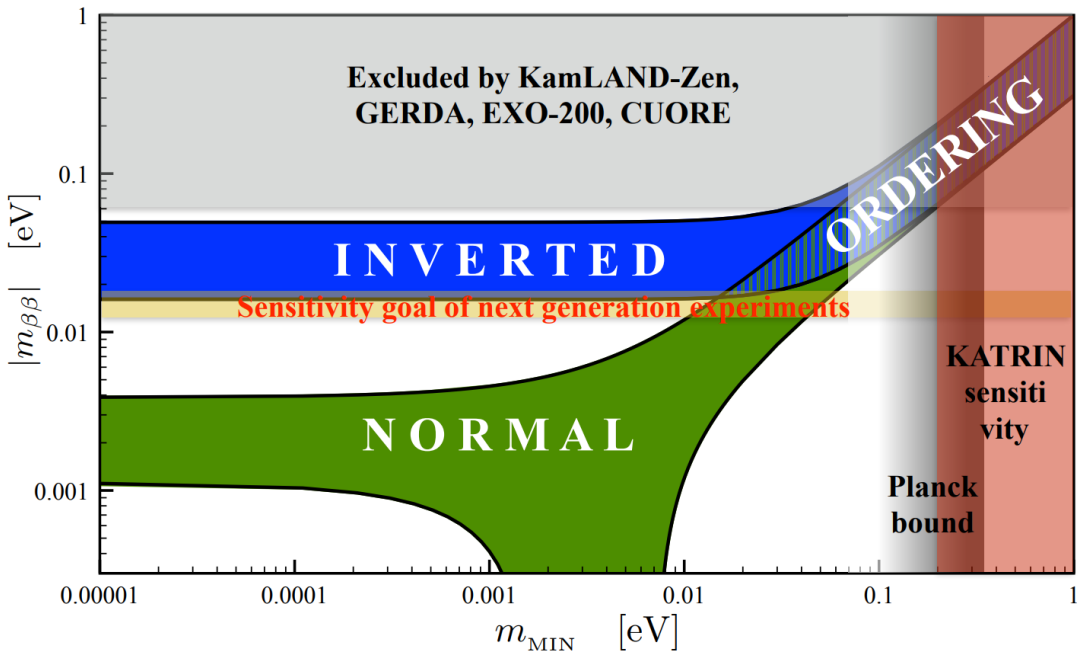


Figure 1.10: Effective neutrino mass $|\langle m_{\beta\beta}\rangle|$ as a function of minimum neutrino mass $m_{min}$. The current best limits lie within the grey shaded area. From [67].

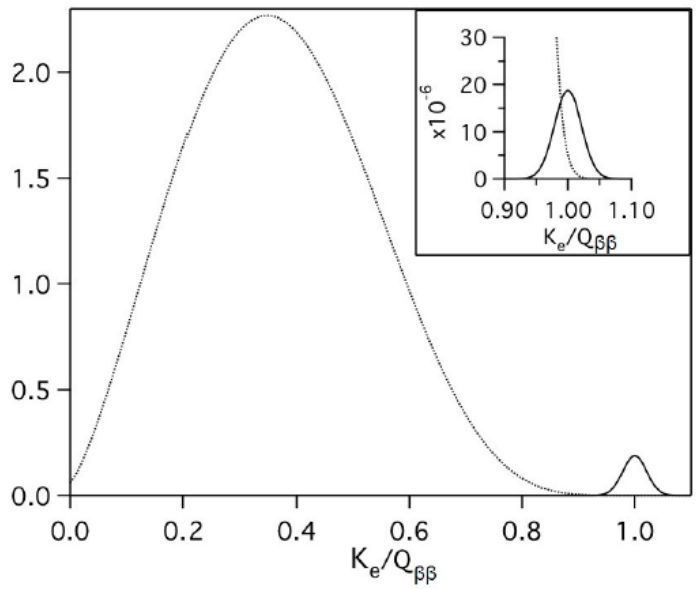


Figure 1.11: Theoretical double beta spectrum. The sum of kinetic energies of both electrons is expressed in units $Q_{\beta\beta}$ on the x-axis. The y-axis is represented in arbitrary units. The top right corner represents shows zoomed in area around the Q-value of the $0\nu\beta\beta$-decay. A clear overlap is visible due to the finite energy resolution of the detector. From [68].

$0\nu\beta\beta$ can be distinguished by looking at the spectrum. In $2\nu\beta\beta$-decay, some of the decay energy (the Q-value) is carried away by the neutrinos. This gives rise to the continuous spectrum with an endpoint at $(E_1 + E_2) \rightarrow Q$ (here, $E_1$ and $E_2$ are the kinetic energies of the emitted electrons). In the case of $0\nu\beta\beta$, the entire disintegration energy of the decay is carried away solely by the two emitted electrons as there are no neutrinos in the final state. The theoretical spectral shape is a delta function at the point where the sum of the two electrons $(E_1+E_2)$ is equal to Q-value. Proper energy cuts can very efficiently help to distinguish $0\nu\beta\beta$ from $2\nu\beta\beta$. If we take into account the finite detector resolution the expected spectral shape of $2\nu\beta\beta$ and $0\nu\beta\beta$ resembles the example in the figure 1.11. Based on the quality of the detector, the $2\nu\beta\beta$ events from vicinity of $Q$ value can be smeared over the Q threshold. In this case, the the spectrum of $2\nu\beta\beta$ can overlap with spectrum of $0\nu\beta\beta$ (see Figure 1.11), making the $2\nu\beta\beta$-decay a background for $0\nu\beta\beta$ searches. The existence of this effect underlines the importance of the detectors with high energy resolution. The $0\nu\beta\beta$ detectors are typically placed underground in order to suppress the background due to the omnipresent cosmic rays on the surface of the Earth.

### 1.3.3 Double Beta-decay Experiments

As $0\nu\beta\beta$-decay provides valuable information on the nature of neutrinos, there naturally are multiple experiments searching for this rare process. The experiments employ a multitude of measuring techniques and study different candidate isotopes. The experimental techniques or approaches can be divided into two main categories.

In the first category are detectors that employ the approach where **the detector and the source are separate** from one another. Such approach is used, for

example by the SuperNEMO experiment [69], or its predecessors (NEMO-1 [70], NEMO-2 [71] and NEMO-3 [72]). The underlying methodology is based on the tracker and calorimeter architecture. A thin foil acting as a source is placed between a series of trackers and calorimeters. In this approach it is possible to reconstruct both the trajectory of the detected particles as well as the energy of the interaction. However, the design of the detector is very complicated and various challenges must be overcome in the construction.

The second category of $0\nu\beta\beta$-decay experiments employs the approach where **detector and the source are the same**. There are experiments where the source is a fluid, such as Enriched Xenon Observatory (EXO) [73] experiment or KamLAND-Zen [74]. Using liquids or gases as the detection medium and the source of the decay allows for building large-scale detectors. This in turn provides for high efficiency of detection. Disadvantage of such detectors is the relatively high background. On the other hand, detectors where the source is crystalline, such as Germanium based GERDA [75] or LEGEND [76] experiments, provide very good detection energy resolution. Having excellent energy resolution is essential in attempting to distinguish between $2\nu\beta\beta$ and $0\nu\beta\beta$. The COBRA Experiment belongs in this category.

CHAPTER 2

# COBRA EXPERIMENT

The **C**admium Zinc Telluride **0**-Neutrino Double-**B**eta **R**esearch **A**pparatus experiment (COBRA experiment) is a $0\nu\beta\beta$ detector based on the technology using semiconductor CdZnTe crystals. Its concept was proposed by Kai Zuber in 2001 [77]. The detector belongs to category of so-called homogeneous detectors – the detector where source serves as a detector at the same time. This brings out a desirable advantage of the design – the detector disposes with a very high efficiency of detection, since the radiation originates inside the crystal. The apparatus also contains an impressive number of nine possible double beta-decay candidate isotopes. In order to lower the background radiation to a minimum, the detector is placed in an underground laboratory – *Laboratori Nazionali del Gran Sasso* (LNGS), located in Italian Appenines below Gran Sasso mountain. The laboratory is shielded by 1400 m of rock formation which accounts for 3800 m.w.e. The cosmic muon flux is suppressed down to $(3.41 \pm 0.01).10^{-4}\mathrm{m}^{-2}\mathrm{s}^{-1}$ [78].

The detector consists of two modules. The detector was, in its first phase composed of 64 CdZnTe semiconductor detectors shaped in form of the cubes (see Figure 2.2 ). Each cube has a volume of 1 $\mathrm{cm}^3$ ($1.0 \times 1.0 \times 1.0$ $\mathrm{cm}^3$). The arrangement of the detectors is depicted in Figure 2.1. The detectors are arranged in 4 layers, containing 16 detectors each, placed on top of one another in $4 \times 4 \times 4$ arrangement. This module is called the COBRA Demonstrator. The demonstrator has been finished in 2013 and has been taking data since. In 2018, an extension has been installed. The second module of the COBRA detector, called the eXtended DEMonstrator (XDEM), consists of 9 CdZnTe cubes of volume 6 $\mathrm{cm}^3$($2.0 \times 2.0 \times 1.5$ $\mathrm{cm}^3$). The nine cubes form another layer, which is placed on top of the existing Demonstrator. A scheme of the geometry and the composition of the detector is shown in Figure 2.1.

The detector is shielded on the outermost side by 7 cm thick layer of borated polyethylene (neutron shielding). Further in, a construction of several 2 mm thick sheet of iron acts as a Faraday cage, shielding the detector from the electromagnetic interference. Inside, the detector itself, with pre-amplifiers, is placed in an air-tight polycarbonate box. The polycarbonate box is constantly flushed with nitrogen in order to prevent dust from settling on the detector and to limit the diffusion of radon into the setup. Two more layers ensure additional shielding from $\gamma$-radiation. A lead castle is built around the inner-most shielding structure – the copper nest. The detector crystals are mounted on a radioactively pure thermoplastic polyoxymethylene (POM) and they are shielded individually with additional layers of copper shielding. Photos of the detector shielding and the detector cubes are presented in Figure 2.2.

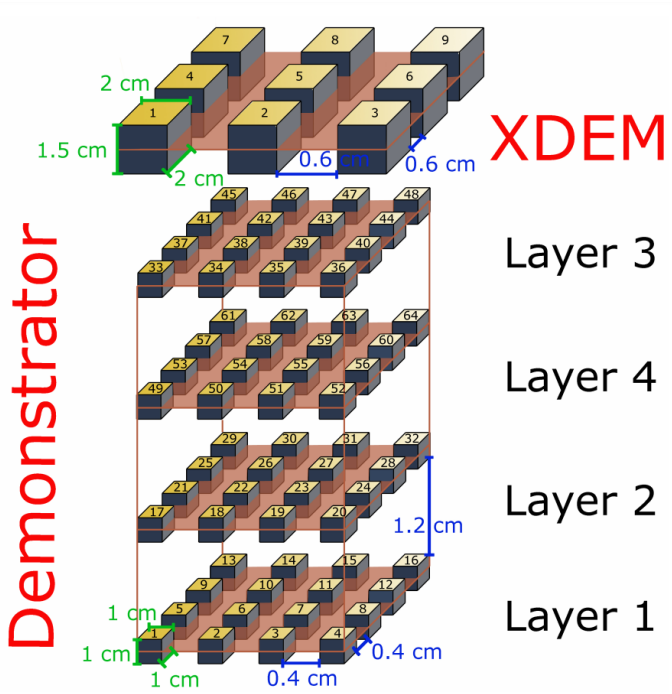


Figure 2.1: Schematic of the COBRA experimental setup. The two phases – COBRA Demonstrator and XDEM – are marked. The geometry of the setup is marked. The individual detectors are labeled, this labelling is used for data analysis. The layers 3 and 4 are swapped, as the 4th layer showed better performance and is therefore placed closed to the middle of the detector. From [56].

## 2.1 COBRA CdZnTe Semiconductor Detector

COBRA profits from the semiconductor detector technology. Semiconductors used as particle detectors have remarkable energy resolution. The principles of detection lie in the properties which define semiconductors, arising from the band theory of solids. Energy states available for electrons within a crystalline lattice of materials form the so-called bands – regions where the possible electron states are so close to each other, they can be considered continuous. The band theory describes the conduction properties of materials and divides them into three distinct categories, based on their conduction properties. These depend on the width of $E_g$ (energy gap) between conduction and valence bands and the number of available/occupied states in each band. Materials can be either conductors, insulators or semiconductors. The group we are interested in are the semiconductors. They are materials with properties "in between" the insulators and the conductors. They have $E_g < 5$ eV , so little energy is required to excite electrons to transition into conduction band. At temperatures $T \to 0$ K they behave as insulators. The valence band is fully occupied, leaving no possible energy states in the conduction band. However, with higher temperatures, it becomes possible that some of the valence electrons gain sufficient energy to breach the energy gap $E_g$ (by thermal excitation). Once the electron in a valence band moves to the conduction band, it leaves behind a vacancy. This vacancy, where an electron should have been, is called a hole. Holes are effectively represented in the theory as if they were positively charged particles. Essentially a missing negatively charged electron in a lattice leaves the surrounding area with

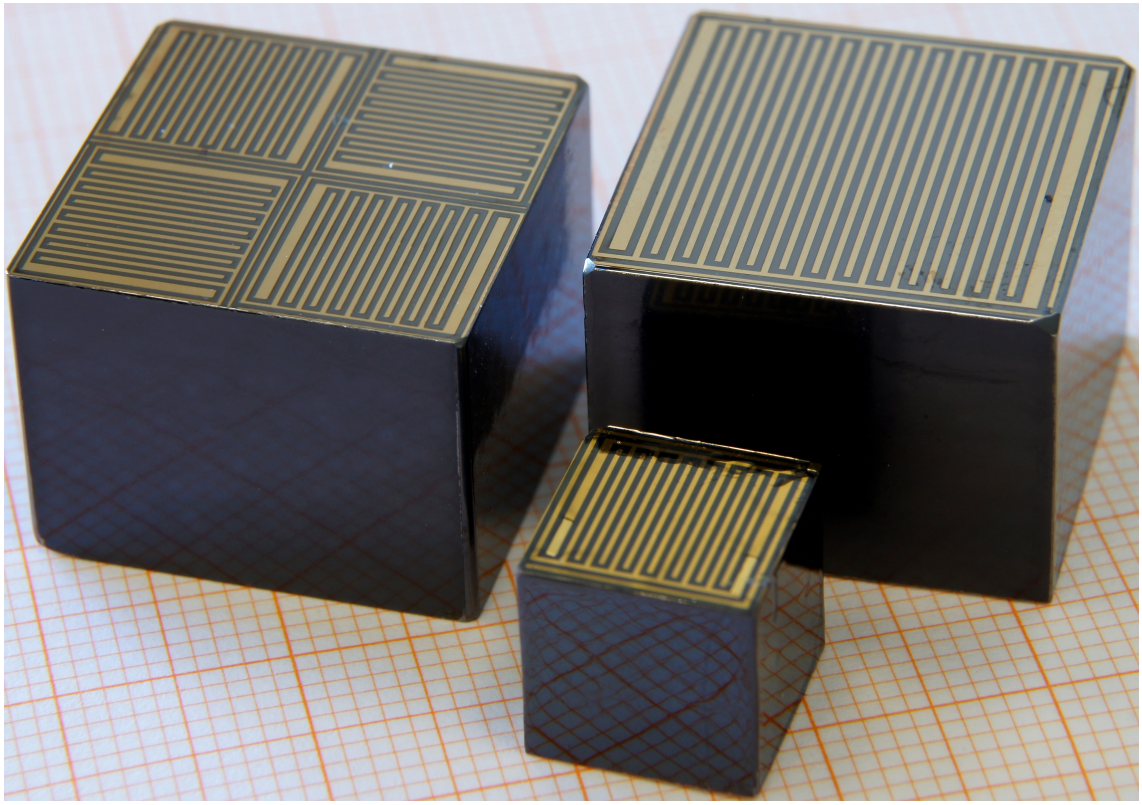

(a)

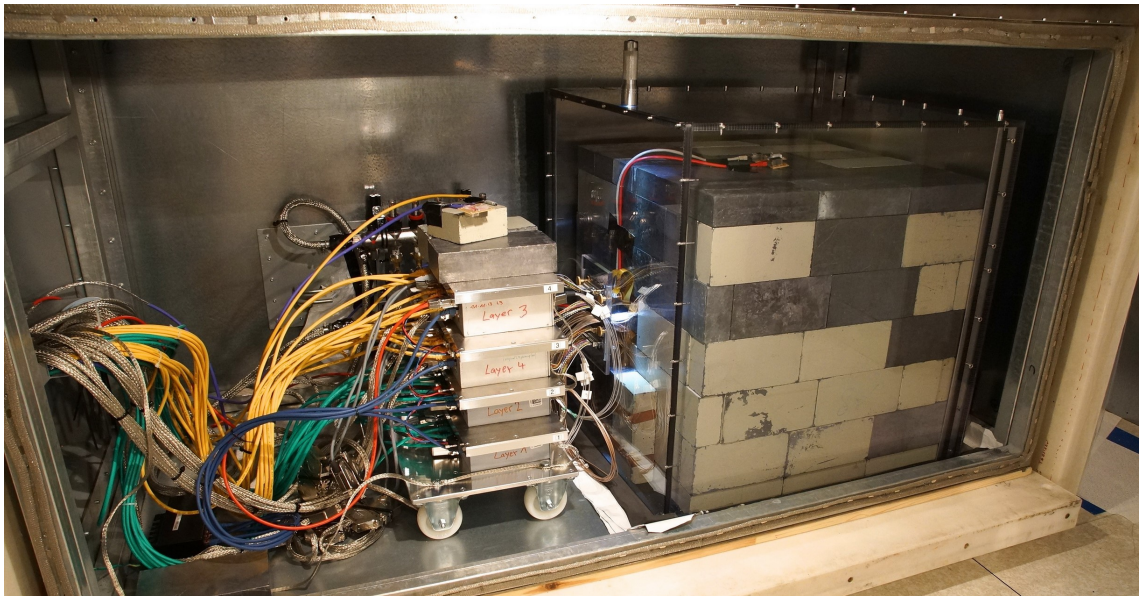


(b)

Figure 2.2: a) Picture of the detector crystals used in COBRA Demonstrator (small cube on the bottom) and COBRA XDEM (bigger cubes). There are two types of the 6 $mm^3$ cubes, only the ones with the quad coplanar grid are used in the final setup. [79] b) Photo of the COBRA detector when one side of the outer shielding was removed. From [80].

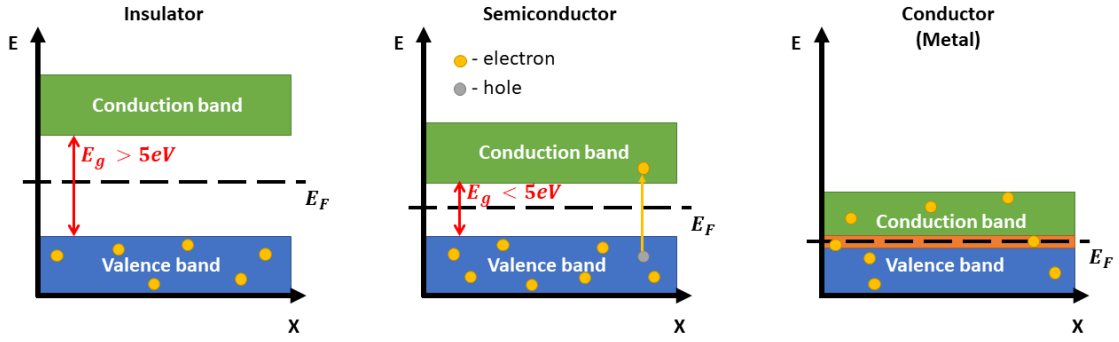


Figure 2.3: Figure depicting the band theory of solids. Inspired by [81, 82]

one extra positive charge, making the hole behave as if it was positively charged. By creating an electron-hole pair, the semiconductor can conduct electric current. Figure 2.3 illustrates the bands for each.

To improve the conduction properties of semiconductors, a process called doping is used. There are two doping variants. Either some atoms with an extra electron in its valence shell are added to the lattice, providing extra weakly bonded electrons. Such addition is called donor doping, which creates an n-type semiconductor. Or, atoms with one less electron in its valence shell are added, creating extra holes. Such dopant is called an acceptor, forming a p-type semiconductor. Most semiconductors used for particle detection are constructed by placing together a p-type semiconductor with an n-type semiconductor forming the so-called p-n junction. When attached to a bias voltage (a fixed DC voltage applied to the semiconductor), a depleted region is formed where the two semiconductors meet. The depleted region is an area where the extra holes and the extra electrons recombine, leaving no free charge carriers available to conduct current. The depleted region is then used as an active detector volume, since there are fewer charge carriers than normally in a semiconductor.

An ionizing particle passing through the depleted region deposits its energy in the detector which creates many electron-hole pairs, subsequently conducting current – movement of charge. The charge carriers, electrons and holes, induce current on the cathode and anode, respectively. The induced charge is then proportional to the deposited energy of the ionizing particle – the so-called ionizing energy. Since one wishes to collect charge only due the passing of an ionizing radiation and not due to random thermal vibration of the lattice (electron-hole pair from thermal excitation), most semiconductor detectors must be cooled down to very low temperatures so that the thermal excitations do not create noise in the measurement [81].

The CdZnTe crystals used for COBRA experiment belong to a special type of semiconductor detectors. The complicated band structure provides for some unique properties of the detector. First, CdZnTe allows for only very few thermal recombinations of electron-hole pairs even at room temperature, making it functional at such temperatures. Some cooling is still advised as it improves the energy resolution and detector performance. Second, the structure of the crystal makes it a viable detector without the need for creating a p-n junction, the whole crystal can be used as an active detector volume. Illustration of this is shown in Figure 2.4.

With respect to the double beta-decay searches, one of the biggest advantages of

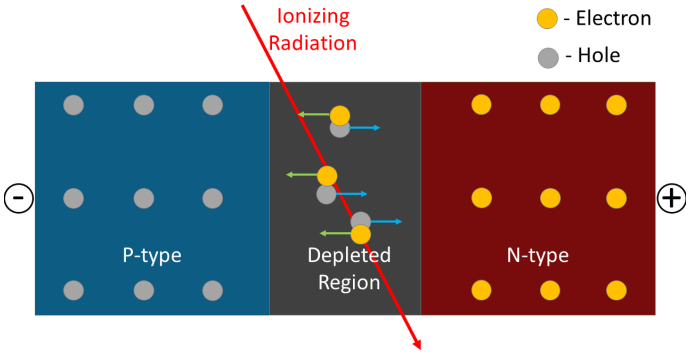


Figure 2.4: Incident radiation passing through depleted region of a p-n junction of a semiconductor detector. Electron-hole pairs created in this process travel through the semiconductor conducting current. Inspired by [83].

CdZnTe crystals is the number of candidate double beta-decay isotopes it contains. All of them, along with their Q-values and natural abundances, are listed in Table 2.1. Especially notable are two isotopes, candidates for $\beta^-\beta^-$-decay, present in the COBRA crystals. $^{116}$Cd has Q-value highest of all isotopes in COBRA – 2813.4 keV, it is larger than the 2615 keV $\gamma$-line of $^{208}$Tl, the topmost contributor to the background from natural decay chains. The second notable candidate isotope is the $^{130}$Te, with Q-value of 2527.5 keV. While, this is not above the $^{208}$Tl background, it lies between its $\gamma$-line and in its Compton edge, making the contamination minimal. It also has a relatively high abundance in the detector. Another advantage of the high Q-values for these two isotopes is that they have greater phase-space factor leading to shorter half-life, as can be seen from equations (1.29) and (1.34).

The manufacturing process of the CdZnTe crystals is such that it is not possible to precisely determine the percentages of each element within the crystal. While 50% of the atoms in the crystal are Tellurium, the other 50% is made up of Cadmium and Zinc collectively. It is not known precisely how much is the Cadmium and how much is the Zinc content, however. Some measurements found that Zinc makes up

| **Isotopes** | **Q-value [keV]** | **Decay Modes** | **Natural Abundance [%]** | **Detector Abundance [%]** |
|---|---|---|---|---|
| $^{108}$Cd | 272.4 [84] | EC/EC | 0.89 | 0.42 |
| $^{114}$Cd | 539.8 [85] | $\beta^-\beta^-$ | 28.73 | 13.42 |
| $^{128}$Te | 865.9 [86] | $\beta^-\beta^-$ | 31.69 | 15.85 |
| $^{70}$Zn | 998.5 [87] | $\beta^-\beta^-$ | 0.61 | 0.02 |
| $^{64}$Zn | 1093.3 [88] | $\beta^+$/EC; EC/EC | 49.17 | 1.60 |
| $^{120}$Te | 1714.8 [86] | $\beta^+$/EC; EC/EC | 0.10 | 0.05 |
| $^{130}$Te | 2527.0 [89] | $\beta^-\beta^-$ | 33.80 | 16.9 |
| $^{106}$Cd | 2775.0 [84] | $\beta^+\beta^+$; $\beta^+$/EC; EC/EC | 1.25 | 0.58 |
| $^{116}$Cd | 2813.5 [89] | $\beta^-\beta^-$ | 7.50 | 3.50 |

Table 2.1: Table presenting the nine isotope candidates for $\beta\beta$-decay and their abundance in the COBRA detector. The values are sorted by their Q-value. The natural abundances of the isotopes are taken from [90].

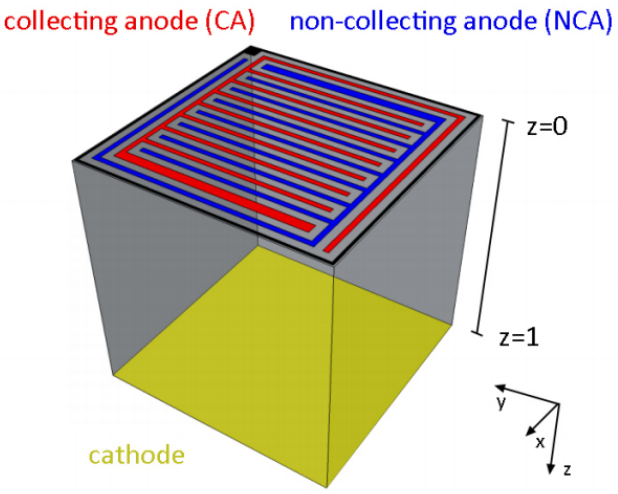


Figure 2.5: Design of the coplanar grid used in COBRA detector. From [56], inspired by [93].

around 3.26% and Cadmium 46.74%. These values are used in the data analysis. The last column of Table 2.1 shows the natural abundances converted to detector abundance according to these percentages [91].

On the other hand, a drawback of using CdZnTe crystals is that it contains impurities in the structure. These impurities can create traps for charge carriers (especially for holes) and stop them within the crystal without contributing to the induced charge. Thus, the ionizing energy converted from the induced charge would be smaller than the deposited energy from the ionizing particle. The trapping of charge carriers leads to dependence of the reconstructed energy (E) on the interaction depth. An undesirable effect. A solution to this is provided by P. Luke in 1994 [92] by proposing the use of the so-called coplanar grid for the electrode structure.

## 2.2 COBRA Coplanar Grid

In order to collect the charge induced by ionizing radiation passing through the detector, a system of one cathode and two anodes is connected to the opposite sides of each detector. This arrangement of electrodes forms the so-called CoPlanar Grid (CPG). Scheme of the design is depicted in Figure 2.5. The side of the detector with a cathode connected to it, collecting holes, is a metallic plate covering the entire surface of that face. The holes are much more prone to being trapped than electrons. This results in an incorrect energy reconstruction. This is a reason why the signal from cathode is ignored. On the opposite side of the detector, there are two types of anodes connected in a special pattern (see Figure 2.5). A charge collecting anode (CA) and a non-collecting anode (NCA). Two different values of bias voltage are applied to the detector. A bias of about 1 kV is between the cathode and CA, noted BV (bias voltage). The second bias, noted as GB (grid bias), is applied between the two anodes. CA is grounded, while NCA is at $-50$ kV. Such an arrangement is crucial in eliminating the inaccuracies of the determination of deposited energy.

An ionizing radiation interacting with the detector creates electron-hole pairs at position $z_0$ ($0 < z < 1$) with charge $q$. Let us take $z_0 = 0.5$ as an example. Under the

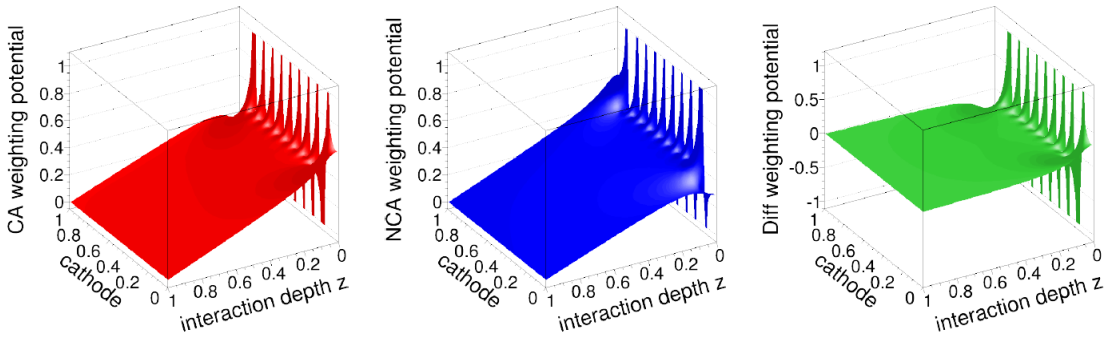


Figure 2.6: Plot of the weighting potentials for CA, NCA and the cathode. From [96].

applied bias, the movement of charges induces a total charge $Q$ at the electrodes. According to the Shockley-Ramo theorem [94, 95], the induced charge $Q$ will be proportional to the charge deposited by the interaction $q$ factored with the so-called weighting potential $\phi_0(z)$:

$$Q = -q\phi_0(z) \tag{2.1}$$

The weighting potential is linear and equal for both anodes, unless the electrons are very close to the anode side – see Figure 2.6. The difference in the weighting potential is due to the different biases applied on the anodes. An electron pulled toward the anode will feel only BV, if it is not in close proximity of the two anodes. The induced charge $Q$ will be the same on both anodes. Once the electron reaches the anode side, it will be pulled to the CA, but not to the NCA. The induced charge $Q$ for CA and NCA will be different. This results in different signal amplitudes ($A$) measured for each anode. Holes on the other hand, will feel only the linear part of the weighting potential (that is, unless created at $z = 0$). The different number of electrons collected at the anodes makes it possible to compensate for the trapped holes (since at creation, number of holes and electrons is the same).

Finally, to extract the signal, only the difference between CA and NCA, due to GB, is accounted for. As holes produce the same signal for both anodes – they only feel the BV – they do not have influence on the difference of the signal due to GB. On the other hand, electrons travelling toward CA and NCA will eventually feel GB resulting in the signal difference. Taking only this difference into account leads to a signal independent of holes (which get trapped much more easily than electrons) and the signal is thus more interaction-depth-independent.

Another feature that needs to be accounted for, is the effect of trapped electrons. This effect is much smaller than that for holes, but is still relevant. For this reason a second weighting factor $\omega$ is introduced, associated with NCA. The reconstructed energy of the interaction is proportional to the difference in the amplitudes of the two anodes.

$$E \propto A_{diff} = A_{CA} - \omega A_{NCA} \tag{2.2}$$

The interaction depth can also be calculated in the CPG, using the ratio of the amplitudes:

$$z = \frac{A_{cathode}}{A_{diff}} = \frac{A_{CA} + A_{NCA}}{A_{CA} - \omega A_{NCA}} \tag{2.3}$$

In processing the recorder pulses, a software called Manticore is used to reconstruct, the interaction depth, signal amplitude, and reconstructed energy of each. These are then saved in the dataset.

The interaction depth is used in the data analysis as one of the filters for choosing the correct data. In general, only events with $0.2 < z < 0.95$ are used. Second filter used in the data analysis is the ratio of signal amplitude to the reconstructed energy, denoted $A/E$. These are discussed further in the data analysis Chapter 4.

CHAPTER 3

# FELDMAN-COUSINS METHOD

Not surprisingly, double beta-decay follows the universal law of radioactive decay. This law states that the number of nuclei within an atom decays exponentially as:

$$N(t) = N_0 e^{-\lambda t}. \tag{3.1}$$

Here, $N(t)$ is the number of nuclei that have not yet decayed, $t$ is the time since we started observing the decay, $N_0$ is the initial number of nuclei capable of decay, and finally $\lambda$ is called a decay constant. The dimension of the decay constant is $s^{-1}$ – it is the rate of decay. Furthermore, one can define the half-life of a decay $T_{1/2}$. The $T_{1/2}$ is defined as the time it takes for half of the initial number of nuclei $N_0$ to decay. It is directly related to the decay constant via well-known relation $T_{1/2} = \ln(2)/\lambda$. The half-life of the double beta process can be obtained experimentally by considering the equation (3.1). However, it is not simple to count the number of nuclei initially present in the observed source and how many of them already decayed. In the following sections, I will describe which observables are accessible from the experiment, how to incorporate them into the equation (3.1) and how to account for the statistical nature of the radioactive decay in the case of rare processes. Based on these considerations, I will, finally, introduce the famous Feldman-Cousins (FC) method and discuss its implementation which I achieved. The derivations in this chapter are based on [97] and [8].

## 3.1 Measurable Parameters of Rare Radioactive Decay

### 3.1.1 Initial Number of Nuclei

In regard to the experimental determination of the initial number of nuclei $N_0$ from equation (3.1), the idea is relatively straightforward. The initial number of observed nuclei of the studied isotope in the source with a total mass $m$ can be calculated with the help of the value of molar mass of the isotope $W$. The molar mass represents the mass contained within one mole of the isotope. Therefore, $N_0$ can be calculated as:

$$N_0 = \frac{mN_A}{W}. \tag{3.2}$$

The Avogadro's constant $N_A$ represents the number of nuclei in one mole. Since $N_A$ is a constant and $W$ is a tabulated value, one only needs to measure the mass $m$ of the isotope contained in the observed radioactive source. The mass $m$ is

actually not measurable directly, but it can be estimated. To obtain the mass of the isotope $m$, one needs to calculate it using an experimentally measurable mass of the detector $m_d$ and multiply it by the isotope abundance within the detector $a$ (a fraction representing what proportion of the full detector mass is composed of the isotope of interest): $m = am_d$. Finally, the initial number of nuclei of the observed isotope in the detector, using only experimentally measurable parameters is given by equation (3.3).

$$N_0 = \frac{N_A a m_d}{W} \tag{3.3}$$

### 3.1.2 Calculation of Half-Life for Rare Events

The standard way of measuring radioactive decay is to collect enough statistics to fit the exponential curve and extract $\lambda$ of the decay. Knowing $N_0$ it is then possible to simply plug into equation (3.1). This is a viable method for any decay, where the $\lambda$ is relatively high (or subsequently $T_{1/2}$ is low). However, as stated already in this thesis, the typical half-life of double beta processes is extremely long. In fact, the shortest cited $T_{1/2}$ (see Table 1.3) is of the order of $\approx 10^{18}$ years. Thus, it is not realistic to collect enough statistics to reliably fit an exponential decay curve to the data. It is vital to introduce a dedicated method to extract the half-life from an experiment observing a rare event. One such method is presented in the lines to follow. Let us define the number of decayed nuclei, $n_D(t)$ as the difference of initial to remaining (undecayed) nuclei:

$$n_D(t) = N_0 - N(t) = N_0 - N_0 e^{-\lambda t} \ . \tag{3.4}$$

Let us consider a half-life of $^{100}$Mo: $T_{1/2} \approx 7.06 \cdot 10^{18}$ yr, the corresponding decay constant can be calculated as:

$$\lambda = \frac{\ln(2)}{T_{1/2}} = \frac{6.9 \cdot 10^{-1}}{7.1 \cdot 10^{18}\text{yr}} \approx 10^{-20}\text{yr}^{-1}. \tag{3.5}$$

The decay constant is very small. Even if the measurement duration was to take a decade (e.g. t = 10 yr), the exponent $\lambda t$ in (3.4) will still be extremely small. Subsequently, all further powers of $\lambda t$ will be ever smaller.

$$1 \gg (\lambda t) \gg (\lambda t)^2 \gg ... \gg (\lambda t)^n \tag{3.6}$$

Let us consider the equation (3.4) and apply Taylor expansion of the exponential $e^x$ around zero ($e^x = 1 + x + \frac{x^2}{2!} + ... + \frac{x^n}{n!}$). Since the duration of the measurement $t$ is very low compared to $T_{1/2}$, we can consider the measurement duration to be effectively close to zero. Finally, the Taylor expansion:

$$\begin{aligned} n_D &= N_0 - N_0 e^{-\lambda t} \\ &= N_0 - N_0 \left(1 - \lambda t + \frac{(\lambda t)^2}{2!} - \frac{(\lambda t)^3}{3!} \pm ... \pm \frac{(\lambda t)^n}{n!}\right) \\ &= N_0 \left(1 - 1 + \lambda t - \frac{(\lambda t)^2}{2!} + \frac{(\lambda t)^3}{3!} \mp ... \mp \frac{(\lambda t)^n}{n!}\right) \approx N_0 \lambda t. \end{aligned} \tag{3.7}$$

Here, we used relation (3.6) to cut off the terms higher than linear. This can be justified, since the additional terms add very little to the final result (consider adding each subsequent term after $\lambda t$). If $\lambda t$ is in the order of $10^{-20}$, then $(\lambda t)^2$ will be in order of $10^{-40}$, $(\lambda t)^3$ in order of $10^{-60}$ and so on. The additional terms play negligible role. Thus, by plugging the result of equation (3.3) into equation (3.7) we obtain:

$$n_D = N_0 \lambda t = \ln(2) \frac{N_A}{W} \frac{a m_d t}{T_{1/2}}. \tag{3.8}$$

The equation (3.8) states that the number of decayed nuclei of a given isotope depends proportionally on the quantity of the isotope we are observing and the duration of the measurement, while it is inversely proportional to the isotope's double beta-decay half life. In a realistic experiment, one must take into account the detector's efficiency, $\mathcal{E}$. No detector can be 100% perfectly efficient. Thus, we need to define an experimental parameter $n_{OS}$ – the number of observed decays. $n_{OS}$ is given by $n_{OS} = \mathcal{E} n_D$. The number of observed decays is given by the product of the detector efficiency and the decayed number of nuclei. Since, $\mathcal{E} \in (0, 1)$ it follows that $n_{OS} < n_D$. If we now substitute this relation in the equation (3.8) and express the half-life we obtain:

$$T_{1/2} = \ln(2) \frac{N_A}{W} \mathcal{E} \frac{a m_d t}{n_{OS}}. \tag{3.9}$$

While it might seem that this is the final form of the equation, the reality is yet more complex. Starting from the *"simple"* law of radioactivity (equation (3.1)) and arriving at the equation for double beta-decay half-life (equation (3.9)), one might think this is all that needs to be said and the experiment can begin. There are, however, more obstacles to be addressed. The statistical nature of radioactive decays along with the low number of signal events and the question of discrimination of signal from the background complicate the situation. These issues and the proposed solutions are addressed in the following section. The section describes the FC statistical method, that provides a tool for dealing with rare processes such as double beta-decay. Based on [8] and [97]. The challenges of implementing the method within a dedicated C++ class, created for the purposes of this thesis are described afterwards.

## 3.2 Feldman and Cousins Approach to Sensitivity

Determining the number of signal events measured in a double beta-decay experiment is one of the key elements of the equation (3.9). This is, in fact, a very complicated task. One must consider two inseparable aspects of $n_{OS}$ in a real experiment. One: the presence of non-zero background in an experiment; two: each radioactive decay (background processes included) is a statistical process. These two aspects have some very crucial consequences on the actual value used in place of $n_{OS}$. Since there is always some background present, one must find a way to decide how many excess detected signals over expected background would be significant in order to consider the claim of discovery. Secondly, since both background and signal are statistical processes, one needs to work within the theory of probability. In other

words, we can introduce a variable $\mu_s$, which replaces $n_{OS}$ in equation (3.9). This value will represent the expected number of signal events, rather than observed. This formally transforms the equation into:

$$T_{1/2} = \ln(2)\frac{N_A}{W}\mathcal{E}\frac{am_d t}{\mu_s}. \tag{3.10}$$

Even though this exchange might look like a formality, in fact, we replaced a variable $n_{OS}$ whose value depends on several unpredictable factors (such as coincidence) by a mean expected value of that variable. The question now is, how does one determine the value $\mu_s$? Naively, one could expect that having a precise background model, it would be enough to predict the expected number of background events $\bar{b}$. One could expect to simply subtract $\bar{b}$ from the observed number of counts $n$:

$$\mu_s = n - \bar{b}. \tag{3.11}$$

Nevertheless, it is not so simple. Decay process is a poissonian process. Let us, for example, assume an experiment which expects 3 background counts. Given the fact that we ignore possibility of signal contribution for the moment, the probability to observe three counts is the highest, but it is not 100%. There is non-negligible chance that the experiment would observe less or more counts. The probability to observe $n$ counts when $\bar{b}$ are expected is given by Poisson distribution:

$$P(n, \bar{b}) = \frac{e^{-\bar{b}}}{n!}\bar{b}^n. \tag{3.12}$$

In the case of 3 expected background counts, it is possible to calculate that there is approximately 10.08 % chance to observe n=5 counts. In other words, there is a 10.08 % chance that there were no signal events, however, the naive approach, based on the equation (3.11), would conclude that there were 2 signal events. On the other hand, the opposite situation may also occur. What if none of the observed counts had an origin in the background? If one plugs n=0 into the equation (3.12), one can show that there is approximately 4.98 % chance of that happening. The experiment truly measured 5 signal counts, however, the naive approach would report only 2. This is a very undesirable result. Of course, any other scenario might occur as well, there is always a non-zero probability of n being essentially any number. It is evident that the statistical nature of these processes complicates the situation.

### 3.2.1 Confidence belts – The Classic Approach

Rather than reporting a single value of the expected number of signals, the way to resolve the previously sketched problem, is to report a range of values. This interval is the so-called confidence interval (or Neyman confidence interval [98]). One can construct an interval of values, ranging from some value $\mu_L$ (the so-called lower limit) to value $\mu_U$ (the so-called upper limit) and claim that the true value of $\mu_s$ lies within this interval with some given probability. This probability is called the confidence level (CL). CL is a number representing the level of trust we have that the $\mu_s$ lies within $(\mu_L, \mu_U)$ interval, where $CL \in \langle 0, 1\rangle$. Let us consider an experiment searching for a rare event. The experiment measures $n_0$ counts. Next, consider a series of perfectly identical experiments, each observing $n_i$ decays ($n_i$ may be the same as $n_0$ but it may also be different). The probability that i-th experiment

would observe $n_i$ decays is given by Poisson distribution $P(n_i, \mu_s)$. Let us define $\alpha$ to be a number representing a probability that randomly chosen repeated identical experiment would observe less than or equal number of counts as the original $n_0$ experiment ($n_i \leq n_0$). We define $\beta$ as a probability that randomly chosen repeated identical experiment would observe greater than or equal the number of counts as the original $n_0$ experiment ($n_i \geq n_0$). The numbers $\alpha$ and $\beta$ can be, therefore, expressed in the form of equations as:

$$\alpha = \sum_{n_i=0}^{n_0} P(n_i, \mu_U), \tag{3.13}$$

$$\beta = \sum_{n_i=n_0}^{\infty} P(n_i, \mu_L). \tag{3.14}$$

These two equations give us the recipe for finding the lower and upper limits of the interval. The lower limit $\mu_L$ is defined as value when the cumulative sum of probabilities from $n_0$ to $n = \infty$ equals $\beta$. The upper limit $\mu_U$ is found when the cumulative sum of probabilities from $n = 0$ to $n_0$ equals $\alpha$. In other words, we are looking for an answer to the question: "Given $n_0$, what is the respective $\mu_U$ so that $\alpha$ fraction of repeated experiments report $n_i \leq n_0$ and what is the respective $\mu_L$ so that $\beta$ fraction of experiments report $n_i \geq n_0$?".

Figure 3.1 depicts the two Poisson distributions with $\mu_L$ and $\mu_U$ calculated for $n_0 = 5$. Based on $\mu_L$ and $\mu_U$ we define a confidence level that real number of the signal counts lies in the interval ($\mu_L$, $\mu_U$) as $CL = 1 - \alpha - \beta$. Using this recipe, the confidence intervals can be built for any given CL and $n_0$. Combining a set of intervals with constant CL, but varying $n$ creates the so-called confidence belt. The confidence belt can be understood as a set of confidence intervals as a function of the number of observed counts by a given experiment. These confidence belts are usually calculated before the experiment is operational, as it provides an insight into what the limits would be for any possible n.

Let us now show an example of construction of the belt. First of all, it is necessary to choose $\alpha$ and $\beta$. This choice determines the CL in return[1]. Next step is to construct a confidence interval for $n_0 = 0$. Subsequently, one needs to increment $n_0$ and construct the respective confidence intervals for each value. The process is repeated until satisfactory number of confidence intervals have been generated. Figure 3.2 depicts a result of calculation of a central confidence belt for $\alpha = 0.05$, $\beta$=0.05. Let us point out a problem. For $n = 0$, the confidence interval is empty. This is given by the fact that $\sum_{n_i=0}^{0} P(n_i, \mu_U) = 0$. It is an undesired result. This is the first drawback of the classical approach of constructing the Neyman confidence belt. Let us investigate the method little further.

So far, we considered only a background-less experiment. If we now consider an experiment with non-zero expected mean background rate $\bar{b} \neq 0$, we need to rewrite equations (3.13) and (3.14) into following form:

[1]Choosing $\alpha \neq 0$ and $\beta \neq 0$ creates the so-called central confidence belt. Choosing $\alpha = 0$ or $\beta = 0$ creates the so-called one-sided confidence belt.

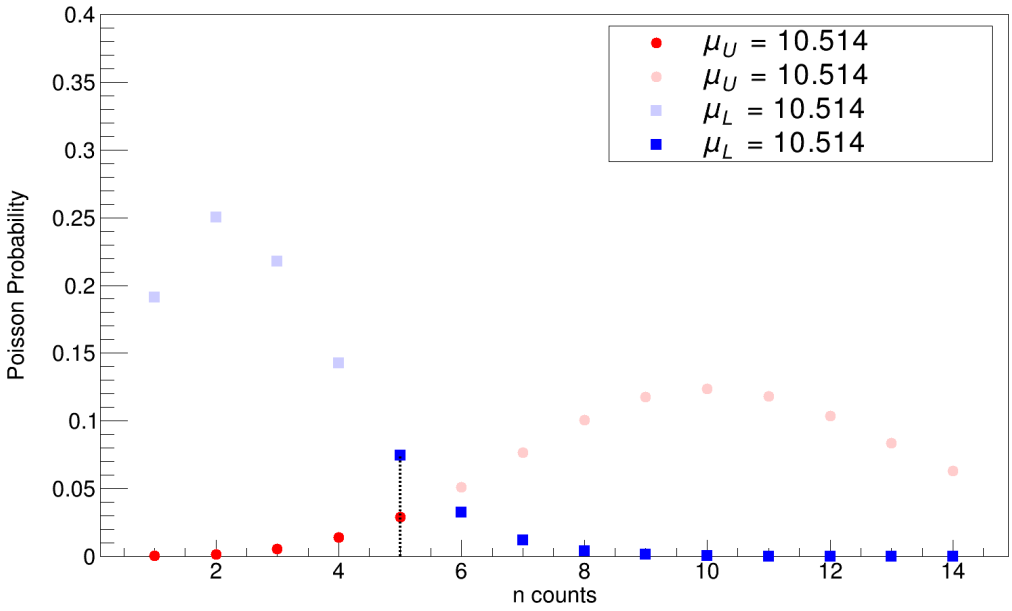


Figure 3.1: Depiction of confidence interval constructed for $\alpha = \beta = 0.05$, around measured $n_0 = 5$. The circles mark the poisson for $\mu_U$, while the squares mark the Poisson distribution for $\mu_L$. The dark red and dark blue colors indicate the experimental outcomes whose sum equals exactly $\alpha$ or $\beta$, respectively. The $n_0$ is marked by the black dotted line.

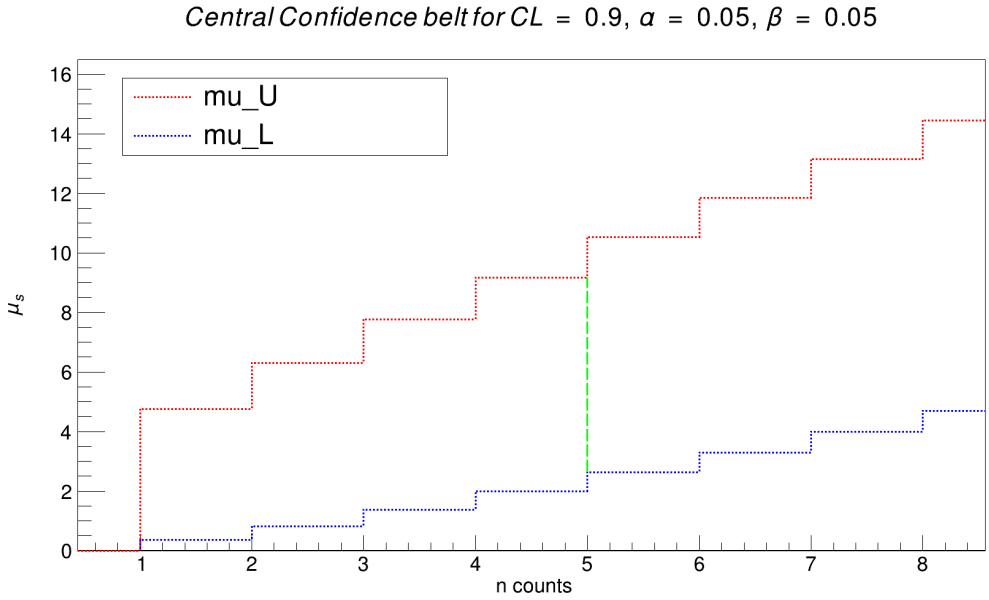


Figure 3.2: Depiction of a central confidence belt constructed for $\alpha = 0.1$, $CL = 0.9$. Using the Neyman confidence belt construction. The green line represents the interval $(\mu_L, \mu_U)$ an experiment with $n_0 = 5$ would choose.

$$\alpha = \sum_{n_i=0}^{n_0} P(n_i, \mu_U + \bar{b}), \tag{3.15}$$

$$\beta = \sum_{n_i=n_0}^{\infty} P(n_i, \mu_L + \bar{b}). \tag{3.16}$$

The mean expected value of total counts in the Poisson distribution has to account for the presence of background as seen in equations (3.15) and (3.16). Consider a series of identical experiments with three expected mean background counts $\bar{b} = 3$. We will construct a one-sided confidence belt with $CL = 0.9$, $\alpha = 0.1$ and $\beta = 0$. Figure 3.3 depicts such one-sided confidence belt.

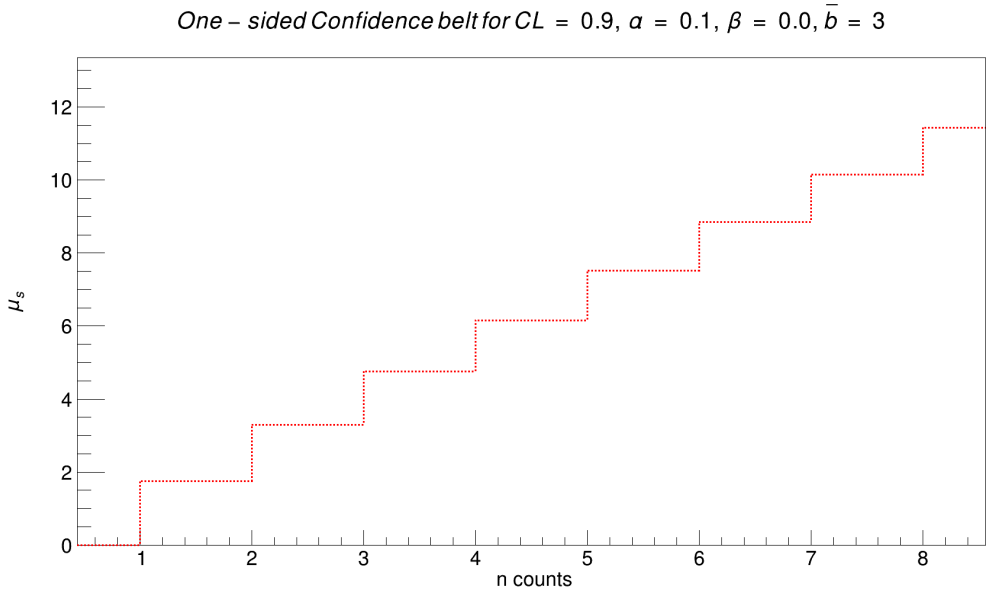


Figure 3.3: Depiction of a one-sided $\mu_U$ confidence belt constructed for $\alpha = 0.1$, $CL = 0.9$, $\bar{b} = 3$.

Notice a very important feature in Figure 3.3. For $n = 0$ the respective upper limit $\mu_U = -0.697$ . This is a non-physical result. The upper limit on the expected number of signal events cannot be a negative number, such a result is impossible to interpret, and it is only an artefact of the calculation. This is another important problem of the classical construction of the confidence belts. Finally, the third drawback of this method is the fact that this method relies on the subjective choice of $\alpha$ and $\beta$ made by the scientist. In the case of small number of observed counts $n$ below $\bar{b}$ one would conservatively expect to report no signal, nevertheless, the method gives a choice to report a central interval which would allow to claim a discovery ($\mu_L > 0$) and this is highly unlikely in such case. The subjectivity in the choice of $\alpha$ and $\beta$ weakens the objectivity of the method. More objective treatment is necessary. Hence, the FC approach.

### 3.2.2 Confidence Belts – *The Feldman Cousins Approach*

An elegant solution to the drawbacks of the classical way of building confidence intervals (subsequently confidence belts) has been provided by Feldman and Cousins in [8]. To understand how the FC method is different from the classical approach, let us look at two features of the classical way of constructing confidence intervals. First, it is inevitable to provide $n_0$, $\alpha$ and $\beta$. Second, the belts are constructed for a given n by the calculation of $\mu_L$ and $\mu_U$. $\mu_L$ is found by summing probabilities from $n_0$ to $\infty$. $\mu_U$ is found by summing probabilities from 0 to $n_0$. Such an approach has disadvantages, which were described before. The FC approach uses a reversed methodology for finding the confidence interval. FC belts are constructed horizontally, i.e. for given value of $\mu_j$ one looks for $n_{min,j}$ and $n_{max,j}$ so that the following condition holds:

$$CL = 1 - \alpha - \beta \leq \sum_{n_i=n_{min,j}}^{n_i=n_{max,j}} P(n_i, \mu_j + \bar{b}) \ . \tag{3.17}$$

In other words, the task is to find the smallest $n_i$ ($n_{min,j}$) and the largest $n_i$ ($n_{max,j}$) given $\mu_j$ so that the cumulative sum is still smaller than or equal to $1-\alpha-\beta$. The use of inequality sign is necessary because now the sum is growing in steps by the addition of terms, as a function of the discrete variable $n$. In the classical method, explained previously, the sum was composed of a stable number of terms and only their values were changing as a function of a continuous variable $\mu_L$ or $\mu_U$ (equations (3.15) and (3.16)). It is unlikely in the FC method that for a chosen $\mu_j$, the cumulative probability would be equal exactly to $CL$. It is always a bit more, which introduces inseparable conservatism in the method. The condition for finding $n_{min,j}$ and $n_{max,j}$ is given by a sum, and the order in which one sums the individual components does not matter. Summation is commutative. The FC method alternates this approach. The underlying principle of the FC method is the choice of the order in which the individual components of the cumulative sum are added. The so-called likelihood ordering ratio factor $R$ dictates which $n_i$ is added to the cumulative sum first, second, third, etc. Until the condition is fulfilled. This leads to an effect which can be considered as one of the triumphs of the FC method. By a unique choice of the order of the terms in the sum the confidence belts are capable to switch between one-sided upper interval to a central interval without the subjective input of the user. Instead of using two variables representing the confidence level ($\alpha$ and $\beta$), only one argument is given – $CL$. This means, that while the total fraction of data rejected by the confidence interval stays the same – for example, if $\alpha = 0.05$ and $\beta = 0.05$, 10% of data is rejected – it is no longer required that a certain amount is rejected from the left and a certain amount from the right. Only the overall proportion is required.

The advantage of the likelihood ordering principle is that, rather than constructing the confidence interval from left to right – as was done in the classical approach – the summation is performed from the "middle" and expands to the sides by adding components either to the right or to the left. This approach automatically decides the best $\alpha$ and $\beta$ based on when the condition for cumulative sum is satisfied. Figure 3.4 shows an interval constructed using the FC approach for $\mu_j = 0.5$, $\bar{b} = 3$, $CL = 0.9$. $n_{min,j} = 0$ and $n_{max,j} = 6$ are marked. The green dots represent the

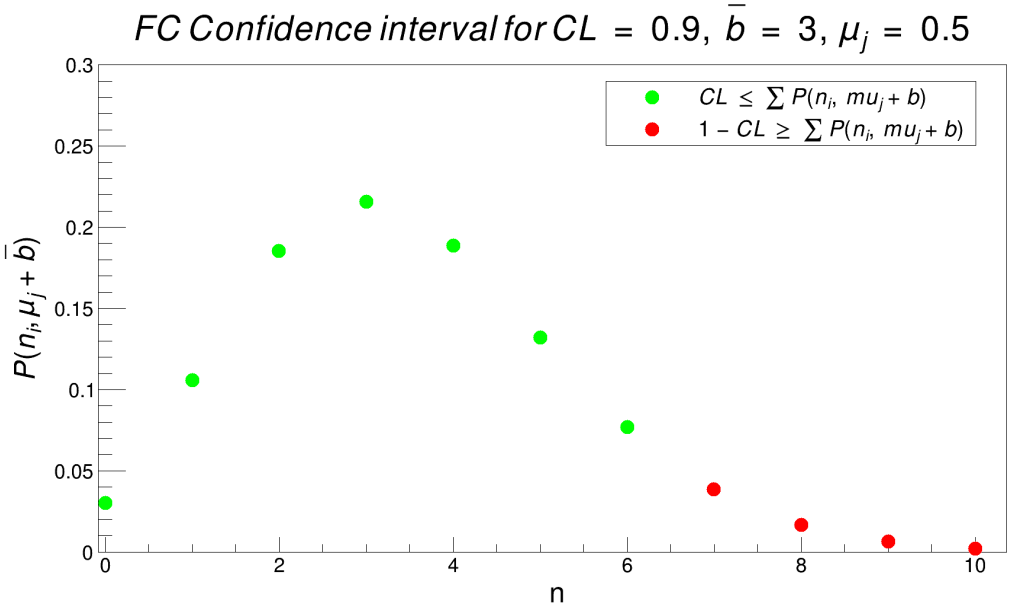


Figure 3.4: An example of the FC Confidence Interval. The interval was generated for $\mu_j = 0.5$, $\bar{b} = 3$, $CL = 0.9$. $n_{min,j}$ and $n_{max,j}$ are marked.

probabilities $P(n_i, \mu_j + \bar{b})$ that fulfill the condition in equation (3.17). Whereas, the red dots represent the rejected $n_i$. The cumulative probability of the marked confidence interval is $\sum_{n_i=0}^{6} P(n_i, 3.5) = 0.93 \geq CL$. It is not exactly equal to $CL$, this is due to the discreteness of $n$. Notice, if we choose $n_{max,j} = 5$, we would obtain $\sum_{n_i=0}^{5} P(n_i, 3.5) \approx 0.86 \leq CL$ – the condition is not yet fulfilled. On the other hand, if we expanded the interval further, for example $n_{max,j} = 7$ we would obtain: $\sum_{n_i=0}^{7} P(n_i, 3.5) \approx 0.97 \geq CL$ – the condition is fulfilled, but we have unnecessarily added an extra data point to the sum. This would create excessive conservatism. We could also choose an interval with $n_{min,j} = 0$ and $n_{max,j} = 6$ – for which we would obtain $\sum_{n_i=1}^{6} P(n_i, 3.5) \approx 0.90 \geq CL$. This may seem as the best option, however, it would give an empty interval for $n = 0$.

It is not evident how to choose the proper interval $\langle n_{min,j}, n_{max,j} \rangle$ objectively. This is solved by the FC ordering principle. However, before showing how to build such a confidence interval, several variables need to be defined:

- $\boldsymbol{\mu_{best} \equiv max(0, n - \bar{b})}$ : $\mu_{best}$ represents the mean expected count that maximizes the Poisson probability. See Figure 3.5.

- $\boldsymbol{R \equiv \frac{P(n,\mu+\bar{b})}{P(n,\mu_{best}+\bar{b})}}$ : $R$ represents the variable which determines the ordering of the components to input into the cumulative probability sum, equations (3.15) and (3.16). The first $n_i = n_0$ to to be added is the one with highest $R_i$, the second $n_i = n_1$ is the one where $R_i$ is the second greatest and so on. Until the condition for the cumulative sum is satisfied. Furthermore, since $\mu_{best}$ is the maximized probability, $P(n, \mu_{best} + \bar{b})$ will always be greater than or equal $P(n, \mu + \bar{b})$, hence $R \in (0, 1]$.

- $\boldsymbol{n_{top} \equiv \lceil \mu + \bar{b} \rceil}$ : $n_{top}$ represents the number of counts where the algorithm begins. At this value, (or at least close to it) we expect to find the highest $R_i$. In case, multiple $R_i$'s are the same value and are the greatest in the array, $n_{top}$ dictates which to take first.

- $\boldsymbol{n_{min}}$ : $n_{min}$ represents the smallest $n_i$, which was added to the cumulative sum of probabilities. The $n_{min}$ is determined when the condition for the cumulative sum is satisfied.

- $\boldsymbol{n_{max}}$ : $n_{max}$ represents the greatest $n_i$, which was added to the cumulative sum of probabilities. The $n_{max}$ is determined when the condition for the cumulative sum is satisfied.

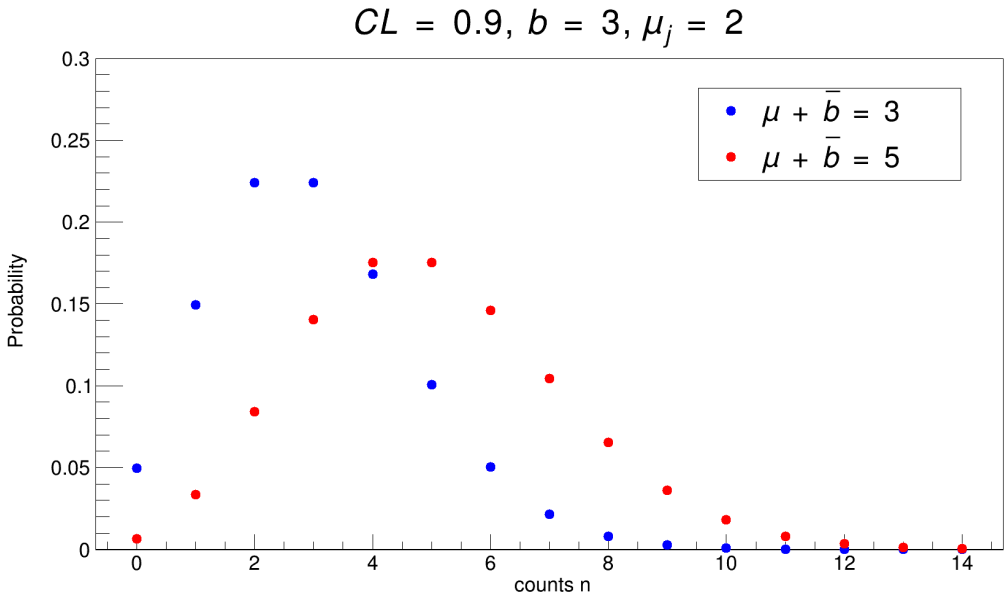


Figure 3.5: Comparison of $P(n, \mu_{best} + \bar{b})$ and $P(n, \mu + \bar{b})$ distributions for $\bar{b} = 2, CL = 0.9, \mu_j = 2$. The $\mu_{best}$ was calculated for $n_i = 0$. Notice that at $n = 0$, the probability given by the $\mu_{best} + \bar{b}$ is the greater one. This is the maximization effect.

To create a confidence belt, multiple confidence intervals must be calculated. To do this, we must choose a range of values ($\mu_j$) for which we want to create the confidence belt. Notice that $\mu_j$ is a continuous variable. Because of this, it is necessary to divide the range into discrete steps if we want to calculate the intervals using a computer algorithm. Thus, depending on how big the steps are, the precision of the computation will be affected. Having defined the necessary variables, we can now describe the algorithm according to which the confidence belts are constructed:

1. Choose some initial $\mu_j$
2. Determine $n_{top}$, $\mu_{best}$ and initialize a variable representing cumulative sum to zero
3. Around $n_{top}$ calculate a set of $R_i$'s
4. Determine highest $R_i$ from the set and add the corresponding $P(n_i, \mu_j)$ to the cumulative sum
5. Recreate the set of $R_i$'s without the value that has been used in step 4.
6. Repeat steps 3. - 4. until cumulative sum reaches or exceeds the desired CL

7. Store the values $n_{min,j}$ and $n_{max,j}$ as the minimum and maximum $n_i$'s present in the cumulative sum for each $\mu_j$

8. Increment $\mu_j$ by chosen step $\Delta\mu$ and repeat steps 2. - 6.

9. Once the desired amount of $\mu_j$'s is reached, stop the algorithm

Table 3.1 demonstrates the individual steps needed to create Figure 3.4. Each row represents $n_i$ counts. The rows are filled out according to the rules laid out in the procedure for FC approach to confidence belts. Except, of course, only one $\mu_j$ has been picked. The table is generated for 11 rows. Second column represents the Poisson probability with given $\mu_j$, $\bar{b}$ and $n_i$. For example in the first row this would be:

$$P(n_i, \mu_j + \bar{b}) = P(0, 3.5) = \frac{e^{-3.5}}{0!} 3.5^0 = 0.030 \ . \tag{3.18}$$

| $\boldsymbol{\mu_j = 0.5, \bar{b} = 3}$ | | | | | |
|---|---|---|---|---|---|
| **n** | $\boldsymbol{P(n_i, \mu_j + \bar{b})}$ | $\boldsymbol{\mu_{best,j}}$ | $\boldsymbol{P(n_i, \mu_{best,j} + \bar{b})}$ | **R** | **Order** |
| 0 | 0.030 | 0 | 0.050 | 0.607 | 6 |
| 1 | 0.106 | 0 | 0.149 | 0.708 | 5 |
| 2 | 0.185 | 0 | 0.224 | 0.826 | 3 |
| 3 | 0.216 | 0 | 0.224 | 0.963 | 2 |
| 4 | 0.189 | 1 | 0.195 | 0.966 | 1 |
| 5 | 0.132 | 2 | 0.175 | 0.753 | 4 |
| 6 | 0.077 | 3 | 0.161 | 0.480 | 7 |
| 7 | 0.039 | 4 | 0.149 | 0.259 | |
| 8 | 0.017 | 5 | 0.140 | 0.121 | |
| 9 | 0.007 | 6 | 0.132 | 0.050 | |
| 10 | 0.002 | 7 | 0.125 | 0.018 | |

Table 3.1: A table presenting the values calculated according to the described procedure for building the FC confidence interval. The table was generated for $\mu = 0.5, \bar{b} = 3, CL = 0.9$. From [97].

The third column represents the variable we defined as $\mu_{best,j}$. For $n_i = 0$ this would be:

$$\mu_{best,j} = max(0, n_i - \bar{b}) = max(0, -3) = 0. \tag{3.19}$$

Notice, that $\mu_{best}$ will be always zero for $n_i < \bar{b}$. In the fourth column, the probability assuming ideal $\mu$ ($\mu_{best,j}$) is calculated for given $n_i$ and $\bar{b}$. In case of $n_i = 0$ it equals:

$$P(n_i, \mu_{best,j} + \bar{b}) = P(0, 3) = \frac{e^{-3}}{0!} 3^0 = 0.050 \ . \tag{3.20}$$

Second to last, $R_i$ is calculated in each row. For $n_i = 0$:

$$R = \frac{P(n_i, \mu_{best,j} + \bar{b})}{P(n_i, \mu_j + \bar{b})} = \frac{0.050}{0.03} = 0.607 \ . \tag{3.21}$$

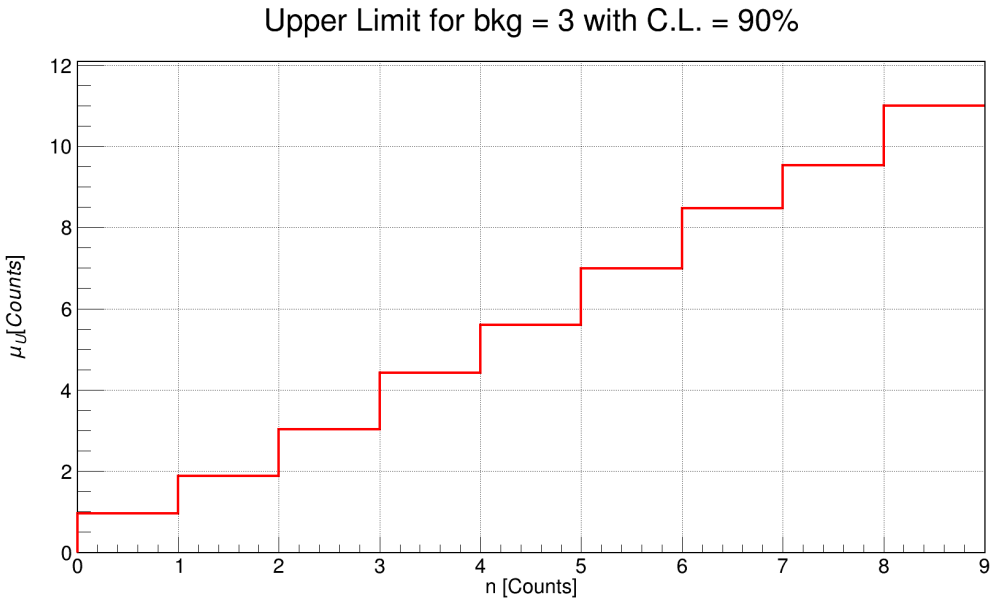


Figure 3.6: Depiction of a confidence belt using the FC approach. The figure was generated with $\Delta\mu_j = 0.01$, $CL = 0.9$ and $\bar{b} = 3$ using my own program. $\mu_L$ was calculated, but not included in the plot.

If one repeats this process for each row, the table can be filled out. Once that is done, the lines of the table are ordered in the direction of the descending R value. It can be seen that this happens at $n_i = 4$. This row also represents the $n_{top}$ ($\lceil 0.5 + 3 \rceil = 4$). That is where (or at least around where) we would expect the highest ratio to lie. The cumulative sum is then filled out according to the ordering principle as:

$$CL \leq P(4, 3.5) + P(3, 3.5) + P(2, 3.5) + P(5, 3.5) + ... + P(6, 3.5) = 0.935. \quad (3.22)$$

The cumulative sum exceeds the wanted $CL = 0.9$ after one adds the term for $n_i = 6$. This was the highest $n_i$ added to the sum and it, therefore, becomes $n_{max,j} = 6$. Similarly, the lowest $n_i$ added to the sum was $n_i = 0$, therefore, $n_{min,j} = 0$. We have produced a single set $(\mu_j, n_{min,j}, n_{max,j}) = (0.5, 0, 6)$. This set we store and repeat the process for another value of $\mu_j$. Once one follows the entire procedure for sufficient number of values $\mu_j$, it is possible to visualize the desired FC confidence belt.

In order to demonstrate, how this approach solves the previously mentioned drawbacks of the classical method a sample confidence belt based on the FC algorithm is presented in Figure 3.6. The figure was produced by using a C++ class written in the scope of this thesis. The belt in the figure is generated for $CL = 0.9$, $\bar{b} = 3$. Note that, the $\mu_U > 0$ for $n = 0$ and the confidence interval is not empty anymore. This occurs thanks to the ordering rules of the FC method. There is a fundamentally minimal value of CL for which the algorithm always produces non-empty confidence interval for $n = 0$. The discussion of how to choose CL so that it is always high enough to guarantee this effect is presented in Section 3.2.5. Another advantage of the algorithm is that there is no need to choose $\alpha$ or $\beta$, only the CL.

At the beginning of the section, it was noted that the goal of this approach is to

figure out what number to input into equation (3.10). Rather than a single number obtained by an experiment, $n_{OS}$, it is desirable to use some number taking into account the presence of background and the probabilistic nature of the measurement. This number would represent the detector's sensitivity toward the neutrinoless double beta-decay given the detector parameters (duration of measurement, detector composition, exposure, etc.). Since the number should represent the detector's sensitivity, it should be independent of the actual number of observed events. It should be dependent only on background level and the desired confidence level. However, when constructing the FC confidence belts, one can notice that $n$ is still necessary to choose the confidence interval out of the confidence belt. The method at this stage, still kept the third drawback of the classical method – from two experiments observing the same $n_0 < \bar{b}$, the one with higher background would report a lower $\mu_U$ which means a better $T_{1/2}$ limit. In order to solve this, one can define a variable $\mathcal{S}(\bar{b})$, which represents an average number which ensemble of infinite number of identical experiments would report as a minimal detectable signal if the experiment expects $\bar{b}$ background counts. This "sensitivity" value is given with some degree of certainty expressed by value $CL$. In fact, this will allow us to provide a limit even if no events are measured. The sensitivity is given as weighted sum of all the upper limits $\mu_U$ for experiment expecting $\bar{b}$ background counts and observing $n_i$ total counts. This upper limit evaluated for given CL, we denote $U(n_i, \bar{b})$. The weight is given by the probability that such experiment would measure $n_i$ total counts, while expecting $\bar{b}$ background counts:

$$\mathcal{S}(\bar{b}) = \sum_{n_i=0}^{\infty} P(n_i, \bar{b}) U(n_i, \bar{b}). \tag{3.23}$$

Summation over the entire range provides a single number $\mathcal{S}(\bar{b})$ dependent only on background and CL, and representing the sensitivity of the detector toward observation of any rare event. Using this approach ensures that experiments with lower background but same observed $n_i$ would report a better $T_{1/2}$ limit. Finally, the sensitivity of the detector to $T_{1/2}$ is given by:

$$T_{1/2} \geq \ln(2) \frac{N_A}{W} \mathcal{E} \frac{a m_d t}{\mathcal{S}(\bar{b})}. \tag{3.24}$$

### 3.2.3 Implementing the Feldman Cousins Approach

Within the scope of this thesis, I have created a program which implements the FC methodology described above. The following lines introduce the program, briefly, describe the verification process of my implementation of the FC approach, and finally provide a more in-depth analysis of the consequences of using the FC method for obtaining the detector sensitivity.

The program package I named MPFC. In the following text, whenever MPFC is mentioned, it represents the output of my implementation of the algorithm. Otherwise, if the abbreviation FC is used, it refers to the original FC method as described in [8]. The program is created so that it is simple to use. To obtain detector sensitivity, only two inputs are required: the average expected background counts $\bar{b}$ and the confidence level $CL$. MPFC has been reliably tested only up to $\bar{b} = 450$. However, a solution for calculating sensitivities for higher $\bar{b}$ is implemented and the

| $CL = 0.9; N = 400$ | | |
|---|---|---|
| **FC - MPFC** | $N_i$ | $(N_i/N) * 100\%$ |
| 0.00 | 171 | 42.75 |
| -0.01 | 208 | 52.00 |
| +0.01 | 19 | 4.75 |
| +0.02 | 0 | 0 |
| -0.02 | 2 | 0.5 |

Table 3.2: Comparison of the generated $\mu_U$ for original FC and generated from MPFC program. The first column represents how much of a difference there is between MPFC and values cited in [8]. Negative values mean that my program overestimated, whereas positive means underestimated. The values were compared with table IV. and V. in [8].

methodology is described in Section 3.2.6. The program is still missing some features, which I plan to add in the future. For example, only upper limits $\mu_U$ are calculated in MPFC. I plan to implement the calculation of the lower limit $\mu_L$.

### 3.2.4 Verification of MPFC Algorithm

Before applying the generated values from MPFC into the data analysis, I have compared the values generated by MPFC with those reported in the original article [8]. First, I compared values for $\mu_U$ (for $\bar{b} \in \langle 0, 15\rangle$ and $n \in \langle 0, 20\rangle$, and $CL = 0.90, 0.95, 0.99$) cited in tables IV. - VII. in [8]. Few disagreements were found in the comparison. However, the difference was in the most extreme cases at the level of $\pm 2\%$. Table 3.2 shows the comparison of my calculated $\mu_U$ values (for CL=0.9) to the original article. It can be seen that in 52% of the cases my program overestimated the $\mu_U$ (more conservative value). In only 5.25% of the cases my program underestimated $\mu_U$ (less conservative value). In overall, my program produced either exactly the same or slightly overestimated results. The differences can mostly be attributed to the different $\Delta\mu_j$ step chosen for the calculation and possible numerical errors rising from the discreetness of $n$, or rounding.

It turns out that the discrepancy between the individual values of $\mu_U$ tends to be further suppressed when the sensitivities $\mathcal{S}(\bar{b})$ are calculated. As a benchmark, I used the table XII. of [8]. I performed a comparison for all cited confidence levels. My program was very close to the cited values. The worst overestimate was by $-1.0\%$. Table 3.3, shows the differences between MPFC and table XII. of [8]. The overall conclusion is that the program is working well within a reasonable margin of error.

### 3.2.5 Minimum Confidence Level Requirements

One of the advantages of using the FC approach for generating the confidence belts is that the method provides an upper limit even if no counts are detected. This is desirable, since it allows for placing a limit on $T_{1/2}$ even if the detector didn't register anything. It provides information about the capabilities of the detector. The MPFC software algorithm does not always provide non-zero interval at n=0. It does so only if large enough $CL$ is chosen. To determine which $CL$ is sufficiently large enough,

| $CL = 0.9$ | | | |
|---|---|---|---|
| $\bar{b}$ | $\mathcal{S}(\bar{b})$ **MPFC** | $\mathcal{S}(\bar{b})$ **FC** | % |
| **0.0** | 2.44 | 2.44 | 0.00% |
| **0.5** | 2.86 | 2.86 | 0.00% |
| **1.0** | 3.28 | 3.28 | 0.00% |
| **1.5** | 3.63 | 3.62 | -1.00% |
| **2.0** | 3.94 | 3.94 | 0.00% |
| **2.5** | 4.20 | 4.20 | 0.00% |
| **3.0** | 4.43 | 4.42 | -1.00% |
| **3.5** | 4.63 | 4.63 | 0.00% |
| **4.0** | 4.83 | 4.83 | 0.00% |
| **5.0** | 5.18 | 5.18 | 0.00% |
| **6.0** | 5.54 | 5.53 | -1.00% |
| **7.0** | 5.90 | 5.90 | 0.00% |
| **8.0** | 6.19 | 6.18 | -1.00% |
| **9.0** | 6.50 | 6.49 | -1.00% |
| **10.0** | 6.76 | 6.76 | 0.00% |
| **11.0** | 7.02 | 7.02 | 0.00% |
| **12.0** | 7.28 | 7.28 | 0.00% |
| **13.0** | 7.52 | 7.51 | -1.00% |
| **14.0** | 7.76 | 7.75 | -1.00% |
| **15.0** | 7.99 | 7.99 | 0.00% |

Table 3.3: Comparison of the generated $\mathcal{S}(\bar{b})$ for original FC and generated from MPFC program. Negative values mean that my program overestimated. The values were compared with table XII. in [8].

I looked at the limiting behaviour of the minimal confidence level ($CL_{min}$) as a function of $\bar{b}$. I looked at what is the cumulative sum when the algorithm reaches $n_{min} = 0$.

Based on the nature of the FC method, it can be shown that the empty confidence interval for the case n = 0 is possible only if the calculation for $\mu_j = 0$ yields $n_{min}$ = 1 or higher. Table 3.4, is similar to Table 3.1, and it is constructed to study the case of $\mu_j = 0$ for any value of non-zero expected background $\bar{b}$. According to the ordering rules described in Section 3.2, the component probabilities of the cumulative sum will be ordered according to the last column of the table. From the table it is obvious that the R value will be always equal to 1 because the respective Poissonian probability in the line is equal to the best scenario for all the $n \leq \lceil \bar{b} \rceil$. This creates an ambiguity which of the values $0 \leq n \leq \lceil \bar{b} \rceil$ should be added first into the sum. The choice is not obvious. Nevertheless, MPFC chooses $n = \lceil \bar{b} \rceil$ first and adds the cumulative probability terms in direction of decreasing n all the way to n = 0. Such an effect sets a minimal requirement for CL in order to reach n = 0. This minimal value $CL_{min}$ is a cumulative sum of all aforementioned lines:

$$CL_{min} = \sum_{n_i=0}^{\lceil \bar{b} \rceil} P(n_i, \bar{b}) = e^{-\lceil \bar{b} \rceil} \sum_{n_i=0}^{\lceil \bar{b} \rceil} \frac{\bar{b}^{n_i}}{n_i!}. \tag{3.25}$$

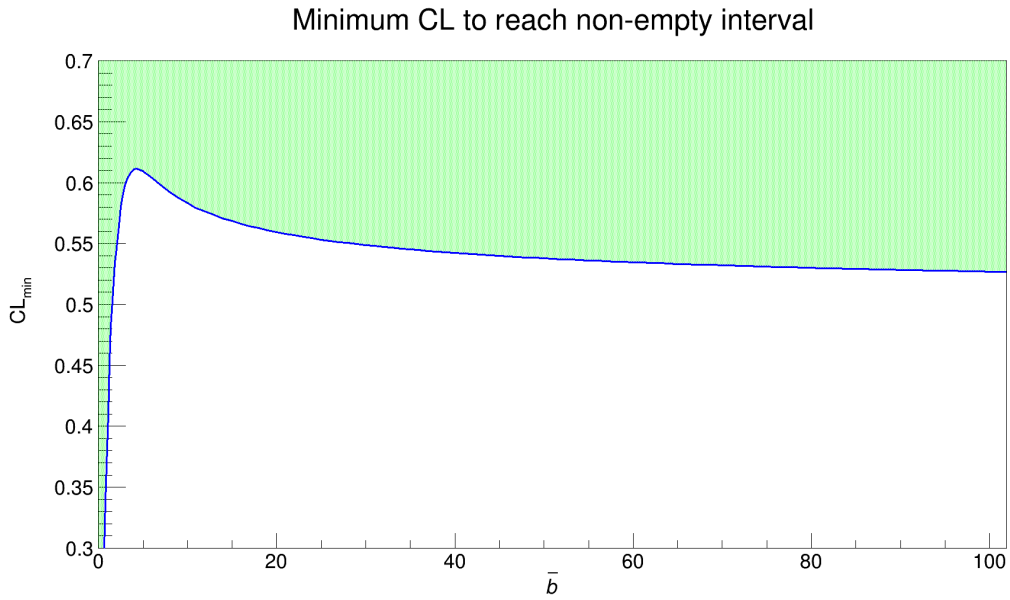


Figure 3.7: MPFC generated values for $CL_{min}$ with $\Delta\bar{b} = 1$. The highest values is at $\bar{b} = 4$, $CL_{min} = 0.61$. The green shaded area represents the *safe-zone*.

| $\boldsymbol{\mu_j = 0, \bar{b} \neq 0}$ | | | | | |
|---|---|---|---|---|---|
| **n** | $\boldsymbol{P(n_i, \mu_j + \bar{b})}$ | $\boldsymbol{\mu_{best,j}}$ | $\boldsymbol{P(n_i, \mu_{best,j} + \bar{b})}$ | **R** | **Order** |
| 0 | $P(0, \bar{b})$ | 0 | $P(0, \bar{b})$ | 1 | $\lceil \bar{b} \rceil$ |
| 1 | $P(1, \bar{b})$ | 0 | $P(1, \bar{b})$ | 1 | $\lceil \bar{b} \rceil - 1$ |
| 2 | $P(2, \bar{b})$ | 0 | $P(2, \bar{b})$ | 1 | $\lceil \bar{b} \rceil - 2$ |
| . | . | . | . | 1 | . |
| . | . | . | . | 1 | . |
| . | . | . | . | 1 | . |
| $\lceil \bar{b} \rceil - 1$ | $P(n-1, \bar{b})$ | 0 | $P(n-1, \bar{b})$ | 1 | 2 |
| $\lceil \bar{b} \rceil$ | $P(n, b)$ | 0 | $P(n, b)$ | 1 | 1 |
| $\lceil \bar{b} \rceil + 1$ | $P(n+1, b)$ | 1 | $P(n+1, 1+b)$ | $< 1$ | n+1 |

Table 3.4: Generalized FC table for $\mu_j = 0$ and $\bar{b} \neq 0$.

Figure 3.7 shows calculated $CL_{min}(\bar{b})$. The area above the line is what I call a *"safe-zone"*. Any $CL$ chosen within the safe-zone will generate non-zero confidence interval for $n_i = 0$ within the given expected background $\bar{b}$. On the other hand, values below the safe-zone will give empty interval for $n_i = 0$. The highest value is at $\bar{b} = 4, CL = 0.61$. If one chooses the CL larger than 0.61, the algorithm will always give desirable limits regardless of the $\bar{b}$.

### 3.2.6 Gaussian Limit of Feldman and Cousins Approach

The FC method is the most useful for experiments where $\bar{b}$ approaches the values close to 0. For increasing value of $\bar{b}$ the Poisson distribution $P(n, \bar{b})$ resembles more and more Gaussian bell curve and the FC method gives results similar to methods assuming simpler Gaussian probabilities. For large values of $\bar{b}$, the $\mathcal{S}(\bar{b})$ can be estimated very precisely by using:

$$\mu_U = \alpha\sqrt{\bar{b}}. \tag{3.26}$$

The square root of $\bar{b}$ represents precisely enough a value of one standard deviation if Gaussian distribution is assumed. The $\alpha$ is therefore, the factor representing the given $CL$ expressed in multiples of standard deviation. For example, when $\alpha = 1$, $CL = 0.683$ (or $1\sigma$). If we wished to obtain $CL = 0.9$ (used for most of the examples in this chapter), we would expect $\alpha = 1.64$. It is very useful to find a maximal value $\bar{b}_{max}$ at which the FC still provides more conservative estimate of sensitivity than previously presented Gaussian method. The $\bar{b}_{max}$ can be found by looking at where $\mu_U$ generated using the FC approach intersects the $\mu_U$ calculated using the equation (3.26). In other words, we are searching for which $\bar{b}$ the Poisson distribution becomes Gaussian with requested precision. Moreover, we expect that given Gaussian approximation would have indistinguishable shape after this point. For the purpose of the thesis we needed only the case for CL=0.9, therefore one would expect that the sought curve beyond $b = \bar{b}_{max}$ should be the one for which $\alpha = 1.64$. Nevertheless, I found out that the most fitting curve is the one slightly more conservative with $\alpha = 1.80$ as it can be seen in Figure 3.8.

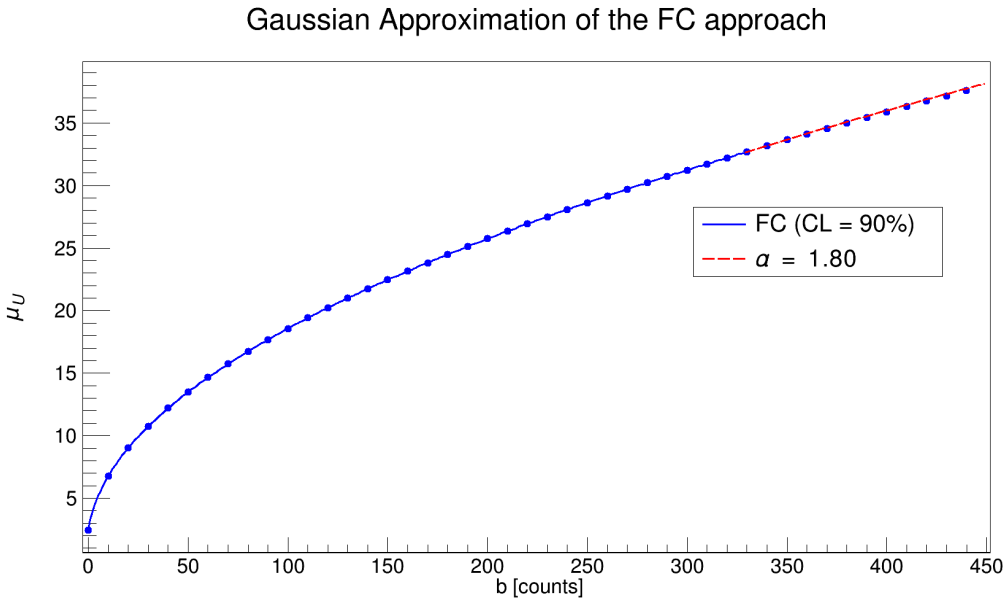


Figure 3.8: Limits $\mu_U$ generated for 450 different $\bar{b}$ with $CL = 0.9$. The blue line represents the values generated by MPFC algorithm. The dashed red line represents limits calculated using equation (3.26) for various $\alpha = 1.8$. The intersection between MPFC and the Gaussian approximation happens at $\bar{b} = 329$, this value is then set for $\bar{b}_{max}$ for the program.

The reason why the Gaussian approximation does not provide the $\alpha = 1.64$ curve might have the following explanation. When implementing the FC method, one needs to resort to several conservative decisions in the process which cannot be omitted due to the discrete nature of Poisson equation. As an example, I would like to point out the fact, that when one is composing the cumulative sum based on the ordering principle, it is almost never possible to reach the CL exactly. One always needs to add another term to the sum and exceed the CL in the majority of cases. This is just one of the intrinsic properties of the algorithm which makes the

FC method fundamentally more conservative compared to the situation if one would assume any continuous probability distribution. Another process which brings more conservatism into the calculation can be found in section B.3.2 of [97]. I would also like to point out that this apparent discrepancy between expected and obtained results is not problematic. The choice of slightly more conservative limit is not against the idea of fair estimation of the sensitivity.

Based on my, calculation, I conclude that the transition from FC to the Gaussian limit approximation happens at $\bar{b}_{max} = 329$. As stated previously, the $\alpha = 1.8$ should be used for $CL = 0.9$.

CHAPTER 4

# CALCULATION OF $T_{1/2}$ SENSITIVITY TO $0\nu\beta\beta$ FOR COBRA DEMONSTRATOR

The following chapter describes the data analysis performed within this thesis. First, some basic information about the data provided by the COBRA collaboration is outlined. Next, the methodology and decision making behind the used data cuts is described. Next, a description and effects of data partitioning are presented. Afterwards, the details of background fitting are provided along with the produced results in the form of spectra. Lastly, the methodology for obtaining various $T_{1/2}$ sensitivities using different approaches is outlined and applied to the partitioned data. The main approach of this thesis is the so-called optimized window counting method. The analysis is performed on four isotopes present in the COBRA detector. This is done so that the numbers can be compared with the values obtained in [1]. The four isotopes are $^{128}$Te, $^{70}$Zn, $^{130}$Te and $^{116}$Cd, their respective Q-values and abundances are provided in Table 2.1.

## 4.1 COBRA Demonstrator Dataset (Years 2013-2019)

In order to perform the data analysis I used data obtained by COBRA Collaboration. I received processed data dating from March 2013 to October 2019, measured uniquely by the COBRA Demonstrator module. Together, there are 18 806 data files. Each data file represents a four hour measurement. The data, on which the analysis in this chapter is based, were already pre-processed from form of the raw waveforms to pre-cleaned event histograms. This has already been done in past by members of the COBRA Collaboration. The data are in form of .root files. Each pre-processed data file contains information about all the detectors that were active (live) within the given data taking period. Furthermore, each file contains information about all the events measured during the data-taking period, their timestamps, interaction depth, the detector number in which they occurred, as well as the energy they each deposited in the detector. The detectors are numbered from 1 to 64. The file also contains information about the detector mass and duration during which the detector was active (this is used to calculate the exposure), detector calibration constants and lot more information less relevant for the topic of this thesis.

### 4.1.1 Measured Spectrum

As the first step to begin the analysis, I looked at the spectrum obtained from the dataset. Figure 4.1 contains the full spectrum integrated over the full dataset. One

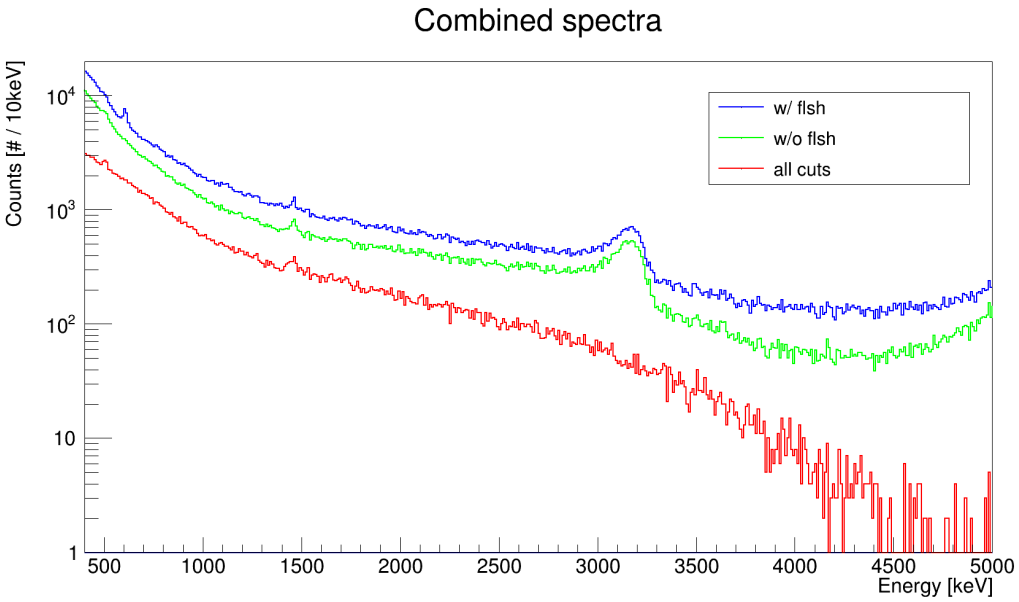


Figure 4.1: Spectrum of the COBRA data. Blue line represents all physical events. Green line represents all physical events excluding the flushing period. Red line represents the spectrum after standard cuts were applied.

can compare the spectrum with the one used for earlier data analysis (2016) in [1]. This publication will be used as a benchmark for evaluating the results of the analysis presented in the thesis.

The spectrum contains several features to be discussed. Analysed .root files contain events which are flagged as "bad" or "injected", these were filtered out and do not appear in any of the provided spectra. The *bad* events are flagged because the waveforms did not meet the basic quality requirements. The *injected* events, on the other hand, are artificially injected pulses coming from the pulse generator. They are used for the purposes of calibration of the detectors, or to help identify whether something is wrong with the data during data taking period. These events are also filtered out. Finally, during the several years of the operation of the Demonstrator, there were certain time periods when issues with nitrogen flushing were observed. This resulted in an unwanted artificial increase of background count rate originating in higher levels of Radon contamination. Such periods (we call them *flushing periods*) are also filtered out and do not appear in the final analysed spectrum. The blue spectrum in Figure 4.1 represents all of the physical events from the full dataset after the elimination of the bad and injected pulses. The green spectrum shows the effects of eliminating the flushing periods, and finally, the red spectrum represents events after applying standard COBRA data cuts. The relevant data cuts are discussed later.

The presented spectra exhibit several defining features. First, at 511 keV, there is a visible $\gamma$-line arising from pair annihilation from $\beta^+$-decay of $^{22}$Na. Around 610 keV, a second peak is visible. This is caused by $\alpha$-decay of $^{222}$Rn. One can notice that this peak appears in the spectrum where the flushing periods are still present (blue line) but it disappears in the other two spectral distributions, where the flushing periods are ignored. At 1275 keV, one can notice a $\gamma$-line arising from $\beta$-decay of $^{22}$Na. This line is caused by emitted gamma quantum as the daughter

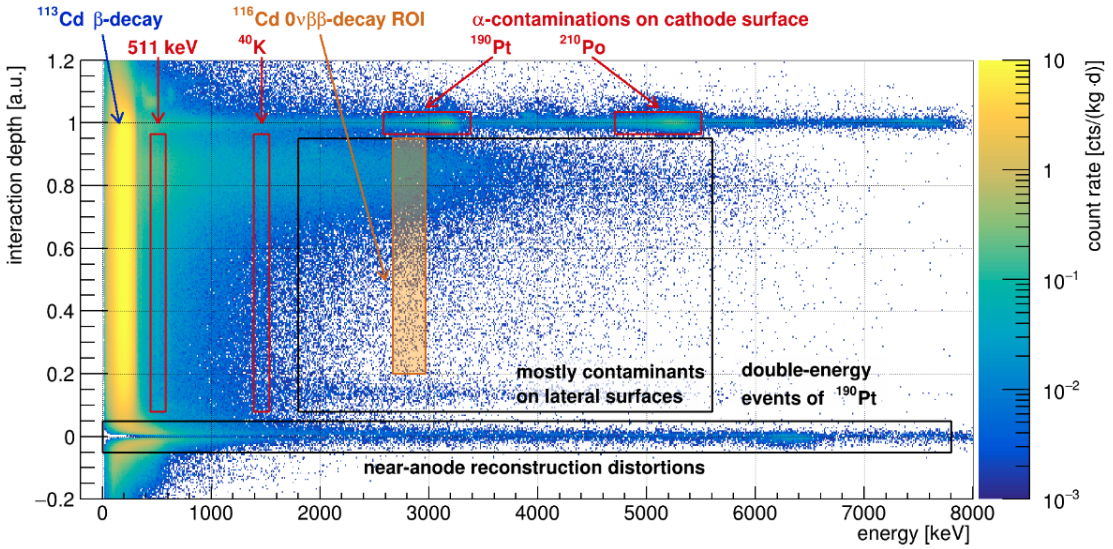


Figure 4.2: A 2D histogram of the Interaction depth ($z$) and Energy. The features visible in the spectrum are marked. From [96].

nucleus ($^{22}$Ne) deexcites. Furthermore, the peak at 1460 keV originates from $\beta$-decay of $^{40}$K. The line belongs to gamma quantum which is produced by deexcitation of its daughter $^{40}$Ar. The peak around 3100 keV originates from $\alpha$-decay of $^{190}$Pt. This decay happens close to the electrodes of the detector, as it is a part of the electrode material, and is suppressed by applying the relevant cuts. As it will be clearer in later sections, neither of the mentioned features are in close proximity to any of the Q-values of the studied decays.

### 4.1.2 Standard Data Cuts

There is a standard set of data cuts used by COBRA collaboration which I applied to achieve a refinement of the spectrum. There are two basic recommended cuts based on the interaction depth of the given event and the so-called amplitude-over-energy (A/E) ratio. The optimal values were studied by the COBRA Collaboration and were provided along with the dataset.

The optimal interaction depth cut (z-cut) was found to be in range $0.2 < z < 0.95$. The interaction depth $z$ can take values from 0 to 1. Where $z = 1$ is an interaction that happened at the cathode side of the detector. On the other hand $z = 0$ represents interaction at the anode side. The geometry of the detector is described in more detail in Chapter 2. Figure 4.2 depicts a 2D histogram of the interaction depth and particle energy. The features of the spectrum described in Section 4.1.1 are marked. The lower bound for the z-cut of ($z > 0.2$) was chosen so that the distortions near the anode would be eliminated along with the signal due to the decay of $^{190}$Pt (double energy events). On the other hand, the upper bound of the z-cut ($z < 0.95$) eliminates the contribution of the $\alpha$-decay of $^{190}$Pt. This contamination is visible in the blue and green lines of Figure 4.1.1 as the peak around 3100 keV [96].

The optimal ratio $A/E$ was found to be within range of $0.872 < \mathrm{A/E} < 1.3$ (detailed analysis of the $A/E$ cut was performed in [99]). The $A/E$ is defined as the amplitude of the current ($A$) divided by the energy extracted from the induced

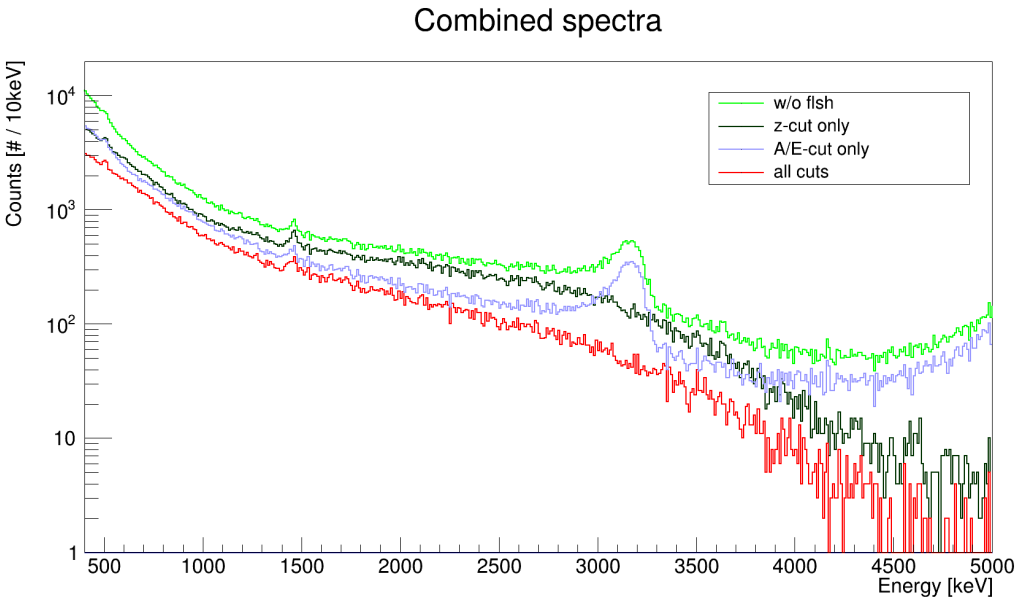


Figure 4.3: Spectra depicting the effects of applying the standard cuts. Green line represents spectrum where bad and injected events, along with flushing periods were filtered out. The dark green line shows the spectrum where only the z-cut was applied. The light blue line represents spectrum where only the A/E-cut was applied. The red line represents spectrum, with all the standard cuts.

charge ($E$). As one expects the both amplitude and integrated charge to be proportional to energy, it is no surprise, that the A/E value is expected to be around 1.

After the application of the cuts it is possible to notice a significant background reduction. Figure 4.3 shows the effects of the three different cuts. The original spectrum (light green line in 4.1 and 4.3) after application of a z-cut is represented by the dark green line in Figure 4.3. Only the events with $0.2 < z < 0.95$ were kept. Reduction in count rate is visible. The 511 keV annihilation peak is now more distinct. One can also notice the disappearance of the peak around 3100 keV which happens thanks to the elimination of $\alpha$-decay signals from $^{190}$Pt from the electrode surface. The light blue line represents the spectrum where only $A/E$ cut was applied to the original (green) spectrum. This resulted in reduction of the background counts. It is clear that this cut did not eliminate the undesired peak at 3100 keV, nor the rising tendency of the spectrum beyond 4500 keV (another peak caused by $\alpha$-decaying elements on the cathode). This is a justification for the use of the z-cut along with A/E cut. The two cuts (z-cut and A/E-cut) together are represented by the red line in the spectrum. The spectrum is much cleaner in comparison to the original, there is a significant reduction in background counts as well as some of the undesired features are eliminated. This (red) spectrum will be used for all data analysis to follow.

Let us now have a look at the cut efficiencies connected to the aforementioned cuts and to the full energy peak efficiency. The overall detector efficiency consists of multiple factors. These can be summarized as:

- Intrinsic full-energy detection efficiency $\boldsymbol{\varepsilon_{fe}}$ represents the fraction of electrons arising from $0\nu\beta\beta$-decay that deposit their full energy in the detector [96].

| Isotope | $\mathcal{E}_{fe}$ [%] |
|---|---|
| $^{128}$Te | 91.9 ± 0.3 |
| $^{70}$Zn | 90.1 ± 0.3 |
| $^{130}$Te | 66.2 ± 0.5 |
| $^{116}$Cd | 62.0 ± 0.9 |

Table 4.1: Table of values used for $\boldsymbol{\mathcal{E}_{fe}}$. The uncertainties are marked in the table, however they are not used in the data analysis. From [96], table 8.29.

Each isotope thus has its own $\boldsymbol{\mathcal{E}_{fe}}$. The values are summarized in Table 4.1.

- Efficiency due to the interaction depth $\boldsymbol{\mathcal{E}_z}$ represents the fraction of data that is left over after application of the z-cut. I use updated values from [96] (table 7.2). These new values have not been published yet, however the COBRA collaboration use them as the standard. The values are: $\boldsymbol{\mathcal{E}_z}$ $(0.2 < z < 0.6) = 0.4170 \pm 0.0005$; $\boldsymbol{\mathcal{E}_z}$ $(0.6 < z < 0.95) = 0.4205 \pm 0.0005$.
- Efficiency due to $A/E$-cut $\boldsymbol{\mathcal{E}_{A/E}}$ represents the fraction of data that is left over after application of the $A/E$-cut. The analysis of this cut was made in [99], the value I use is $\boldsymbol{\mathcal{E}_{A/E}} = 0.9$.

To obtain the overall detector efficiency, all these factors need to be multiplied together, i.e.:

$$\mathcal{E}_D = \mathcal{E}_{fe}\mathcal{E}_z\mathcal{E}_{A/E}. \tag{4.1}$$

### 4.1.3 Data Partitions

COBRA Demonstrator is composed of 64 different CdZnTe crystals with different resolutions and calibration periods. It is beneficial to divide previously discussed full dataset into individual data partitions. A partition used in our analysis represents a subset of the full dataset defined uniquely by the following parameters: the detector number, calibration constants (in other words, calibration period), and the interaction depth (high vs. low – explained in the text below). The detector number represents a unique value assigned to each detector $(1-64)$ which defines where the detector is placed within the setup. The numbering is described in Figure 2.1. The dataset for a given detector must further be partitioned based on the calibration parameters. Over the several years of data taking campaign, each detector was re-calibrated multiple times and the detector resolution, therefore, does not depend only on the quality of the detector but also on its evolution over time. The detector resolution function $\sigma(E)$ is considered stable within a calibration period for given detector. The function is approximated within COBRA experiment in the following form:

$$\sigma(E) = \sqrt{(p_0)^2 + \left(p_1\sqrt{\frac{E}{keV}}\right)^2 + \left(p_2\frac{E}{keV}\right)^2}. \tag{4.2}$$

Here, $p_0$, $p_1$ and $p_2$ are calibration parameters independent of energy, expressed in keV. Note that, the energy needs to be plugged in keV to obtain a proper value for

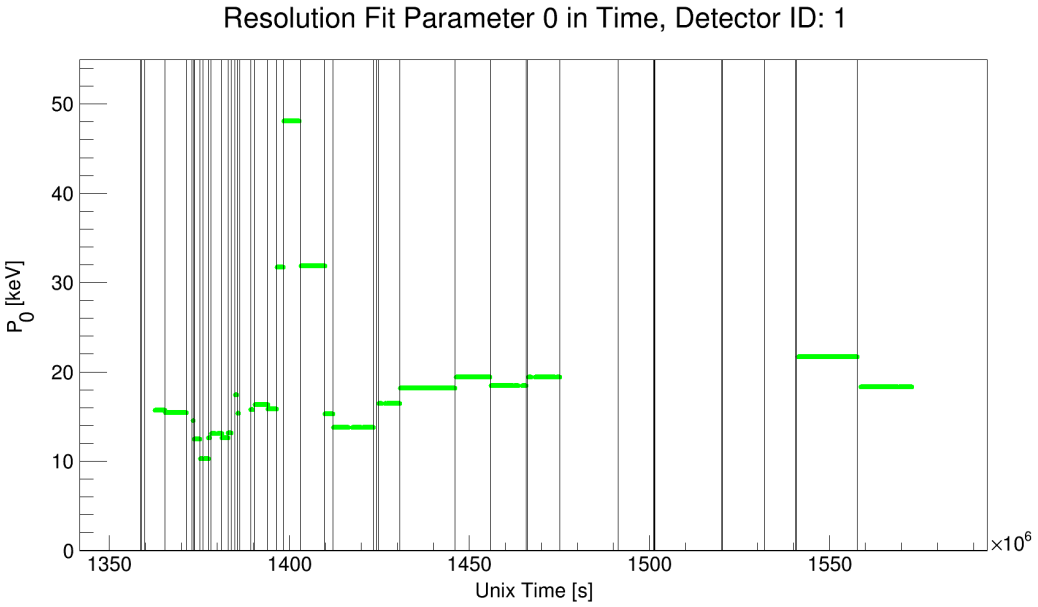


Figure 4.4: The time evolution of the calibration parameter $p_0$. The x-axis represents unix time – number of seconds since the Epoch on January 1st, 1970 at UTC. Each vertical line represents the date of the on-site calibration. The calibration period without a $p_0$ value signifies that the detector was not measuring during the given period.

resolution. The calibration parameters change with each on-site calibration of the detectors. Thus, there is a need to split the detector partitions according to their calibration parameters. These then have their own $\sigma(E)$. As an example, Figure 4.4 shows an evolution of parameter $p_0$ for detector No. 1. The vertical lines split the measurement duration into each separate calibration periods.

The calibration of the detectors was not always performed simultaneously, therefore, it can happen that the parameters do not change between two successive calibration periods. This is accounted for. The partition is defined as a dataset from a continuous time period during which the calibration parameters remained the same. Partitions defined this way are not necessarily coincident with the calibration periods. One partition can be in principle composed by several calibration periods if the parameters remained unchanged for a given detector.

Finally, each detector is sensitive to the interaction depth. The efficiency of the detector is different whether the interaction happened closer to the cathode or anode side. The quality of the data differs based on the z – coordinate of the detector. Based on the previous analyses, it is beneficial to distinguish between the high-z dataset ($0.6 < z < 0.95$) and low-z dataset ($0.2 < z < 0.6$) [100]. Previously defined data partitions – defined by the detector number and the calibration parameters – are further split into two partitions based on the high-z/low-z criterion. Figure 4.5 shows the difference in total spectra for high-z and low-z. It is visible that there are significantly more events in the partitions with high $z$. This behaviour is attributed to the possible contamination on the Delrin holder, in which the detector cubes are placed [101]. Partitioning of the entire dataset, based on the criteria discussed above, results in 2806 total partitions. From now, the 2806 partitions defined in this section should be understood as the basic data analysis unit used in my calculations.

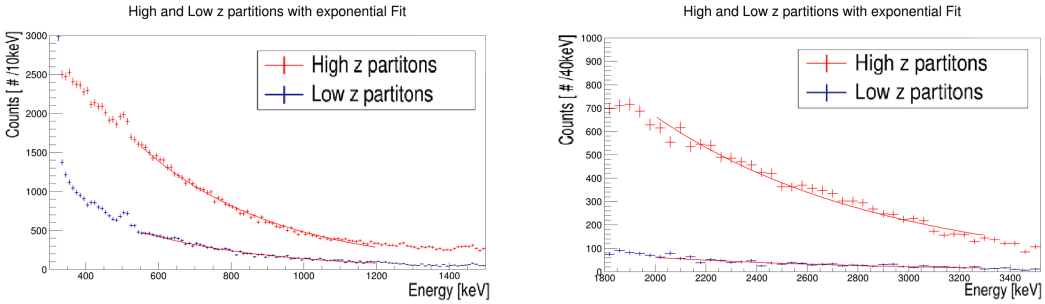


(a) $E \in \langle 550\text{keV} - 1200\text{keV} \rangle$ (b) $E \in \langle 2000\text{keV} - 3300\text{keV} \rangle$

Figure 4.5: Exponential background fit containing events from all of the high-z (red line) and all of the low-z (blue line) partitions in the specified energy ranges.

In text to follow, summation over variable p (occasionally also variable q) in the equations should always be understood as a summation over all the data partitions. Each partition can be identified by its unique ID number (1-2806) and it can be identified by the following parameters: detector number, start time, total duration ($t_p$), detector mass ($m_p$), number of events, calibration parameters and interaction depth $z$ (high-z or low-z). Table with all partition parameters is provided in Table B.1.

### 4.1.4 Background Extraction From the Data

The goal of my data analysis is to apply so-called optimized window counting method in order to estimate half-life sensitivity for $0\nu\beta\beta$ to ground state in case of four isotopes: $^{128}$Te (Q= 865.9 keV), $^{70}$Zn (Q= 998.5 keV), $^{130}$Te (Q= 2527.0 keV) and $^{116}$Cd (Q= 2813.5 keV). Only by looking at the spectrum (red line in Figure 4.5), it is evident that there are no peak-like features in the vicinity of these Q-values, therefore, I do not aspire to test the probability of the presence of $0\nu\beta\beta$ in the dataset. Instead, I assumed that the $0\nu\beta\beta$ is not present and decided to consider the spectrum to consist merely of the background counts. Accordingly, I decided to only estimate the half-life sensitivity of COBRA demonstrator to $0\nu\beta\beta$ for aforementioned isotopes. This approach is further justified by the fact that COBRA Collaboration does not dispose of satisfactory background model yet.

As mentioned in the previous section, each partition contains a subset of events which composes the given spectrum for the partition. It is important to clarify how the number of the background counts can be extracted for a given partition. In the thesis, I used two different methods: the **direct extraction** and a **model**.

Let me start with the direct extraction. For a given partition and a given ROI, the number of background counts in the window is simply summed over the bins in the spectrum belonging to the partition. In case when the boundaries of the ROI ended up inside of a bin, only the proportional number of counts belonging inside the ROI was added. This method is very simple and straightforward. $\bar{b}$ is obtained as:

$$\bar{b} = \xi_0 b_0 + \sum_{i=1}^{n-1} b_i + \xi_n b_n \ . \tag{4.3}$$

Here, $b_i$ represents the number of counts in the the i-th bin. Here i = 0 (i = n) represents the bin containing the left (right) ROI boundary. Furthermore, $\xi_0$ and $\xi_n$ represent the proportion of events (between 0 and 1) of the boundary bins belonging inside of the ROI.

The other (model) method is based on the surrogate model in absence of the proper background model. If one splits the spectrum from Figure 4.1.1 (red line) into two spectra of low-z ($0.2 < z < 0.6$) and high-z ($0.6 < z < 0.95$) and investigates it only in two regions in vicinity of the four Q-values of interest[1], it is possible to see that the spectrum can be (within a reasonable precision) approximated by exponential function:

$$\beta(E) = \beta_0 e^{-\lambda E}. \tag{4.4}$$

These spectra as well as their fits can be seen in Figure 4.5. $\beta_0$ is the norm of the exponential normalized to the total exposure, in units $\mathrm{kg}^{-1}\mathrm{yr}^{-1}\mathrm{kev}^{-1}$ and $\lambda$ is the rate of how fast the background drops with increasing energy, in units $\mathrm{kev}^{-1}$. These are two parameters required by our simplified background model. In order to fit the data with an exponential function, I have written an algorithm which employs the least squares method minimizing the chi-squared value to find the best fit parameters $\beta_0$ and $\lambda$. I decided not to perform the fit independently for each partition as it would result in questionable fit quality because of the insufficient statistics. At around 1200keV there is a visible change in the spectrum, where the spectrum still decreases exponentially, nevertheless slope of the spectrum is not so steep anymore. A different fit would be required for the higher energies. As the Gaussian peak – originating from annihilation 511 keV $\gamma$s – is very close to the Q-value of $0\nu\beta\beta$ of $^{114}Cd$ (Q=539.8 keV), I have decided to exclude this isotope in order to simplify the analysis presented in the thesis. This isotope will be included in the future. Thus, the fitting range was finally chosen to be $550\mathrm{keV} - 1200\mathrm{keV}$.

The second fit I applied was in the range of energies: $2000\mathrm{keV} - 3300\mathrm{keV}$. This range covers $^{130}Te$ and $^{116}Cd$. Here, no peaks are apparent. The resulting fits are depicted in figures 4.5a and 4.5b. Fit parameters are summarized in Table 4.2.

To conclude, each partition possesses two sets of $\beta_0$ and $\lambda$ - for low ($550\mathrm{keV} - 1200\mathrm{keV}$) and high ($2000\mathrm{keV} - 3300\mathrm{keV}$) energy part of the spectrum. Nevertheless, for the reasons described above, half of the partitions (high-z partitions) share one set of the same fit parameters while the other half (low-z partitions) share the other. Once the background fit parameters are known for each partition, it is possible to calculate number of expected background counts in the given ROI ($E_{p,1}$, $E_{p,2}$) by integration:

$$\bar{b}_p(E_{p,1}, E_{p,2}) = m_p t_p \int_{E_{p,1}}^{E_{p,2}} \beta_{0p} e^{-\lambda_p E} dE \ . \tag{4.5}$$

The integral is multiplied by the exposure in order to obtain a dimensionless number of background counts in the region (independent of the exposure). This equation is used whenever I refer to the background estimation method based on the model.

[1](550 keV, 1200 keV) as low energy fit region and (2000 keV, 3300 keV) as high energy fit region.

| | High z | | Low z | |
|---|---|---|---|---|
| E Range [keV] | 550 - 1200 | 2000 - 3300 | 550-1200 | 2000-3300 |
| $\beta_0$ $[keV^{-1}kg^{-1}yr^{-1}]$ | 545.38 | 124.68 | 177.71 | 10.49 |
| $\lambda$ $[keV^{-1}]$ | $2.65 \cdot 10^{-3}$ | $1.08 \cdot 10^{-3}$ | $2.78 \cdot 10^{-3}$ | $1.12 \cdot 10^{-3}$ |
| $\chi^2/ndf$ | 1.69 | 1.85 | 1.42 | 1.45 |

Table 4.2: Fit parameters of the various fits used in data analysis. The fitted spectra can be seen in Figure 4.5.

## 4.2 Data Analysis

As it was explained in the previous chapter, the estimation of the $T_{1/2}$ sensitivity of a rare decay can be obtained based on the following equation:

$$T_{1/2} \geq N_A \frac{\ln(2)}{W} \mathcal{E} \frac{a m_d t}{\mathcal{S}(\bar{b})} \tag{4.6}$$

Let us now have a closer look at the components of this equation. In the previous chapter, I discussed in detail how the sensitivity $\mathcal{S}(\bar{b})$ can be estimated with help of the FC method and earlier in this chapter, I briefly discussed how to obtain the number of background counts from COBRA Demonstrator dataset. In order to proceed with the calculation, we now need to discuss the choice of region of interest (ROI), the efficiency of the energy cut and their implementation to the equation (4.6).

### 4.2.1 Choice of The Region of Interest

The equation (4.6) can be used to calculate a $T_{1/2}$ limit if we provide all the necessary components. However, if our goal is to provide the best possible $T_{1/2}$ limit with a given experimental setup, a few adjustments have to be made. The equation in this form does not explicitly take into account the choice of the region of interest (ROI). The ROI can be chosen almost arbitrarily, however, some choices might lead to sub-optimal results. The larger the ROI is, the more signal counts are accepted along with more background counts. If one shrinks ROI, the acceptance for both the background and signal counts is smaller. It is desirable to find the most optimal window with the signal counts accepted and the most background counts rejected.

#### 4.2.1.1 Cut Efficiency

The efficiency term $\mathcal{E}$ in equation (4.6) can be formally split into two factors, $\mathcal{E}_d$ – the efficiencies representing the limitation by the physics principles and the detection imperfections (presented at the end of Section 4.1.2) and $\mathcal{E}_c(ROI)$ – the efficiency arising from the fact that one performs an energy cut (let us call it "cut efficiency"). The cut efficiency is dependent only on the choice of ROI. Formally, total efficiency $\mathcal{E}$ can be expressed as a function of the ROI:

$$\mathcal{E}(ROI) = \mathcal{E}(l, r) = \mathcal{E}_d \cdot \mathcal{E}_C(l, r) \tag{4.7}$$

$l$ and $r$ stand for the left and right bound of the ROI (in units of energy). Let us now introduce an expected spectral shape of the signal $\rho(E)$ normalized to unity:

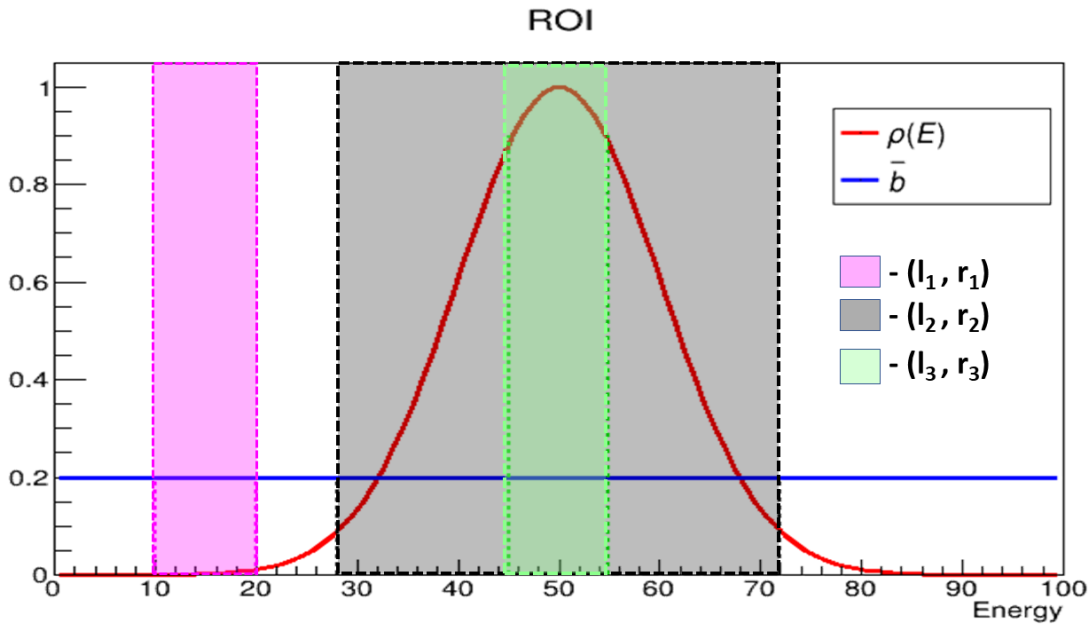


Figure 4.6: Depiction of a response function for $0\nu\beta\beta$ signal. Background is constant. Three possible ROIs are depicted in the figure with different colors: magenta - $(l_1, r_1)$, black - $(l_2, r_2)$, and green - $(l_3, r_3)$.

$$\int_{l=0}^{r=+\infty} \rho(E)dE = 1. \tag{4.8}$$

$\rho(E)$ represents the probability density of detecting a signal at energy E. The dimension of $\rho(E)$ is kev$^{-1}$. Finally, the cut efficiency $\mathcal{E}_c(l, r)$ can be expressed as the integral of $\rho(E)$ between the boundaries of ROI:

$$\int_{l}^{r} \rho(E)dE \equiv \mathcal{E}_c(l, r) \tag{4.9}$$

The closer the boundaries are to each other, the smaller $\mathcal{E}_c(l, r)$ gets. By combination of equations (4.6), (4.7) and (4.9) we obtain:

$$T_{1/2} \geq N_A \frac{\ln(2)}{W} a \frac{m_d t \mathcal{E}(l, r)}{\mathcal{S}(\bar{b})} = N_A \frac{\ln(2)}{W} a \frac{\mathcal{E}_d m_d t \int_l^r \rho(E)dE}{\mathcal{S}(\bar{b})} \ . \tag{4.10}$$

Introducing the cut efficiency effectively limits the exposure of the detector (I refer to this as the *effective exposure*). This may seem counter-intuitive as it seemingly decreases the calculated $T_{1/2}$ limit. However, applying an energy cut also limits the background counts. The expressions which take this fact into account are presented in the following section.

#### 4.2.1.2 ROI Dependent Sensitivity

Choosing a specific ROI results in reducing the effective exposure of the detector. How much the exposure is reduced is in turn dependent on the width of ROI and the shape of the response function. The same reasoning can be used for reducing the effective number of background counts used for calculating $\mathcal{S}(\bar{b})$.

Let us define a function $B(E)$ which holds the information about the shape of the background spectrum. If the shape of background spectrum B(E) is known, it is enough to integrate the function over the ROI and obtain the number of expected background counts $\bar{b}$:

$$\bar{b} = \int_l^r B(E)dE. \tag{4.11}$$

In this case, $B(E)$ has the units of $keV^{-1}$. One can introduce the exposure normalized form of the background function $\beta(E)$:

$$\beta(E) \equiv \frac{B(E)}{m_d t}. \tag{4.12}$$

Thus,

$$\bar{b} = m_d t \int_l^r \beta(E)dE. \tag{4.13}$$

The units of $\beta(E)$ are $keV^{-1}kg^{-1}yr^{-1}$. Equation (4.13) helps us to introduce an expression for the expected number of background counts $\bar{b}$ with explicit dependence on ROI.

In order to demonstrate the benefits of the introduction of ROI, I will consider $\beta(E)$ to be constant and $\rho(E)$ of a Gaussian shape as depicted in Figure 4.6. There are three examples of possible choices of ROI indicated in Figure 4.6. Each choice of the ROI in the figure influences the number of accepted signal counts as well as the background counts. It is evident that the choice of $(l_1, r_1)$ is far from optimal. Such a cut rejects too many signal counts in favour of background counts. It is more interesting to compare $(l_2, r_2)$ and $(l_3, r_3)$. Interval $(l_2, r_2)$ accepts more signal counts in comparison to $(l_3, r_3)$. However, it also accepts more background counts. It is, therefore, desirable to look at the ratio of the accepted signal divided by the accepted number of background counts, the so-called signal-to-background ratio:

$$\alpha(l, r) = \frac{n_s(l, r)}{n_b(l, r)}. \tag{4.14}$$

Here, $n_s(l, r)$ and $n_b(l, r)$ are the number of signal and number of background events within the boundaries $(l, r)$, respectively. They are both obtained by integration of their respective spectral function within the interval $(l, r)$. It is desirable to choose such a couple of ROI boundaries which maximizes $\alpha(l, r)$.

To summarise, I introduced an explicit dependence of efficiency (subsequently exposure) and background (subsequently sensitivity) on ROI. I also showed that this choice has a direct influence on the signal-to-background ratio. It is important to introduce an efficient method capable to choose the optimal boundaries of ROI which are otherwise arbitrary. Before introducing the main method of choosing optimal ROI boundaries in Section 4.2, I first present a simplified example in Section 4.2.2 to demonstrate how the $T_{1/2}$ can be calculated for a certain choice of ROI.

### 4.2.2 Naive Calculation

The equation (4.10) can be used for a quick (naive) estimation of the expected half-life limits from the data. All that is missing now, is to define $\rho(E)$, $\bar{b}$ and the choice

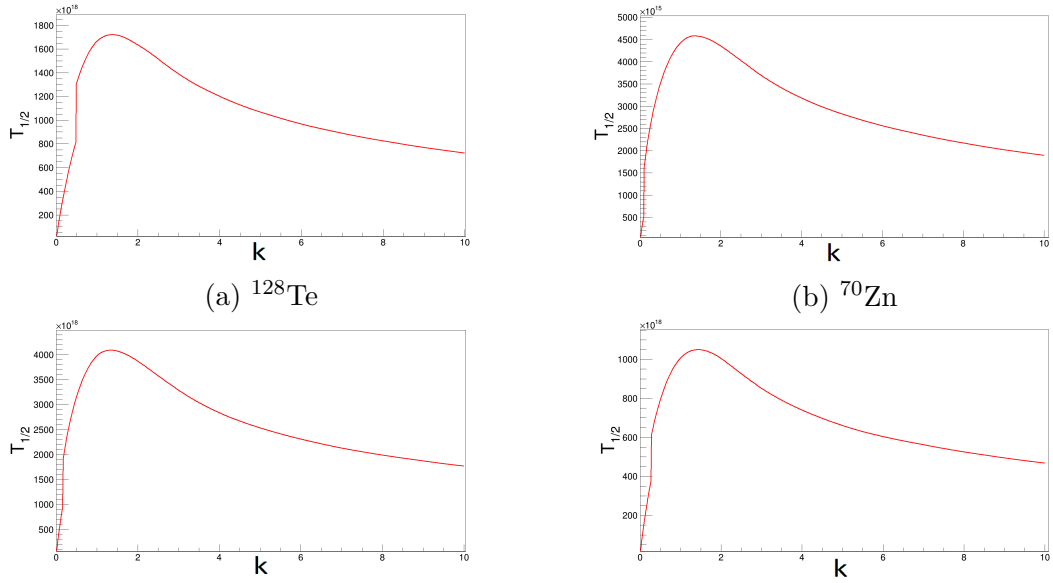


(a) $^{128}$Te (b) $^{70}$Zn

(c) $^{130}$Te (d) $^{116}$Cd

Figure 4.7: $T_{1/2}$ calculated for each isotope using the Naive $k\bar{\sigma}$ method. Each point was calculated for a different ROI by varying $k$. The best obtained limit is the maximum of each function.

of ROI. $\rho(E)$ represents the signal spectral shape which will be assumed to have a Gaussian shape, where $\mu = Q$ and $\sigma$ is the detector resolution:

$$\rho(E) = \frac{1}{\sigma\sqrt{2\pi}} e^{-\frac{(E-Q)^2}{2\sigma^2}} \tag{4.15}$$

Let us, for the moment, leave the model-based estimation of background counts $\bar{b}$ (equation (4.13)) aside and use the direct background method introduced by equation (4.3). The equation for half-life limit estimation then becomes:

$$T_{1/2} \geq N_A \frac{\ln(2)}{W} a \frac{\mathcal{E}_d m_d t \int_l^r \rho(E) dE}{\mathcal{S}(\bar{b})} \ , \tag{4.16}$$

with

$$\bar{b} = \xi_0 b_0 + \sum_{i=1}^{n-1} b_i + \xi_n b_n \ . \tag{4.17}$$

The last choice to make is the choice of ROI. I will study a ROI symmetrically distributed around the Q-value of the studied isotope:

$$l = Q - k\bar{\sigma}, \quad r = Q + k\bar{\sigma}. \tag{4.18}$$

Here, $\bar{\sigma}$ is a detector resolution averaged over all the data partitions. k is a unitless factor representing the distance from the center of ROI in multiples of average detector resolution. The equation (4.16) can, therefore, be written as:

$$T_{1/2} \geq N_A \frac{\ln(2)}{W} a \frac{\bar{\mathcal{E}}_d m_d t \int_{Q-k\bar{\sigma}}^{Q+k\bar{\sigma}} \rho(E) dE}{\mathcal{S}(\bar{b})} \ . \tag{4.19}$$

| Isotope | Limit | Best k |
|---|---|---|
| $^{128}$Te | $1.7 \cdot 10^{21}$ yr | 1.38 |
| $^{70}$Zn | $4.6 \cdot 10^{18}$ yr | 1.34 |
| $^{130}$Te | $4.1 \cdot 10^{21}$ yr | 1.34 |
| $^{116}$Cd | $1.0 \cdot 10^{21}$ yr | 1.44 |

Table 4.3: Results of the application of the naive $k\bar{\sigma}$ approach to calculation of $T_{1/2}$ limits. The last column represents the best $k$ value in the ROI defined as $ROI = Q \pm k\bar{\sigma}$.

Here, $\bar{\mathcal{E}}_d$ is a detector efficiency averaged over all the partitions. It is possible to obtain a value of $T_{1/2}$ for a chosen value of $k$. For a given isotope I varied $k$ from $k = 0.01$ to $k = 10$, in steps of $\Delta k = 0.01$, and calculated the respective $T_{1/2}$. Because of such choice of the ROI, I call this method the naive-$k\bar{\sigma}$ method. Figure 4.7 shows the calculated $T_{1/2}$ as a function of $k$. After the calculation was finished, I extracted the best ROI as the boundaries, where $T_{1/2i}$ is the highest. Using this method, I obtained the results summarized in Table 4.3. The detector abundances used in the calculation are summarized in Table 2.1. It is clear that the most optimal result is given by ROI with boundaries 1.34 up to 1.44 average detector resolutions away from Q-value.

This method is the simple and quick approach to obtain half-life estimation. Nevertheless, it is based only on the average values for $\bar{\mathcal{E}}_d$, $\bar{\sigma}$ completely neglecting the differences between the partitions. The choice of ROI was very intuitive, but – as it will be made clear later – it is not optimal. Furthermore, this method does not take into account the data partitions and the differences in their quality. It is possible to introduce a more refined approach which takes into account these differences and, on top of that, it optimizes the ROI for each partition separately. This method is the key analysis method of the thesis and will be discussed in the following section.

## 4.3 Optimized Window Counting Method

In order to introduce a data partition structure into the equation (4.10) it is sufficient to add a summation of the effective exposures over all partitions $p$:

$$T_{1/2} \geq N_A \frac{\ln(2)}{W} a \frac{\sum_{p=1}^{n} m_p t_p \mathcal{E}_p \int_{l_p}^{r_p} \rho_p(E) dE}{\mathcal{S}(\bar{b})} \ , \tag{4.20}$$

In the following text, I will introduce the method described in [102]. This method is based on the choice of model background as introduced in equation (4.13). To introduce the structure of data partitions into the equation, it is sufficient to sum all the expected background counts over all the partitions:

$$\bar{b} = \sum_{p=1}^{n} m_p t_p \int_{l_p}^{r_p} \beta_p(E) dE. \tag{4.21}$$

The half-life sensitivity estimation in equation (4.20) is a function of 2n parameters, where n = 2086 is the number of all data partitions. In order to find an

optimized ROI for each partition, one needs to find the 2n left and right boundary values which maximizes $T_{1/2}(l_p, r_p)$. For any integer value of q ($1 \leq q \leq 2086$) the following should be satisfied:

$$\frac{\partial}{\partial l_q} T_{1/2}(l_p, r_p) = 0, \quad \frac{\partial}{\partial r_q} T_{1/2}(l_p, r_p) = 0. \tag{4.22}$$

After derivation, one obtains:

$$T_{1/2}\left(-\frac{m_q t_q \rho_q(l_q)}{\sum_{p=1}^{n} m_p t_p \mathcal{E}_p(l_p, r_p)} + \frac{\mathcal{S}'(\bar{b}) m_q t_q \beta_q(l_q)}{\mathcal{S}(\bar{b})}\right) = 0 \ , \tag{4.23}$$

and

$$T_{1/2}\left(\frac{m_q t_q \rho_q(r_q)}{\sum_{p=1}^{n} m_p t_p \mathcal{E}_p(l_p, r_p)} - \frac{\mathcal{S}'(\bar{b}) m_q t_q \beta_q(r_q)}{\mathcal{S}(\bar{b})}\right) = 0. \tag{4.24}$$

Only a derivation of $\partial T_{1/2}/\partial r_q$ is provided in appendix A.1 due to the similarity to derivation of $\partial T_{1/2}/\partial l_q$. $\bar{b}$ is given by the Equation (4.21). We obtained a system of 2n equations with 2n variables. The solution gives ideal ROI for each partition separately. Luckily, it is possible to reduce number of the free parameters. If we now simplify equations (4.23) and (4.24) by multiplication of both sides by factor $T_{1/2}/(m_q t_q)$ and by subsequent expression of $\frac{\rho_q(r_q)}{\beta_q(r_q)}$ and $\frac{\rho_q(l_q)}{\beta_q(l_q)}$, we obtain:

$$\frac{\rho_q(r_q)}{\beta_q(r_q)} = \frac{\mathcal{S}'(\bar{b})}{\mathcal{S}(\bar{b})} \sum_{p=1}^{n} m_p t_p \mathcal{E}_p(l_p, r_p) \tag{4.25}$$

and

$$\frac{\rho_q(l_q)}{\beta_q(l_q)} = \frac{\mathcal{S}'(\bar{b})}{\mathcal{S}(\bar{b})} \sum_{p=1}^{n} m_p t_p \mathcal{E}_p(l_p, r_p) \ . \tag{4.26}$$

Both of these equations represent 2n equalities, one for given partition q. It is evident that the right-hand sides for a given q are equal. One can, therefore, merge the equations into one equation and lower the number of equalities by a factor of two:

$$\frac{\rho_q(r_q)}{\beta_q(r_q)} \ = \ \frac{\mathcal{S}'(\bar{b})}{\mathcal{S}(\bar{b})} \sum_{p=1}^{n} m_p t_p \mathcal{E}_p(l_p, r_p) = \frac{\rho_q(l_q)}{\beta_q(l_q)} \ \equiv \ (\rho/\beta). \tag{4.27}$$

Even though we managed to simplify the task, the equation (4.27) still represents 2806 equations. From the form of the equation, it is clear that the minimal condition for the best ROI (for a given partition q) is given by the boundaries ($l_q$, $r_q$) for which the ratio $\rho(\mathrm{E})/\beta(\mathrm{E})$ is equal at the boundaries. Not all of the regions of this type are optimal, nevertheless, each optimal ROI satisfies this condition. Finally, this still 2086-dimensional problem can be shrunk to one single parameter. If one considers the form of the intermediate term, it includes the sum over the effective exposures (recognizable from the numerator of the right side of the equation (4.20)) and the ratio of the first derivative of the sensitivity and the sensitivity itself. For a given

set of partition quantities $m_p$, $t_p$ and $\mathcal{E}_p$ this middle term is the same for each of the 2086 equations. This means that the term $\rho(\mathrm{E})/\beta(\mathrm{E})$ should be equal to the left and right boundary of a given partition, and it should be equal to the ROI boundary of each partition. This allows us to introduce a single parameter which we will simply call $(\rho/\beta)$. It can be noticed that not all sets of partition ROI boundaries for a given $(\rho/\beta)$ give the optimal result, nevertheless, each optimal ROI result will always be the one where $(\rho/\beta)$ is the same on the boundaries of every ROI of each partition.

The optimal set of ROI can be found by variation of one parameter $(\rho/\beta)$. This result holds regardless of the choice of signal $\rho(\mathrm{E})$ or background $\beta(\mathrm{E})$ spectral shapes. In the following section, I will introduce a simplified calculation which explains how to use this method.

### 4.3.1 Simplified Example of Implementation of Optimized Window Counting Method

In order to explain how the equation (4.27) can be implemented in a real calculation, I decided to present a simple toy model calculation. For this purpose I will assume the exponentially decreasing background spectral shape:

$$\beta_p(E) = \beta_{0p} e^{(-\lambda_p E)}, \tag{4.28}$$

and a signal spectrum of a Gaussian shape as described in Section 4.2.2:

$$\rho_p(E) = \frac{1}{\sigma_p\sqrt{2\pi}} e^{-\frac{(E-Q)^2}{2\sigma_p^2}} \quad . \tag{4.29}$$

Note that p stands for the partition number. Therefore, the variables $\beta_{0p}$, $\lambda_p$, (background fitting parameters), and $\sigma_p$ (detector resolution) are partition dependent. In this toy model, for simplicity, I will assume only two partitions. The equation (4.27) suggests to study the ratio $\rho_p(\mathrm{E})/\beta_p(\mathrm{E})$:

$$\frac{\rho_p(E)}{\beta_p(E)} = \frac{1}{\beta_{0p}\sigma_p\sqrt{2\pi}} e^{(\lambda_p E - \frac{(E-Q)^2}{2\sigma_p^2})}. \tag{4.30}$$

Thanks to the derivation in the previous section, we know that the value of $(\rho/\beta)$ has to be a unique value regardless of partition. We can, therefore consider this as a parameter and express the left $(l_p)$ and right $(r_p)$ ROI boundaries from equation (4.30) as:

$$l_p = Q + \lambda_p\sigma_p^2 - \sigma_p\sqrt{(\lambda_p\sigma_p)^2 + 2\lambda_p Q - 2\ln\left(\frac{\beta_{0p}\sigma_p\sqrt{2\pi}}{\mathcal{E}_p}\left(\frac{\rho}{\beta}\right)\right)}, \tag{4.31}$$

$$r_p = Q + \lambda_p\sigma_p^2 + \sigma_p\sqrt{(\lambda_p\sigma_p)^2 + 2\lambda_p Q - 2\ln\left(\frac{\beta_{0p}\sigma_p\sqrt{2\pi}}{\mathcal{E}_p}\left(\frac{\rho}{\beta}\right)\right)}. \tag{4.32}$$

The detailed derivation is provided in appendix A.2. Having the equations (4.31) and (4.32), one can obtain a candidate for optimal set of ROIs (one ROI per partition) for each value of $(\rho/\beta)$. By variation of this variable it is possible to change the

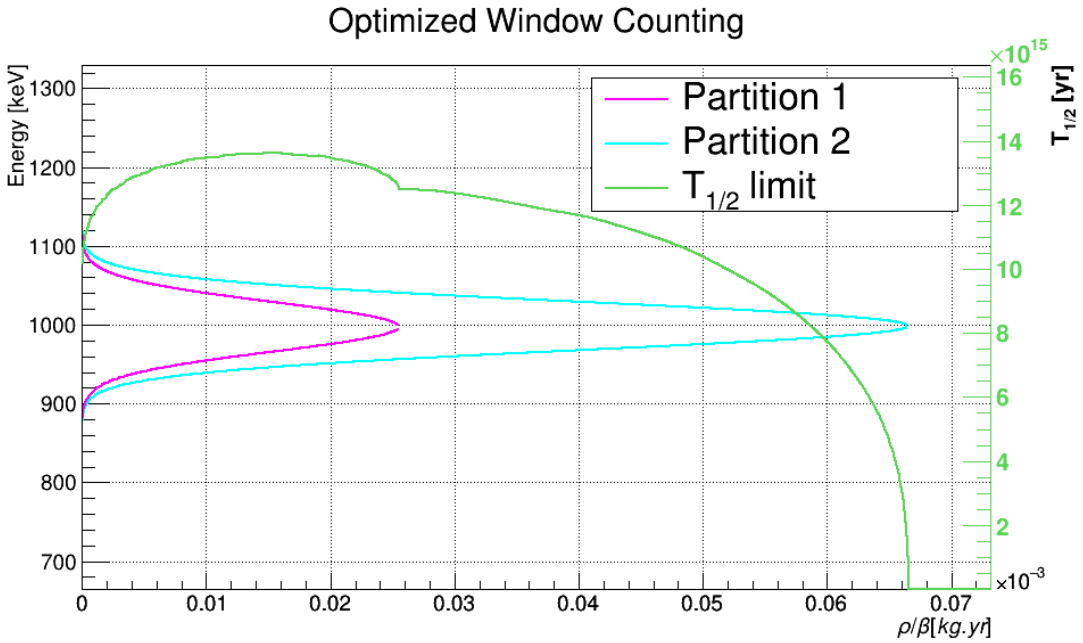


Figure 4.8: Optimized Window Counting Method example. The cyan and magenta lines represent the left and right bounds calculated according to the equations (4.31) and (4.32). The green line represent the corresponding calculated $T_{1/2}$.

width of the ROI for each partition and obtain a $T_{1/2}$ limit for each value. Finally, there would be a value of $(\rho/\beta)$ for which the given ensemble of ROIs yields the highest $T_{1/2}$. This set of ROIs should be considered as ideal.

Figure 4.8 represents the results of my simplified two-partition toy model. The x-axis represents the $(\rho/\beta)$ parameter. Magenta (cyan) curve represents the left and right boundaries of the ROI for partition 1 (partition 2). If one draws a vertical line for a given $(\rho/\beta)$ this line would cross the magenta (or cyan) curve twice. The y-value (energy scale on the left) of higher intersection point represents the right ROI boundary $r_p$ for given $(\rho/\beta)$ while the y-value (also energy scale on the left) of lower intersection point represents left ROI boundary $l_p$. The value of the respective $T_{1/2}$ for a given set of ROIs is represented by the green curve with the time scale on the right side of the plot. Note that, with the increasing value of $(\rho/\beta)$ both ROIs are getting smaller. Moreover, at the value of $(\rho/\beta) = 2.6 \cdot 10^{-5}$ kg.yr, the partition number 1 is closed completely and ignored beyond that. This is a key feature of the method. The algorithm tends to close (or completely closes) the partitions of lower quality sooner in order to improve the final half-life estimation. The decision to exclude (partially or completely) is done automatically without the need of subjective input of the person analysing the data.

The concept of the partition quality can be expressed by a well-defined variable. The point at which the partition is completely closed happens when $(\rho/\beta)$ reaches a value when the left ROI boundary is equal to the right ROI boundary, i.e. $l_p = r_p$ for a given partition p. Based on the equations (4.31) and (4.32) it can be seen that it happens when the term under the square root (the same for both boundaries) is exactly equal to zero. This happens for the following value of $(\rho/\beta)$:

$$\left(\frac{\rho}{\beta}\right)_p = \frac{\mathcal{E}_p}{\beta_{0p}\sigma_p\sqrt{2\pi}} e^{\lambda_p\left(Q+\frac{\lambda_p\sigma_p^2}{2}\right)} \equiv q_p. \tag{4.33}$$

This value I will call a partition quality $q_p$. Finally, if we look at Figure 4.8, it is possible to notice that the best $T_{1/2}$ is obtained for $(\rho/\beta) = 1.5 \cdot 10^{-5}$ kg.yr, for which $T_{1/2} = 1.36 \cdot 10^{16}$ yr. The partition 2 is of higher quality ($q_2 = 6.6 \cdot 10^{-5}$ kg.yr) and, therefore it contributes in a wider range than partition 1 with quality of $q_1 = 2.6 \cdot 10^{-5}$ kg.yr.

The last noticeable feature of the result in equations (4.31) and (4.32) is the fact that the ROI for each of the partitions is not centered around the Q-value of the decay as it was assumed in our naive approach presented in the previous section. The center is always shifted to the higher energies from the Q-value at the point $E = Q+\lambda_p\sigma_p^2$. This is expected if we take into account the fact that the shape of the signal Gaussian distribution is symmetric around Q-value, but the background energy spectrum is considered as an exponential. Within this assumption, there are always more background counts to the left from the Q-value than to the right. Therefore, the ROI prefers the energy cuts centered to the right of Q-value to improve signal-over-background ratio.

### 4.3.2 Application of Optimized Window Counting Method to Data from COBRA Demonstrator

The approach demonstrated in the previous toy model can be easily applied for any number of partitions. I applied this method for the COBRA dataset composed of 2086 partitions as described in the Section 4.1.3. In the calculation, I assume the exponential background spectrum shape. In general, the fit parameters should be extracted separately for each of the partitions. Nevertheless, the fits are the same within the same category of the partition and energy range as described in Section 4.1.4, and are summarized in Table 4.2. The results are summarized in Figures 4.9a - 4.10b. Each figure shows the calculated $T_{1/2}$ as a function of $(\rho/\beta)$. For clarity, the ROI curves (similar to the magenta and cyan curves from Figure 4.8) are omitted. For comparison, the results from [1] are marked with a black dotted horizontal line. The full red line represents values of inverse sensitivity:

$$\frac{1}{\mathcal{S}(\bar{b})} = \frac{1}{\mathcal{S}(\sum_{p=1}^{n} m_p t_p \int_{l_p}^{r_p} \beta_p(E)dE)}, \tag{4.34}$$

while the red dashed line represents the value of effective exposure given by equation:

$$e_{eff} = \sum_{p=1}^{n} m_p t_p \mathcal{E}_p \int_{l_p}^{r_p} \rho_p(E)dE. \tag{4.35}$$

The product of these two values, as can be seen from equation (4.20), is proportional to the final half-life limit estimation $T_{1/2}$. The comparison of the best limits extracted from the figures 4.9a - 4.10b with the limits from the reference article can be found in Table 4.4. It can be seen that the calculated limits of $T_{1/2}$ are slightly worse for $^{128}$Te and $^{70}$Zn, and the limits are improved for $^{130}$Te and for $^{116}$Cd. As expected, all limits are better than the ones calculated by the "naive" approach

| Isotope | 2016 Limit | My Limit | Q-Value | $\bar{b}$ | $1/\mathcal{S}(\bar{b})$ | Exp |
|---|---|---|---|---|---|---|
| $^{128}$Te | $1.9 \cdot 10^{21}$yr | $1.8 \cdot 10^{21}$yr | 866.5 keV | 3280 | $9.70 \cdot 10^{-3}$ | 0.368 kg.yr |
| $^{70}$Zn | $6.8 \cdot 10^{18}$yr | $4.9 \cdot 10^{18}$yr | 997.1 keV | 1854 | $1.30 \cdot 10^{-2}$ | 0.321 kg.yr |
| $^{130}$Te | $6.1 \cdot 10^{21}$yr | $6.9 \cdot 10^{21}$yr | 2527.5 keV | 108 | $5.20 \cdot 10^{-2}$ | 0.244 kg.yr |
| $^{116}$Cd | $1.1 \cdot 10^{21}$yr | $1.8 \cdot 10^{21}$yr | 2813.4 keV | 84 | $5.84 \cdot 10^{-2}$ | 0.244 kg.yr |

Table 4.4: Summary of the $T_{1/2}$ limit results using the optimized window method. The values are compared to the limits cited in [1].

(compare with Table 4.3).

Let us have a look at the evolution of $\frac{1}{\mathcal{S}(\bar{b})}$ and $e_{eff}$ as a function of $(\rho/\beta)$ in the figures 4.9a - 4.10b. Regardless of the isotope, the effective exposure drops as the ROIs are closing with the increasing $(\rho/\beta)$ value. On the other hand, the inverse sensitivity grows. In the figures, it is possible to study the interplay of the two variables and compare their relative importance. The uncertainty of the values can influence directly the uncertainty of the final half-life limit. While the uncertainty of the effective exposure is negligible, because the partial efficiencies (values are summarized at the end of Section 4.1.2), detector masses, and measurement periods are known with high precision, the inverse sensitivity depends on the estimation of the background counts. The optimized window counting method is sensitive to the background model. Figure 4.11 shows the spectrum composed of all high-z partitions of detector No. 39. The blue lines show the fit used as an input for the optimized window counting method. The fit was normalized to the exposure of the detector 39 ($mt = 0.02$ kg.yr). It can be seen that the fit significantly underestimates the real background counts. In this case, the shape of the spectrum is visibly not exponential. This is the most extreme case but it still points to the important imperfection. The reason for the discrepancy is the fact that the fit is extracted and re-scaled from the global spectrum as it was explained in Section 4.1.4. Such a simplified approach seems not to take into account the possible differences in spectral shapes between the partitions.

In order to obtain a more precise idea how much the model underestimates or overestimates the real background count in the ROI for each separate partition, I defined a quantity:

$$d_p = \frac{b_p^{direct} - b_p^{model}}{b_p^{model}} \tag{4.36}$$

The quantity $d_p$ is defined for each partition p. It represents the relative difference of the background counts in the most optimal ROI from the direct counting method $b_p^{direct}$ (see Section 4.1.4) minus the background counts in the most optimal ROI as calculated from the model for given partition $b_p^{model}$. One expects the difference to be zero in the ideal case. The case when $d_p = b_p^{model}$ can happen only when the partition p is ignored, i.e. its ROI window is completely closed: $l_p = r_p$. In such a case, the direct method, of course, meets the expected value of the prediction, by definition. Such partitions for $b_p^{model} = 0$ are excluded from the study. In case when $b_p^{direct} = 0$ the $d_p$ = -1. This is the case when no counts are present in the ROI but the model expects $b_p^{model} > 0$. It is a clear case of the background overestimation. Figure 4.12 shows four histograms of the relative differences $d_p$ in the optimal ROI obtained as a result of optimized window counting method. It is evident that the

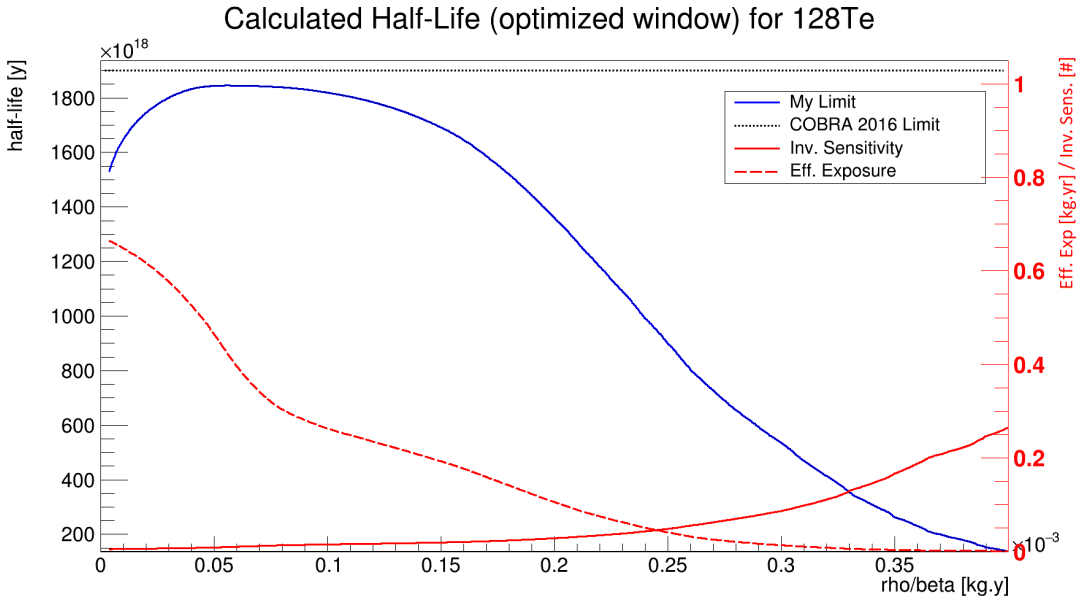


(a)

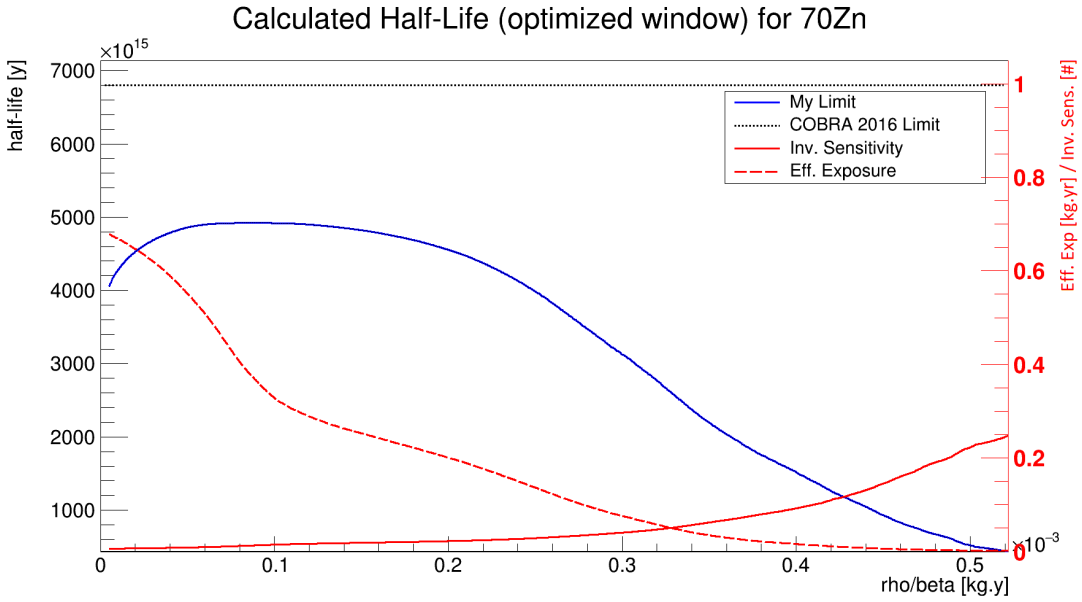


(b)

Figure 4.9: Optimized window counting method for a) $^{128}$Te and b) $^{70}$Zn. Blue line represents calculated $T_{1/2}$ with background obtained from model. Black line represent the limit cited in [1].

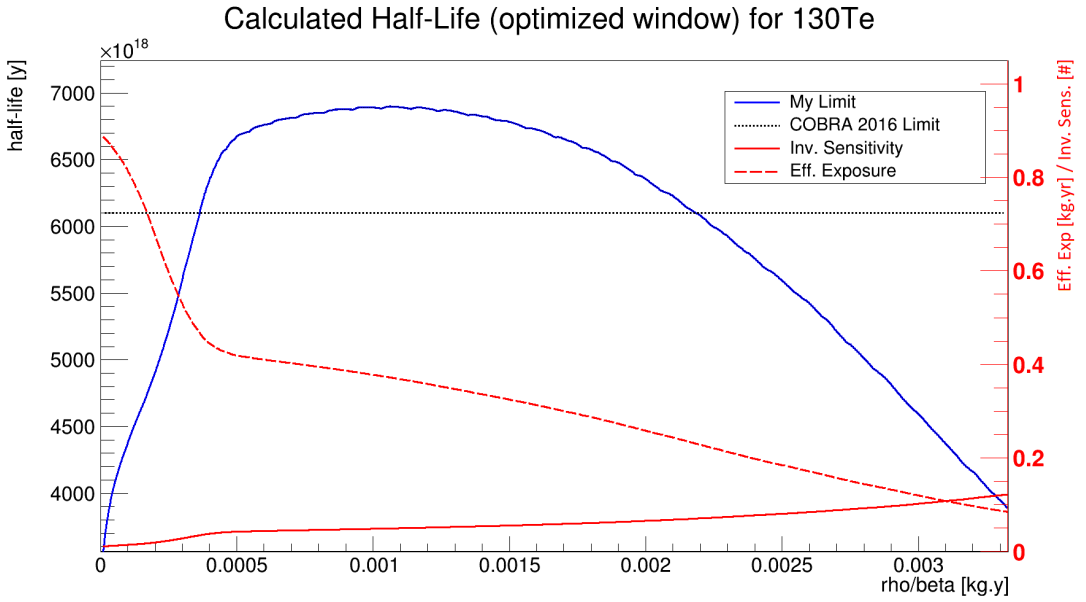


(a)

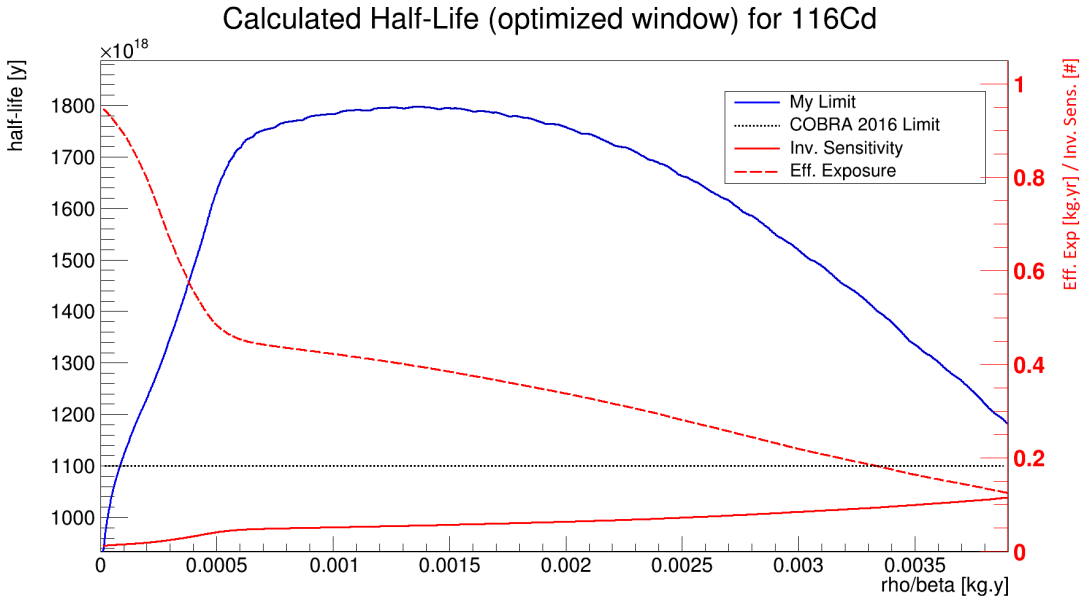


(b)

Figure 4.10: Optimized window counting method for a) $^{130}$Te and b) $^{116}$Cd. Blue line represents calculated $T_{1/2}$ with background obtained from model. Black line represent the limit cited in [1].

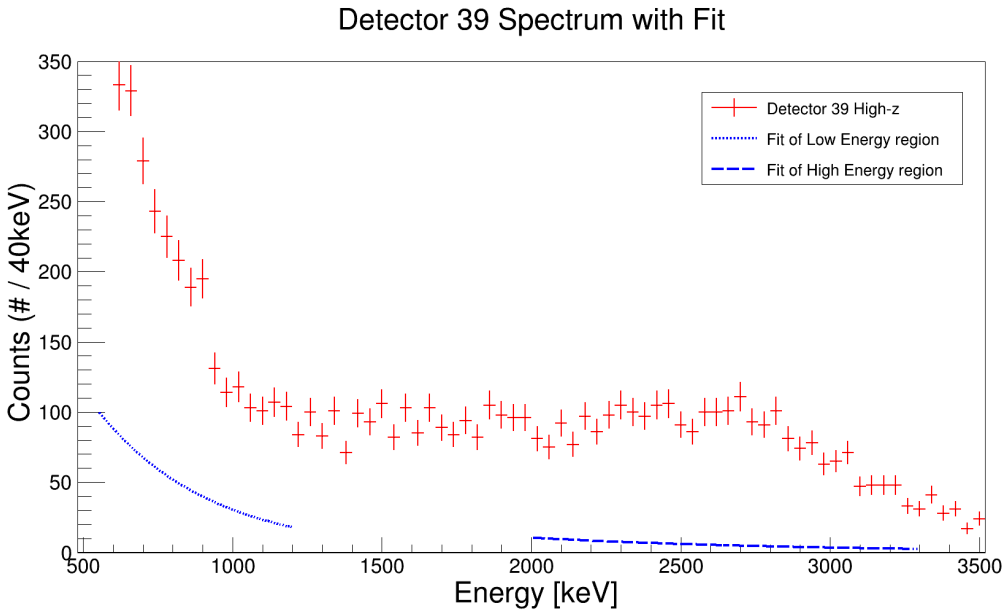


Figure 4.11: High-z partitions spectrum of the detector No. 39. The dotted blue line represents the fit of the low energy region $E \in \langle 550, 1200 \rangle$. The dashed blue line represents the fit of the high energy region $E \in \langle 2000, 3300 \rangle$. The fit was done for the global spectrum as described in Section 4.1.4 and then adjusted to the detector 39 spectrum based on its exposure.

case of $d_p$ = -1 is dominant in all four cases. Moreover, there are only a few partitions when $d_p > 0$. It means that the overestimation of the background happens for the majority of the partitions and leads to unnecessarily conservative half-life sensitivity.

The optimized window counting method is capable of discarding or keeping the partitions based on their quality which depends on the precision with which the model describes the background spectrum. The discrepancy between the model and the real measurement can penalize (in case of overestimation of the background) or prioritize (in case of underestimation of the background) some partitions over others. This fact gives hope to further improve the limits for the isotopes with the highest Q-values $^{130}$Te and $^{116}$Cd. The background contributions are $\bar{b} = 108$ and $\bar{b} = 84$ for these isotopes. As can be deduced from Figure 3.8, the sensitivity changes the most in the region of the $\bar{b}$ close to zero. Even a slight change in the estimation of background counts can cause a relatively large change in the sensitivity. It would be desirable to better tailor the background model to the real data in each partition, but this requires an enormous amount of effort. Possibilities of such an approach will be studied as a work beyond the scope of this thesis.

Except for the hypothesis about the imprecise background modelling, another reason for slightly lower limit in the case of $^{128}$Te (in comparison to [1]) lies in the difference of the used values of abundance. The values used in this work are summarized in Table 2.1. Nevertheless, in [1] they report the abundances recalculated into the number of nuclei per kilogram of the isotope $N_0/m_d$ which can be expressed by slight modification of equation 3.3:

$$\frac{N_0}{m_d} = \frac{N_A a}{W}. \tag{4.37}$$

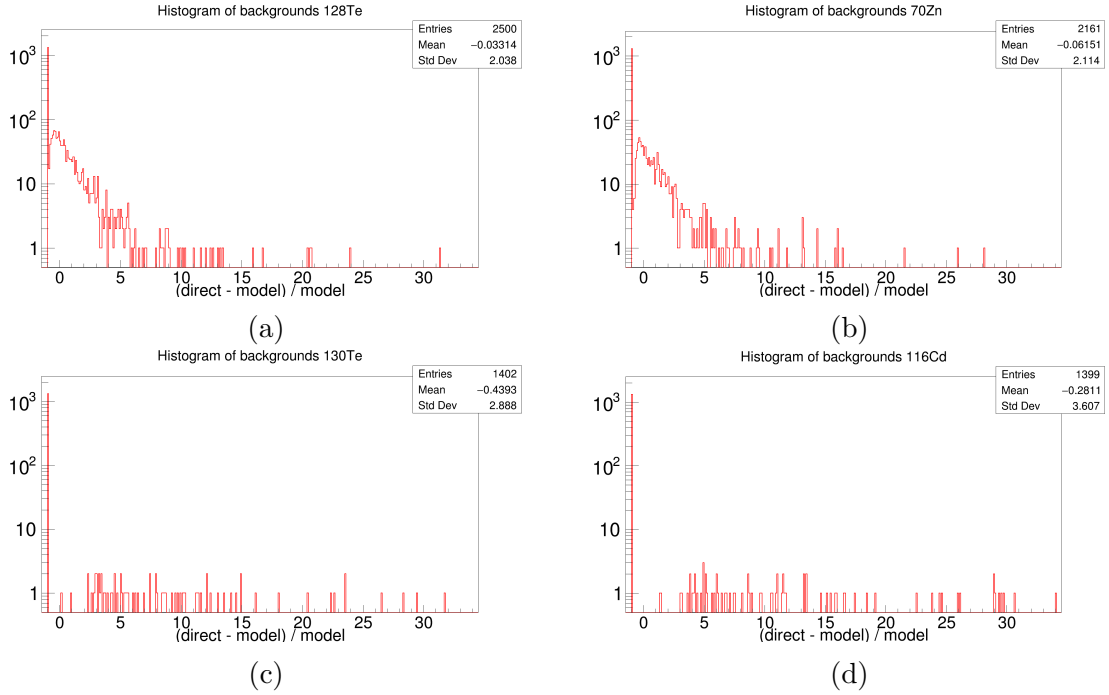


Figure 4.12: Histogram of the differences between the model and the direct background, for the best ROI of each isotope.

| **Isotope** | **2016 Article** $\mathbf{N/10^{23}}$ **(atoms/kg)** | **My values** $\mathbf{N/10^{23}}$ **(atoms/kg)** |
|---|---|---|
| $^{128}$Te | 8.08 | 7.46 |
| $^{70}$Zn | 0.015 | 0.017 |
| $^{130}$Te | 8.62 | 7.83 |
| $^{116}$Cd | 1.73 | 1.82 |

Table 4.5: Comparison of the isotope contents of the COBRA demonstrator. The second column shows values cited in table III of [1]. The third column shows the calculated values I used (equation 4.37).

The abundances used in this work were plugged into the equation and compared to the values from [1]. They are compared in Table 4.5. It is clear that the value for $^{128}$Te is larger by 8% which causes our limit to be penalised by 8% in comparison to the article. In general, the abundances are known within a relatively large uncertainty and the values can differ between the publications. Further investigations of the uncertainties of the experimental quantities need to be performed beyond the scope of the thesis. There is almost no discrepancy in the abundances in the case of $^{70}$Zn, therefore, the most probable reason for the weak limit provided in this work lies in the discrepancy of the background model. Furthermore, the partitions of low quality were excluded in the article by hand. The Optimized Window Counting method might have kept some significantly bad partitions more opened as due to the underestimation of the real background for the majority of the partitions. This will be studied in more detail in the future.

CHAPTER 5

# CONCLUSION

The goal of this thesis was to analyze data from the COBRA Demonstrator and calculate $T_{1/2}$ sensitivity to $0\nu\beta\beta$-decay for four different isotopes present in the detector.

In Chapter 1 I outlined the relevant physics. The fermions and bosons of the SM were introduced. A dedicated section to neutrino physics detailed the history of the postulation and the discovery of this particle. The Solar Neutrino Problem was described and the solution presented. This further imposed a new problem in neutrino physics – the Neutrino Mass Hierarchy. The description of the ordinary and double beta-decay was outlined next. $0\nu\beta\beta$-decay as a possible key to answering the the Neutrino Mass Hierarchy problem, as well as the experimental tool for determining the nature of neutrino, was introduced.

Chapter 2 was dedicated to the COBRA experiment. Here, the detector construction, semiconductor detection technology, and the composition of the detector crystals were detailed. Importance of the relevant isotopes, their abundance in the detector was summarized. Lastly, the CPG technology was briefly introduced.

Chapter 3, dedicated to the FC approach to calculating sensitivity, followed next. The justification of why this method is important for the $0\nu\beta\beta$ experiments was provided first. Second, the method itself was described in detail, some examples were provided. Lastly, the MPFC program developed within the scope of this thesis was introduced. The limitations and verification of the program were outlined first. Lastly, some of the challenges of applying the package were detailed and resolved.

The main results of this thesis are provided in Chapter 4. The Chapter begins with the description of the COBRA Demonstrator data. The total exposure of the obtained dataset, collected between 2013 and 2019, was 1.252 kg.yr. The analysis of the spectrum and the data cuts are provided next. Standard cuts, used by the members of the COBRA Collaboration, were used. These include the so-called z-cut and the $A/E$-cut, described in detail in Section 4.1.2. Next, the importance and the procedure used for the data partitioning is provided. Partitioning the full data set results in 2806 partitions. These are created based on the detector number, calibration parameters, and split into high-z and low-z partitions. Two methods for the extraction of background counts are presented in Section 4.1.4. The direct extraction method is used as a complementary method to the discussion of the results. The main background extraction method used for the data analysis is based on the exponential fit of the spectrum. The fit was performed for a global spectrum, taking into account the high-z and low-z partitions. The results of the fit are provided at the end of the section. Within the Data Analysis chapter, the importance of choosing the correct ROI is described first. The main method used for obtaining the optimal ROI for the calculation of the $T_{1/2}$ sensitivity is the so-called Optimized Window

Counting method. This method is described in detail in Section 4.8. The main advantage of the method is that it optimizes the ROI for each partition individually. In combination with the Gaussian signal function and the exponential background function, this method provides a single-parameter ($\rho/\beta$) dependent ROI.

Having defined all the necessary components, the results of applying the Optimized Window Counting method – using exponential background fit and MPFC for determining the sensitivity – are provided. $T_{1/2}$ limits are calculated for four isotopes: $^{128}$Te ($T_{1/2} \geq 1.8{\cdot}10^{21}$ yr), $^{70}$Zn ($T_{1/2} \geq 4.9{\cdot}10^{18}$ yr), $^{130}$Te ($T_{1/2} \geq 6.9{\cdot}10^{21}$ yr), and $^{116}$Cd ($T_{1/2} \geq 1.8 \cdot 10^{21}$ yr). The results are then compared to the publication of the COBRA Collaboration from 2016 [1] (with exposure of 0.643 kg.yr). In comparison, the limits calculated in this thesis were better for $^{130}$Te and $^{116}$Cd. The results were, on the other hand, worse for $^{128}$Te and $^{70}$Zn. Possible hypotheses why this could have occurred are presented at the end of Chapter 4. First, the global background model used in the analysis is not sufficiently adapted to each individual data partition. Some of the detectors exhibit worse properties than others. The second hypothesis is that the values used in [1] for the abundances of the isotopes are different (compared in Table 4.5). This could be attributed to the fact that the uncertainties of the quantities were not accounted for in the data analysis. The abundance significantly influences the effective exposure in the calculation, thus providing for inconsistent results.

# Bibliography


[1] Joachim Ebert et al. "Results of a search for neutrinoless double-$\beta$ decay using the COBRA demonstrator". In: *Phys. Rev. C* 94 (2 Aug. 2016), p. 024603. DOI: 10.1103/PhysRevC.94.024603. URL: https://link.aps.org/doi/10.1103/PhysRevC.94.024603.

[2] S. L. Glashow. "Partial-symmetries of weak interactions". In: *Nuclear Physics* 22.4 (1961), pp. 579–588. DOI: 10.1016/0029-5582(61)90469-2.

[3] A. Salam. "Elementary particle theory". In: *Prog. Of the Nobel Symposium, 1968, Stockholm, Sweden*. Vol. 367. 1968.

[4] S. Weinberg. "A Model of Leptons". In: *Physical Review Letters* 19.21 (1967), pp. 1264–1266. DOI: 10.1103/physrevlett.19.1264.

[5] Y. Fukuda et al. "Evidence for oscillation of atmospheric neutrinos". In: *Phys. Rev. Lett.* 81 (1998), pp. 1562–1567. DOI: 10.1103/PhysRevLett.81.1562. arXiv: hep-ex/9807003.

[6] Q. R. Ahmad et al. "Measurement of the rate of $\nu_e + d \rightarrow p + p + e^-$ interactions produced by $^8$B solar neutrinos at the Sudbury Neutrino Observatory". In: *Phys. Rev. Lett.* 87 (2001), p. 071301. DOI: 10.1103/PhysRevLett.87.071301. arXiv: nucl-ex/0106015.

[7] E. Majorana. "Über die Kerntheorie". In: *Zeitschrift für Physik* 82.3-4 (1933), pp. 137–145. DOI: 10.1007/bf01341484.

[8] Gary J. Feldman and Robert D. Cousins. "A Unified approach to the classical statistical analysis of small signals". In: *Phys. Rev. D* 57 (1998), pp. 3873–3889. DOI: 10.1103/PhysRevD.57.3873. arXiv: physics/9711021.

[9] MJ Cush. *Standard Model of Elementary Particles*. URL: https://en.wikipedia.org/wiki/File:Standard_Model_of_Elementary_Particles.svg.

[10] J. J. Thomson. *The discharge of electricity through gases*. 1898.

[11] J. Street and E. Stevenson. "New Evidence for the Existence of a Particle of Mass Intermediate Between the Proton and Electron". In: *Physical Review* 52 (1937), pp. 1003–1004.

[12] M. L. Perl et al. "Evidence for Anomalous Lepton Production in $e^+ - e^-$ Annihilation". In: *Phys. Rev. Lett.* 35 (22 Dec. 1975), pp. 1489–1492. DOI: 10.1103/PhysRevLett.35.1489. URL: https://link.aps.org/doi/10.1103/PhysRevLett.35.1489.

[13] Professor E. Rutherford F.R.S. "LXXIX. The scattering of  and  particles by matter and the structure of the atom". In: *The London, Edinburgh, and Dublin Philosophical Magazine and Journal of Science* (1911). DOI: 10.1080/14786440508637080.

[14] C. M. LATTES et al. "PROCESSES INVOLVING CHARGED MESONS". In: *Nature* 159.4047 (1947), pp. 694–697. DOI: 10.1038/159694a0.

[15] J. A. Angelo. *Nuclear Technology (Sourcebooks in modern technology)*. Greenwood Publishing Group, 2004.

[16] C. L. Cowan et al. "Detection of the Free Neutrino: a Confirmation". In: *Science* 124.3212 (1956), pp. 103–104. DOI: 10.1126/science.124.3212.103.

[17] F. Englert and R. Brout. "Broken Symmetry and the Mass of Gauge Vector Mesons". In: *Physical Review Letters* 13.9 (1964), pp. 321–323. DOI: 10.1103/physrevlett.13.321.

[18] P. W. Higgs. "Broken Symmetries and the Masses of Gauge Bosons". In: *Physical Review Letters* 13.16 (1964), pp. 508–509. DOI: 10.1103/physrevlett.13.508.

[19] G. S. Guralnik, C. R. Hagen, and T. W. Kibble. "Global Conservation Laws and Massless Particles". In: *Physical Review Letters* 13.20 (1964), pp. 585–587. DOI: 10.1103/physrevlett.13.585.

[20] S.M. Bilenky and J. Hošek. "Glashow-Weinberg-Salam theory of electroweak interactions and the neutral currents". In: *Physics Reports* 90.2 (1982), pp. 73–157. ISSN: 0370-1573. DOI: https://doi.org/10.1016/0370-1573(82)90016-3. URL: https://www.sciencedirect.com/science/article/pii/0370157382900163.

[21] Steven Weinberg. "Implications of Dynamical Symmetry Breaking". In: *Phys. Rev. D* 13 (1976). [Addendum: Phys.Rev.D 19, 1277–1280 (1979)], pp. 974–996. DOI: 10.1103/PhysRevD.19.1277.

[22] F. Capozzi et al. "Neutrino masses and mixings: Status of known and unknown 3  parameters". In: *Nuclear Physics B* 908 (2016), pp. 218–234. DOI: 10.1016/j.nuclphysb.2016.02.016.

[23] W. Heisenberg. "Über den Bau der Atomkerne. I". In: *Zeitschrift für Physik* 77.1-2 (1932), pp. 1–11. DOI: 10.1007/bf01342433.

[24] *the numerical approach to the strong force*$_2$016. June 2016. URL: https://webific.ific.uv.es/web/en/content/lattice-qcd-numerical-approach-strong-force.

[25] A. Das and T. Ferbel. *Introduction to nuclear and particle physics*. World Scientific, 2003.

[26] D. J. Gross and F. Wilczek. "Ultraviolet Behavior of Non-Abelian Gauge Theories". In: *Physical Review Letters* 30.26 (1973), pp. 1343–1346. DOI: 10.1103/physrevlett.30.1343.

[27] H. D. Politzer. "Reliable Perturbative Results for Strong Interactions?" In: *Physical Review Letters* 30.26 (1973), pp. 1346–1349. DOI: 10.1103/physrevlett.30.1346.

[28] D. J. Gross and F. Wilczek. "Asymptotically Free Gauge Theories. I". In: *Physical Review D* 8.10 (1973), pp. 3633–3652. DOI: 10.1103/physrevd.8.3633.

[29] D. J. Gross and F. Wilczek. "Asymptotically Free Gauge Theories. I". In: *Physical Review D* 8.10 (1973), pp. 3633–3652. DOI: 10.1103/physrevd.8.3633.

[30] Klaus Grotz, Hans V. Klapdor-Kleingrothaus, and Klaus Grotz. In: *The weak interaction in nuclear, particle and astrophysics*. Hilger, 1990, pp. 10–16.

[31] S. Chatrchyan et al. "Observation of a new boson at a mass of 125 GeV with the CMS experiment at the LHC". In: *Physics Letters B* 716.1 (2012), pp. 30–61. ISSN: 0370-2693. DOI: https://doi.org/10.1016/j.physletb.2012.08.021. URL: https://www.sciencedirect.com/science/article/pii/S0370269312008581.

[32] E. Rutherford. "VIII. Uranium radiation and the electrical conduction produced by it". In: *The London, Edinburgh, and Dublin Philosophical Magazine and Journal of Science* 47.284 (1899), pp. 109–163. DOI: 10.1080/14786449908621245.

[33] P. Villard. "Cathode Rays". In: *Scientific American* 83.19 (1900), pp. 291–291. DOI: 10.1038/scientificamerican11101900-291.

[34] Michael F. L'Annunziata. *Radioactivity Introduction and History, From the Quantum to Quarks*. Elsevier Science, 2016, pp. 123–134.

[35] Tosaka. *File:Decay chain(4n+2, Uranium series).PNG*. URL: https://commons.wikimedia.org/wiki/File:Decay_chain(4n%5C%2B2,_Uranium_series).PNG.

[36] Allan Franklin. "The prehistory of the neutrino". In: *International Conference on History of the Neutrino: 1930-2018*. 2019.

[37] "The average energy of disintegration of radium E". In: *Proceedings of the Royal Society of London. Series A, Containing Papers of a Mathematical and Physical Character* 117.776 (1927), pp. 109–123. DOI: 10.1098/rspa.1927.0168.

[38] V. Barger, D. Marfatia, and K. L. Whisnant. *The physics of neutrinos*. Princeton University Press, 2012.

[39] J. Chadwick. "Possible Existence of a Neutron". In: *Nature* 129.3252 (1932), pp. 312–312. DOI: 10.1038/129312a0.

[40] E. Fermi. "Versuch einer Theorie der $\beta$-Strahlen. I". In: *Zeitschrift für Physik* 88.3-4 (1934), pp. 161–177. DOI: 10.1007/bf01351864.

[41] Fred L. Wilson. "Fermi's Theory of Beta Decay". In: *American Journal of Physics* 36.12 (1968), pp. 1150–1160. DOI: 10.1119/1.1974382.

[42] Carl D. Anderson. "The Positive Electron". In: *Physical Review* 43.6 (1933), pp. 491–494. DOI: 10.1103/physrev.43.491.

[43] Augusto Gandini. "From the Chicago Pile 1 to next-generation reactors". In: *Enrico Fermi* (2004). DOI: 10.1007/978-3-662-01160-7_12.

[44] URL: http://hyperphysics.phy-astr.gsu.edu/hbase/Particles/cowan.html.

[45] Maurizio Salaris and Santi Cassisi. *Evolution of stars and stellar populationsTexte imprimé*. John Wiley, 2005.

[46] Boehm Félix and Petr Vogel. *Physics of massive neutrinos*. Cambridge University Press, 1992.

[47] V. Gribov and B. Pontecorvo. "Neutrino astronomy and lepton charge". In: *Physics Letters B* 28.7 (1969), pp. 493–496. ISSN: 0370-2693. DOI: https://doi.org/10.1016/0370-2693(69)90525-5. URL: https://www.sciencedirect.com/science/article/pii/0370269369905255.

[48] Y. Fukuda et al. "Evidence for Oscillation of Atmospheric Neutrinos". In: *Phys. Rev. Lett.* 81 (8 Aug. 1998), pp. 1562–1567. DOI: 10.1103/PhysRevLett.81.1562. URL: https://link.aps.org/doi/10.1103/PhysRevLett.81.1562.

[49] Q. R. Ahmad et al. "Measurement of the Rate of $\nu_e + d \rightarrow p + p + e^-$ Interactions Produced by $^8B$ Solar Neutrinos at the Sudbury Neutrino Observatory". In: *Phys. Rev. Lett.* 87 (7 July 2001), p. 071301. DOI: 10.1103/PhysRevLett.87.071301. URL: https://link.aps.org/doi/10.1103/PhysRevLett.87.071301.

[50] B. Pontecorvo. "Inverse beta processes and nonconservation of lepton charge". In: *Zh. Eksp. Teor. Fiz.* 34 (1957), p. 247.

[51] Ziro Maki, Masami Nakagawa, and Shoichi Sakata. "Remarks on the unified model of elementary particles". In: *Prog. Theor. Phys.* 28 (1962), pp. 870–880. DOI: 10.1143/PTP.28.870.

[52] Ivan Esteban et al. "Global analysis of three-flavour neutrino oscillations: synergies and tensions in the determination of $\theta_{23}$, $\delta_{CP}$, and the mass ordering". In: *JHEP* 01 (2019), p. 106. DOI: 10.1007/JHEP01(2019)106. arXiv: 1811.05487 [hep-ph].

[53] R. N. Cahn et al. "White Paper: Measuring the Neutrino Mass Hierarchy". In: *Community Summer Study 2013: Snowmass on the Mississippi*. July 2013. arXiv: 1307.5487 [hep-ex].

[54] K. Zuber. *Neutrino physics*. Taylor amp; Francis, 2012.

[55] John Dirk Walecka. In: *Introduction to modern physics: theoretical foundations*. World Scientific, 2008, pp. 157–161.

[56] J. Volkmer. "Prospects of the Iinvestigation of EC/Beta+ Decays With the COBRA Experiment". MA thesis. 2018.

[57] Bernhard Schwingenheuer. "Status and prospects of searches for neutrinoless double beta decay". In: *Annalen der Physik* 525.4 (2013), pp. 269–280. DOI: https://doi.org/10.1002/andp.201200222. eprint: https://onlinelibrary.wiley.com/doi/pdf/10.1002/andp.201200222. URL: https://onlinelibrary.wiley.com/doi/abs/10.1002/andp.201200222.

[58] M. Goeppert-Mayer. "Double Beta-Disintegration". In: *Physical Review* 48.6 (1935), pp. 512–516. DOI: 10.1103/physrev.48.512.

[59] S. R. Elliott, A. A. Hahn, and M. K. Moe. "Direct evidence for two-neutrino double-beta decay in Se82". In: *Physical Review Letters* 59.18 (1987), pp. 2020–2023. DOI: 10.1103/physrevlett.59.2020.

[60] Alexander Barabash. "Precise Half-Life Values for Two-Neutrino Double-$\beta$ Decay: 2020 Review". In: *Universe* 6.10 (2020), p. 159. DOI: 10.3390/universe6100159. arXiv: 2009.14451 [nucl-ex].

[61] R. Álvarez-Rodríguez et al. "Testing the single-state dominance hypothesis". In: *AIP Conference Proceedings* 1572.1 (2013), pp. 3–6. DOI: 10.1063/1.4856536. eprint: https://aip.scitation.org/doi/pdf/10.1063/1.4856536. URL: https://aip.scitation.org/doi/abs/10.1063/1.4856536.

[62] Ettore Majorana and Luciano Maiani. "A symmetric theory of electrons and positrons". In: *Ettore Majorana Scientific Papers: On occasion of the centenary of his birth*. Ed. by Giuseppe Franco Bassani. Berlin, Heidelberg: Springer Berlin Heidelberg, 2006, pp. 201–233. ISBN: 978-3-540-48095-2. DOI: 10.1007/978-3-540-48095-2_10. URL: https://doi.org/10.1007/978-3-540-48095-2_10.

[63] Alexey Vlasenko, George M. Fuller, and Vincenzo Cirigliano. "Neutrino Quantum Kinetics". In: *Phys. Rev. D* 89.10 (2014), p. 105004. DOI: 10.1103/PhysRevD.89.105004. arXiv: 1309.2628 [hep-ph].

[64] Mihai Horoi. "Shell model nuclear matrix elements for competing mechanisms contributing to double beta decay". In: *AIP Conference Proceedings* 1572.1 (2013), pp. 61–64. DOI: 10.1063/1.4856550. eprint: https://aip.scitation.org/doi/pdf/10.1063/1.4856550. URL: https://aip.scitation.org/doi/abs/10.1063/1.4856550.

[65] Ziro Maki, Masami Nakagawa, and Shoichi Sakata. "Remarks on the Unified Model of Elementary Particles". In: *Progress of Theoretical Physics* 28.5 (Nov. 1962), pp. 870–880. ISSN: 0033-068X. DOI: 10.1143/PTP.28.870. eprint: https://academic.oup.com/ptp/article-pdf/28/5/870/5258750/28-5-870.pdf. URL: https://doi.org/10.1143/PTP.28.870.

[66] A. S. Barabash. *Brief review of double beta decay experiments*. 2017. arXiv: 1702.06340 [nucl-ex].

[67] A. Giuliani et al. "Double Beta Decay APPEC Committee Report". In: (Oct. 2019). arXiv: 1910.04688 [hep-ex].

[68] Steven R. Elliott. "Experiments for neutrinoless double beta decay". In: *Int. J. Mod. Phys. A* 18 (2003). Ed. by R. Shrock, pp. 4097–4112. DOI: 10.1142/S0217751X03017397. arXiv: nucl-ex/0301011.

[69] R. Arnold et al. "Probing New Physics Models of Neutrinoless Double Beta Decay with SuperNEMO". In: *Eur. Phys. J. C* 70 (2010), pp. 927–943. DOI: 10.1140/epjc/s10052-010-1481-5. arXiv: 1005.1241 [hep-ex].

[70] R. Arnold et al. "Double-beta decay prototype detector with multiwire drift tubes in the Geiger mode". In: *Nucl. Phys. B Proc. Suppl.* 28 (1992). Ed. by A. Morales, J. Morales, and J. A. Villar, pp. 223–225. DOI: 10.1016/0920-5632(92)90175-R.

[71] R. Arnold et al. "Performance of a prototype tracking detector for double beta decay measurements". In: *Nucl. Instrum. Meth. A* 354 (1995), pp. 338–351. DOI: 10.1016/0168-9002(94)01025-0.

[72] R. Arnold et al. "Technical design and performance of the NEMO 3 detector". In: *Nucl. Instrum. Meth. A* 536 (2005), pp. 79–122. DOI: 10.1016/j.nima.2004.07.194. arXiv: physics/0402115.

[73] G. Anton et al. "Search for Neutrinoless Double-$\beta$ Decay with the Complete EXO-200 Dataset". In: *Phys. Rev. Lett.* 123.16 (2019), p. 161802. DOI: 10.1103/PhysRevLett.123.161802. arXiv: 1906.02723 [hep-ex].

[74] A. Gando et al. "Search for Majorana Neutrinos near the Inverted Mass Hierarchy Region with KamLAND-Zen". In: *Phys. Rev. Lett.* 117.8 (2016). [Addendum: Phys.Rev.Lett. 117, 109903 (2016)], p. 082503. DOI: 10.1103/PhysRevLett.117.082503. arXiv: 1605.02889 [hep-ex].

[75] M. Agostini et al. "GERDA results and the future perspectives for the neutrinoless double beta decay search using $^{76}$Ge". In: *Int. J. Mod. Phys. A* 33.09 (2018), p. 1843004. DOI: 10.1142/S0217751X18430042.

[76] N. Abgrall et al. "The Large Enriched Germanium Experiment for Neutrinoless Double Beta Decay (LEGEND)". In: *AIP Conf. Proc.* 1894.1 (2017). Ed. by Osvaldo Civitarese, Ivan Stekl, and Jouni Suhonen, p. 020027. DOI: 10.1063/1.5007652. arXiv: 1709.01980 [physics.ins-det].

[77] K. Zuber. "COBRA—double beta decay searches using CdTe detectors". In: *Physics Letters B* 519.1 (2001), pp. 1–7. ISSN: 0370-2693. DOI: https://doi.org/10.1016/S0370-2693(01)01056-5. URL: https://www.sciencedirect.com/science/article/pii/S0370269301010565.

[78] G. Bellini et al. "Cosmic-muon flux and annual modulation in Borexino at 3800 m water-equivalent depth". In: *Journal of Cosmology and Astroparticle Physics* 2012.05 (May 2012), pp. 015–015. DOI: 10.1088/1475-7516/2012/05/015. URL: https://doi.org/10.1088/1475-7516/2012/05/015.

[79] *The COBRA detector crystals*. Nov. 2020. URL: https://www.cobra-experiment.org/the_cobra_experiment/detectors/.

[80] K. Zuber. Aug. 2011. URL: https://www.cobra-experiment.org/.

[81] G. F. Knoll. "Chapter 11 - Semiconductor Diode Detectors". In: *Radiation Detection and Measurement*. 3rd. JOHN WILEY, 2009.

[82] *File:Electronic band diagram.svg*. URL: https://commons.wikimedia.org/wiki/File:Electronic_band_diagram.svg.

[83] S. N. Ahmed. *Physics and engineering of radiation detection*. ELSEVIER, 2017.

[84] J. Ketelaer et al. "TRIGA-SPEC: a setup for mass spectrometry and laser spectroscopy at the research reactor TRIGA Mainz". In: *Nuclear Instruments and Methods in Physics Research Section A: Accelerators, Spectrometers, Detectors and Associated Equipment* 594 (Sept. 2008), pp. 162–177. DOI: 10.1016/j.nima.2008.06.023.

[85] S.I. Sukhoruchkin and Z.N. Soroko. "Atomic Mass and Nuclear Binding Energy for Cd-114 (Cadmium)". In: Jan. 2009. DOI: 10.1007/978-3-540-69945-3_2845.

[86] ND Scielzo et al. "Double-$\beta$-decay Q values of Te 130, Te 128, and Te 120". In: *Physical Review C* 80.2 (2009), p. 025501.

[87] S.I. Sukhoruchkin and Z.N. Soroko. "Atomic Mass and Nuclear Binding Energy for Zn-70 (Zinc)". In: Jan. 2009. ISBN: 978-3-540-69944-6. DOI: 10.1007/978-3-540-69945-3_1315.

[88] S.I. Sukhoruchkin and Z.N. Soroko. "Atomic Mass and Nuclear Binding Energy for Zn-64 (Zinc)". In: Jan. 2009. DOI: 10.1007/978-3-540-69945-3_1309.

[89] S. Rahaman et al. "Double-beta decay Q values of 116Cd and 130Te". In: *Physics Letters B* 703.4 (2011), pp. 412–416. ISSN: 0370-2693. DOI: https://doi.org/10.1016/j.physletb.2011.07.078. URL: https://www.sciencedirect.com/science/article/pii/S0370269311008975.

[90] J. Meija et al. "Isotopic compositions of the elements 2013 (IUPAC Technical Report)". In: *Chemistry International* (2016).

[91] R. Temminghoff. *Updates on Radio-Purity and Zn Content, Presentation at the COBRA Collaboration Meeting in Dresden*. 2018.

[92] P. N. Luke. "Single-polarity charge sensing in ionization detectors using coplanar electrodes". In: *Applied Physics Letters* 65.22 (1994), pp. 2884–2886. DOI: 10.1063/1.112523.

[93] M. Fritts et al. "Pulse-shape discrimination of surface events in CdZnTe detectors for the COBRA experiment". In: *Nucl. Instrum. Meth. A* 749 (2014), pp. 27–34. DOI: 10.1016/j.nima.2014.02.038. arXiv: 1401.5844 [nucl-ex].

[94] W. Shockley. "Currents to Conductors Induced by a Moving Point Charge". In: *Journal of Applied Physics* 9.10 (1938), pp. 635–636. DOI: 10.1063/1.1710367.

[95] S. Ramo. "Currents Induced by Electron Motion". In: *Proceedings of the IRE* 27.9 (1939), pp. 584–585. DOI: 10.1109/jrproc.1939.228757.

[96] S. Zatschler. "Pulse-shape studies with coplanar grid CdZnTe detectors and searches for rare nuclear decays with the COBRA experiment". PhD thesis. Dresden, Tech. U., TU, Dresden (main), 2020.

[97] Miroslav Macko. "SuperNEMO Experiment: Study of Systematic Uncertainties of Track Reconstruction and Energy Calibration. Evaluation of Sensitivity to 0nbb with Emission of Majoron for 82 Se." 2018BORD0368. PhD thesis. 2018. URL: http://www.theses.fr/2018BORD0368/document.

[98] "Outline of a Theory of Statistical Estimation Based on the Classical Theory of Probability". In: *Philosophical Transactions of the Royal Society of London. Series A, Mathematical and Physical Sciences* 236.767 (1937), pp. 333–380. DOI: 10.1098/rsta.1937.0005.

[99] J. Kuttler. "Investigation of the 2nuBB-spectrum of 116Cd with the COBRA experiment". MA thesis. 2019.

[100] S. Zatschler. *Potential of various double beta decay searches, Presentation at the COBRA Collaboration Meeting*. 2020.

[101] Lucas Bodenstein-Dresler et al. "The COBRA Experiment Annual Report 2018)". In: (2018).

[102] Joachim Ebert et al. "Results of a search for neutrinoless double-$\beta$ decay using the COBRA demonstrator". In: *Phys. Rev. C* 94 (2 Aug. 2016), p. 024603. DOI: 10.1103/PhysRevC.94.024603. URL: https://link.aps.org/doi/10.1103/PhysRevC.94.024603.

Appendix A

# APPENDIX A

## A.1 Step-By-Step Derivation of $\frac{\partial T_{1/2}}{\partial r_q} = 0$

To derive $\frac{\partial T_{1/2}}{\partial r_q} = 0$, I will make use of the Fundamental Theorem of Calculus which can be summarized as:

$$\mathrm{F}(x) = \int_a^b f(x)dx, \qquad \mathrm{F}'(x) = f(x)\ ,$$

then

$$\int_a^b f(x) = \ \mathrm{F}(b) - \mathrm{F}(a).$$

This can be applied as follows:

$$\frac{\partial}{\partial r_q}\int_{l_p}^{r_p} \rho_p(E)dE = \frac{\partial(R_p(r_p) - R_p(l_p))}{\partial r_q} = \delta_{pq}\rho_p(r_p), \tag{A.1}$$

$$\frac{\partial}{\partial r_q}\int_{l_p}^{r_p} \beta_p(E)dE = \frac{\partial(B_p(r_p) - B_p(l_p))}{\partial r_q} = \delta_{pq}\beta_p(r_p). \tag{A.2}$$

Here, $\delta_{pq}$ is the Kronecker delta. This result will be used in the derivation.

$$\frac{\partial T_{1/2}}{\partial r_q} = \frac{\partial}{\partial r_q}\left(N_A\frac{ln(2)}{W}a\frac{\sum_p m_p t_p \mathcal{E}_{dp}\int_{l_p}^{r_p}\rho_p(E)dE}{\mathcal{S}(\bar{b})}\right) \tag{A.3}$$

$$= N_A\frac{ln(2)}{W}a\frac{\partial}{\partial r_q}\left(\frac{\sum_p m_p t_p \mathcal{E}_{dp}\int_{l_p}^{r_p}\rho_p(E)dE}{\mathcal{S}(\sum_p m_p t_p\int_{l_p}^{r_p}\beta_p(E)dE)}\right) \tag{A.4}$$

$$= N_A\frac{ln(2)}{W}a\left(\frac{\sum_p m_p t_p \mathcal{E}_{dp}\delta_{pq}\rho_p(r_p)}{\mathcal{S}(\bar{b})} - \right.$$

$$\left. - \ \frac{\sum_p m_p t_p \mathcal{E}_p \mathcal{S}'(\bar{b})\sum_\varrho m_\varrho t_\varrho \delta_{\varrho q}\beta_p(r_p)}{\mathcal{S}^2(\bar{b})}\right) \tag{A.5}$$

Where I used a different index for the second sum $\varrho$ in the numerator of the second term, and I used the fact that $\mathcal{E} = \mathcal{E}_d\mathcal{E}_C$ as defined in equation 4.7. The equation

can be simplified:

$$\frac{\partial T_{1/2}}{\partial r_q} = N_A \frac{ln(2)}{W} a \left( \frac{m_q t_q \mathcal{E}_{dq} \rho_q(r_q)}{\mathcal{S}(\bar{b})} \frac{\sum_p m_p t_p \mathcal{E}_p}{\sum_p m_p t_p \mathcal{E}_p} - \frac{\sum_p m_p t_p \mathcal{E}_p \mathcal{S}'(\bar{b}) m_q t_q \beta_q(r_q)}{\mathcal{S}^2(\bar{b})} \right) \quad \text{(A.6)}$$

$$= N_A \frac{ln(2)}{W} a \frac{\sum_p m_p t_p \mathcal{E}_p}{\mathcal{S}(\bar{b})} \left( \frac{m_p t_p \rho_q(r_q)}{\sum_p m_p t_p \mathcal{E}_p} - \frac{\mathcal{S}'(\bar{b}) m_q t_q \beta_q(r_q)}{\mathcal{S}(\bar{b})} \right) \quad \text{(A.7)}$$

$$= T_{1/2} \left( \frac{m_p t_p \rho_q(r_q)}{\sum_p m_p t_p \mathcal{E}_p} - \frac{\mathcal{S}'(\bar{b}) m_q t_q \beta_q(r_q)}{\mathcal{S}(\bar{b})} \right) = 0. \quad \text{(A.8)}$$

## A.2 Step-By-Step Derivation of Bounds For Exponential Background

Gaussian signal function $\rho$:

$$\rho = \frac{\mathcal{E}}{\sigma\sqrt{2\pi}} e^{-\frac{(E-Q)^2}{2\sigma^2}}. \quad \text{(A.9)}$$

Exponential Background function $\beta$:

$$\beta = \beta_0 e^{-\lambda E}. \quad \text{(A.10)}$$

To derive equations for left and right bounds, the equation $\frac{\rho}{\beta}$ is solved for $E$:

$$\frac{\rho}{\beta} = \frac{\mathcal{E}}{\sigma\sqrt{2\pi}} e^{-\frac{(E-Q)^2}{2\sigma^2}} \frac{1}{\beta_0} e^{\lambda E} \quad \text{(A.11)}$$

$$\frac{\beta_0 \sigma\sqrt{2\pi}}{\mathcal{E}} \frac{\rho}{\beta} = e^{\lambda E - \frac{1}{2\sigma^2}(E-Q)^2} \quad \text{(A.12)}$$

$$ln\left( \frac{\beta_0 \sigma\sqrt{2\pi}}{\mathcal{E}} \frac{\rho}{\beta} \right) = \lambda E - \frac{1}{2\sigma^2} E^2 + \frac{Q}{\sigma^2} E - \frac{Q^2}{2\sigma^2} \quad \text{(A.13)}$$

$$0 = \frac{1}{2\sigma^2} E^2 - \left( \lambda + \frac{Q}{\sigma^2} \right) E + \frac{Q^2}{2\sigma^2} + ln\left( \frac{\beta_0 \sigma\sqrt{2\pi}}{\mathcal{E}} \frac{\rho}{\beta} \right) \quad \text{(A.14)}$$

We have obtained a quadratic equation for $E$. The roots can be found by the application of quadratic formula:

$$E_{1,2} = \frac{\lambda + \frac{Q}{\sigma^2} \pm \sqrt{\lambda^2 + 2\frac{\lambda Q}{\sigma^2} - \frac{2}{\sigma^2} ln\left( \frac{\beta_0 \sigma\sqrt{2\pi}}{\mathcal{E}} \frac{\rho}{\beta} \right)}}{\frac{1}{\sigma^2}} \quad \text{(A.15)}$$

$$= Q + \sigma^2 \lambda \pm \sigma^2 \sqrt{\lambda^2 + 2\frac{\lambda Q}{\sigma^2} - \frac{2}{\sigma^2} ln\left( \frac{\beta_0 \sigma\sqrt{2\pi}}{\mathcal{E}} \frac{\rho}{\beta} \right)} \quad \text{(A.16)}$$

$$= Q + \sigma^2 \lambda \pm \sigma \sqrt{(\lambda\sigma)^2 + 2\lambda Q - 2ln\left( \frac{\beta_0 \sigma\sqrt{2\pi}}{\mathcal{E}} \frac{\rho}{\beta} \right)} \quad \text{(A.17)}$$

Finally, we can define $r \equiv E_1$ and $l \equiv E_2$:

$$r = Q + \sigma^2\lambda + \sigma\sqrt{(\lambda\sigma)^2 + 2\lambda Q - 2ln\left(\frac{\beta_0\sigma\sqrt{2\pi}}{\mathcal{E}}\frac{\rho}{\beta}\right)} \quad \text{(A.18)}$$

$$l = Q + \sigma^2\lambda - \sigma\sqrt{(\lambda\sigma)^2 + 2\lambda Q - 2ln\left(\frac{\beta_0\sigma\sqrt{2\pi}}{\mathcal{E}}\frac{\rho}{\beta}\right)} \quad \text{(A.19)}$$

Appendix B

# TABLE OF PARTITIONS

Table B.1: List of all partitions from the entire COBRA Demonstrator dataset (2013 - 2019). The partitions are described in detail in Section 4.1.3. There are two partitions per row, one for low-z and one for high-z. The first column of the table contains the partition number for low-z/high-z partition. The second column contains the detector number. The third column contains the start date of the partition in format: Day/Month/Year. The fourth column contains the total duration in days for which the partition was active. The fifth column contains the mass of the partition (detector) in grams. The sixth column contains the number of events within the partition for low-z/high-z partitions. The last three columns contain the calibration constants $p_0$, $p_1$, $p_2$.

| **Partition No.** | **D. No.** | **Start date** | **Dur. [d]** | **m [g]** | **Events** | **$p_0$ [keV]** | **$p_1$ [keV]** | **$p_2$ [keV]** |
|---|---|---|---|---|---|---|---|---|
| 1/1404 | 1 | 8/3/2013 | 31.5 | 5.90 | 1338/1300 | 15.7 | 0.86 | 6.5E-07 |
| 2/1405 | 1 | 10/4/2013 | 65.7 | 5.90 | 2663/2632 | 15.4 | 0.83 | -2.2E-07 |
| 3/1406 | 1 | 9/7/2013 | 0.3 | 5.90 | 11/16 | 14.5 | 0.84 | 1.3E-06 |
| 4/1407 | 1 | 11/7/2013 | 18.3 | 5.90 | 563/572 | 12.5 | 0.87 | 7.0E-07 |
| 5/1408 | 1 | 1/8/2013 | 8.0 | 5.90 | 257/259 | 10.3 | 0.91 | 1.6E-07 |
| 6/1409 | 1 | 12/8/2013 | 11.6 | 5.90 | 379/331 | 10.3 | 0.93 | 2.3E-06 |
| 7/1410 | 1 | 27/8/2013 | 2.5 | 5.90 | 76/88 | 12.6 | 0.85 | -4.9E-03 |
| 8/1411 | 1 | 5/9/2013 | 23.0 | 5.90 | 718/671 | 13.1 | 0.83 | -4.9E-03 |
| 9/1412 | 1 | 9/10/2013 | 14.6 | 5.90 | 435/447 | 12.6 | 0.86 | 3.6E-08 |
| 10/1413 | 1 | 29/10/2013 | 7.9 | 5.90 | 223/220 | 13.2 | 0.86 | 5.2E-06 |
| 11/1414 | 1 | 21/11/2013 | 4.8 | 5.90 | 67/81 | 17.4 | 0.75 | 2.5E-03 |
| 12/1415 | 1 | 29/11/2013 | 1.3 | 5.90 | 25/20 | 15.4 | 0.78 | 2.5E-03 |
| 13/1416 | 1 | 10/1/2014 | 4.6 | 5.90 | 120/98 | 15.8 | 0.83 | 3.1E-07 |
| 14/1417 | 1 | 24/1/2014 | 38.4 | 5.90 | 691/745 | 16.3 | 0.79 | 5.7E-07 |
| 15/1418 | 1 | 6/3/2014 | 22.6 | 5.90 | 311/374 | 15.8 | 0.79 | 1.5E-06 |
| 16/1419 | 1 | 3/4/2014 | 18.4 | 5.90 | 130/174 | 31.7 | 0.79 | 2.3E-06 |
| 17/1420 | 1 | 26/4/2014 | 46.9 | 5.90 | 225/416 | 48.1 | 0.77 | 2.1E-06 |
| 18/1421 | 1 | 19/6/2014 | 73.9 | 5.90 | 329/763 | 31.9 | 0.76 | 1.1E-06 |
| 19/1422 | 1 | 5/9/2014 | 24.5 | 5.90 | 249/315 | 15.3 | 0.78 | 1.2E-06 |
| 20/1423 | 1 | 2/10/2014 | 102.5 | 5.90 | 1417/1660 | 13.8 | 0.87 | 1.2E-06 |
| 21/1424 | 1 | 25/2/2015 | 50.1 | 5.90 | 528/530 | 16.5 | 0.75 | 2.6E-08 |
| 22/1425 | 1 | 6/5/2015 | 157.0 | 5.90 | 1533/1560 | 18.2 | 0.70 | 2.7E-06 |
| 23/1426 | 1 | 1/11/2015 | 99.7 | 5.90 | 489/498 | 19.4 | 0.66 | 5.7E-06 |
| 24/1427 | 1 | 22/2/2016 | 89.1 | 5.90 | 664/737 | 18.5 | 0.70 | 4.9E-06 |
| 25/1428 | 1 | 20/6/2016 | 72.0 | 5.90 | 1107/1199 | 19.4 | 0.66 | 5.7E-06 |
| 26/1429 | 1 | 5/11/2018 | 173.1 | 5.90 | 3558/3708 | 21.7 | 0.70 | 9.5E-03 |
| 27/1430 | 1 | 25/5/2019 | 126.3 | 5.90 | 2661/2626 | 18.3 | 0.61 | 1.0E-02 |
| 28/1431 | 2 | 8/3/2013 | 31.5 | 5.89 | 975/935 | 15.2 | 0.64 | 5.4E-03 |
| 29/1432 | 2 | 10/4/2013 | 65.7 | 5.89 | 1991/1934 | 16.0 | 0.67 | 1.1E-03 |
| 30/1433 | 2 | 9/7/2013 | 0.3 | 5.89 | 12/6 | 17.1 | 0.59 | -2.6E-07 |
| 31/1434 | 2 | 11/7/2013 | 18.3 | 5.89 | 357/361 | 15.6 | 0.63 | -1.7E-07 |
| 32/1435 | 2 | 1/8/2013 | 8.0 | 5.89 | 52/68 | 14.9 | 0.65 | 3.7E-07 |
| 33/1436 | 2 | 12/8/2013 | 11.6 | 5.89 | 82/100 | 15.3 | 0.67 | 7.1E-07 |
| 34/1437 | 2 | 27/8/2013 | 2.5 | 5.89 | 24/31 | 15.8 | 0.68 | 4.2E-04 |
| 35/1438 | 2 | 5/9/2013 | 23.0 | 5.89 | 259/278 | 15.3 | 0.71 | 4.2E-04 |
| 36/1439 | 2 | 9/10/2013 | 14.6 | 5.89 | 72/83 | 15.2 | 0.70 | -1.0E-07 |
| 37/1440 | 2 | 29/10/2013 | 7.9 | 5.89 | 16/26 | 15.7 | 0.67 | 2.5E-03 |
| 38/1441 | 2 | 21/11/2013 | 4.8 | 5.89 | 60/67 | 19.0 | 0.59 | 1.8E-03 |
| 39/1442 | 2 | 29/11/2013 | 1.3 | 5.89 | 21/23 | 17.6 | 0.60 | 9.6E-04 |
| 40/1443 | 2 | 10/1/2014 | 4.6 | 5.89 | 40/50 | 19.2 | 0.55 | 1.2E-03 |

| Partition No. | D. No. | Start date | Dur. [d] | m [g] | Events | $p_0$ [keV] | $p_1$ [keV] | $p_2$ [keV] |
|---|---|---|---|---|---|---|---|---|
| 41/1444 | 2 | 24/1/2014 | 38.4 | 5.89 | 290/315 | 19.3 | 0.56 | 1.6E-03 |
| 42/1445 | 2 | 6/3/2014 | 22.6 | 5.89 | 199/201 | 18.8 | 0.55 | 2.3E-03 |
| 43/1446 | 2 | 3/4/2014 | 65.3 | 5.89 | 491/478 | 18.5 | 0.55 | 3.8E-03 |
| 44/1447 | 2 | 19/6/2014 | 73.9 | 5.89 | 500/484 | 18.3 | 0.58 | 1.9E-03 |
| 45/1448 | 2 | 5/9/2014 | 24.5 | 5.89 | 240/269 | 19.3 | 0.56 | 4.6E-03 |
| 46/1449 | 2 | 2/10/2014 | 102.5 | 5.89 | 2096/2070 | 20.5 | 0.52 | 4.6E-03 |
| 47/1450 | 2 | 25/2/2015 | 50.1 | 5.89 | 617/593 | 19.5 | 0.63 | 9.1E-07 |
| 48/1451 | 2 | 6/5/2015 | 157.0 | 5.89 | 1821/1791 | 20.9 | 0.63 | 1.7E-07 |
| 49/1452 | 2 | 1/11/2015 | 99.7 | 5.89 | 542/480 | 22.0 | 0.55 | 4.3E-08 |
| 50/1453 | 2 | 22/2/2016 | 89.1 | 5.89 | 690/661 | 21.9 | 0.48 | 1.7E-06 |
| 51/1454 | 2 | 20/6/2016 | 72.0 | 5.89 | 640/628 | 22.2 | 0.48 | -6.4E-08 |
| 52/1455 | 2 | 5/11/2018 | 173.1 | 5.89 | 5306/4920 | 23.0 | 0.28 | 5.4E-03 |
| 53/1456 | 2 | 25/5/2019 | 126.3 | 5.89 | 1748/1697 | 23.9 | 0.31 | 8.1E-03 |
| 54/1457 | 3 | 8/3/2013 | 31.5 | 5.85 | 967/903 | 22.1 | 0.72 | -1.4E-08 |
| 55/1458 | 3 | 10/4/2013 | 65.7 | 5.85 | 1905/1763 | 21.7 | 0.70 | -2.3E-07 |
| 56/1459 | 3 | 25/2/2015 | 50.1 | 5.85 | 1497/1341 | 19.4 | 0.85 | 3.6E-07 |
| 57/1460 | 3 | 6/5/2015 | 157.0 | 5.85 | 4007/3456 | 21.8 | 0.75 | 8.3E-08 |
| 58/1461 | 3 | 1/11/2015 | 99.7 | 5.85 | 1324/1137 | 19.5 | 0.79 | -5.3E-07 |
| 59/1462 | 3 | 22/2/2016 | 89.1 | 5.85 | 1646/2587 | 13.1 | 1.01 | 2.3E-06 |
| 60/1463 | 3 | 20/6/2016 | 72.0 | 5.85 | 398/375 | 16.4 | 0.90 | -1.1E-06 |
| 61/1464 | 3 | 31/7/2017 | 174.1 | 5.85 | 1000/768 | 22.4 | 0.57 | 2.3E-02 |
| 62/1465 | 3 | 5/11/2018 | 173.1 | 5.85 | 3686/3628 | 20.5 | 0.68 | 1.2E-02 |
| 63/1466 | 3 | 25/5/2019 | 126.3 | 5.85 | 70/287 | 20.9 | 0.80 | 1.5E-02 |
| 64/1467 | 4 | 8/3/2013 | 31.5 | 5.91 | 1047/998 | 17.8 | 0.84 | 1.2E-03 |
| 65/1468 | 4 | 10/4/2013 | 65.7 | 5.91 | 2120/1993 | 18.6 | 0.82 | 1.2E-03 |
| 66/1469 | 4 | 9/7/2013 | 0.3 | 5.91 | 5/7 | 17.0 | 0.85 | 1.1E-06 |
| 67/1470 | 4 | 11/7/2013 | 18.3 | 5.91 | 437/399 | 17.5 | 0.75 | 4.0E-03 |
| 68/1471 | 4 | 1/8/2013 | 8.0 | 5.91 | 183/154 | 17.2 | 0.74 | 4.0E-03 |
| 69/1472 | 4 | 12/8/2013 | 11.6 | 5.91 | 251/230 | 16.9 | 0.80 | 8.9E-07 |
| 70/1473 | 4 | 27/8/2013 | 2.5 | 5.91 | 55/54 | 16.9 | 0.82 | -2.2E-07 |
| 71/1474 | 4 | 5/9/2013 | 23.0 | 5.91 | 515/488 | 16.7 | 0.82 | -9.9E-07 |
| 72/1475 | 4 | 9/10/2013 | 14.6 | 5.91 | 332/299 | 16.3 | 0.82 | 3.0E-07 |
| 73/1476 | 4 | 29/10/2013 | 7.9 | 5.91 | 182/163 | 15.5 | 0.83 | 1.5E-06 |
| 74/1477 | 5 | 8/3/2013 | 31.5 | 5.86 | 1482/1515 | 14.2 | 0.63 | -1.1E-07 |
| 75/1478 | 5 | 10/4/2013 | 65.6 | 5.86 | 3048/3230 | 14.4 | 0.60 | -5.3E-08 |
| 76/1479 | 5 | 9/7/2013 | 0.3 | 5.86 | 9/17 | 17.7 | 0.59 | -4.2E-07 |
| 77/1480 | 5 | 11/7/2013 | 19.3 | 5.86 | 579/621 | 14.0 | 0.67 | 3.5E-03 |
| 78/1481 | 5 | 1/8/2013 | 8.0 | 5.86 | 70/111 | 13.5 | 0.65 | 6.4E-03 |
| 79/1482 | 5 | 12/8/2013 | 11.6 | 5.86 | 132/182 | 15.6 | 0.56 | 2.9E-03 |
| 80/1483 | 5 | 27/8/2013 | 2.5 | 5.86 | 27/34 | 16.1 | 0.61 | 2.8E-07 |
| 81/1484 | 5 | 5/9/2013 | 23.0 | 5.86 | 368/420 | 12.9 | 0.76 | 8.1E-07 |
| 82/1485 | 5 | 9/10/2013 | 14.6 | 5.86 | 283/373 | 12.4 | 0.73 | 5.2E-07 |
| 83/1486 | 5 | 29/10/2013 | 8.1 | 5.86 | 28/76 | 14.9 | 0.60 | 2.3E-03 |
| 84/1487 | 5 | 21/11/2013 | 4.8 | 5.86 | 174/176 | 18.5 | 0.68 | 8.5E-07 |
| 85/1488 | 5 | 29/11/2013 | 1.3 | 5.86 | 53/55 | 17.4 | 0.70 | 1.5E-06 |
| 86/1489 | 5 | 10/1/2014 | 4.6 | 5.86 | 201/201 | 19.9 | 0.65 | 7.1E-06 |
| 87/1490 | 5 | 24/1/2014 | 38.7 | 5.86 | 1336/1449 | 18.6 | 0.76 | 7.0E-06 |
| 88/1491 | 5 | 6/3/2014 | 26.5 | 5.86 | 1035/1037 | 18.7 | 0.74 | 1.1E-07 |
| 89/1492 | 5 | 3/4/2014 | 18.4 | 5.86 | 808/889 | 18.6 | 0.71 | 5.9E-07 |
| 90/1493 | 5 | 26/4/2014 | 47.0 | 5.86 | 1876/2013 | 19.9 | 0.72 | -2.1E-07 |
| 91/1494 | 5 | 19/6/2014 | 74.2 | 5.86 | 2750/2843 | 20.5 | 0.69 | -1.9E-08 |
| 92/1495 | 5 | 5/9/2014 | 24.4 | 5.86 | 919/962 | 20.2 | 0.67 | 2.2E-08 |
| 93/1496 | 5 | 2/10/2014 | 102.6 | 5.86 | 3958/3929 | 20.8 | 0.69 | -1.2E-06 |
| 94/1497 | 5 | 25/2/2015 | 48.9 | 5.86 | 1187/1183 | 22.1 | 0.75 | 1.8E-06 |
| 95/1498 | 5 | 6/5/2015 | 152.7 | 5.86 | 3603/3627 | 23.0 | 0.72 | -4.0E-07 |
| 96/1499 | 5 | 1/11/2015 | 95.1 | 5.86 | 1035/1042 | 23.7 | 0.67 | 2.5E-07 |
| 97/1500 | 5 | 21/2/2016 | 88.6 | 5.86 | 1233/1241 | 23.0 | 0.74 | 1.1E-05 |
| 98/1501 | 5 | 21/6/2016 | 67.4 | 5.86 | 696/811 | 23.8 | 0.63 | 3.6E-07 |
| 99/1502 | 5 | 2/10/2016 | 134.1 | 5.86 | 3356/3545 | 24.4 | 0.64 | 5.0E-04 |
| 100/1503 | 5 | 20/5/2017 | 56.2 | 5.86 | 1382/1547 | 19.9 | 0.68 | 1.0E-03 |
| 101/1504 | 5 | 31/7/2017 | 168.6 | 5.86 | 2688/2667 | 14.8 | 0.72 | 1.0E-03 |
| 102/1505 | 5 | 23/7/2018 | 3.7 | 5.86 | 11/23 | 20.9 | 0.77 | 8.0E-03 |
| 103/1506 | 5 | 5/11/2018 | 174.0 | 5.86 | 3723/4014 | 22.1 | 0.25 | 1.3E-02 |
| 104/1507 | 5 | 25/5/2019 | 126.7 | 5.86 | 299/370 | 24.3 | 0.37 | 1.5E-02 |
| 105/1508 | 6 | 8/3/2013 | 31.5 | 5.88 | 1106/1177 | 16.3 | 0.76 | 3.1E-07 |
| 106/1509 | 6 | 10/4/2013 | 65.6 | 5.88 | 2435/2423 | 15.7 | 0.80 | 1.8E-07 |
| 107/1510 | 6 | 9/7/2013 | 0.3 | 5.88 | 11/18 | 15.8 | 0.52 | -4.6E-07 |
| 108/1511 | 6 | 11/7/2013 | 19.3 | 5.88 | 582/608 | 15.7 | 0.50 | 3.2E-03 |
| 109/1512 | 6 | 1/8/2013 | 8.0 | 5.88 | 122/117 | 15.8 | 0.49 | 3.5E-03 |
| 110/1513 | 6 | 12/8/2013 | 11.6 | 5.88 | 198/179 | 15.7 | 0.55 | 3.2E-04 |
| 111/1514 | 6 | 27/8/2013 | 2.5 | 5.88 | 40/26 | 15.4 | 0.56 | 8.2E-08 |
| 112/1515 | 6 | 5/9/2013 | 23.0 | 5.88 | 517/581 | 15.0 | 0.54 | 4.0E-08 |

| Partition No. | D. No. | Start date | Dur. [d] | m [g] | Events | $p_0$ [keV] | $p_1$ [keV] | $p_2$ [keV] |
|---|---|---|---|---|---|---|---|---|
| 113/1516 | 6 | 9/10/2013 | 14.6 | 5.88 | 489/511 | 15.4 | 0.52 | -3.3E-07 |
| 114/1517 | 6 | 29/10/2013 | 8.1 | 5.88 | 139/150 | 15.1 | 0.55 | -3.3E-07 |
| 115/1518 | 6 | 21/11/2013 | 4.8 | 5.88 | 108/87 | 16.8 | 0.48 | 2.8E-03 |
| 116/1519 | 6 | 29/11/2013 | 1.3 | 5.88 | 44/47 | 16.1 | 0.44 | 2.8E-03 |
| 117/1520 | 6 | 10/1/2014 | 4.6 | 5.88 | 181/163 | 16.8 | 0.47 | -3.7E-03 |
| 118/1521 | 6 | 24/1/2014 | 38.7 | 5.88 | 1315/1268 | 17.4 | 0.44 | -3.7E-03 |
| 119/1522 | 6 | 6/3/2014 | 26.5 | 5.88 | 894/801 | 16.4 | 0.48 | -3.9E-08 |
| 120/1523 | 6 | 3/4/2014 | 18.4 | 5.88 | 623/591 | 19.9 | 0.54 | 1.1E-07 |
| 121/1524 | 6 | 26/4/2014 | 47.0 | 5.88 | 1396/1282 | 23.8 | 0.60 | 9.5E-08 |
| 122/1525 | 6 | 19/6/2014 | 74.2 | 5.88 | 1787/1672 | 19.5 | 0.56 | 8.4E-07 |
| 123/1526 | 6 | 5/9/2014 | 24.4 | 5.88 | 734/750 | 16.2 | 0.48 | 2.9E-03 |
| 124/1527 | 6 | 2/10/2014 | 102.6 | 5.88 | 3294/3256 | 16.9 | 0.49 | 2.9E-03 |
| 125/1528 | 6 | 25/2/2015 | 48.9 | 5.88 | 1206/1175 | 17.9 | 0.51 | 1.2E-06 |
| 126/1529 | 6 | 6/5/2015 | 152.7 | 5.88 | 3455/3261 | 18.9 | 0.53 | 2.8E-06 |
| 127/1530 | 6 | 1/11/2015 | 95.1 | 5.88 | 946/924 | 20.9 | 0.51 | 1.6E-06 |
| 128/1531 | 6 | 21/2/2016 | 88.6 | 5.88 | 1273/1214 | 21.1 | 0.57 | 1.3E-06 |
| 129/1532 | 6 | 21/6/2016 | 67.4 | 5.88 | 1260/1226 | 22.0 | 0.49 | -2.8E-07 |
| 130/1533 | 6 | 2/10/2016 | 134.1 | 5.88 | 2824/2845 | 21.6 | 0.50 | 1.6E-03 |
| 131/1534 | 6 | 20/5/2017 | 56.2 | 5.88 | 1086/1080 | 17.8 | 0.52 | 4.2E-03 |
| 132/1535 | 6 | 31/7/2017 | 168.6 | 5.88 | 3134/3072 | 18.7 | 0.50 | 6.7E-03 |
| 133/1536 | 6 | 23/7/2018 | 3.7 | 5.88 | 13/13 | 22.5 | 0.37 | 4.0E-03 |
| 134/1537 | 6 | 5/11/2018 | 174.0 | 5.88 | 4471/4237 | 20.2 | 0.19 | 7.6E-03 |
| 135/1538 | 6 | 25/5/2019 | 126.7 | 5.88 | 1702/1669 | 19.4 | 0.54 | 3.0E-03 |
| 136/1539 | 7 | 8/3/2013 | 31.5 | 5.83 | 1152/1233 | 14.5 | 0.69 | 1.6E-07 |
| 137/1540 | 7 | 10/4/2013 | 65.6 | 5.83 | 2613/2634 | 14.7 | 0.64 | 5.9E-03 |
| 138/1541 | 7 | 9/7/2013 | 0.3 | 5.83 | 13/18 | 16.7 | 0.55 | 6.5E-03 |
| 139/1542 | 7 | 11/7/2013 | 19.3 | 5.83 | 601/554 | 16.9 | 0.56 | 2.1E-03 |
| 140/1543 | 7 | 1/8/2013 | 8.0 | 5.83 | 73/96 | 15.9 | 0.56 | 2.4E-03 |
| 141/1544 | 7 | 12/8/2013 | 11.6 | 5.83 | 108/149 | 16.2 | 0.57 | 9.5E-04 |
| 142/1545 | 7 | 27/8/2013 | 2.5 | 5.83 | 33/19 | 16.5 | 0.62 | -3.2E-07 |
| 143/1546 | 7 | 5/9/2013 | 23.0 | 5.83 | 362/391 | 16.6 | 0.64 | 3.8E-07 |
| 144/1547 | 7 | 9/10/2013 | 14.6 | 5.83 | 381/434 | 17.2 | 0.59 | 8.3E-07 |
| 145/1548 | 7 | 29/10/2013 | 8.1 | 5.83 | 71/92 | 16.6 | 0.58 | 3.3E-07 |
| 146/1549 | 7 | 21/11/2013 | 4.8 | 5.83 | 140/119 | 16.6 | 0.66 | 3.5E-06 |
| 147/1550 | 7 | 29/11/2013 | 1.3 | 5.83 | 42/50 | 16.2 | 0.63 | 3.6E-03 |
| 148/1551 | 7 | 10/1/2014 | 4.6 | 5.83 | 188/156 | 18.1 | 0.67 | -3.8E-07 |
| 149/1552 | 7 | 24/1/2014 | 38.7 | 5.83 | 1196/1266 | 18.9 | 0.71 | -1.3E-06 |
| 150/1553 | 7 | 6/3/2014 | 44.9 | 5.83 | 1273/1435 | 19.8 | 0.71 | -1.9E-06 |
| 151/1554 | 7 | 26/4/2014 | 47.0 | 5.83 | 977/1150 | 22.4 | 0.69 | -5.3E-07 |
| 152/1555 | 7 | 19/6/2014 | 74.2 | 5.83 | 1266/1440 | 22.6 | 0.65 | 1.3E-03 |
| 153/1556 | 7 | 5/9/2014 | 24.4 | 5.83 | 678/655 | 21.1 | 0.65 | 1.3E-03 |
| 154/1557 | 7 | 2/10/2014 | 102.6 | 5.83 | 2612/2868 | 23.3 | 0.65 | 1.9E-06 |
| 155/1558 | 7 | 25/2/2015 | 48.9 | 5.83 | 1099/1167 | 25.8 | 0.66 | 5.0E-07 |
| 156/1559 | 7 | 6/5/2015 | 152.7 | 5.83 | 2656/2837 | 27.1 | 0.69 | 1.5E-06 |
| 157/1560 | 7 | 1/11/2015 | 95.1 | 5.83 | 737/821 | 27.0 | 0.70 | 8.6E-07 |
| 158/1561 | 7 | 21/2/2016 | 88.6 | 5.83 | 1140/1087 | 19.7 | 0.77 | 1.8E-06 |
| 159/1562 | 7 | 21/6/2016 | 67.4 | 5.83 | 1718/1631 | 26.5 | 0.67 | 4.3E-07 |
| 160/1563 | 7 | 2/10/2016 | 134.1 | 5.83 | 4501/4429 | 27.4 | 0.67 | 5.0E-04 |
| 161/1564 | 7 | 20/5/2017 | 56.2 | 5.83 | 1690/1683 | 25.1 | 0.63 | 3.5E-03 |
| 162/1565 | 7 | 31/7/2017 | 168.6 | 5.83 | 4639/4762 | 23.8 | 0.60 | 7.2E-03 |
| 163/1566 | 7 | 23/7/2018 | 3.7 | 5.83 | 1/10 | 29.2 | 0.61 | 3.6E-03 |
| 164/1567 | 7 | 5/11/2018 | 174.0 | 5.83 | 5493/5687 | 24.5 | 0.68 | 1.0E-03 |
| 165/1568 | 7 | 25/5/2019 | 126.7 | 5.83 | 3300/3393 | 26.9 | 0.57 | 6.3E-03 |
| 166/1569 | 8 | 8/3/2013 | 31.5 | 5.85 | 1275/1201 | 13.1 | 0.61 | 3.8E-03 |
| 167/1570 | 8 | 10/4/2013 | 65.6 | 5.85 | 2773/2524 | 13.5 | 0.60 | 3.9E-03 |
| 168/1571 | 8 | 9/7/2013 | 0.3 | 5.85 | 15/11 | 15.2 | 0.50 | 6.7E-03 |
| 169/1572 | 8 | 11/7/2013 | 19.3 | 5.85 | 619/627 | 14.6 | 0.50 | 7.5E-03 |
| 170/1573 | 8 | 1/8/2013 | 8.0 | 5.85 | 101/126 | 12.4 | 0.58 | 4.4E-03 |
| 171/1574 | 8 | 12/8/2013 | 11.6 | 5.85 | 192/193 | 11.3 | 0.67 | 2.2E-07 |
| 172/1575 | 8 | 27/8/2013 | 2.5 | 5.85 | 36/36 | 12.2 | 0.65 | 5.8E-07 |
| 173/1576 | 8 | 5/9/2013 | 23.0 | 5.85 | 455/494 | 12.3 | 0.66 | 9.4E-07 |
| 174/1577 | 8 | 9/10/2013 | 14.6 | 5.85 | 326/349 | 12.0 | 0.66 | 1.2E-03 |
| 175/1578 | 8 | 29/10/2013 | 8.1 | 5.85 | 93/101 | 12.4 | 0.62 | 1.2E-03 |
| 176/1579 | 8 | 21/11/2013 | 4.8 | 5.85 | 140/130 | 17.0 | 0.66 | 2.0E-03 |
| 177/1580 | 8 | 29/11/2013 | 1.3 | 5.85 | 38/36 | 16.1 | 0.62 | 2.0E-03 |
| 178/1581 | 8 | 10/1/2014 | 4.6 | 5.85 | 168/144 | 14.6 | 0.59 | 4.9E-03 |
| 179/1582 | 8 | 24/1/2014 | 38.7 | 5.85 | 1560/1433 | 8.4 | 0.63 | 9.3E-03 |
| 180/1583 | 8 | 6/3/2014 | 26.5 | 5.85 | 1078/1047 | 7.3 | 0.68 | 6.7E-03 |
| 181/1584 | 8 | 3/4/2014 | 18.4 | 5.85 | 783/766 | 12.0 | 0.66 | 5.7E-03 |
| 182/1585 | 8 | 26/4/2014 | 47.0 | 5.85 | 1679/1649 | 14.7 | 0.62 | 7.7E-03 |
| 183/1586 | 8 | 19/6/2014 | 74.2 | 5.85 | 2351/2127 | 10.8 | 0.57 | 8.2E-03 |
| 184/1587 | 8 | 5/9/2014 | 24.4 | 5.85 | 1058/883 | 9.9 | 0.58 | 6.6E-03 |

| Partition No. | D. No. | Start date | Dur. [d] | m [g] | Events | $p_0$ [keV] | $p_1$ [keV] | $p_2$ [keV] |
|---|---|---|---|---|---|---|---|---|
| 185/1588 | 8 | 2/10/2014 | 102.6 | 5.85 | 4917/4584 | 9.3 | 0.62 | 4.1E-03 |
| 186/1589 | 8 | 25/2/2015 | 48.9 | 5.85 | 1337/1195 | 25.1 | 0.68 | 4.0E-07 |
| 187/1590 | 8 | 6/5/2015 | 247.8 | 5.85 | 4251/3725 | 24.9 | 0.72 | 4.1E-07 |
| 188/1591 | 8 | 21/2/2016 | 88.6 | 5.85 | 1222/1132 | 19.9 | 0.80 | 3.2E-07 |
| 189/1592 | 8 | 21/6/2016 | 67.4 | 5.85 | 1380/1291 | 24.9 | 0.72 | 4.1E-07 |
| 190/1593 | 8 | 2/10/2016 | 134.1 | 5.85 | 3611/3439 | 27.1 | 0.71 | 5.0E-04 |
| 191/1594 | 8 | 23/7/2018 | 3.7 | 5.85 | 1/4 | 33.5 | 0.16 | 1.1E-02 |
| 192/1595 | 8 | 5/11/2018 | 174.0 | 5.85 | 4315/3789 | 27.0 | 0.46 | 1.1E-02 |
| 193/1596 | 8 | 25/5/2019 | 126.7 | 5.85 | 2266/2087 | 27.8 | 0.69 | 4.7E-03 |
| 194/1597 | 9 | 8/3/2013 | 30.5 | 5.89 | 1330/1324 | 10.5 | 0.56 | 2.5E-02 |
| 195/1598 | 9 | 10/4/2013 | 65.7 | 5.89 | 3041/3034 | 10.8 | 0.57 | 2.5E-02 |
| 196/1599 | 9 | 9/7/2013 | 0.3 | 5.89 | 17/20 | 11.3 | 0.59 | 2.5E-02 |
| 197/1600 | 9 | 11/7/2013 | 19.3 | 5.89 | 705/707 | 11.3 | 0.59 | 2.4E-02 |
| 198/1601 | 9 | 1/8/2013 | 8.0 | 5.89 | 145/150 | 11.3 | 0.58 | 2.3E-02 |
| 199/1602 | 9 | 12/8/2013 | 11.6 | 5.89 | 194/226 | 5.6 | 0.70 | 2.1E-02 |
| 200/1603 | 9 | 27/8/2013 | 2.5 | 5.89 | 45/53 | 0.0 | 0.80 | 2.0E-02 |
| 201/1604 | 9 | 5/9/2013 | 22.9 | 5.89 | 598/589 | 8.0 | 0.39 | 2.3E-02 |
| 202/1605 | 9 | 9/10/2013 | 14.6 | 5.89 | 296/301 | 15.2 | 0.00 | 2.5E-02 |
| 203/1606 | 9 | 29/10/2013 | 8.1 | 5.89 | 132/141 | 15.2 | 0.00 | 2.6E-02 |
| 204/1607 | 9 | 5/11/2018 | 168.8 | 5.89 | 8299/8028 | 11.4 | 0.01 | 2.7E-02 |
| 205/1608 | 9 | 25/5/2019 | 92.7 | 5.89 | 4346/4544 | 11.5 | 0.13 | 2.8E-02 |
| 206/1609 | 10 | 8/3/2013 | 30.5 | 5.90 | 1513/1506 | 14.8 | 0.33 | 4.6E-03 |
| 207/1610 | 10 | 10/4/2013 | 65.7 | 5.90 | 3599/3442 | 13.8 | 0.35 | 5.3E-03 |
| 208/1611 | 10 | 9/7/2013 | 0.3 | 5.90 | 14/16 | 10.2 | 0.43 | 3.3E-03 |
| 209/1612 | 10 | 11/7/2013 | 19.3 | 5.90 | 754/756 | 9.1 | 0.45 | 7.5E-07 |
| 210/1613 | 10 | 1/8/2013 | 8.0 | 5.90 | 95/109 | 9.2 | 0.47 | 3.1E-07 |
| 211/1614 | 10 | 12/8/2013 | 11.6 | 5.90 | 144/179 | 9.4 | 0.48 | 2.9E-08 |
| 212/1615 | 10 | 27/8/2013 | 2.5 | 5.90 | 28/42 | 9.0 | 0.50 | -2.0E-07 |
| 213/1616 | 10 | 5/9/2013 | 45.5 | 5.90 | 820/948 | 8.4 | 0.51 | -5.9E-07 |
| 214/1617 | 10 | 5/11/2018 | 168.8 | 5.90 | 8485/8093 | 10.0 | 0.37 | 8.8E-03 |
| 215/1618 | 10 | 25/5/2019 | 92.7 | 5.90 | 4641/4476 | 10.7 | 0.34 | 1.0E-02 |
| 216/1619 | 11 | 8/3/2013 | 30.5 | 5.88 | 1513/1473 | 11.2 | 0.52 | 1.3E-02 |
| 217/1620 | 11 | 10/4/2013 | 65.7 | 5.88 | 3518/3410 | 10.5 | 0.63 | 2.2E-02 |
| 218/1621 | 11 | 9/7/2013 | 19.7 | 5.88 | 828/749 | 12.0 | 0.59 | 2.2E-02 |
| 219/1622 | 11 | 1/8/2013 | 8.0 | 5.88 | 115/145 | 8.1 | 0.74 | 1.1E-02 |
| 220/1623 | 11 | 12/8/2013 | 11.6 | 5.88 | 184/194 | 3.4 | 0.87 | 4.4E-03 |
| 221/1624 | 11 | 27/8/2013 | 2.5 | 5.88 | 34/49 | 2.6 | 0.85 | 8.8E-03 |
| 222/1625 | 11 | 5/9/2013 | 22.9 | 5.88 | 481/602 | 2.2 | 0.84 | 9.6E-03 |
| 223/1626 | 11 | 9/10/2013 | 22.7 | 5.88 | 370/455 | 1.8 | 0.83 | 1.0E-02 |
| 224/1627 | 11 | 21/11/2013 | 4.6 | 5.88 | 105/82 | 14.0 | 0.56 | 6.1E-07 |
| 225/1628 | 11 | 29/11/2013 | 1.3 | 5.88 | 38/36 | 13.5 | 0.55 | 9.3E-04 |
| 226/1629 | 11 | 10/1/2014 | 4.6 | 5.88 | 225/197 | 13.2 | 0.50 | -3.6E-03 |
| 227/1630 | 11 | 24/1/2014 | 65.0 | 5.88 | 2334/2263 | 14.5 | 0.42 | -7.1E-03 |
| 228/1631 | 11 | 3/4/2014 | 18.5 | 5.88 | 511/480 | 26.2 | 0.27 | 9.7E-04 |
| 229/1632 | 11 | 26/4/2014 | 46.4 | 5.88 | 1092/1088 | 36.8 | 0.36 | 4.5E-03 |
| 230/1633 | 11 | 19/6/2014 | 74.0 | 5.88 | 1566/1512 | 23.8 | 0.57 | 3.4E-03 |
| 231/1634 | 11 | 5/9/2014 | 24.0 | 5.88 | 834/792 | 12.0 | 0.53 | 6.8E-03 |
| 232/1635 | 11 | 2/10/2014 | 102.6 | 5.88 | 3681/3533 | 12.2 | 0.56 | 3.4E-03 |
| 233/1636 | 11 | 25/2/2015 | 49.5 | 5.88 | 1858/1830 | 13.1 | 0.58 | 1.7E-03 |
| 234/1637 | 11 | 6/5/2015 | 155.7 | 5.88 | 4826/4581 | 13.9 | 0.61 | 1.7E-03 |
| 235/1638 | 11 | 1/11/2015 | 99.7 | 5.88 | 784/898 | 14.2 | 0.63 | 4.4E-08 |
| 236/1639 | 11 | 31/7/2017 | 180.1 | 5.88 | 7126/6701 | 14.8 | 0.60 | 4.5E-03 |
| 237/1640 | 11 | 5/11/2018 | 168.8 | 5.88 | 7347/7124 | 17.7 | 0.40 | 8.7E-03 |
| 238/1641 | 11 | 25/5/2019 | 92.7 | 5.88 | 3974/3729 | 18.8 | 0.35 | 1.0E-02 |
| 239/1642 | 12 | 8/3/2013 | 30.5 | 5.90 | 1323/1316 | 10.8 | 0.56 | 8.4E-03 |
| 240/1643 | 12 | 10/4/2013 | 65.7 | 5.90 | 2922/2714 | 10.4 | 0.63 | 5.2E-03 |
| 241/1644 | 12 | 9/7/2013 | 0.3 | 5.90 | 12/10 | 10.4 | 0.60 | 8.8E-03 |
| 242/1645 | 12 | 11/7/2013 | 19.3 | 5.90 | 646/596 | 8.9 | 0.67 | 5.7E-03 |
| 243/1646 | 12 | 1/8/2013 | 8.0 | 5.90 | 103/132 | 8.9 | 0.66 | 2.6E-03 |
| 244/1647 | 12 | 12/8/2013 | 11.6 | 5.90 | 198/201 | 9.4 | 0.65 | 2.1E-03 |
| 245/1648 | 12 | 27/8/2013 | 2.5 | 5.90 | 54/49 | 8.4 | 0.68 | 1.8E-03 |
| 246/1649 | 12 | 5/9/2013 | 22.9 | 5.90 | 539/544 | 8.0 | 0.69 | 3.7E-07 |
| 247/1650 | 12 | 9/10/2013 | 14.6 | 5.90 | 220/260 | 9.1 | 0.64 | 3.6E-03 |
| 248/1651 | 12 | 29/10/2013 | 8.1 | 5.90 | 94/103 | 9.8 | 0.59 | 8.6E-03 |
| 249/1652 | 12 | 21/11/2013 | 4.6 | 5.90 | 155/142 | 10.6 | 0.67 | 4.4E-03 |
| 250/1653 | 12 | 29/11/2013 | 1.3 | 5.90 | 47/40 | 10.2 | 0.63 | 4.4E-03 |
| 251/1654 | 12 | 10/1/2014 | 4.6 | 5.90 | 161/178 | 12.3 | 0.59 | 8.0E-03 |
| 252/1655 | 12 | 24/1/2014 | 38.7 | 5.90 | 1387/1287 | 11.6 | 0.60 | 7.9E-03 |
| 253/1656 | 12 | 6/3/2014 | 26.4 | 5.90 | 963/962 | 10.3 | 0.63 | 6.5E-03 |
| 254/1657 | 12 | 3/4/2014 | 18.5 | 5.90 | 685/672 | 10.3 | 0.62 | 7.9E-03 |
| 255/1658 | 12 | 26/4/2014 | 46.4 | 5.90 | 1656/1507 | 13.4 | 0.58 | 9.0E-03 |
| 256/1659 | 12 | 19/6/2014 | 74.0 | 5.90 | 2325/2295 | 14.3 | 0.52 | 1.0E-02 |

| Partition No. | D. No. | Start date | Dur. [d] | m [g] | Events | $p_0$ [keV] | $p_1$ [keV] | $p_2$ [keV] |
|---|---|---|---|---|---|---|---|---|
| 257/1660 | 12 | 5/9/2014 | 24.0 | 5.90 | 903/869 | 13.0 | 0.45 | 1.1E-02 |
| 258/1661 | 12 | 2/10/2014 | 102.6 | 5.90 | 3880/3763 | 13.6 | 0.45 | 1.1E-02 |
| 259/1662 | 12 | 25/2/2015 | 49.5 | 5.90 | 1789/1712 | 11.9 | 0.57 | 9.4E-03 |
| 260/1663 | 12 | 6/5/2015 | 155.7 | 5.90 | 4548/4278 | 12.1 | 0.62 | 6.7E-03 |
| 261/1664 | 12 | 1/11/2015 | 99.7 | 5.90 | 2876/3049 | 12.2 | 0.62 | 5.9E-03 |
| 262/1665 | 13 | 8/3/2013 | 30.5 | 5.86 | 1254/1414 | 12.8 | 0.73 | 1.8E-06 |
| 263/1666 | 13 | 10/4/2013 | 65.7 | 5.86 | 2656/3117 | 12.6 | 0.73 | 1.3E-03 |
| 264/1667 | 13 | 9/7/2013 | 0.3 | 5.86 | 11/14 | 15.2 | 0.66 | 2.6E-07 |
| 265/1668 | 13 | 11/7/2013 | 19.3 | 5.86 | 736/861 | 14.0 | 0.65 | 2.5E-07 |
| 266/1669 | 13 | 1/8/2013 | 8.0 | 5.86 | 283/326 | 13.2 | 0.64 | 2.3E-03 |
| 267/1670 | 13 | 12/8/2013 | 11.6 | 5.86 | 439/453 | 14.4 | 0.61 | 6.1E-03 |
| 268/1671 | 13 | 27/8/2013 | 2.5 | 5.86 | 105/125 | 14.5 | 0.62 | 3.8E-03 |
| 269/1672 | 13 | 5/9/2013 | 22.7 | 5.86 | 726/862 | 13.7 | 0.66 | 2.5E-06 |
| 270/1673 | 13 | 9/10/2013 | 13.9 | 5.86 | 193/240 | 14.1 | 0.63 | 3.6E-03 |
| 271/1674 | 13 | 29/10/2013 | 8.1 | 5.86 | 246/290 | 13.6 | 0.66 | 5.3E-03 |
| 272/1675 | 13 | 21/11/2013 | 4.7 | 5.86 | 70/70 | 18.4 | 0.64 | -5.3E-03 |
| 273/1676 | 13 | 29/11/2013 | 1.3 | 5.86 | 27/31 | 16.0 | 0.67 | -3.5E-03 |
| 274/1677 | 13 | 10/1/2014 | 4.6 | 5.86 | 137/188 | 17.8 | 0.70 | 9.7E-06 |
| 275/1678 | 13 | 24/1/2014 | 38.5 | 5.86 | 978/1194 | 16.3 | 0.76 | 1.1E-05 |
| 276/1679 | 13 | 6/3/2014 | 26.4 | 5.86 | 569/657 | 15.9 | 0.70 | 1.3E-06 |
| 277/1680 | 13 | 3/4/2014 | 18.3 | 5.86 | 433/526 | 15.9 | 0.65 | -1.9E-07 |
| 278/1681 | 13 | 26/4/2014 | 45.7 | 5.86 | 952/1133 | 20.8 | 0.67 | -1.9E-07 |
| 279/1682 | 13 | 19/6/2014 | 74.1 | 5.86 | 1302/1510 | 21.1 | 0.62 | 3.6E-03 |
| 280/1683 | 13 | 5/9/2014 | 24.2 | 5.86 | 671/852 | 16.2 | 0.60 | 3.6E-03 |
| 281/1684 | 13 | 2/10/2014 | 102.7 | 5.86 | 3153/3678 | 15.9 | 0.64 | 4.1E-07 |
| 282/1685 | 13 | 25/2/2015 | 49.5 | 5.86 | 1412/1673 | 15.6 | 0.68 | 2.8E-07 |
| 283/1686 | 13 | 6/5/2015 | 155.9 | 5.86 | 3601/4151 | 15.6 | 0.71 | 5.3E-07 |
| 284/1687 | 13 | 1/11/2015 | 99.9 | 5.86 | 1128/1218 | 16.2 | 0.68 | -1.3E-08 |
| 285/1688 | 13 | 22/2/2016 | 96.1 | 5.86 | 1632/2009 | 15.7 | 0.64 | 4.7E-03 |
| 286/1689 | 13 | 20/6/2016 | 76.1 | 5.86 | 2042/2440 | 16.4 | 0.57 | 5.1E-03 |
| 287/1690 | 13 | 2/10/2016 | 142.2 | 5.86 | 7190/8669 | 17.7 | 0.44 | 1.5E-02 |
| 288/1691 | 13 | 20/5/2017 | 58.8 | 5.86 | 2955/3497 | 16.7 | 0.38 | 1.6E-02 |
| 289/1692 | 13 | 31/7/2017 | 160.9 | 5.86 | 5969/6837 | 15.3 | 0.36 | 1.2E-02 |
| 290/1693 | 14 | 8/3/2013 | 30.5 | 5.91 | 1118/1093 | 14.1 | 0.74 | 3.5E-06 |
| 291/1694 | 14 | 10/4/2013 | 65.7 | 5.91 | 2374/2442 | 14.9 | 0.73 | 5.2E-07 |
| 292/1695 | 14 | 9/7/2013 | 0.3 | 5.91 | 9/8 | 11.1 | 0.72 | -3.2E-07 |
| 293/1696 | 14 | 11/7/2013 | 19.3 | 5.91 | 974/996 | 11.7 | 0.74 | -2.5E-03 |
| 294/1697 | 14 | 1/8/2013 | 8.0 | 5.91 | 72/63 | 10.9 | 0.72 | 2.5E-03 |
| 295/1698 | 14 | 12/8/2013 | 11.6 | 5.91 | 99/139 | 10.6 | 0.72 | 5.0E-03 |
| 296/1699 | 14 | 27/8/2013 | 2.5 | 5.91 | 8/4 | 9.8 | 0.78 | 4.3E-03 |
| 297/1700 | 14 | 5/9/2013 | 22.7 | 5.91 | 270/339 | 8.8 | 0.75 | 8.0E-03 |
| 298/1701 | 14 | 9/10/2013 | 13.9 | 5.91 | 172/282 | 6.3 | 0.85 | 3.7E-03 |
| 299/1702 | 14 | 29/10/2013 | 8.1 | 5.91 | 31/44 | 4.7 | 1.00 | 1.1E-02 |
| 300/1703 | 14 | 21/11/2013 | 4.7 | 5.91 | 74/74 | 14.4 | 0.60 | 5.0E-07 |
| 301/1704 | 14 | 29/11/2013 | 1.3 | 5.91 | 25/38 | 13.8 | 0.58 | -2.9E-08 |
| 302/1705 | 14 | 10/1/2014 | 4.6 | 5.91 | 166/171 | 15.3 | 0.53 | 4.7E-03 |
| 303/1706 | 14 | 24/1/2014 | 38.5 | 5.91 | 1216/1241 | 13.9 | 0.57 | 4.7E-03 |
| 304/1707 | 14 | 6/3/2014 | 26.4 | 5.91 | 665/685 | 12.6 | 0.63 | 2.1E-06 |
| 305/1708 | 14 | 3/4/2014 | 18.3 | 5.91 | 476/498 | 13.1 | 0.60 | 4.0E-08 |
| 306/1709 | 14 | 26/4/2014 | 45.7 | 5.91 | 1046/1041 | 17.5 | 0.63 | 2.7E-07 |
| 307/1710 | 14 | 19/6/2014 | 74.1 | 5.91 | 1333/1434 | 16.4 | 0.67 | 2.4E-03 |
| 308/1711 | 14 | 5/9/2014 | 24.2 | 5.91 | 735/729 | 11.1 | 0.68 | 4.9E-03 |
| 309/1712 | 14 | 2/10/2014 | 102.7 | 5.91 | 2899/3167 | 11.8 | 0.64 | 2.4E-03 |
| 310/1713 | 14 | 25/2/2015 | 49.5 | 5.91 | 729/748 | 13.8 | 0.61 | 2.4E-07 |
| 311/1714 | 14 | 6/5/2015 | 155.9 | 5.91 | 2386/2450 | 14.0 | 0.65 | -9.7E-08 |
| 312/1715 | 14 | 1/11/2015 | 99.9 | 5.91 | 645/656 | 15.2 | 0.65 | 7.8E-07 |
| 313/1716 | 14 | 22/2/2016 | 96.1 | 5.91 | 916/1018 | 15.3 | 0.66 | 1.7E-06 |
| 314/1717 | 14 | 20/6/2016 | 76.1 | 5.91 | 1536/1528 | 14.8 | 0.62 | 1.1E-06 |
| 315/1718 | 14 | 2/10/2016 | 142.2 | 5.91 | 4461/4659 | 14.7 | 0.65 | 5.0E-04 |
| 316/1719 | 14 | 20/5/2017 | 58.8 | 5.91 | 1502/1487 | 13.8 | 0.64 | 1.0E-03 |
| 317/1720 | 14 | 31/7/2017 | 160.9 | 5.91 | 1626/1541 | 14.1 | 0.61 | 1.0E-03 |
| 318/1721 | 15 | 8/3/2013 | 30.5 | 5.87 | 1416/1409 | 11.9 | 0.60 | 1.3E-07 |
| 319/1722 | 15 | 10/4/2013 | 65.7 | 5.87 | 3315/3188 | 12.0 | 0.59 | -2.4E-07 |
| 320/1723 | 15 | 9/7/2013 | 0.3 | 5.87 | 23/10 | 13.5 | 0.49 | 5.4E-07 |
| 321/1724 | 15 | 11/7/2013 | 19.3 | 5.87 | 758/755 | 12.2 | 0.53 | -4.1E-07 |
| 322/1725 | 15 | 1/8/2013 | 8.0 | 5.87 | 63/92 | 10.8 | 0.57 | 1.6E-03 |
| 323/1726 | 15 | 12/8/2013 | 11.6 | 5.87 | 134/139 | 10.7 | 0.61 | 1.6E-03 |
| 324/1727 | 15 | 27/8/2013 | 2.5 | 5.87 | 27/19 | 10.6 | 0.60 | 1.1E-06 |
| 325/1728 | 15 | 5/9/2013 | 22.7 | 5.87 | 420/457 | 10.6 | 0.57 | 1.2E-07 |
| 326/1729 | 15 | 9/10/2013 | 13.9 | 5.87 | 229/299 | 11.2 | 0.57 | 2.3E-07 |
| 327/1730 | 15 | 29/10/2013 | 8.1 | 5.87 | 54/74 | 10.4 | 0.64 | 6.3E-07 |
| 328/1731 | 15 | 21/11/2013 | 4.7 | 5.87 | 84/96 | 15.8 | 0.51 | 4.0E-04 |

| Partition No. | D. No. | Start date | Dur. [d] | m [g] | Events | $p_0$ [keV] | $p_1$ [keV] | $p_2$ [keV] |
|---|---|---|---|---|---|---|---|---|
| 329/1732 | 15 | 29/11/2013 | 1.3 | 5.87 | 38/43 | 15.2 | 0.48 | 4.0E-04 |
| 330/1733 | 15 | 10/1/2014 | 4.6 | 5.87 | 177/189 | 15.6 | 0.52 | 3.7E-03 |
| 331/1734 | 15 | 24/1/2014 | 38.5 | 5.87 | 1263/1269 | 15.7 | 0.48 | 3.7E-03 |
| 332/1735 | 15 | 6/3/2014 | 26.4 | 5.87 | 769/705 | 14.9 | 0.49 | 1.2E-07 |
| 333/1736 | 15 | 3/4/2014 | 18.3 | 5.87 | 443/464 | 14.4 | 0.50 | 5.7E-09 |
| 334/1737 | 15 | 26/4/2014 | 45.7 | 5.87 | 845/1031 | 17.4 | 0.52 | 2.3E-03 |
| 335/1738 | 15 | 19/6/2014 | 74.1 | 5.87 | 1015/1281 | 17.1 | 0.53 | 2.3E-03 |
| 336/1739 | 15 | 5/9/2014 | 24.2 | 5.87 | 695/667 | 13.8 | 0.52 | -3.1E-08 |
| 337/1740 | 15 | 2/10/2014 | 102.7 | 5.87 | 2910/3008 | 14.0 | 0.52 | -5.7E-08 |
| 338/1741 | 15 | 25/2/2015 | 49.5 | 5.87 | 1133/1075 | 15.2 | 0.54 | -6.1E-07 |
| 339/1742 | 15 | 6/5/2015 | 155.9 | 5.87 | 3654/3432 | 15.7 | 0.53 | 2.0E-06 |
| 340/1743 | 15 | 1/11/2015 | 99.9 | 5.87 | 993/1000 | 15.9 | 0.51 | 2.1E-06 |
| 341/1744 | 15 | 22/2/2016 | 96.1 | 5.87 | 1360/1284 | 15.9 | 0.56 | 1.2E-06 |
| 342/1745 | 15 | 20/6/2016 | 76.1 | 5.87 | 1579/1507 | 14.4 | 0.59 | 7.6E-07 |
| 343/1746 | 15 | 2/10/2016 | 142.2 | 5.87 | 4630/4543 | 15.3 | 0.60 | 5.0E-04 |
| 344/1747 | 15 | 20/5/2017 | 58.8 | 5.87 | 1439/1281 | 14.9 | 0.54 | 1.0E-03 |
| 345/1748 | 15 | 31/7/2017 | 160.9 | 5.87 | 2783/2388 | 18.7 | 0.55 | 1.0E-03 |
| 346/1749 | 16 | 8/3/2013 | 30.5 | 5.91 | 957/895 | 22.6 | 0.74 | 3.1E-07 |
| 347/1750 | 16 | 10/4/2013 | 65.7 | 5.91 | 1913/1811 | 22.8 | 0.73 | 3.0E-07 |
| 348/1751 | 16 | 9/7/2013 | 0.3 | 5.91 | 12/10 | 21.1 | 0.70 | 1.1E-06 |
| 349/1752 | 16 | 11/7/2013 | 19.3 | 5.91 | 485/481 | 21.4 | 0.76 | 8.0E-07 |
| 350/1753 | 16 | 1/8/2013 | 8.0 | 5.91 | 30/67 | 20.2 | 0.84 | -3.1E-07 |
| 351/1754 | 16 | 12/8/2013 | 11.6 | 5.91 | 60/101 | 19.3 | 0.89 | 1.5E-06 |
| 352/1755 | 16 | 27/8/2013 | 2.5 | 5.91 | 12/25 | 19.2 | 0.86 | 1.6E-06 |
| 353/1756 | 16 | 5/9/2013 | 22.7 | 5.91 | 316/448 | 19.2 | 0.80 | 2.3E-06 |
| 354/1757 | 16 | 9/10/2013 | 13.9 | 5.91 | 118/111 | 20.2 | 0.87 | 2.4E-06 |
| 355/1758 | 16 | 29/10/2013 | 8.1 | 5.91 | 16/13 | 19.7 | 0.95 | 1.4E-03 |
| 356/1759 | 16 | 21/11/2013 | 4.7 | 5.91 | 4/3 | 21.3 | 0.78 | 1.4E-06 |
| 357/1760 | 16 | 29/11/2013 | 1.3 | 5.91 | 1/5 | 20.5 | 0.73 | 1.7E-06 |
| 358/1761 | 16 | 10/1/2014 | 4.6 | 5.91 | 59/44 | 21.4 | 0.63 | 4.0E-07 |
| 359/1762 | 16 | 5/9/2014 | 24.2 | 5.91 | 150/112 | 17.9 | 0.71 | 1.4E-06 |
| 360/1763 | 16 | 2/10/2014 | 102.7 | 5.91 | 877/879 | 18.5 | 0.68 | 3.9E-03 |
| 361/1764 | 16 | 25/2/2015 | 49.5 | 5.91 | 399/420 | 19.3 | 0.75 | 1.3E-06 |
| 362/1765 | 16 | 6/5/2015 | 155.9 | 5.91 | 1450/1500 | 20.5 | 0.71 | 1.6E-06 |
| 363/1766 | 16 | 1/11/2015 | 99.9 | 5.91 | 456/516 | 21.2 | 0.70 | 2.6E-07 |
| 364/1767 | 16 | 22/2/2016 | 96.1 | 5.91 | 498/524 | 18.7 | 0.79 | 2.0E-07 |
| 365/1768 | 16 | 20/6/2016 | 76.1 | 5.91 | 246/207 | 20.6 | 0.75 | -8.0E-07 |
| 366/1769 | 16 | 2/10/2016 | 142.2 | 5.91 | 1747/1766 | 23.7 | 0.78 | 1.7E-03 |
| 367/1770 | 17 | 8/3/2013 | 31.5 | 5.87 | 515/535 | 12.3 | 0.77 | 1.2E-02 |
| 368/1771 | 17 | 10/4/2013 | 66.0 | 5.87 | 1013/1018 | 11.9 | 0.78 | 1.2E-02 |
| 369/1772 | 17 | 9/7/2013 | 0.3 | 5.87 | 7/5 | 10.4 | 0.84 | -1.0E-07 |
| 370/1773 | 17 | 11/7/2013 | 19.3 | 5.87 | 266/247 | 9.5 | 0.88 | 6.1E-07 |
| 371/1774 | 17 | 1/8/2013 | 8.0 | 5.87 | 101/140 | 11.1 | 0.80 | 5.8E-03 |
| 372/1775 | 17 | 12/8/2013 | 13.4 | 5.87 | 178/204 | 11.6 | 0.80 | 8.8E-03 |
| 373/1776 | 17 | 27/8/2013 | 2.5 | 5.87 | 29/38 | 10.6 | 0.88 | 6.0E-03 |
| 374/1777 | 17 | 5/9/2013 | 23.0 | 5.87 | 406/367 | 10.6 | 0.85 | 8.6E-03 |
| 375/1778 | 17 | 9/10/2013 | 14.6 | 5.87 | 214/212 | 9.9 | 0.85 | 1.0E-02 |
| 376/1779 | 17 | 29/10/2013 | 8.1 | 5.87 | 111/113 | 8.4 | 0.92 | 4.8E-03 |
| 377/1780 | 17 | 21/11/2013 | 4.9 | 5.87 | 2/17 | 12.8 | 0.79 | -2.8E-07 |
| 378/1781 | 17 | 29/11/2013 | 1.3 | 5.87 | 0/8 | 11.7 | 0.76 | 7.3E-04 |
| 379/1782 | 17 | 10/1/2014 | 4.6 | 5.87 | 68/51 | 14.4 | 0.73 | 4.5E-03 |
| 380/1783 | 17 | 24/1/2014 | 38.6 | 5.87 | 463/453 | 13.3 | 0.76 | 6.4E-03 |
| 381/1784 | 17 | 6/3/2014 | 26.4 | 5.87 | 199/220 | 12.4 | 0.75 | 6.2E-03 |
| 382/1785 | 17 | 3/4/2014 | 18.4 | 5.87 | 66/77 | 19.6 | 0.78 | 4.3E-03 |
| 383/1786 | 17 | 26/4/2014 | 47.8 | 5.87 | 33/67 | 25.0 | 0.80 | -3.6E-07 |
| 384/1787 | 17 | 19/6/2014 | 73.4 | 5.87 | 116/208 | 23.2 | 0.75 | 1.0E-06 |
| 385/1788 | 17 | 5/9/2014 | 24.3 | 5.87 | 41/101 | 17.3 | 0.73 | 3.4E-03 |
| 386/1789 | 17 | 2/10/2014 | 103.7 | 5.87 | 238/625 | 11.2 | 0.74 | 3.4E-03 |
| 387/1790 | 17 | 25/2/2015 | 49.1 | 5.87 | 663/842 | 12.4 | 0.71 | 2.9E-03 |
| 388/1791 | 17 | 6/5/2015 | 149.7 | 5.87 | 1925/2001 | 14.1 | 0.65 | 7.7E-03 |
| 389/1792 | 17 | 1/11/2015 | 95.4 | 5.87 | 536/614 | 14.1 | 0.66 | 9.9E-03 |
| 390/1793 | 17 | 22/2/2016 | 85.2 | 5.87 | 965/1067 | 11.7 | 0.72 | 1.2E-02 |
| 391/1794 | 17 | 20/6/2016 | 80.8 | 5.87 | 2159/2321 | 13.2 | 0.70 | 1.0E-02 |
| 392/1795 | 17 | 2/10/2016 | 148.9 | 5.87 | 5479/5655 | 14.3 | 0.67 | 1.0E-02 |
| 393/1796 | 17 | 23/7/2018 | 3.7 | 5.87 | 0/1 | 15.8 | 0.34 | 1.1E-02 |
| 394/1797 | 18 | 8/3/2013 | 31.5 | 5.87 | 779/758 | 10.4 | 0.42 | 9.1E-03 |
| 395/1798 | 18 | 10/4/2013 | 66.0 | 5.87 | 1509/1460 | 10.6 | 0.68 | 4.6E-03 |
| 396/1799 | 18 | 9/7/2013 | 0.3 | 5.87 | 8/6 | 11.9 | 0.73 | 2.1E-03 |
| 397/1800 | 18 | 11/7/2013 | 19.3 | 5.87 | 342/339 | 12.9 | 0.51 | 4.2E-03 |
| 398/1801 | 18 | 1/8/2013 | 8.0 | 5.87 | 159/137 | 12.9 | 0.45 | -2.0E-03 |
| 399/1802 | 18 | 12/8/2013 | 13.4 | 5.87 | 271/227 | 12.9 | 0.43 | -1.9E-03 |
| 400/1803 | 18 | 27/8/2013 | 2.5 | 5.87 | 46/46 | 11.6 | 0.49 | -9.3E-04 |

| Partition No. | D. No. | Start date | Dur. [d] | m [g] | Events | $p_0$ [keV] | $p_1$ [keV] | $p_2$ [keV] |
|---|---|---|---|---|---|---|---|---|
| 401/1804 | 18 | 5/9/2013 | 23.0 | 5.87 | 398/367 | 9.9 | 0.51 | -5.1E-03 |
| 402/1805 | 18 | 9/10/2013 | 14.6 | 5.87 | 269/249 | 9.6 | 0.52 | -3.8E-03 |
| 403/1806 | 18 | 29/10/2013 | 8.1 | 5.87 | 152/139 | 10.5 | 0.45 | -7.9E-03 |
| 404/1807 | 18 | 21/11/2013 | 4.9 | 5.87 | 34/30 | 11.9 | 0.61 | 8.2E-09 |
| 405/1808 | 18 | 29/11/2013 | 1.3 | 5.87 | 8/6 | 11.5 | 0.58 | 7.3E-07 |
| 406/1809 | 18 | 10/1/2014 | 4.6 | 5.87 | 67/60 | 11.9 | 0.50 | -3.9E-03 |
| 407/1810 | 18 | 24/1/2014 | 38.6 | 5.87 | 508/516 | 11.6 | 0.49 | -3.3E-03 |
| 408/1811 | 18 | 6/3/2014 | 26.4 | 5.87 | 251/244 | 11.2 | 0.52 | 1.2E-03 |
| 409/1812 | 18 | 3/4/2014 | 18.4 | 5.87 | 184/185 | 22.7 | 0.26 | 5.2E-03 |
| 410/1813 | 18 | 26/4/2014 | 47.8 | 5.87 | 485/506 | 31.9 | 0.18 | 1.0E-02 |
| 411/1814 | 18 | 19/6/2014 | 73.4 | 5.87 | 606/589 | 29.6 | 0.35 | 1.1E-02 |
| 412/1815 | 18 | 5/9/2014 | 24.3 | 5.87 | 264/269 | 19.4 | 0.47 | 4.0E-03 |
| 413/1816 | 18 | 2/10/2014 | 103.7 | 5.87 | 2008/1993 | 10.1 | 0.55 | 1.5E-03 |
| 414/1817 | 18 | 25/2/2015 | 198.8 | 5.87 | 3701/3423 | 11.1 | 0.56 | 4.4E-03 |
| 415/1818 | 18 | 1/11/2015 | 95.4 | 5.87 | 789/718 | 12.0 | 0.53 | 2.2E-03 |
| 416/1819 | 18 | 22/2/2016 | 85.2 | 5.87 | 1270/1165 | 13.2 | 0.51 | 2.6E-06 |
| 417/1820 | 18 | 20/6/2016 | 80.8 | 5.87 | 2521/2307 | 13.0 | 0.50 | 3.8E-07 |
| 418/1821 | 18 | 2/10/2016 | 148.9 | 5.87 | 5541/5489 | 13.9 | 0.47 | 2.6E-03 |
| 419/1822 | 18 | 21/5/2017 | 50.5 | 5.87 | 1030/1069 | 13.6 | 0.37 | 7.0E-03 |
| 420/1823 | 18 | 31/7/2017 | 175.9 | 5.87 | 3501/3733 | 13.0 | 0.33 | 8.4E-03 |
| 421/1824 | 18 | 23/7/2018 | 3.7 | 5.87 | 1/3 | 14.7 | 0.18 | 8.9E-03 |
| 422/1825 | 19 | 8/3/2013 | 31.5 | 5.88 | 707/685 | 9.8 | 0.37 | 7.2E-03 |
| 423/1826 | 19 | 10/4/2013 | 66.0 | 5.88 | 1356/1455 | 10.7 | 0.36 | 6.4E-03 |
| 424/1827 | 19 | 9/7/2013 | 41.1 | 5.88 | 704/747 | 11.1 | 0.36 | 6.1E-03 |
| 425/1828 | 19 | 27/8/2013 | 2.5 | 5.88 | 40/53 | 11.4 | 0.40 | 3.0E-03 |
| 426/1829 | 19 | 5/9/2013 | 45.7 | 5.88 | 819/860 | 11.8 | 0.44 | -9.2E-07 |
| 427/1830 | 19 | 21/11/2013 | 4.9 | 5.88 | 44/58 | 14.8 | 0.48 | -1.2E-03 |
| 428/1831 | 19 | 29/11/2013 | 1.3 | 5.88 | 18/14 | 14.2 | 0.46 | -1.2E-03 |
| 429/1832 | 19 | 10/1/2014 | 4.6 | 5.88 | 63/58 | 15.1 | 0.50 | -6.5E-08 |
| 430/1833 | 19 | 24/1/2014 | 38.6 | 5.88 | 425/474 | 15.8 | 0.50 | -8.2E-07 |
| 431/1834 | 19 | 6/3/2014 | 26.4 | 5.88 | 333/388 | 14.9 | 0.52 | 6.9E-08 |
| 432/1835 | 19 | 3/4/2014 | 18.4 | 5.88 | 246/270 | 15.5 | 0.50 | 6.1E-07 |
| 433/1836 | 19 | 26/4/2014 | 47.8 | 5.88 | 644/689 | 16.9 | 0.47 | 2.5E-07 |
| 434/1837 | 19 | 19/6/2014 | 73.4 | 5.88 | 934/971 | 15.5 | 0.46 | 9.8E-07 |
| 435/1838 | 19 | 5/9/2014 | 24.3 | 5.88 | 334/363 | 15.0 | 0.49 | 8.7E-07 |
| 436/1839 | 19 | 2/10/2014 | 103.7 | 5.88 | 2465/2613 | 17.4 | 0.48 | 2.9E-03 |
| 437/1840 | 19 | 25/2/2015 | 49.1 | 5.88 | 1196/1167 | 17.9 | 0.55 | 6.0E-07 |
| 438/1841 | 19 | 6/5/2015 | 149.7 | 5.88 | 2726/2778 | 19.5 | 0.51 | 1.5E-03 |
| 439/1842 | 19 | 1/11/2015 | 95.4 | 5.88 | 844/787 | 19.6 | 0.48 | 1.5E-03 |
| 440/1843 | 19 | 22/2/2016 | 85.2 | 5.88 | 1110/1119 | 19.3 | 0.46 | 2.4E-07 |
| 441/1844 | 19 | 20/6/2016 | 80.8 | 5.88 | 2233/2208 | 19.0 | 0.44 | 1.0E-07 |
| 442/1845 | 19 | 2/10/2016 | 148.9 | 5.88 | 5958/5982 | 20.1 | 0.39 | 2.6E-03 |
| 443/1846 | 19 | 21/5/2017 | 50.5 | 5.88 | 1550/1625 | 18.2 | 0.35 | 5.4E-03 |
| 444/1847 | 19 | 31/7/2017 | 175.9 | 5.88 | 4334/4618 | 16.0 | 0.40 | 3.3E-03 |
| 445/1848 | 19 | 23/7/2018 | 3.7 | 5.88 | 1/8 | 21.2 | 0.24 | 5.2E-03 |
| 446/1849 | 20 | 8/3/2013 | 31.5 | 5.88 | 556/562 | 17.4 | 0.65 | 2.3E-07 |
| 447/1850 | 20 | 10/4/2013 | 66.0 | 5.88 | 1209/1205 | 18.0 | 0.63 | 1.7E-03 |
| 448/1851 | 20 | 9/7/2013 | 0.3 | 5.88 | 6/4 | 17.0 | 0.62 | 1.2E-07 |
| 449/1852 | 20 | 11/7/2013 | 19.3 | 5.88 | 342/305 | 16.6 | 0.66 | 5.6E-08 |
| 450/1853 | 20 | 1/8/2013 | 8.0 | 5.88 | 156/129 | 17.3 | 0.66 | 1.6E-03 |
| 451/1854 | 20 | 12/8/2013 | 13.4 | 5.88 | 232/249 | 17.9 | 0.68 | 1.6E-03 |
| 452/1855 | 20 | 27/8/2013 | 2.5 | 5.88 | 49/47 | 16.8 | 0.68 | 2.5E-03 |
| 453/1856 | 20 | 5/9/2013 | 23.0 | 5.88 | 456/424 | 17.0 | 0.64 | 2.5E-03 |
| 454/1857 | 20 | 9/10/2013 | 14.6 | 5.88 | 250/261 | 17.4 | 0.68 | 5.2E-07 |
| 455/1858 | 20 | 29/10/2013 | 8.1 | 5.88 | 160/130 | 16.7 | 0.72 | 4.5E-07 |
| 456/1859 | 20 | 21/11/2013 | 4.9 | 5.88 | 18/18 | 19.9 | 0.66 | 1.5E-06 |
| 457/1860 | 20 | 29/11/2013 | 1.3 | 5.88 | 3/4 | 19.7 | 0.56 | 3.8E-03 |
| 458/1861 | 20 | 10/1/2014 | 4.6 | 5.88 | 31/33 | 18.1 | 0.63 | 2.0E-03 |
| 459/1862 | 20 | 24/1/2014 | 38.6 | 5.88 | 219/218 | 17.5 | 0.62 | 1.3E-03 |
| 460/1863 | 20 | 6/3/2014 | 26.4 | 5.88 | 182/178 | 16.3 | 0.60 | 1.3E-03 |
| 461/1864 | 20 | 3/4/2014 | 18.4 | 5.88 | 132/135 | 16.3 | 0.60 | 4.4E-07 |
| 462/1865 | 20 | 26/4/2014 | 47.8 | 5.88 | 342/305 | 16.0 | 0.61 | 4.4E-04 |
| 463/1866 | 20 | 19/6/2014 | 73.4 | 5.88 | 518/474 | 15.8 | 0.61 | 4.4E-04 |
| 464/1867 | 20 | 5/9/2014 | 24.3 | 5.88 | 239/282 | 15.7 | 0.60 | 5.5E-06 |
| 465/1868 | 20 | 2/10/2014 | 103.7 | 5.88 | 2689/2630 | 15.6 | 0.63 | 2.3E-07 |
| 466/1869 | 20 | 25/2/2015 | 49.1 | 5.88 | 1322/1305 | 16.0 | 0.63 | 7.8E-07 |
| 467/1870 | 20 | 6/5/2015 | 149.7 | 5.88 | 3602/3388 | 16.7 | 0.61 | 1.2E-07 |
| 468/1871 | 20 | 1/11/2015 | 95.4 | 5.88 | 1002/1016 | 17.0 | 0.59 | 8.9E-08 |
| 469/1872 | 20 | 22/2/2016 | 85.2 | 5.88 | 1515/1470 | 22.0 | 0.64 | 2.2E-07 |
| 470/1873 | 20 | 20/6/2016 | 80.8 | 5.88 | 2044/2027 | 16.9 | 0.61 | -8.9E-08 |
| 471/1874 | 20 | 2/10/2016 | 148.9 | 5.88 | 5537/5452 | 18.0 | 0.60 | 5.0E-04 |
| 472/1875 | 20 | 21/5/2017 | 50.5 | 5.88 | 1514/1407 | 16.7 | 0.48 | 5.4E-03 |

| Partition No. | D. No. | Start date | Dur. [d] | m [g] | Events | $p_0$ [keV] | $p_1$ [keV] | $p_2$ [keV] |
|---|---|---|---|---|---|---|---|---|
| 473/1876 | 20 | 31/7/2017 | 175.9 | 5.88 | 4542/4729 | 13.2 | 0.46 | 6.3E-03 |
| 474/1877 | 20 | 23/7/2018 | 3.7 | 5.88 | 0/3 | 18.3 | 0.34 | 9.9E-03 |
| 475/1878 | 21 | 8/3/2013 | 31.5 | 5.87 | 1051/1067 | 8.6 | 0.58 | 5.5E-04 |
| 476/1879 | 21 | 10/4/2013 | 65.6 | 5.87 | 2087/2065 | 8.6 | 0.57 | 5.5E-04 |
| 477/1880 | 21 | 9/7/2013 | 0.3 | 5.87 | 14/13 | 9.4 | 0.58 | 4.7E-07 |
| 478/1881 | 21 | 11/7/2013 | 19.3 | 5.87 | 521/499 | 9.2 | 0.57 | 7.3E-07 |
| 479/1882 | 21 | 1/8/2013 | 8.0 | 5.87 | 188/204 | 9.7 | 0.51 | 2.2E-03 |
| 480/1883 | 21 | 12/8/2013 | 11.8 | 5.87 | 335/329 | 9.7 | 0.54 | 2.2E-03 |
| 481/1884 | 21 | 27/8/2013 | 2.5 | 5.87 | 73/56 | 9.2 | 0.59 | 2.9E-03 |
| 482/1885 | 21 | 5/9/2013 | 23.0 | 5.87 | 790/727 | 9.7 | 0.52 | 2.9E-03 |
| 483/1886 | 21 | 9/10/2013 | 14.6 | 5.87 | 511/506 | 9.8 | 0.53 | 1.7E-03 |
| 484/1887 | 21 | 29/10/2013 | 8.1 | 5.87 | 227/228 | 9.3 | 0.58 | 3.5E-03 |
| 485/1888 | 21 | 21/11/2013 | 4.8 | 5.87 | 75/83 | 11.6 | 0.58 | 1.4E-08 |
| 486/1889 | 21 | 29/11/2013 | 1.3 | 5.87 | 27/30 | 11.2 | 0.55 | 6.9E-09 |
| 487/1890 | 21 | 10/1/2014 | 69.6 | 5.87 | 1923/1830 | 10.4 | 0.55 | -6.4E-07 |
| 488/1891 | 21 | 3/4/2014 | 18.3 | 5.87 | 520/480 | 11.9 | 0.55 | -3.2E-07 |
| 489/1892 | 21 | 26/4/2014 | 47.8 | 5.87 | 1161/1135 | 13.4 | 0.55 | 2.6E-03 |
| 490/1893 | 21 | 19/6/2014 | 73.9 | 5.87 | 1988/1902 | 11.6 | 0.52 | 2.6E-03 |
| 491/1894 | 21 | 5/9/2014 | 23.9 | 5.87 | 640/666 | 10.2 | 0.48 | -2.8E-07 |
| 492/1895 | 21 | 2/10/2014 | 104.0 | 5.87 | 4350/4151 | 10.7 | 0.47 | -6.3E-07 |
| 493/1896 | 21 | 25/2/2015 | 49.8 | 5.87 | 1735/1654 | 10.5 | 0.50 | -1.3E-05 |
| 494/1897 | 21 | 6/5/2015 | 156.3 | 5.87 | 4320/4213 | 11.1 | 0.46 | 2.4E-03 |
| 495/1898 | 21 | 1/11/2015 | 100.3 | 5.87 | 1389/1302 | 11.8 | 0.43 | 2.4E-03 |
| 496/1899 | 21 | 20/2/2016 | 92.4 | 5.87 | 1992/1965 | 11.6 | 0.45 | 2.4E-06 |
| 497/1900 | 21 | 20/6/2016 | 82.8 | 5.87 | 3971/4145 | 11.8 | 0.44 | -9.3E-08 |
| 498/1901 | 21 | 2/10/2016 | 121.1 | 5.87 | 6452/6509 | 12.2 | 0.42 | 1.4E-03 |
| 499/1902 | 21 | 20/5/2017 | 52.3 | 5.87 | 1816/1942 | 12.0 | 0.32 | 5.4E-03 |
| 500/1903 | 21 | 31/7/2017 | 174.1 | 5.87 | 5328/5632 | 11.7 | 0.32 | 7.0E-03 |
| 501/1904 | 21 | 23/7/2018 | 3.7 | 5.87 | 1/11 | 11.1 | 0.38 | 3.4E-03 |
| 502/1905 | 22 | 8/3/2013 | 31.5 | 5.85 | 875/970 | 15.1 | 0.41 | 6.4E-03 |
| 503/1906 | 22 | 10/4/2013 | 65.6 | 5.85 | 1569/1665 | 15.4 | 0.42 | 6.0E-03 |
| 504/1907 | 22 | 9/7/2013 | 0.3 | 5.85 | 7/10 | 18.8 | 0.71 | -8.4E-09 |
| 505/1908 | 22 | 11/7/2013 | 19.3 | 5.85 | 456/489 | 17.1 | 0.72 | -2.8E-07 |
| 506/1909 | 22 | 1/8/2013 | 8.0 | 5.85 | 203/181 | 17.2 | 0.65 | -6.2E-07 |
| 507/1910 | 22 | 12/8/2013 | 11.8 | 5.85 | 269/273 | 17.6 | 0.63 | -3.1E-07 |
| 508/1911 | 22 | 27/8/2013 | 2.5 | 5.85 | 55/70 | 17.5 | 0.61 | -1.0E-03 |
| 509/1912 | 22 | 5/9/2013 | 23.0 | 5.85 | 455/458 | 18.8 | 0.55 | -1.0E-03 |
| 510/1913 | 22 | 9/10/2013 | 14.6 | 5.85 | 294/291 | 18.0 | 0.67 | -1.7E-07 |
| 511/1914 | 22 | 29/10/2013 | 8.1 | 5.85 | 202/184 | 16.9 | 0.71 | -2.0E-07 |
| 512/1915 | 22 | 21/11/2013 | 4.8 | 5.85 | 90/110 | 19.3 | 0.68 | -1.2E-07 |
| 513/1916 | 22 | 29/11/2013 | 1.3 | 5.85 | 24/22 | 18.2 | 0.69 | -3.9E-07 |
| 514/1917 | 22 | 10/1/2014 | 4.6 | 5.85 | 129/153 | 19.9 | 0.64 | -3.6E-07 |
| 515/1918 | 22 | 24/1/2014 | 38.6 | 5.85 | 913/914 | 19.5 | 0.66 | -4.8E-07 |
| 516/1919 | 22 | 6/3/2014 | 26.4 | 5.85 | 632/689 | 20.5 | 0.63 | -2.8E-07 |
| 517/1920 | 22 | 3/4/2014 | 18.3 | 5.85 | 442/465 | 22.1 | 0.63 | 2.1E-08 |
| 518/1921 | 22 | 26/4/2014 | 47.8 | 5.85 | 1049/1096 | 23.6 | 0.66 | -4.5E-07 |
| 519/1922 | 22 | 19/6/2014 | 73.9 | 5.85 | 1528/1483 | 22.8 | 0.70 | -2.1E-06 |
| 520/1923 | 22 | 5/9/2014 | 23.9 | 5.85 | 544/573 | 22.4 | 0.70 | -1.8E-06 |
| 521/1924 | 22 | 2/10/2014 | 104.0 | 5.85 | 2598/2597 | 24.8 | 0.69 | 2.5E-08 |
| 522/1925 | 22 | 25/2/2015 | 49.8 | 5.85 | 952/963 | 26.0 | 0.68 | 4.8E-07 |
| 523/1926 | 22 | 6/5/2015 | 156.3 | 5.85 | 2542/2608 | 27.4 | 0.68 | 5.9E-06 |
| 524/1927 | 22 | 1/11/2015 | 100.3 | 5.85 | 761/711 | 28.7 | 0.69 | 1.1E-05 |
| 525/1928 | 22 | 20/2/2016 | 92.4 | 5.85 | 1098/1175 | 29.3 | 0.70 | 6.4E-06 |
| 526/1929 | 22 | 20/6/2016 | 82.8 | 5.85 | 2195/2294 | 28.7 | 0.69 | 1.1E-05 |
| 527/1930 | 22 | 2/10/2016 | 121.1 | 5.85 | 4101/4033 | 29.0 | 0.69 | 5.1E-04 |
| 528/1931 | 22 | 20/5/2017 | 52.3 | 5.85 | 1296/1434 | 27.5 | 0.56 | 4.5E-03 |
| 529/1932 | 22 | 31/7/2017 | 174.1 | 5.85 | 3537/3738 | 25.5 | 0.53 | 4.5E-03 |
| 530/1933 | 22 | 23/7/2018 | 3.7 | 5.85 | 3/1 | 30.3 | 0.61 | 3.0E-03 |
| 531/1934 | 23 | 9/7/2013 | 0.3 | 5.90 | 8/11 | 10.5 | 0.63 | -4.6E-07 |
| 532/1935 | 23 | 11/7/2013 | 19.3 | 5.90 | 481/473 | 5.6 | 0.64 | 1.3E-03 |
| 533/1936 | 23 | 1/8/2013 | 8.0 | 5.90 | 177/177 | 5.7 | 0.57 | -2.6E-03 |
| 534/1937 | 23 | 12/8/2013 | 11.8 | 5.90 | 291/267 | 11.6 | 0.48 | -8.1E-03 |
| 535/1938 | 23 | 27/8/2013 | 2.5 | 5.90 | 49/37 | 5.8 | 0.56 | -2.5E-03 |
| 536/1939 | 23 | 5/9/2013 | 23.0 | 5.90 | 528/531 | 0.0 | 0.66 | 3.4E-03 |
| 537/1940 | 23 | 9/10/2013 | 14.6 | 5.90 | 327/306 | 4.0 | 0.66 | 1.7E-03 |
| 538/1941 | 23 | 29/10/2013 | 8.1 | 5.90 | 204/201 | 8.0 | 0.66 | -3.3E-07 |
| 539/1942 | 23 | 21/11/2013 | 4.8 | 5.90 | 105/111 | 11.8 | 0.49 | -8.3E-03 |
| 540/1943 | 23 | 29/11/2013 | 1.3 | 5.90 | 29/35 | 11.4 | 0.43 | -8.9E-03 |
| 541/1944 | 23 | 10/1/2014 | 4.6 | 5.90 | 131/128 | 8.9 | 0.53 | -4.1E-03 |
| 542/1945 | 23 | 24/1/2014 | 38.6 | 5.90 | 1098/1069 | 12.1 | 0.41 | -8.2E-03 |
| 543/1946 | 23 | 6/3/2014 | 26.4 | 5.90 | 703/689 | 11.3 | 0.44 | -7.9E-03 |
| 544/1947 | 23 | 3/4/2014 | 18.3 | 5.90 | 461/477 | 12.5 | 0.51 | -6.8E-03 |

| Partition No. | D. No. | Start date | Dur. [d] | m [g] | Events | $p_0$ [keV] | $p_1$ [keV] | $p_2$ [keV] |
|---|---|---|---|---|---|---|---|---|
| 545/1948 | 23 | 26/4/2014 | 47.8 | 5.90 | 1047/1101 | 15.6 | 0.57 | -6.4E-03 |
| 546/1949 | 23 | 19/6/2014 | 73.9 | 5.90 | 1736/1710 | 13.7 | 0.50 | -7.6E-03 |
| 547/1950 | 23 | 5/9/2014 | 23.9 | 5.90 | 503/517 | 8.1 | 0.54 | -4.2E-03 |
| 548/1951 | 23 | 2/10/2014 | 104.0 | 5.90 | 2550/2675 | 5.4 | 0.67 | -1.1E-07 |
| 549/1952 | 23 | 25/2/2015 | 49.8 | 5.90 | 1768/1715 | 11.1 | 0.42 | 2.9E-04 |
| 550/1953 | 23 | 6/5/2015 | 256.6 | 5.90 | 5669/5533 | 11.4 | 0.43 | -9.4E-03 |
| 551/1954 | 23 | 20/2/2016 | 92.4 | 5.90 | 1912/1961 | 11.5 | 0.47 | -9.5E-04 |
| 552/1955 | 23 | 20/6/2016 | 82.8 | 5.90 | 3100/2815 | 11.1 | 0.41 | 1.1E-03 |
| 553/1956 | 23 | 2/10/2016 | 121.1 | 5.90 | 5707/5686 | 12.2 | 0.41 | 8.8E-03 |
| 554/1957 | 23 | 20/5/2017 | 52.3 | 5.90 | 1905/1915 | 12.0 | 0.36 | 8.1E-03 |
| 555/1958 | 23 | 31/7/2017 | 174.1 | 5.90 | 5213/5541 | 11.6 | 0.27 | 1.0E-02 |
| 556/1959 | 23 | 23/7/2018 | 3.7 | 5.90 | 2/4 | 11.9 | 0.36 | 8.2E-03 |
| 557/1960 | 24 | 8/3/2013 | 31.5 | 6.46 | 1096/1020 | 8.9 | 0.80 | 4.6E-02 |
| 558/1961 | 24 | 10/4/2013 | 65.6 | 6.46 | 2128/2049 | 9.2 | 0.73 | 4.7E-02 |
| 559/1962 | 24 | 9/7/2013 | 0.3 | 6.46 | 21/7 | 9.8 | 0.69 | 5.1E-02 |
| 560/1963 | 24 | 11/7/2013 | 19.3 | 6.46 | 693/702 | 5.2 | 0.89 | 4.2E-02 |
| 561/1964 | 24 | 1/8/2013 | 8.0 | 6.46 | 276/231 | 0.0 | 1.20 | 3.3E-02 |
| 562/1965 | 24 | 12/8/2013 | 11.8 | 6.46 | 440/329 | 0.5 | 1.06 | 4.2E-02 |
| 563/1966 | 24 | 27/8/2013 | 2.5 | 6.46 | 107/76 | 1.0 | 0.84 | 4.9E-02 |
| 564/1967 | 24 | 5/9/2013 | 23.0 | 6.46 | 1073/852 | 2.1 | 0.90 | 4.1E-02 |
| 565/1968 | 24 | 9/10/2013 | 14.6 | 6.46 | 663/539 | 2.1 | 0.96 | 3.7E-02 |
| 566/1969 | 24 | 29/10/2013 | 8.1 | 6.46 | 307/260 | 0.4 | 1.04 | 3.4E-02 |
| 567/1970 | 24 | 21/11/2013 | 4.8 | 5.72 | 75/62 | 5.4 | 0.92 | 7.8E-03 |
| 568/1971 | 24 | 29/11/2013 | 1.3 | 5.72 | 23/16 | 7.3 | 0.81 | 1.5E-02 |
| 569/1972 | 24 | 10/1/2014 | 4.6 | 5.72 | 101/68 | 6.6 | 0.85 | 1.6E-02 |
| 570/1973 | 24 | 24/1/2014 | 38.6 | 5.72 | 898/620 | 2.5 | 0.95 | 7.0E-03 |
| 571/1974 | 24 | 6/3/2014 | 26.4 | 5.72 | 631/414 | 0.5 | 0.94 | 7.3E-03 |
| 572/1975 | 24 | 3/4/2014 | 18.3 | 5.72 | 460/284 | 0.9 | 0.92 | 1.3E-02 |
| 573/1976 | 24 | 26/4/2014 | 47.8 | 5.72 | 1086/737 | 4.4 | 0.86 | 1.7E-02 |
| 574/1977 | 24 | 19/6/2014 | 73.9 | 5.72 | 1722/1220 | 6.1 | 0.84 | 1.7E-02 |
| 575/1978 | 24 | 5/9/2014 | 23.9 | 5.72 | 592/465 | 4.4 | 0.88 | 1.3E-02 |
| 576/1979 | 24 | 2/10/2014 | 104.0 | 5.72 | 3904/2649 | 2.9 | 0.91 | 1.3E-02 |
| 577/1980 | 24 | 25/2/2015 | 49.8 | 5.72 | 1649/1067 | 0.9 | 0.98 | 1.1E-02 |
| 578/1981 | 24 | 6/5/2015 | 256.6 | 5.72 | 5330/3822 | 0.9 | 0.98 | 1.1E-02 |
| 579/1982 | 24 | 20/2/2016 | 92.4 | 5.72 | 1879/1352 | 5.6 | 0.81 | 1.4E-02 |
| 580/1983 | 24 | 20/6/2016 | 82.8 | 5.72 | 3191/2096 | 0.9 | 0.98 | 1.1E-02 |
| 581/1984 | 24 | 2/10/2016 | 121.1 | 5.72 | 6335/4494 | 5.7 | 0.83 | 1.4E-02 |
| 582/1985 | 24 | 20/5/2017 | 52.3 | 5.72 | 1950/1447 | 8.1 | 0.70 | 1.8E-02 |
| 583/1986 | 24 | 31/7/2017 | 174.1 | 5.72 | 5813/4131 | 6.9 | 0.70 | 2.0E-02 |
| 584/1987 | 24 | 23/7/2018 | 3.7 | 5.72 | 1/2 | 11.6 | 0.55 | 2.2E-02 |
| 585/1988 | 25 | 9/7/2013 | 0.3 | 5.88 | 6/13 | 9.4 | 0.60 | 3.8E-03 |
| 586/1989 | 25 | 11/7/2013 | 19.3 | 5.88 | 631/653 | 8.8 | 0.59 | 2.5E-04 |
| 587/1990 | 25 | 1/8/2013 | 8.0 | 5.88 | 267/264 | 4.3 | 0.67 | -2.1E-03 |
| 588/1991 | 25 | 12/8/2013 | 13.4 | 5.88 | 453/466 | 4.4 | 0.70 | 3.7E-03 |
| 589/1992 | 25 | 27/8/2013 | 2.5 | 5.88 | 88/86 | 8.9 | 0.62 | 7.2E-03 |
| 590/1993 | 25 | 5/9/2013 | 11.2 | 5.88 | 304/372 | 10.2 | 0.43 | -3.6E-03 |
| 591/1994 | 25 | 9/10/2013 | 22.7 | 5.88 | 676/742 | 11.5 | 0.25 | -1.7E-02 |
| 592/1995 | 25 | 21/11/2013 | 4.5 | 5.88 | 105/103 | 8.9 | 0.60 | 1.0E-02 |
| 593/1996 | 25 | 29/11/2013 | 1.3 | 5.88 | 46/32 | 8.6 | 0.60 | 6.8E-03 |
| 594/1997 | 25 | 10/1/2014 | 4.6 | 5.88 | 152/141 | 8.7 | 0.62 | -7.7E-07 |
| 595/1998 | 25 | 24/1/2014 | 38.4 | 5.88 | 1107/1254 | 8.4 | 0.61 | 1.1E-03 |
| 596/1999 | 25 | 6/3/2014 | 26.4 | 5.88 | 817/884 | 8.9 | 0.54 | 5.7E-03 |
| 597/2000 | 25 | 3/4/2014 | 18.3 | 5.88 | 524/574 | 17.8 | 0.24 | -1.4E-03 |
| 598/2001 | 25 | 26/4/2014 | 635.1 | 5.88 | 14655/15896 | 26.0 | 0.00 | -1.2E-02 |
| 599/2002 | 25 | 20/6/2016 | 82.2 | 5.88 | 3739/3840 | 17.9 | 0.21 | -1.5E-03 |
| 600/2003 | 25 | 2/10/2016 | 148.1 | 5.88 | 7772/8346 | 10.0 | 0.46 | 8.8E-03 |
| 601/2004 | 25 | 21/5/2017 | 52.9 | 5.88 | 1123/1092 | 10.2 | 0.44 | 8.7E-03 |
| 602/2005 | 25 | 31/7/2017 | 174.8 | 5.88 | 3456/3770 | 14.3 | 0.48 | 7.6E-03 |
| 603/2006 | 25 | 23/7/2018 | 3.7 | 5.88 | 4/5 | 9.5 | 0.44 | 7.7E-03 |
| 604/2007 | 26 | 8/3/2013 | 91.9 | 5.88 | 3005/3458 | 12.2 | 0.50 | -8.4E-08 |
| 605/2008 | 26 | 9/7/2013 | 0.3 | 5.88 | 9/6 | 6.8 | 0.54 | 5.5E-03 |
| 606/2009 | 26 | 11/7/2013 | 19.3 | 5.88 | 586/646 | 8.3 | 0.47 | 7.8E-03 |
| 607/2010 | 26 | 1/8/2013 | 8.0 | 5.88 | 240/239 | 11.2 | 0.36 | 7.8E-04 |
| 608/2011 | 26 | 12/8/2013 | 13.4 | 5.88 | 349/420 | 10.3 | 0.39 | -6.3E-04 |
| 609/2012 | 26 | 27/8/2013 | 2.5 | 5.88 | 74/78 | 8.7 | 0.49 | 1.8E-03 |
| 610/2013 | 26 | 5/9/2013 | 11.2 | 5.88 | 281/311 | 8.3 | 0.54 | -2.1E-03 |
| 611/2014 | 26 | 9/10/2013 | 14.6 | 5.88 | 372/383 | 8.5 | 0.53 | 1.4E-06 |
| 612/2015 | 26 | 29/10/2013 | 8.1 | 5.88 | 234/245 | 8.1 | 0.51 | 3.7E-03 |
| 613/2016 | 26 | 21/11/2013 | 4.5 | 5.88 | 129/168 | 9.9 | 0.53 | -4.8E-03 |
| 614/2017 | 26 | 29/11/2013 | 44.4 | 5.88 | 1334/1419 | 8.6 | 0.55 | -4.1E-03 |
| 615/2018 | 26 | 6/3/2014 | 26.4 | 5.88 | 878/944 | 8.3 | 0.56 | -2.0E-03 |
| 616/2019 | 26 | 3/4/2014 | 18.3 | 5.88 | 659/622 | 8.8 | 0.55 | 2.2E-03 |

| Partition No. | D. No. | Start date | Dur. [d] | m [g] | Events | $p_0$ [keV] | $p_1$ [keV] | $p_2$ [keV] |
|---|---|---|---|---|---|---|---|---|
| 617/2020 | 26 | 26/4/2014 | 47.0 | 5.88 | 1448/1510 | 6.6 | 0.57 | 2.2E-03 |
| 618/2021 | 26 | 19/6/2014 | 71.7 | 5.88 | 2495/2417 | 1.7 | 0.58 | 2.6E-03 |
| 619/2022 | 26 | 5/9/2014 | 24.3 | 5.88 | 724/756 | 0.0 | 0.56 | 5.3E-03 |
| 620/2023 | 26 | 2/10/2014 | 103.5 | 5.88 | 3963/4514 | 0.0 | 0.57 | 5.5E-03 |
| 621/2024 | 26 | 25/2/2015 | 49.6 | 5.88 | 1463/1566 | 10.4 | 0.43 | -8.6E-03 |
| 622/2025 | 26 | 6/5/2015 | 154.8 | 5.88 | 3702/3913 | 10.5 | 0.45 | -8.3E-03 |
| 623/2026 | 26 | 1/11/2015 | 89.9 | 5.88 | 963/993 | 10.6 | 0.46 | -8.1E-03 |
| 624/2027 | 26 | 20/2/2016 | 94.3 | 5.88 | 1886/1966 | 11.4 | 0.42 | 3.5E-04 |
| 625/2028 | 26 | 20/6/2016 | 82.2 | 5.88 | 3739/3803 | 12.3 | 0.46 | 3.7E-04 |
| 626/2029 | 26 | 2/10/2016 | 148.1 | 5.88 | 7459/7744 | 11.4 | 0.43 | 9.1E-03 |
| 627/2030 | 26 | 21/5/2017 | 52.9 | 5.88 | 1738/1828 | 12.0 | 0.30 | 9.9E-03 |
| 628/2031 | 26 | 31/7/2017 | 174.8 | 5.88 | 5194/5505 | 11.2 | 0.28 | 8.9E-03 |
| 629/2032 | 26 | 23/7/2018 | 3.7 | 5.88 | 3/13 | 11.8 | 0.34 | 8.4E-03 |
| 630/2033 | 27 | 8/3/2013 | 92.2 | 5.88 | 2968/2753 | 1.2 | 0.06 | 1.6E-03 |
| 631/2034 | 27 | 11/7/2013 | 19.3 | 5.88 | 446/403 | 6.4 | 0.23 | -4.1E-03 |
| 632/2035 | 27 | 1/8/2013 | 8.0 | 5.88 | 202/167 | 12.4 | 0.31 | -1.1E-02 |
| 633/2036 | 27 | 12/8/2013 | 13.4 | 5.88 | 315/305 | 11.5 | 0.34 | -3.7E-05 |
| 634/2037 | 27 | 27/8/2013 | 2.5 | 5.88 | 58/48 | 11.7 | 0.28 | 1.2E-02 |
| 635/2038 | 27 | 5/9/2013 | 11.2 | 5.88 | 247/222 | 11.4 | 0.35 | 5.9E-03 |
| 636/2039 | 27 | 9/10/2013 | 22.7 | 5.88 | 490/549 | 9.2 | 0.59 | 1.3E-06 |
| 637/2040 | 27 | 21/11/2013 | 4.5 | 5.88 | 100/92 | 12.0 | 0.53 | 4.2E-04 |
| 638/2041 | 27 | 29/11/2013 | 1.3 | 5.88 | 22/37 | 11.2 | 0.54 | 1.5E-03 |
| 639/2042 | 27 | 10/1/2014 | 4.6 | 5.88 | 122/106 | 10.1 | 0.70 | -1.1E-07 |
| 640/2043 | 27 | 24/1/2014 | 38.4 | 5.88 | 958/795 | 11.3 | 0.61 | -3.6E-03 |
| 641/2044 | 27 | 6/3/2014 | 26.4 | 5.88 | 683/626 | 6.2 | 0.59 | -1.6E-03 |
| 642/2045 | 27 | 3/4/2014 | 18.3 | 5.88 | 487/441 | 5.7 | 0.58 | -2.2E-03 |
| 643/2046 | 27 | 26/4/2014 | 47.0 | 5.88 | 1093/1136 | 12.9 | 0.46 | -9.4E-03 |
| 644/2047 | 27 | 19/6/2014 | 71.7 | 5.88 | 1800/1638 | 14.7 | 0.22 | -1.2E-02 |
| 645/2048 | 27 | 5/9/2014 | 24.3 | 5.88 | 589/581 | 14.2 | 0.21 | -1.2E-02 |
| 646/2049 | 27 | 2/10/2014 | 103.5 | 5.88 | 3732/3483 | 12.2 | 0.52 | -1.0E-02 |
| 647/2050 | 27 | 25/2/2015 | 49.6 | 5.88 | 853/879 | 13.3 | 0.40 | -7.3E-04 |
| 648/2051 | 27 | 6/5/2015 | 154.8 | 5.88 | 2631/2661 | 14.4 | 0.33 | -1.4E-02 |
| 649/2052 | 27 | 1/11/2015 | 89.9 | 5.88 | 650/664 | 14.6 | 0.35 | -1.3E-02 |
| 650/2053 | 27 | 20/2/2016 | 94.3 | 5.88 | 1465/1323 | 13.4 | 0.50 | -3.3E-03 |
| 651/2054 | 27 | 20/6/2016 | 82.2 | 5.88 | 2978/2859 | 15.9 | 0.36 | 1.1E-02 |
| 652/2055 | 27 | 2/10/2016 | 148.1 | 5.88 | 6344/6140 | 14.6 | 0.42 | 9.4E-03 |
| 653/2056 | 27 | 21/5/2017 | 52.9 | 5.88 | 1190/1288 | 14.7 | 0.33 | 1.1E-02 |
| 654/2057 | 27 | 31/7/2017 | 174.8 | 5.88 | 4016/4155 | 13.6 | 0.32 | 1.1E-02 |
| 655/2058 | 27 | 23/7/2018 | 3.7 | 5.88 | 1/1 | 15.9 | 0.14 | 1.1E-02 |
| 656/2059 | 28 | 8/3/2013 | 29.0 | 6.53 | 1433/1330 | 12.0 | 0.80 | 2.5E-02 |
| 657/2060 | 28 | 10/4/2013 | 62.9 | 6.53 | 2269/2196 | 13.1 | 0.80 | 2.3E-02 |
| 658/2061 | 28 | 9/7/2013 | 19.7 | 6.53 | 520/445 | 12.2 | 0.94 | 1.7E-02 |
| 659/2062 | 28 | 1/8/2013 | 8.0 | 6.53 | 231/183 | 10.2 | 0.92 | 1.9E-02 |
| 660/2063 | 28 | 12/8/2013 | 13.4 | 6.53 | 379/242 | 7.9 | 0.95 | 1.5E-02 |
| 661/2064 | 28 | 27/8/2013 | 2.5 | 6.53 | 51/46 | 6.2 | 1.00 | 1.1E-02 |
| 662/2065 | 28 | 6/3/2014 | 26.4 | 6.53 | 817/614 | 9.1 | 0.88 | 1.6E-02 |
| 663/2066 | 28 | 3/4/2014 | 18.3 | 6.53 | 540/395 | 4.6 | 0.85 | 1.8E-02 |
| 664/2067 | 28 | 26/4/2014 | 47.0 | 6.53 | 1306/1021 | 3.0 | 0.87 | 1.8E-02 |
| 665/2068 | 28 | 19/6/2014 | 71.7 | 6.53 | 1962/1404 | 8.9 | 0.83 | 1.7E-02 |
| 666/2069 | 28 | 5/9/2014 | 24.3 | 6.53 | 928/620 | 11.1 | 0.74 | 2.0E-02 |
| 667/2070 | 28 | 2/10/2014 | 103.5 | 6.53 | 6225/4425 | 10.7 | 0.76 | 2.1E-02 |
| 668/2071 | 28 | 25/2/2015 | 49.6 | 6.53 | 2587/2227 | -1.1 | 0.82 | 1.6E-02 |
| 669/2072 | 28 | 6/5/2015 | 154.8 | 6.53 | 6033/4957 | -11.3 | 0.72 | 2.0E-02 |
| 670/2073 | 28 | 1/11/2015 | 89.9 | 6.53 | 1171/886 | 1.1 | 0.89 | 9.9E-03 |
| 671/2074 | 28 | 20/2/2016 | 94.3 | 6.53 | 2008/1482 | 18.2 | 1.11 | 7.1E-06 |
| 672/2075 | 28 | 20/6/2016 | 82.2 | 6.53 | 3791/2858 | 13.5 | 1.06 | 3.7E-06 |
| 673/2076 | 28 | 2/10/2016 | 148.1 | 6.53 | 11230/9223 | 20.2 | 0.93 | 1.1E-02 |
| 674/2077 | 29 | 8/3/2013 | 31.4 | 5.88 | 886/870 | 11.5 | 0.76 | 2.7E-03 |
| 675/2078 | 29 | 10/4/2013 | 65.8 | 5.88 | 1791/1791 | 11.9 | 0.77 | 2.7E-03 |
| 676/2079 | 29 | 9/7/2013 | 0.3 | 5.88 | 11/7 | 12.5 | 0.75 | 2.0E-03 |
| 677/2080 | 29 | 11/7/2013 | 19.3 | 5.88 | 476/438 | 11.0 | 0.75 | 2.0E-03 |
| 678/2081 | 29 | 1/8/2013 | 8.0 | 5.88 | 205/198 | 11.2 | 0.73 | 4.2E-07 |
| 679/2082 | 29 | 12/8/2013 | 11.6 | 5.88 | 281/275 | 11.9 | 0.75 | -3.3E-07 |
| 680/2083 | 29 | 27/8/2013 | 2.5 | 5.88 | 65/66 | 13.8 | 0.62 | -6.4E-03 |
| 681/2084 | 29 | 5/9/2013 | 20.5 | 5.88 | 562/506 | 13.5 | 0.62 | -6.4E-03 |
| 682/2085 | 29 | 9/10/2013 | 13.1 | 5.88 | 326/323 | 11.1 | 0.76 | 4.2E-08 |
| 683/2086 | 29 | 29/10/2013 | 8.1 | 5.88 | 207/215 | 11.2 | 0.75 | 1.1E-03 |
| 684/2087 | 29 | 21/11/2013 | 4.7 | 5.88 | 45/38 | 15.3 | 0.67 | 4.1E-03 |
| 685/2088 | 29 | 29/11/2013 | 1.3 | 5.88 | 23/15 | 12.9 | 0.72 | 6.3E-07 |
| 686/2089 | 29 | 10/1/2014 | 4.6 | 5.88 | 85/85 | 14.5 | 0.70 | 4.5E-04 |
| 687/2090 | 29 | 24/1/2014 | 38.4 | 5.88 | 596/566 | 14.3 | 0.70 | 4.5E-04 |
| 688/2091 | 29 | 6/3/2014 | 26.3 | 5.88 | 415/417 | 12.8 | 0.70 | 4.2E-08 |

| Partition No. | D. No. | Start date | Dur. [d] | m [g] | Events | $p_0$ [keV] | $p_1$ [keV] | $p_2$ [keV] |
|---|---|---|---|---|---|---|---|---|
| 689/2092 | 29 | 3/4/2014 | 18.3 | 5.88 | 309/277 | 14.6 | 0.66 | 5.3E-03 |
| 690/2093 | 29 | 26/4/2014 | 47.8 | 5.88 | 735/707 | 17.1 | 0.63 | 6.5E-03 |
| 691/2094 | 29 | 19/6/2014 | 74.0 | 5.88 | 1034/1028 | 14.8 | 0.66 | 1.2E-03 |
| 692/2095 | 29 | 5/9/2014 | 24.3 | 5.88 | 463/425 | 13.9 | 0.60 | 4.9E-03 |
| 693/2096 | 29 | 2/10/2014 | 104.0 | 5.88 | 3287/3134 | 14.4 | 0.60 | 4.9E-03 |
| 694/2097 | 29 | 7/5/2015 | 150.9 | 5.88 | 4175/4121 | 13.4 | 0.69 | 3.5E-07 |
| 695/2098 | 29 | 1/11/2015 | 99.6 | 5.88 | 1270/1273 | 14.1 | 0.67 | 2.8E-03 |
| 696/2099 | 29 | 20/2/2016 | 98.6 | 5.88 | 1847/1833 | 13.4 | 0.68 | 3.9E-03 |
| 697/2100 | 29 | 20/6/2016 | 80.9 | 5.88 | 2977/3040 | 14.5 | 0.58 | 8.0E-03 |
| 698/2101 | 29 | 2/10/2016 | 141.7 | 5.88 | 6251/6494 | 15.2 | 0.63 | 5.8E-03 |
| 699/2102 | 29 | 21/5/2017 | 54.5 | 5.88 | 1802/1924 | 14.6 | 0.61 | 5.9E-03 |
| 700/2103 | 29 | 31/7/2017 | 178.2 | 5.88 | 4789/5258 | 12.3 | 0.52 | 9.6E-03 |
| 701/2104 | 29 | 24/7/2018 | 3.3 | 5.88 | 2/0 | 14.1 | 0.58 | 8.0E-03 |
| 702/2105 | 30 | 8/3/2013 | 31.4 | 5.86 | 766/807 | 11.6 | 0.53 | 1.7E-02 |
| 703/2106 | 30 | 10/4/2013 | 65.8 | 5.86 | 1452/1469 | 11.5 | 0.54 | 1.7E-02 |
| 704/2107 | 30 | 9/7/2013 | 0.3 | 5.86 | 5/9 | 11.7 | 0.73 | -1.4E-07 |
| 705/2108 | 30 | 11/7/2013 | 19.3 | 5.86 | 363/362 | 12.1 | 0.65 | 7.7E-03 |
| 706/2109 | 30 | 1/8/2013 | 8.0 | 5.86 | 162/161 | 13.3 | 0.52 | 1.5E-02 |
| 707/2110 | 30 | 12/8/2013 | 11.6 | 5.86 | 270/217 | 13.3 | 0.50 | 1.7E-02 |
| 708/2111 | 30 | 27/8/2013 | 2.5 | 5.86 | 48/44 | 15.0 | 0.24 | 2.1E-02 |
| 709/2112 | 30 | 5/9/2013 | 20.5 | 5.86 | 454/445 | 16.8 | 0.00 | 2.3E-02 |
| 710/2113 | 30 | 9/10/2013 | 13.1 | 5.86 | 278/260 | 14.7 | 0.18 | 2.3E-02 |
| 711/2114 | 30 | 29/10/2013 | 8.1 | 5.86 | 168/176 | 12.6 | 0.36 | 2.3E-02 |
| 712/2115 | 30 | 21/11/2013 | 4.7 | 5.86 | 47/51 | 17.1 | 0.66 | 7.6E-06 |
| 713/2116 | 30 | 29/11/2013 | 1.3 | 5.86 | 17/14 | 16.6 | 0.61 | 3.8E-06 |
| 714/2117 | 30 | 10/1/2014 | 4.6 | 5.86 | 78/107 | 15.5 | 0.61 | 3.3E-07 |
| 715/2118 | 30 | 24/1/2014 | 38.4 | 5.86 | 580/600 | 14.7 | 0.61 | 3.8E-08 |
| 716/2119 | 30 | 6/3/2014 | 44.6 | 5.86 | 773/754 | 14.0 | 0.59 | 1.1E-07 |
| 717/2120 | 30 | 26/4/2014 | 47.8 | 5.86 | 785/690 | 15.0 | 0.60 | 1.4E-07 |
| 718/2121 | 30 | 19/6/2014 | 236.1 | 5.86 | 6523/6499 | 16.0 | 0.60 | 1.7E-07 |
| 719/2122 | 30 | 7/5/2015 | 150.9 | 5.86 | 4637/4807 | 15.8 | 0.54 | -3.6E-03 |
| 720/2123 | 30 | 1/11/2015 | 99.6 | 5.86 | 1338/1375 | 15.6 | 0.53 | -3.6E-03 |
| 721/2124 | 30 | 20/2/2016 | 98.6 | 5.86 | 1990/2035 | 13.8 | 0.61 | 6.1E-07 |
| 722/2125 | 30 | 20/6/2016 | 80.9 | 5.86 | 3786/3948 | 14.5 | 0.53 | 2.8E-03 |
| 723/2126 | 30 | 2/10/2016 | 141.7 | 5.86 | 7074/7091 | 14.4 | 0.51 | 6.2E-03 |
| 724/2127 | 30 | 21/5/2017 | 54.5 | 5.86 | 1873/2075 | 13.9 | 0.42 | 7.8E-03 |
| 725/2128 | 30 | 31/7/2017 | 178.2 | 5.86 | 5403/6124 | 12.2 | 0.34 | 7.2E-03 |
| 726/2129 | 30 | 24/7/2018 | 3.3 | 5.86 | 0/0 | 14.2 | 0.43 | 4.5E-03 |
| 727/2130 | 31 | 8/3/2013 | 31.4 | 5.89 | 904/863 | 10.9 | 0.45 | 7.2E-03 |
| 728/2131 | 31 | 10/4/2013 | 65.8 | 5.89 | 1720/1588 | 11.0 | 0.45 | 6.7E-03 |
| 729/2132 | 31 | 9/7/2013 | 0.3 | 5.89 | 6/3 | 15.0 | 0.75 | -1.4E-08 |
| 730/2133 | 31 | 11/7/2013 | 19.3 | 5.89 | 388/351 | 14.4 | 0.66 | -1.8E-08 |
| 731/2134 | 31 | 1/8/2013 | 8.0 | 5.89 | 155/166 | 14.2 | 0.60 | 1.9E-08 |
| 732/2135 | 31 | 12/8/2013 | 11.6 | 5.89 | 224/232 | 13.9 | 0.61 | 1.4E-06 |
| 733/2136 | 31 | 27/8/2013 | 2.5 | 5.89 | 58/49 | 13.2 | 0.60 | 2.7E-06 |
| 734/2137 | 31 | 5/9/2013 | 20.5 | 5.89 | 132/125 | 25.3 | 0.88 | 1.9E-06 |
| 735/2138 | 31 | 6/3/2014 | 26.3 | 5.89 | 251/231 | 9.3 | 0.73 | 1.7E-06 |
| 736/2139 | 31 | 3/4/2014 | 18.3 | 5.89 | 170/154 | 18.3 | 0.71 | 1.3E-06 |
| 737/2140 | 31 | 26/4/2014 | 47.8 | 5.89 | 325/321 | 27.4 | 0.68 | 8.8E-07 |
| 738/2141 | 31 | 19/6/2014 | 74.0 | 5.89 | 390/420 | 18.5 | 0.65 | 2.2E-03 |
| 739/2142 | 31 | 5/9/2014 | 24.3 | 5.89 | 242/218 | 7.7 | 0.67 | 4.2E-03 |
| 740/2143 | 31 | 2/10/2014 | 104.0 | 5.89 | 1833/1715 | 5.9 | 0.72 | 4.1E-03 |
| 741/2144 | 31 | 3/3/2015 | 33.8 | 5.89 | 824/701 | 10.1 | 0.69 | -5.4E-03 |
| 742/2145 | 31 | 7/5/2015 | 150.9 | 5.89 | 2951/2732 | 10.1 | 0.70 | -2.7E-03 |
| 743/2146 | 31 | 1/11/2015 | 99.6 | 5.89 | 861/862 | 11.9 | 0.68 | -1.4E-07 |
| 744/2147 | 31 | 20/2/2016 | 98.6 | 5.89 | 1243/1191 | 11.5 | 0.71 | 8.0E-07 |
| 745/2148 | 31 | 20/6/2016 | 80.9 | 5.89 | 1839/1926 | 13.6 | 0.65 | 1.9E-07 |
| 746/2149 | 31 | 2/10/2016 | 141.7 | 5.89 | 4099/3974 | 14.6 | 0.61 | 5.3E-03 |
| 747/2150 | 32 | 8/3/2013 | 31.4 | 5.87 | 834/843 | 5.1 | 0.90 | 5.9E-04 |
| 748/2151 | 32 | 10/4/2013 | 65.8 | 5.87 | 1651/1597 | 5.4 | 0.90 | 1.3E-03 |
| 749/2152 | 32 | 9/7/2013 | 0.3 | 5.87 | 7/5 | 4.8 | 0.87 | 7.5E-03 |
| 750/2153 | 32 | 11/7/2013 | 19.3 | 5.87 | 367/356 | 8.3 | 0.72 | 1.2E-02 |
| 751/2154 | 32 | 1/8/2013 | 8.0 | 5.87 | 154/147 | 11.3 | 0.69 | 1.3E-02 |
| 752/2155 | 32 | 12/8/2013 | 11.6 | 5.87 | 226/223 | 10.5 | 0.77 | 9.7E-03 |
| 753/2156 | 32 | 27/8/2013 | 2.5 | 5.87 | 56/52 | 11.1 | 0.67 | 1.2E-02 |
| 754/2157 | 32 | 5/9/2013 | 20.5 | 5.87 | 431/437 | 11.3 | 0.66 | 1.3E-02 |
| 755/2158 | 32 | 9/10/2013 | 13.1 | 5.87 | 274/290 | 11.2 | 0.72 | 1.1E-02 |
| 756/2159 | 32 | 29/10/2013 | 8.1 | 5.87 | 165/173 | 12.1 | 0.73 | 9.9E-03 |
| 757/2160 | 32 | 21/11/2013 | 4.7 | 5.87 | 44/43 | 9.8 | 0.83 | 1.1E-02 |
| 758/2161 | 32 | 29/11/2013 | 1.3 | 5.87 | 22/14 | 9.2 | 0.81 | 7.7E-03 |
| 759/2162 | 32 | 10/1/2014 | 4.6 | 5.87 | 83/66 | 14.0 | 0.70 | 1.4E-02 |
| 760/2163 | 32 | 24/1/2014 | 38.4 | 5.87 | 470/493 | 15.6 | 0.81 | 1.0E-02 |

| Partition No. | D. No. | Start date | Dur. [d] | m [g] | Events | $p_0$ [keV] | $p_1$ [keV] | $p_2$ [keV] |
|---|---|---|---|---|---|---|---|---|
| 761/2164 | 32 | 6/3/2014 | 26.3 | 5.87 | 267/309 | 16.1 | 0.90 | 3.1E-03 |
| 762/2165 | 32 | 3/4/2014 | 18.3 | 5.87 | 150/197 | 17.4 | 0.93 | 4.1E-07 |
| 763/2166 | 32 | 26/4/2014 | 47.8 | 5.87 | 349/453 | 16.8 | 0.95 | 2.3E-03 |
| 764/2167 | 32 | 19/6/2014 | 74.0 | 5.87 | 409/566 | 23.4 | 1.03 | 2.3E-03 |
| 765/2168 | 32 | 5/9/2014 | 24.3 | 5.87 | 273/283 | 28.7 | 1.14 | 4.4E-08 |
| 766/2169 | 32 | 2/10/2014 | 104.0 | 5.87 | 931/1042 | 26.3 | 1.14 | -3.0E-08 |
| 767/2170 | 33 | 9/7/2013 | 19.3 | 6.24 | 801/942 | 8.9 | 0.79 | 1.2E-02 |
| 768/2171 | 33 | 1/8/2013 | 8.0 | 6.24 | 253/322 | 9.9 | 0.81 | 1.4E-02 |
| 769/2172 | 33 | 12/8/2013 | 11.4 | 6.24 | 341/449 | 10.1 | 0.83 | 1.4E-02 |
| 770/2173 | 33 | 27/8/2013 | 2.5 | 6.24 | 58/87 | 9.5 | 0.84 | 1.3E-02 |
| 771/2174 | 33 | 5/9/2013 | 30.1 | 6.24 | 825/1143 | 8.4 | 0.96 | 6.4E-03 |
| 772/2175 | 33 | 9/10/2013 | 22.8 | 6.24 | 581/771 | 7.2 | 1.07 | -2.1E-07 |
| 773/2176 | 33 | 21/11/2013 | 2.0 | 6.24 | 38/56 | 11.1 | 0.79 | 2.3E-03 |
| 774/2177 | 33 | 29/11/2013 | 1.2 | 6.24 | 25/31 | 9.4 | 0.77 | 4.2E-03 |
| 775/2178 | 33 | 10/1/2014 | 4.4 | 6.24 | 135/146 | 14.7 | 0.60 | 1.1E-02 |
| 776/2179 | 33 | 24/1/2014 | 39.5 | 6.24 | 945/1217 | 13.9 | 0.67 | 9.3E-03 |
| 777/2180 | 33 | 6/3/2014 | 26.5 | 6.24 | 705/938 | 12.6 | 0.72 | 1.0E-02 |
| 778/2181 | 33 | 3/4/2014 | 17.0 | 6.24 | 484/597 | 6.3 | 0.92 | 7.1E-03 |
| 779/2182 | 33 | 26/4/2014 | 42.2 | 6.24 | 1100/1344 | 6.3 | 0.96 | -6.9E-06 |
| 780/2183 | 33 | 19/6/2014 | 61.0 | 6.24 | 1502/1780 | 11.5 | 0.82 | 5.6E-03 |
| 781/2184 | 33 | 5/9/2014 | 23.1 | 6.24 | 642/770 | 13.8 | 0.74 | 1.2E-02 |
| 782/2185 | 33 | 2/10/2014 | 117.4 | 6.24 | 4718/5554 | 14.1 | 0.74 | 9.2E-03 |
| 783/2186 | 33 | 25/2/2015 | 50.2 | 6.24 | 904/1072 | 14.5 | 0.86 | -1.2E-07 |
| 784/2187 | 33 | 6/5/2015 | 126.9 | 6.24 | 1764/2123 | 16.7 | 0.90 | 2.1E-06 |
| 785/2188 | 33 | 1/11/2015 | 100.8 | 6.24 | 762/850 | 18.7 | 0.91 | 5.2E-06 |
| 786/2189 | 33 | 20/2/2016 | 84.0 | 6.24 | 840/987 | 21.2 | 0.70 | 7.0E-03 |
| 787/2190 | 33 | 18/6/2016 | 84.0 | 6.24 | 623/686 | 18.7 | 0.91 | 5.2E-06 |
| 788/2191 | 33 | 2/10/2016 | 146.5 | 6.24 | 3535/2690 | 24.1 | 0.46 | 1.5E-02 |
| 789/2192 | 33 | 21/7/2018 | 6.4 | 6.24 | 7/20 | 25.0 | 0.14 | 2.0E-02 |
| 790/2193 | 33 | 2/11/2018 | 170.9 | 6.24 | 6275/7659 | 15.7 | 0.80 | 2.0E-02 |
| 791/2194 | 34 | 9/7/2013 | 19.3 | 6.13 | 794/851 | 12.5 | 0.45 | 1.4E-02 |
| 792/2195 | 34 | 1/8/2013 | 8.0 | 6.13 | 214/272 | 11.9 | 0.53 | 1.4E-02 |
| 793/2196 | 34 | 12/8/2013 | 11.4 | 6.13 | 333/365 | 11.3 | 0.60 | 1.3E-02 |
| 794/2197 | 34 | 27/8/2013 | 2.5 | 6.13 | 89/81 | 5.6 | 0.74 | 1.3E-02 |
| 795/2198 | 34 | 5/9/2013 | 30.1 | 6.13 | 927/1021 | -4.9 | 0.77 | 1.4E-02 |
| 796/2199 | 34 | 9/10/2013 | 22.8 | 6.13 | 682/791 | -9.7 | 0.67 | 1.5E-02 |
| 797/2200 | 34 | 21/11/2013 | 2.0 | 6.13 | 39/46 | 13.4 | 0.62 | 8.5E-03 |
| 798/2201 | 34 | 29/11/2013 | 1.2 | 6.13 | 25/30 | 12.8 | 0.58 | 9.6E-03 |
| 799/2202 | 34 | 10/1/2014 | 4.4 | 6.13 | 91/125 | 16.6 | 0.53 | 9.6E-03 |
| 800/2203 | 34 | 24/1/2014 | 39.5 | 6.13 | 783/1017 | 16.8 | 0.49 | 1.1E-02 |
| 801/2204 | 34 | 6/3/2014 | 26.5 | 6.13 | 571/833 | 13.9 | 0.65 | 7.1E-03 |
| 802/2205 | 34 | 3/4/2014 | 17.0 | 6.13 | 353/492 | 13.9 | 0.75 | 7.0E-03 |
| 803/2206 | 34 | 26/4/2014 | 42.2 | 6.13 | 862/1256 | 17.5 | 0.72 | 9.5E-03 |
| 804/2207 | 34 | 19/6/2014 | 61.0 | 6.13 | 1170/1635 | 15.9 | 0.77 | 9.0E-03 |
| 805/2208 | 34 | 5/9/2014 | 23.1 | 6.13 | 518/662 | 15.0 | 0.87 | 7.1E-03 |
| 806/2209 | 34 | 2/10/2014 | 117.4 | 6.13 | 4625/5830 | 14.7 | 0.92 | 9.1E-03 |
| 807/2210 | 34 | 25/2/2015 | 50.2 | 6.13 | 1447/1978 | 15.4 | 1.08 | 1.5E-02 |
| 808/2211 | 34 | 6/5/2015 | 126.9 | 6.13 | 2048/2844 | 14.7 | 1.22 | 1.2E-02 |
| 809/2212 | 34 | 1/11/2015 | 100.8 | 6.13 | 331/554 | 11.2 | 1.33 | 5.8E-03 |
| 810/2213 | 34 | 20/2/2016 | 84.0 | 6.13 | 368/583 | 3.9 | 2.01 | 7.7E-06 |
| 811/2214 | 34 | 18/6/2016 | 84.0 | 6.13 | 2967/4066 | 12.6 | 1.25 | 2.9E-02 |
| 812/2215 | 34 | 2/10/2016 | 146.5 | 6.13 | 8395/10391 | 19.5 | 1.02 | 3.2E-02 |
| 813/2216 | 34 | 20/5/2017 | 51.5 | 6.13 | 3012/3831 | 20.8 | 0.80 | 3.8E-02 |
| 814/2217 | 34 | 31/7/2017 | 189.7 | 6.13 | 8337/10513 | 15.2 | 0.80 | 4.0E-02 |
| 815/2218 | 34 | 21/7/2018 | 6.4 | 6.13 | 4/35 | 27.7 | 0.80 | 4.0E-02 |
| 816/2219 | 34 | 2/11/2018 | 170.9 | 6.13 | 9642/11847 | 25.9 | 0.68 | 4.0E-02 |
| 817/2220 | 35 | 9/7/2013 | 0.3 | 6.23 | 24/23 | 12.7 | 0.48 | 3.7E-02 |
| 818/2221 | 35 | 12/7/2013 | 19.0 | 6.23 | 1285/1097 | 6.3 | 0.84 | 2.9E-02 |
| 819/2222 | 35 | 1/8/2013 | 8.0 | 6.23 | 505/423 | 0.0 | 1.20 | 2.1E-02 |
| 820/2223 | 35 | 12/8/2013 | 11.4 | 6.23 | 737/566 | 10.1 | 0.60 | 2.9E-02 |
| 821/2224 | 35 | 27/8/2013 | 2.5 | 6.23 | 162/110 | 17.5 | 0.40 | 3.5E-02 |
| 822/2225 | 35 | 5/9/2013 | 30.1 | 6.23 | 1899/1651 | 18.1 | 0.40 | 3.3E-02 |
| 823/2226 | 35 | 9/10/2013 | 22.8 | 6.23 | 1390/1085 | 21.5 | 0.00 | 3.2E-02 |
| 824/2227 | 35 | 21/11/2013 | 3.2 | 6.23 | 98/63 | 7.6 | 0.97 | 1.2E-02 |
| 825/2228 | 35 | 10/1/2014 | 4.4 | 6.23 | 128/115 | 12.3 | 0.84 | 1.4E-02 |
| 826/2229 | 35 | 24/1/2014 | 39.5 | 6.23 | 975/878 | 16.0 | 0.67 | 1.6E-02 |
| 827/2230 | 35 | 6/3/2014 | 26.5 | 6.23 | 797/696 | 12.3 | 0.85 | 8.0E-03 |
| 828/2231 | 35 | 3/4/2014 | 17.0 | 6.23 | 549/462 | 12.1 | 1.09 | 3.4E-07 |
| 829/2232 | 35 | 26/4/2014 | 42.2 | 6.23 | 1106/957 | 13.4 | 1.16 | -5.4E-08 |
| 830/2233 | 35 | 19/6/2014 | 61.0 | 6.23 | 1549/1435 | 10.0 | 1.17 | 2.9E-04 |
| 831/2234 | 35 | 5/9/2014 | 23.1 | 6.23 | 699/710 | 9.7 | 1.19 | 2.9E-04 |
| 832/2235 | 35 | 2/10/2014 | 117.4 | 6.23 | 5757/5568 | -1.8 | 0.63 | 1.3E-02 |

| Partition No. | D. No. | Start date | Dur. [d] | m [g] | Events | $p_0$ [keV] | $p_1$ [keV] | $p_2$ [keV] |
|---|---|---|---|---|---|---|---|---|
| 833/2236 | 35 | 25/2/2015 | 50.2 | 6.23 | 1822/1785 | 24.3 | 0.61 | 1.5E-02 |
| 834/2237 | 35 | 6/5/2015 | 126.9 | 6.23 | 3167/2877 | 33.1 | 0.00 | 3.1E-02 |
| 835/2238 | 35 | 1/11/2015 | 100.8 | 6.23 | 938/962 | 22.9 | 0.39 | 2.0E-02 |
| 836/2239 | 35 | 20/2/2016 | 84.0 | 6.23 | 980/964 | 16.9 | 0.39 | 1.5E-02 |
| 837/2240 | 35 | 18/6/2016 | 84.0 | 6.23 | 2950/2601 | 12.7 | 0.77 | 9.8E-03 |
| 838/2241 | 35 | 2/10/2016 | 146.5 | 6.23 | 8825/8216 | 16.7 | 0.58 | 1.6E-02 |
| 839/2242 | 35 | 20/5/2017 | 51.5 | 6.23 | 3440/3065 | 17.4 | 0.37 | 2.3E-02 |
| 840/2243 | 35 | 31/7/2017 | 189.7 | 6.23 | 11995/10942 | 14.9 | 0.30 | 2.3E-02 |
| 841/2244 | 35 | 21/7/2018 | 6.4 | 6.23 | 24/22 | 18.6 | 0.42 | 2.3E-02 |
| 842/2245 | 35 | 2/11/2018 | 170.9 | 6.23 | 8744/7951 | 14.3 | 0.44 | 2.5E-02 |
| 843/2246 | 35 | 25/5/2019 | 125.3 | 6.23 | 5831/5228 | 15.5 | 0.46 | 2.0E-02 |
| 844/2247 | 36 | 12/7/2013 | 19.0 | 6.20 | 823/822 | 0.0 | 0.97 | 1.1E-02 |
| 845/2248 | 36 | 27/8/2013 | 2.5 | 6.20 | 2/10 | 12.8 | 0.88 | 2.9E-02 |
| 846/2249 | 36 | 5/9/2013 | 30.1 | 6.20 | 16/145 | 12.1 | 0.82 | 1.9E-02 |
| 847/2250 | 36 | 9/10/2013 | 14.7 | 6.20 | 15/47 | 6.0 | 0.91 | 1.7E-02 |
| 848/2251 | 36 | 29/10/2013 | 8.1 | 6.20 | 1/18 | 0.0 | 1.10 | 1.5E-02 |
| 849/2252 | 36 | 29/11/2013 | 1.2 | 6.20 | 12/15 | 4.5 | 0.81 | 1.1E-02 |
| 850/2253 | 36 | 10/1/2014 | 4.4 | 6.20 | 65/88 | 5.8 | 0.78 | 1.5E-02 |
| 851/2254 | 36 | 24/1/2014 | 39.5 | 6.20 | 505/634 | 5.7 | 0.82 | 8.6E-03 |
| 852/2255 | 36 | 6/3/2014 | 26.5 | 6.20 | 372/512 | 5.7 | 0.81 | 1.1E-02 |
| 853/2256 | 36 | 3/4/2014 | 17.0 | 6.20 | 165/222 | 0.0 | 0.93 | 1.3E-02 |
| 854/2257 | 36 | 26/4/2014 | 42.2 | 6.20 | 82/104 | 6.0 | 0.89 | 9.6E-03 |
| 855/2258 | 36 | 25/2/2015 | 50.2 | 6.20 | 1848/2215 | 14.0 | 0.85 | 1.5E-03 |
| 856/2259 | 36 | 6/5/2015 | 126.9 | 6.20 | 3570/4357 | 15.4 | 0.94 | 1.3E-06 |
| 857/2260 | 36 | 18/6/2016 | 84.0 | 6.20 | 2403/2820 | 0.0 | 0.95 | 1.7E-02 |
| 858/2261 | 37 | 21/11/2013 | 2.3 | 6.28 | 56/69 | 10.2 | 0.69 | 1.3E-02 |
| 859/2262 | 37 | 29/11/2013 | 1.2 | 6.28 | 23/44 | 9.1 | 0.72 | 1.0E-02 |
| 860/2263 | 37 | 10/1/2014 | 4.6 | 6.28 | 127/206 | 4.5 | 0.75 | 4.3E-03 |
| 861/2264 | 37 | 24/1/2014 | 39.0 | 6.28 | 998/1248 | 0.0 | 0.75 | 7.9E-03 |
| 862/2265 | 37 | 6/3/2014 | 26.1 | 6.28 | 780/1053 | 3.1 | 0.78 | 6.9E-03 |
| 863/2266 | 37 | 3/4/2014 | 17.0 | 6.28 | 478/636 | 6.1 | 0.84 | 4.3E-03 |
| 864/2267 | 37 | 26/4/2014 | 46.4 | 6.28 | 1258/1459 | 9.0 | 0.85 | 2.2E-03 |
| 865/2268 | 37 | 19/6/2014 | 60.9 | 6.28 | 1600/1931 | 11.8 | 0.87 | -8.7E-08 |
| 866/2269 | 37 | 5/9/2014 | 23.1 | 6.28 | 788/920 | 13.0 | 0.87 | 1.1E-06 |
| 867/2270 | 37 | 2/10/2014 | 113.6 | 6.28 | 5984/6964 | 7.1 | 0.77 | 3.1E-03 |
| 868/2271 | 37 | 25/2/2015 | 49.9 | 6.28 | 1722/1933 | 10.8 | 0.79 | 6.2E-03 |
| 869/2272 | 37 | 6/5/2015 | 141.9 | 6.28 | 3998/4530 | 9.8 | 0.93 | 4.7E-03 |
| 870/2273 | 37 | 1/11/2015 | 100.3 | 6.28 | 1391/1577 | 11.0 | 0.87 | 2.8E-03 |
| 871/2274 | 37 | 20/2/2016 | 79.7 | 6.28 | 1380/1564 | 11.4 | 0.81 | 6.6E-03 |
| 872/2275 | 37 | 18/6/2016 | 86.3 | 6.28 | 1854/2244 | 13.7 | 0.67 | 5.7E-03 |
| 873/2276 | 37 | 2/10/2016 | 146.2 | 6.28 | 4978/5835 | 16.7 | 0.68 | 7.3E-03 |
| 874/2277 | 37 | 20/5/2017 | 54.0 | 6.28 | 1938/2200 | 16.4 | 0.61 | 9.3E-03 |
| 875/2278 | 37 | 31/7/2017 | 181.6 | 6.28 | 9240/9670 | 17.1 | 0.67 | 7.1E-03 |
| 876/2279 | 37 | 21/7/2018 | 6.4 | 6.28 | 28/82 | 17.6 | 0.36 | 2.9E-02 |
| 877/2280 | 37 | 2/11/2018 | 170.7 | 6.28 | 7468/8311 | 16.3 | 0.39 | 1.4E-02 |
| 878/2281 | 37 | 25/5/2019 | 112.9 | 6.28 | 5408/5667 | 21.8 | 0.50 | 2.3E-02 |
| 879/2282 | 38 | 9/7/2013 | 0.3 | 6.23 | 28/31 | 7.6 | 0.59 | 1.5E-02 |
| 880/2283 | 38 | 11/7/2013 | 19.3 | 6.23 | 1466/1738 | 7.2 | 0.60 | 1.7E-02 |
| 881/2284 | 38 | 1/8/2013 | 8.0 | 6.23 | 566/740 | 7.2 | 0.62 | 2.0E-02 |
| 882/2285 | 38 | 12/8/2013 | 11.5 | 6.23 | 816/955 | -0.7 | 0.62 | 2.0E-02 |
| 883/2286 | 38 | 27/8/2013 | 2.5 | 6.23 | 181/204 | 3.1 | 0.31 | 2.3E-02 |
| 884/2287 | 38 | 5/9/2013 | 30.1 | 6.23 | 2231/2530 | 15.1 | 0.00 | 2.5E-02 |
| 885/2288 | 38 | 9/10/2013 | 14.7 | 6.23 | 994/1182 | 3.7 | 0.31 | 2.3E-02 |
| 886/2289 | 38 | 29/10/2013 | 8.1 | 6.23 | 576/688 | 0.3 | 0.62 | 2.2E-02 |
| 887/2290 | 38 | 21/11/2013 | 2.3 | 6.23 | 58/67 | 8.9 | 0.70 | 1.0E-02 |
| 888/2291 | 38 | 29/11/2013 | 1.2 | 6.23 | 33/29 | 10.9 | 0.70 | 1.2E-02 |
| 889/2292 | 38 | 2/10/2014 | 113.6 | 6.23 | 4460/4994 | 19.2 | 0.83 | 6.3E-03 |
| 890/2293 | 38 | 25/2/2015 | 49.9 | 6.23 | 1103/1233 | 16.9 | 0.79 | 2.4E-03 |
| 891/2294 | 38 | 6/5/2015 | 141.9 | 6.23 | 2701/2969 | 12.7 | 1.00 | 3.9E-07 |
| 892/2295 | 38 | 1/11/2015 | 100.3 | 6.23 | 862/943 | 9.5 | 0.88 | 6.9E-03 |
| 893/2296 | 38 | 20/2/2016 | 79.7 | 6.23 | 823/897 | 15.6 | 0.27 | 1.4E-02 |
| 894/2297 | 38 | 18/6/2016 | 86.3 | 6.23 | 1599/2042 | 13.2 | 0.55 | 1.4E-02 |
| 895/2298 | 38 | 2/10/2016 | 146.2 | 6.23 | 5434/5965 | 14.0 | 0.65 | 8.9E-03 |
| 896/2299 | 38 | 20/5/2017 | 54.0 | 6.23 | 1873/1984 | 13.6 | 0.61 | 7.4E-03 |
| 897/2300 | 38 | 21/7/2018 | 6.4 | 6.23 | 10/38 | 19.4 | 0.31 | 1.2E-02 |
| 898/2301 | 38 | 2/11/2018 | 170.7 | 6.23 | 3754/4119 | 16.1 | 0.57 | 9.9E-03 |
| 899/2302 | 38 | 25/5/2019 | 112.9 | 6.23 | 3027/3338 | 15.1 | 0.53 | 1.1E-02 |
| 900/2303 | 39 | 9/7/2013 | 0.3 | 6.25 | 29/28 | 9.9 | 0.48 | 1.2E-02 |
| 901/2304 | 39 | 11/7/2013 | 19.3 | 6.25 | 1441/1958 | 5.0 | 0.53 | 1.3E-02 |
| 902/2305 | 39 | 1/8/2013 | 8.0 | 6.25 | 526/620 | 6.4 | 0.45 | 1.5E-02 |
| 903/2306 | 39 | 12/8/2013 | 11.5 | 6.25 | 745/997 | 6.4 | 0.46 | 1.5E-02 |
| 904/2307 | 39 | 27/8/2013 | 2.5 | 6.25 | 163/216 | -7.0 | 0.31 | 1.6E-02 |

| Partition No. | D. No. | Start date | Dur. [d] | m [g] | Events | $p_0$ [keV] | $p_1$ [keV] | $p_2$ [keV] |
|---|---|---|---|---|---|---|---|---|
| 905/2308 | 39 | 5/9/2013 | 30.1 | 6.25 | 1964/2666 | -5.7 | 0.40 | 1.2E-02 |
| 906/2309 | 39 | 9/10/2013 | 14.7 | 6.25 | 895/1196 | 6.0 | 0.65 | 1.0E-02 |
| 907/2310 | 39 | 29/10/2013 | 8.1 | 6.25 | 502/705 | -1.3 | 0.41 | 1.6E-02 |
| 908/2311 | 39 | 21/11/2013 | 2.3 | 6.25 | 44/66 | 12.3 | 0.48 | 1.3E-02 |
| 909/2312 | 39 | 29/11/2013 | 1.2 | 6.25 | 23/37 | 11.9 | 0.46 | 9.6E-03 |
| 910/2313 | 39 | 2/10/2014 | 113.6 | 6.25 | 4612/5763 | 21.1 | 0.60 | -4.0E-03 |
| 911/2314 | 39 | 25/2/2015 | 49.9 | 6.25 | 988/1426 | 14.5 | 0.63 | 2.0E-03 |
| 912/2315 | 39 | 6/5/2015 | 141.9 | 6.25 | 2833/3964 | 15.7 | 0.71 | -3.1E-07 |
| 913/2316 | 39 | 1/11/2015 | 100.3 | 6.25 | 1035/1402 | 14.3 | 0.67 | 1.9E-03 |
| 914/2317 | 39 | 20/2/2016 | 79.7 | 6.25 | 869/1074 | 10.3 | 0.66 | 1.9E-03 |
| 915/2318 | 39 | 18/6/2016 | 86.3 | 6.25 | 1204/1878 | 12.6 | 0.57 | 3.9E-03 |
| 916/2319 | 39 | 2/10/2016 | 146.2 | 6.25 | 5425/6735 | 14.8 | 0.53 | 5.1E-03 |
| 917/2320 | 39 | 20/5/2017 | 54.0 | 6.25 | 1803/2309 | 15.2 | 0.40 | 8.0E-03 |
| 918/2321 | 39 | 21/7/2018 | 6.4 | 6.25 | 31/73 | 16.3 | 0.31 | 9.6E-03 |
| 919/2322 | 39 | 2/11/2018 | 170.7 | 6.25 | 3038/4742 | 14.6 | 0.32 | 1.1E-02 |
| 920/2323 | 39 | 25/5/2019 | 112.9 | 6.25 | 2165/3190 | 16.0 | 0.36 | 9.7E-03 |
| 921/2324 | 40 | 9/7/2013 | 0.3 | 6.24 | 37/26 | -9.5 | 0.64 | 2.4E-02 |
| 922/2325 | 40 | 11/7/2013 | 19.3 | 6.24 | 1515/1562 | -11.7 | 0.32 | 3.0E-02 |
| 923/2326 | 40 | 1/8/2013 | 8.0 | 6.24 | 610/536 | -6.9 | 0.44 | 3.0E-02 |
| 924/2327 | 40 | 12/8/2013 | 11.5 | 6.24 | 822/779 | 4.0 | 0.83 | 2.6E-02 |
| 925/2328 | 40 | 27/8/2013 | 2.5 | 6.24 | 208/169 | -3.4 | 0.38 | 3.1E-02 |
| 926/2329 | 40 | 5/9/2013 | 30.1 | 6.24 | 2251/2281 | -7.0 | 0.46 | 2.8E-02 |
| 927/2330 | 40 | 9/10/2013 | 14.7 | 6.24 | 1167/1091 | 0.9 | 0.92 | 2.3E-02 |
| 928/2331 | 40 | 29/10/2013 | 8.1 | 6.24 | 605/563 | -5.7 | 0.46 | 2.9E-02 |
| 929/2332 | 40 | 21/11/2013 | 2.3 | 6.24 | 39/50 | 11.1 | 0.55 | 1.9E-02 |
| 930/2333 | 40 | 29/11/2013 | 1.2 | 6.24 | 21/22 | 9.7 | 0.61 | 1.7E-02 |
| 931/2334 | 40 | 10/1/2014 | 4.6 | 6.24 | 118/149 | 5.9 | 0.69 | 1.4E-02 |
| 932/2335 | 40 | 24/1/2014 | 39.0 | 6.24 | 1053/1027 | 0.0 | 0.73 | 1.3E-02 |
| 933/2336 | 40 | 6/3/2014 | 26.1 | 6.24 | 484/522 | 7.3 | 0.72 | 1.3E-02 |
| 934/2337 | 40 | 3/4/2014 | 17.0 | 6.24 | 361/328 | 14.6 | 0.75 | 1.4E-02 |
| 935/2338 | 40 | 26/4/2014 | 46.4 | 6.24 | 834/842 | 18.6 | 0.90 | 6.9E-03 |
| 936/2339 | 40 | 19/6/2014 | 60.9 | 6.24 | 862/938 | 17.1 | 0.87 | 6.0E-03 |
| 937/2340 | 40 | 5/9/2014 | 23.1 | 6.24 | 644/623 | 11.2 | 0.83 | 6.0E-03 |
| 938/2341 | 40 | 2/10/2014 | 113.6 | 6.24 | 4415/4318 | 5.4 | 0.79 | 7.7E-03 |
| 939/2342 | 40 | 25/2/2015 | 49.9 | 6.24 | 739/760 | 18.7 | 0.93 | 9.8E-07 |
| 940/2343 | 40 | 6/5/2015 | 141.9 | 6.24 | 1931/2085 | 11.7 | 1.17 | 5.1E-03 |
| 941/2344 | 40 | 1/11/2015 | 100.3 | 6.24 | 535/534 | 3.6 | 1.32 | 1.0E-02 |
| 942/2345 | 40 | 20/2/2016 | 79.7 | 6.24 | 454/472 | 6.1 | 0.94 | 1.2E-02 |
| 943/2346 | 40 | 18/6/2016 | 86.3 | 6.24 | 240/359 | 3.6 | 1.32 | 1.0E-02 |
| 944/2347 | 40 | 2/10/2016 | 146.2 | 6.24 | 2798/3042 | 5.3 | 1.05 | 5.6E-03 |
| 945/2348 | 40 | 20/5/2017 | 54.0 | 6.24 | 1060/1007 | 8.3 | 0.64 | 7.8E-03 |
| 946/2349 | 40 | 21/7/2018 | 6.4 | 6.24 | 25/31 | 14.1 | 0.08 | 1.9E-02 |
| 947/2350 | 40 | 2/11/2018 | 170.7 | 6.24 | 3326/3561 | 12.9 | 0.17 | 1.8E-02 |
| 948/2351 | 40 | 25/5/2019 | 112.9 | 6.24 | 2180/2393 | 14.1 | 0.20 | 1.8E-02 |
| 949/2352 | 41 | 9/7/2013 | 0.3 | 6.25 | 28/30 | 6.8 | 0.74 | 2.5E-02 |
| 950/2353 | 41 | 11/7/2013 | 19.3 | 6.25 | 1598/1434 | 10.4 | 0.42 | 3.6E-02 |
| 951/2354 | 41 | 1/8/2013 | 8.0 | 6.25 | 660/553 | 13.6 | 0.11 | 4.4E-02 |
| 952/2355 | 41 | 12/8/2013 | 11.5 | 6.25 | 912/717 | 10.0 | 0.50 | 4.1E-02 |
| 953/2356 | 41 | 27/8/2013 | 2.5 | 6.25 | 226/190 | 8.9 | 0.67 | 4.2E-02 |
| 954/2357 | 41 | 5/9/2013 | 30.1 | 6.25 | 2557/2236 | 10.3 | 0.61 | 4.2E-02 |
| 955/2358 | 41 | 9/10/2013 | 22.8 | 6.25 | 1735/1543 | 9.1 | 0.76 | 3.9E-02 |
| 956/2359 | 41 | 21/11/2013 | 2.2 | 6.25 | 61/57 | 9.6 | 0.79 | 1.4E-02 |
| 957/2360 | 41 | 29/11/2013 | 0.5 | 6.25 | 14/15 | 10.7 | 0.69 | 1.7E-02 |
| 958/2361 | 41 | 10/1/2014 | 4.6 | 6.25 | 119/105 | 20.8 | 0.88 | 8.1E-03 |
| 959/2362 | 41 | 24/1/2014 | 34.7 | 6.25 | 688/629 | 17.6 | 0.91 | 1.2E-02 |
| 960/2363 | 41 | 6/3/2014 | 25.9 | 6.25 | 637/589 | 18.0 | 1.11 | 4.4E-03 |
| 961/2364 | 41 | 3/4/2014 | 17.0 | 6.25 | 428/404 | 20.6 | 1.02 | 9.8E-03 |
| 962/2365 | 41 | 26/4/2014 | 46.4 | 6.25 | 1121/1010 | 19.8 | 1.01 | 9.8E-03 |
| 963/2366 | 41 | 19/6/2014 | 60.7 | 6.25 | 1250/1281 | 17.6 | 1.04 | 6.1E-03 |
| 964/2367 | 41 | 5/9/2014 | 22.9 | 6.25 | 555/551 | 18.8 | 1.07 | 6.1E-03 |
| 965/2368 | 41 | 2/10/2014 | 112.2 | 6.25 | 3776/3683 | 16.6 | 0.97 | 6.0E-03 |
| 966/2369 | 41 | 25/2/2015 | 45.0 | 6.25 | 2219/2178 | 6.0 | 1.10 | 1.4E-02 |
| 967/2370 | 41 | 6/5/2015 | 131.0 | 6.25 | 3927/3825 | 13.2 | 1.07 | 5.8E-06 |
| 968/2371 | 41 | 1/11/2015 | 100.7 | 6.25 | 1379/1261 | 13.5 | 0.93 | 5.2E-03 |
| 969/2372 | 41 | 20/2/2016 | 84.1 | 6.25 | 1341/1195 | 16.4 | 0.38 | 1.7E-02 |
| 970/2373 | 41 | 18/6/2016 | 83.6 | 6.25 | 1980/1840 | 12.6 | 0.76 | 1.0E-02 |
| 971/2374 | 41 | 31/7/2017 | 182.3 | 6.25 | 3134/3020 | 16.6 | 0.37 | 2.0E-02 |
| 972/2375 | 41 | 21/7/2018 | 6.2 | 6.25 | 31/30 | 18.1 | 0.43 | 1.8E-02 |
| 973/2376 | 41 | 2/11/2018 | 159.5 | 6.25 | 3488/3159 | 16.3 | 0.35 | 1.7E-02 |
| 974/2377 | 41 | 25/5/2019 | 103.8 | 6.25 | 2464/2677 | 19.5 | 0.33 | 2.1E-02 |
| 975/2378 | 42 | 9/7/2013 | 0.3 | 6.20 | 32/26 | -6.8 | 0.77 | 2.2E-02 |
| 976/2379 | 42 | 11/7/2013 | 19.3 | 6.20 | 1843/1684 | -8.6 | 0.69 | 2.5E-02 |

| Partition No. | D. No. | Start date | Dur. [d] | m [g] | Events | $p_0$ [keV] | $p_1$ [keV] | $p_2$ [keV] |
|---|---|---|---|---|---|---|---|---|
| 977/2380 | 42 | 1/8/2013 | 8.0 | 6.20 | 743/701 | -3.4 | 0.81 | 4.1E-02 |
| 978/2381 | 42 | 12/8/2013 | 11.5 | 6.20 | 1064/900 | -4.4 | 0.80 | 4.1E-02 |
| 979/2382 | 42 | 27/8/2013 | 2.5 | 6.20 | 232/213 | -6.2 | 0.79 | 2.0E-02 |
| 980/2383 | 42 | 5/9/2013 | 52.9 | 6.20 | 4985/4425 | 0.0 | 0.98 | 1.4E-02 |
| 981/2384 | 42 | 21/11/2013 | 2.2 | 6.20 | 54/55 | 14.3 | 0.35 | 1.7E-02 |
| 982/2385 | 42 | 29/11/2013 | 0.5 | 6.20 | 6/8 | 14.5 | 0.33 | 1.9E-02 |
| 983/2386 | 42 | 10/1/2014 | 39.3 | 6.20 | 808/860 | 9.4 | 0.98 | 5.2E-07 |
| 984/2387 | 42 | 6/3/2014 | 25.9 | 6.20 | 611/592 | 18.9 | 1.02 | 4.1E-07 |
| 985/2388 | 42 | 3/4/2014 | 63.4 | 6.20 | 1280/1235 | 28.5 | 1.05 | 3.0E-07 |
| 986/2389 | 42 | 19/6/2014 | 60.7 | 6.20 | 1018/1024 | 27.7 | 1.06 | 2.8E-07 |
| 987/2390 | 42 | 5/9/2014 | 22.9 | 6.20 | 450/473 | 32.0 | 1.21 | 3.8E-07 |
| 988/2391 | 42 | 2/10/2014 | 112.2 | 6.20 | 3770/3822 | 22.0 | 0.99 | 7.5E-03 |
| 989/2392 | 42 | 25/2/2015 | 45.0 | 6.20 | 1573/1581 | 17.2 | 1.00 | -7.2E-07 |
| 990/2393 | 42 | 6/5/2015 | 131.0 | 6.20 | 3001/2873 | 10.1 | 1.05 | 1.6E-02 |
| 991/2394 | 42 | 1/11/2015 | 100.7 | 6.20 | 2013/1881 | 5.5 | 0.85 | 2.2E-02 |
| 992/2395 | 42 | 20/2/2016 | 84.1 | 6.20 | 2096/2013 | 8.2 | 0.66 | 1.4E-02 |
| 993/2396 | 42 | 18/6/2016 | 83.6 | 6.20 | 2694/2594 | 10.2 | 0.61 | 1.2E-02 |
| 994/2397 | 42 | 2/10/2016 | 140.3 | 6.20 | 5674/5517 | 14.5 | 0.71 | 1.2E-02 |
| 995/2398 | 42 | 21/7/2018 | 6.2 | 6.20 | 58/73 | 13.3 | 0.48 | 1.7E-02 |
| 996/2399 | 42 | 2/11/2018 | 159.5 | 6.20 | 5013/4793 | 13.5 | 0.48 | 1.7E-02 |
| 997/2400 | 42 | 25/5/2019 | 103.8 | 6.20 | 7042/6114 | 12.6 | 0.40 | 1.8E-02 |
| 998/2401 | 43 | 9/7/2013 | 0.3 | 6.26 | 29/34 | 8.8 | 0.62 | 1.3E-02 |
| 999/2402 | 43 | 11/7/2013 | 19.3 | 6.26 | 1612/1645 | 9.1 | 0.60 | 1.5E-02 |
| 1000/2403 | 43 | 1/8/2013 | 8.0 | 6.26 | 687/661 | 8.2 | 0.70 | 8.3E-03 |
| 1001/2404 | 43 | 12/8/2013 | 11.5 | 6.26 | 1004/916 | 7.5 | 0.82 | 4.0E-03 |
| 1002/2405 | 43 | 27/8/2013 | 2.5 | 6.26 | 195/215 | -0.5 | 0.68 | 9.1E-03 |
| 1003/2406 | 43 | 5/9/2013 | 30.1 | 6.26 | 2262/2514 | 1.2 | 0.60 | 1.3E-02 |
| 1004/2407 | 43 | 9/10/2013 | 14.7 | 6.26 | 1169/1101 | 8.9 | 0.74 | 6.4E-03 |
| 1005/2408 | 43 | 29/10/2013 | 8.1 | 6.26 | 598/592 | 10.9 | 0.42 | 1.0E-02 |
| 1006/2409 | 43 | 21/11/2013 | 2.2 | 6.26 | 53/54 | 11.6 | 0.32 | -8.0E-03 |
| 1007/2410 | 43 | 29/11/2013 | 0.5 | 6.26 | 14/10 | 11.8 | 0.29 | -3.9E-03 |
| 1008/2411 | 43 | 10/1/2014 | 4.6 | 6.26 | 190/179 | 10.6 | 0.55 | 1.0E-02 |
| 1009/2412 | 43 | 24/1/2014 | 34.7 | 6.26 | 913/1015 | 11.8 | 0.53 | 1.1E-02 |
| 1010/2413 | 43 | 6/3/2014 | 25.9 | 6.26 | 785/846 | 12.2 | 0.65 | 5.6E-03 |
| 1011/2414 | 43 | 3/4/2014 | 17.0 | 6.26 | 519/572 | 14.3 | 0.81 | 4.3E-08 |
| 1012/2415 | 43 | 26/4/2014 | 46.4 | 6.26 | 1322/1326 | 18.1 | 0.82 | 2.8E-07 |
| 1013/2416 | 43 | 19/6/2014 | 60.7 | 6.26 | 1600/1627 | 16.1 | 0.77 | 2.3E-06 |
| 1014/2417 | 43 | 5/9/2014 | 22.9 | 6.26 | 679/622 | 13.6 | 0.86 | 2.1E-06 |
| 1015/2418 | 43 | 2/10/2014 | 112.2 | 6.26 | 4979/4925 | 10.3 | 0.82 | 2.8E-06 |
| 1016/2419 | 43 | 25/2/2015 | 45.0 | 6.26 | 960/977 | 14.7 | 1.33 | -2.1E-07 |
| 1017/2420 | 43 | 6/5/2015 | 131.0 | 6.26 | 1586/1568 | 7.0 | 1.59 | -5.3E-07 |
| 1018/2421 | 43 | 1/11/2015 | 100.7 | 6.26 | 1248/1258 | 8.3 | 1.14 | -2.4E-07 |
| 1019/2422 | 43 | 20/2/2016 | 84.1 | 6.26 | 1223/1140 | 4.8 | 0.91 | 1.2E-02 |
| 1020/2423 | 43 | 18/6/2016 | 83.6 | 6.26 | 1828/1972 | 9.6 | 0.70 | 4.3E-08 |
| 1021/2424 | 43 | 2/10/2016 | 140.3 | 6.26 | 4959/5205 | 11.3 | 0.70 | 5.0E-04 |
| 1022/2425 | 43 | 20/5/2017 | 49.4 | 6.26 | 1819/1750 | 11.4 | 0.57 | 6.0E-03 |
| 1023/2426 | 43 | 21/7/2018 | 6.2 | 6.26 | 35/44 | 12.4 | 0.41 | 1.2E-02 |
| 1024/2427 | 43 | 25/5/2019 | 103.8 | 6.26 | 5877/5406 | 13.4 | 0.44 | 1.0E-02 |
| 1025/2428 | 44 | 9/7/2013 | 0.3 | 6.31 | 36/18 | 10.0 | 0.87 | 2.6E-02 |
| 1026/2429 | 44 | 11/7/2013 | 19.3 | 6.31 | 974/785 | 9.1 | 0.86 | 3.2E-02 |
| 1027/2430 | 44 | 1/8/2013 | 8.0 | 6.31 | 102/119 | 9.9 | 0.87 | 3.6E-02 |
| 1028/2431 | 44 | 12/8/2013 | 11.5 | 6.31 | 203/229 | 10.2 | 0.91 | 3.5E-02 |
| 1029/2432 | 44 | 27/8/2013 | 2.5 | 6.31 | 62/53 | 4.4 | 1.15 | 2.9E-02 |
| 1030/2433 | 44 | 5/9/2013 | 30.1 | 6.31 | 662/593 | 6.3 | 1.02 | 3.1E-02 |
| 1031/2434 | 44 | 9/10/2013 | 14.7 | 6.31 | 220/215 | 7.7 | 0.90 | 3.1E-02 |
| 1032/2435 | 44 | 29/10/2013 | 8.1 | 6.31 | 55/78 | 2.7 | 1.10 | 2.4E-02 |
| 1033/2436 | 44 | 21/11/2013 | 2.2 | 6.31 | 46/31 | 9.7 | 0.77 | 1.3E-02 |
| 1034/2437 | 44 | 29/11/2013 | 0.5 | 6.31 | 11/10 | 10.1 | 0.83 | 1.3E-02 |
| 1035/2438 | 44 | 10/1/2014 | 39.3 | 6.31 | 916/836 | 11.9 | 0.87 | -2.0E-07 |
| 1036/2439 | 44 | 6/3/2014 | 25.9 | 6.31 | 536/480 | 15.7 | 1.02 | 5.7E-08 |
| 1037/2440 | 44 | 3/4/2014 | 17.0 | 6.31 | 327/288 | 20.8 | 1.24 | 6.2E-07 |
| 1038/2441 | 44 | 26/4/2014 | 46.4 | 6.31 | 801/794 | 27.0 | 1.20 | 5.1E-07 |
| 1039/2442 | 44 | 19/6/2014 | 60.7 | 6.31 | 1041/909 | 24.9 | 1.08 | 5.3E-03 |
| 1040/2443 | 44 | 5/9/2014 | 22.9 | 6.31 | 429/390 | 17.8 | 1.06 | 1.1E-02 |
| 1041/2444 | 44 | 2/10/2014 | 112.2 | 6.31 | 3051/2814 | 13.6 | 0.81 | 1.2E-02 |
| 1042/2445 | 44 | 25/2/2015 | 45.0 | 6.31 | 1350/1274 | 19.6 | 0.93 | 4.6E-07 |
| 1043/2446 | 44 | 6/5/2015 | 131.0 | 6.31 | 2333/2195 | 10.5 | 1.09 | 1.5E-02 |
| 1044/2447 | 44 | 1/11/2015 | 100.7 | 6.31 | 490/444 | 8.2 | 0.84 | 2.2E-02 |
| 1045/2448 | 44 | 20/2/2016 | 84.1 | 6.31 | 474/484 | 9.8 | 0.60 | 1.1E-02 |
| 1046/2449 | 44 | 18/6/2016 | 83.6 | 6.31 | 2887/2530 | 15.1 | 0.42 | 1.4E-02 |
| 1047/2450 | 44 | 2/10/2016 | 140.3 | 6.31 | 7718/6681 | 16.2 | 0.61 | 1.1E-02 |
| 1048/2451 | 44 | 20/5/2017 | 49.4 | 6.31 | 3020/2539 | 15.3 | 0.60 | 1.2E-02 |

| Partition No. | D. No. | Start date | Dur. [d] | m [g] | Events | $p_0$ [keV] | $p_1$ [keV] | $p_2$ [keV] |
|---|---|---|---|---|---|---|---|---|
| 1049/2452 | 44 | 31/7/2017 | 182.3 | 6.31 | 9719/8467 | 13.9 | 0.43 | 1.4E-02 |
| 1050/2453 | 44 | 21/7/2018 | 6.2 | 6.31 | 34/41 | 15.8 | 0.54 | 1.5E-02 |
| 1051/2454 | 44 | 2/11/2018 | 159.5 | 6.31 | 6059/5530 | 16.3 | 0.31 | 2.1E-02 |
| 1052/2455 | 44 | 25/5/2019 | 103.8 | 6.31 | 3505/3204 | 17.9 | 0.37 | 1.7E-02 |
| 1053/2456 | 45 | 9/7/2013 | 0.3 | 6.23 | 22/18 | 9.9 | 0.83 | 1.5E-02 |
| 1054/2457 | 45 | 11/7/2013 | 19.3 | 6.23 | 975/1048 | 5.0 | 0.82 | 1.5E-02 |
| 1055/2458 | 45 | 1/8/2013 | 8.0 | 6.23 | 354/347 | 6.6 | 0.74 | 1.5E-02 |
| 1056/2459 | 45 | 12/8/2013 | 11.5 | 6.23 | 522/597 | 11.2 | 0.76 | 1.4E-02 |
| 1057/2460 | 45 | 27/8/2013 | 2.5 | 6.23 | 107/140 | 9.1 | 0.87 | 1.4E-02 |
| 1058/2461 | 45 | 5/9/2013 | 26.6 | 6.23 | 1170/1271 | 10.5 | 0.79 | 1.8E-02 |
| 1059/2462 | 45 | 9/10/2013 | 12.6 | 6.23 | 587/600 | 10.5 | 0.80 | 1.9E-02 |
| 1060/2463 | 45 | 29/10/2013 | 8.1 | 6.23 | 378/396 | 9.5 | 0.89 | 1.4E-02 |
| 1061/2464 | 45 | 21/11/2013 | 1.8 | 6.23 | 23/39 | 13.5 | 0.88 | 7.1E-03 |
| 1062/2465 | 45 | 29/11/2013 | 1.0 | 6.23 | 22/14 | 12.5 | 0.93 | 6.0E-03 |
| 1063/2466 | 45 | 10/1/2014 | 4.6 | 6.23 | 116/121 | 17.3 | 0.84 | 8.9E-03 |
| 1064/2467 | 45 | 24/1/2014 | 38.2 | 6.23 | 777/871 | 17.5 | 0.65 | 1.9E-02 |
| 1065/2468 | 45 | 6/3/2014 | 26.3 | 6.23 | 603/672 | 20.4 | 0.83 | 1.0E-02 |
| 1066/2469 | 45 | 4/4/2014 | 14.1 | 6.23 | 265/309 | 22.4 | 1.15 | 6.1E-07 |
| 1067/2470 | 45 | 26/4/2014 | 33.8 | 6.23 | 588/688 | 27.4 | 1.16 | 3.0E-07 |
| 1068/2471 | 45 | 19/6/2014 | 59.6 | 6.23 | 782/939 | 28.2 | 1.06 | 9.7E-03 |
| 1069/2472 | 45 | 5/9/2014 | 22.0 | 6.23 | 347/473 | 27.8 | 1.12 | 9.7E-03 |
| 1070/2473 | 45 | 2/10/2014 | 105.4 | 6.23 | 1826/2238 | 31.7 | 1.29 | -9.2E-08 |
| 1071/2474 | 45 | 26/2/2015 | 37.9 | 6.23 | 527/635 | 31.7 | 1.30 | 2.2E-02 |
| 1072/2475 | 45 | 18/6/2016 | 82.9 | 6.23 | 1672/1963 | 0.0 | 1.38 | 1.7E-02 |
| 1073/2476 | 45 | 2/10/2016 | 144.4 | 6.23 | 5049/5712 | 15.4 | 0.69 | 2.6E-02 |
| 1074/2477 | 45 | 20/5/2017 | 55.4 | 6.23 | 1487/1649 | 23.0 | 0.39 | 3.6E-02 |
| 1075/2478 | 45 | 31/7/2017 | 182.9 | 6.23 | 3080/3178 | 15.2 | 0.77 | 3.6E-02 |
| 1076/2479 | 46 | 9/7/2013 | 0.3 | 6.21 | 21/26 | 0.0 | 0.94 | 3.1E-02 |
| 1077/2480 | 46 | 11/7/2013 | 19.3 | 6.21 | 1501/1400 | 4.1 | 0.98 | 3.8E-02 |
| 1078/2481 | 46 | 1/8/2013 | 21.9 | 6.21 | 1484/1293 | 8.2 | 1.03 | 4.5E-02 |
| 1079/2482 | 46 | 5/9/2013 | 26.6 | 6.21 | 1662/1507 | 4.1 | 1.29 | 3.4E-02 |
| 1080/2483 | 46 | 9/10/2013 | 12.6 | 6.21 | 724/695 | 0.0 | 1.56 | 2.4E-02 |
| 1081/2484 | 46 | 29/10/2013 | 8.1 | 6.21 | 473/387 | 0.0 | 1.50 | 2.6E-02 |
| 1082/2485 | 46 | 21/11/2013 | 1.8 | 6.21 | 39/41 | 8.9 | 0.92 | 1.0E-02 |
| 1083/2486 | 46 | 29/11/2013 | 1.0 | 6.21 | 14/21 | 9.9 | 0.93 | 1.0E-02 |
| 1084/2487 | 46 | 10/1/2014 | 4.6 | 6.21 | 142/130 | 8.0 | 1.07 | 5.5E-03 |
| 1085/2488 | 46 | 24/1/2014 | 38.2 | 6.21 | 768/840 | 8.6 | 0.90 | 1.5E-02 |
| 1086/2489 | 46 | 6/3/2014 | 26.3 | 6.21 | 603/550 | 22.0 | 1.04 | 1.4E-02 |
| 1087/2490 | 46 | 4/4/2014 | 14.1 | 6.21 | 256/258 | 26.9 | 1.38 | 8.2E-03 |
| 1088/2491 | 46 | 26/4/2014 | 33.8 | 6.21 | 581/565 | 34.2 | 1.37 | 1.6E-02 |
| 1089/2492 | 46 | 19/6/2014 | 59.6 | 6.21 | 836/823 | 39.2 | 1.09 | 2.4E-02 |
| 1090/2493 | 46 | 5/9/2014 | 22.0 | 6.21 | 362/309 | 39.4 | 1.28 | 1.2E-02 |
| 1091/2494 | 46 | 2/10/2014 | 105.4 | 6.21 | 1650/1742 | 24.4 | 1.29 | 6.2E-03 |
| 1092/2495 | 46 | 20/2/2016 | 83.6 | 6.21 | 0/0 | 5.5 | 0.83 | 1.6E-02 |
| 1093/2496 | 46 | 18/6/2016 | 82.9 | 6.21 | 1949/1942 | 10.9 | 0.73 | 1.6E-02 |
| 1094/2497 | 46 | 2/10/2016 | 144.4 | 6.21 | 7528/6980 | 18.0 | 0.77 | 1.8E-02 |
| 1095/2498 | 46 | 20/5/2017 | 55.4 | 6.21 | 2696/2352 | 19.8 | 0.60 | 2.1E-02 |
| 1096/2499 | 46 | 31/7/2017 | 182.9 | 6.21 | 7573/7159 | 19.8 | 0.40 | 2.1E-02 |
| 1097/2500 | 47 | 9/7/2013 | 0.3 | 6.26 | 12/19 | 17.3 | 0.96 | -1.3E-08 |
| 1098/2501 | 47 | 11/7/2013 | 19.3 | 6.26 | 757/853 | 16.5 | 0.87 | 4.8E-03 |
| 1099/2502 | 47 | 1/8/2013 | 8.0 | 6.26 | 196/218 | 18.8 | 0.84 | 4.8E-03 |
| 1100/2503 | 47 | 12/8/2013 | 14.0 | 6.26 | 367/396 | 21.9 | 0.90 | 1.2E-07 |
| 1101/2504 | 47 | 5/9/2013 | 26.6 | 6.26 | 571/709 | 29.9 | 0.45 | 1.7E-02 |
| 1102/2505 | 47 | 9/10/2013 | 20.7 | 6.26 | 408/382 | 38.0 | 0.00 | 3.4E-02 |
| 1103/2506 | 47 | 21/11/2013 | 1.8 | 6.26 | 28/29 | 20.0 | 0.83 | -2.6E-03 |
| 1104/2507 | 47 | 29/11/2013 | 1.0 | 6.26 | 10/3 | 22.6 | 0.82 | 2.9E-03 |
| 1105/2508 | 47 | 10/1/2014 | 4.6 | 6.26 | 135/133 | 18.3 | 0.72 | 5.9E-03 |
| 1106/2509 | 47 | 24/1/2014 | 38.2 | 6.26 | 682/839 | 23.3 | 0.82 | 7.1E-03 |
| 1107/2510 | 47 | 6/3/2014 | 26.3 | 6.26 | 614/662 | 31.4 | 1.37 | 4.1E-03 |
| 1108/2511 | 47 | 4/4/2014 | 14.1 | 6.26 | 155/197 | 17.3 | 2.15 | 1.8E-02 |
| 1109/2512 | 47 | 26/2/2015 | 37.9 | 6.26 | 141/239 | 12.8 | 1.65 | -6.3E-07 |
| 1110/2513 | 47 | 8/5/2015 | 122.7 | 6.26 | 503/821 | 1.7 | 1.89 | 1.2E-02 |
| 1111/2514 | 47 | 1/11/2015 | 101.0 | 6.26 | 312/452 | 5.6 | 1.53 | 1.4E-02 |
| 1112/2515 | 47 | 20/2/2016 | 83.6 | 6.26 | 270/325 | 5.6 | 1.07 | 1.4E-02 |
| 1113/2516 | 47 | 18/6/2016 | 82.9 | 6.26 | 1993/2506 | 11.1 | 1.17 | 5.8E-03 |
| 1114/2517 | 47 | 2/10/2016 | 144.4 | 6.26 | 5076/6353 | 16.7 | 0.99 | 2.2E-02 |
| 1115/2518 | 47 | 20/5/2017 | 55.4 | 6.26 | 1946/2491 | 18.6 | 0.77 | 3.4E-02 |
| 1116/2519 | 47 | 31/7/2017 | 182.9 | 6.26 | 5543/7129 | 21.7 | 0.38 | 2.9E-02 |
| 1117/2520 | 48 | 6/3/2014 | 26.3 | 6.22 | 0/0 | 19.7 | 1.04 | -2.2E-07 |
| 1118/2521 | 48 | 4/4/2014 | 47.9 | 6.22 | 0/0 | 28.3 | 1.13 | 5.5E-07 |
| 1119/2522 | 48 | 19/6/2014 | 59.6 | 6.22 | 0/0 | 25.9 | 1.12 | 1.4E-07 |
| 1120/2523 | 48 | 5/9/2014 | 22.0 | 6.22 | 31/63 | 30.1 | 1.14 | -1.9E-06 |

| Partition No. | D. No. | Start date | Dur. [d] | m [g] | Events | $p_0$ [keV] | $p_1$ [keV] | $p_2$ [keV] |
|---|---|---|---|---|---|---|---|---|
| 1121/2524 | 48 | 2/10/2014 | 105.4 | 6.22 | 1118/1708 | 20.0 | 1.04 | 5.6E-03 |
| 1122/2525 | 48 | 26/2/2015 | 37.9 | 6.22 | 435/717 | 39.3 | 1.11 | 8.1E-03 |
| 1123/2526 | 48 | 8/5/2015 | 223.8 | 6.22 | 547/1038 | 49.3 | 1.01 | 1.6E-02 |
| 1124/2527 | 48 | 20/2/2016 | 83.6 | 6.22 | 21/42 | 40.2 | 0.83 | 1.7E-02 |
| 1125/2528 | 48 | 18/6/2016 | 82.9 | 6.22 | 756/1008 | 49.3 | 1.01 | 1.6E-02 |
| 1126/2529 | 49 | 21/11/2013 | 3.8 | 5.68 | 170/118 | 10.7 | 0.63 | 1.7E-02 |
| 1127/2530 | 49 | 10/1/2014 | 4.6 | 5.68 | 192/149 | 10.2 | 0.67 | 1.7E-02 |
| 1128/2531 | 49 | 24/1/2014 | 39.6 | 5.68 | 1435/1085 | 8.4 | 0.72 | 1.6E-02 |
| 1129/2532 | 49 | 6/3/2014 | 26.4 | 5.68 | 1177/914 | 6.9 | 0.74 | 1.8E-02 |
| 1130/2533 | 49 | 3/4/2014 | 17.1 | 5.68 | 766/568 | 6.7 | 0.78 | 2.0E-02 |
| 1131/2534 | 49 | 26/4/2014 | 102.9 | 5.68 | 4509/2876 | 6.8 | 0.81 | 2.0E-02 |
| 1132/2535 | 49 | 5/9/2014 | 23.1 | 5.68 | 1077/800 | 7.0 | 0.86 | 1.7E-02 |
| 1133/2536 | 49 | 2/10/2014 | 111.5 | 5.68 | 7177/5805 | 3.6 | 0.88 | 1.7E-02 |
| 1134/2537 | 49 | 25/2/2015 | 48.6 | 5.68 | 1857/1575 | 9.9 | 1.00 | 9.7E-03 |
| 1135/2538 | 49 | 6/5/2015 | 122.7 | 5.68 | 3065/2584 | 12.7 | 1.09 | 7.5E-03 |
| 1136/2539 | 49 | 1/11/2015 | 68.5 | 5.68 | 692/567 | 10.3 | 0.89 | 1.1E-02 |
| 1137/2540 | 49 | 21/2/2016 | 50.7 | 5.68 | 915/706 | 10.7 | 0.58 | 1.4E-02 |
| 1138/2541 | 50 | 21/11/2013 | 3.8 | 5.71 | 83/81 | 12.6 | 0.56 | 3.8E-03 |
| 1139/2542 | 50 | 10/1/2014 | 4.6 | 5.71 | 133/115 | 12.5 | 0.55 | 1.9E-03 |
| 1140/2543 | 50 | 24/1/2014 | 39.6 | 5.71 | 936/810 | 11.8 | 0.53 | 1.3E-06 |
| 1141/2544 | 50 | 6/3/2014 | 26.4 | 5.71 | 775/642 | 11.2 | 0.53 | 7.4E-07 |
| 1142/2545 | 50 | 3/4/2014 | 17.1 | 5.71 | 502/445 | 11.0 | 0.53 | 2.7E-07 |
| 1143/2546 | 50 | 26/4/2014 | 41.3 | 5.71 | 1139/996 | 11.5 | 0.52 | -3.4E-07 |
| 1144/2547 | 50 | 19/6/2014 | 61.5 | 5.71 | 1718/1484 | 11.8 | 0.48 | -2.0E-03 |
| 1145/2548 | 50 | 5/9/2014 | 23.1 | 5.71 | 744/588 | 11.2 | 0.50 | -2.0E-03 |
| 1146/2549 | 50 | 2/10/2014 | 111.5 | 5.71 | 5498/4901 | 10.9 | 0.56 | 6.8E-08 |
| 1147/2550 | 50 | 25/2/2015 | 48.6 | 5.71 | 2305/1977 | 11.4 | 0.59 | 2.3E-07 |
| 1148/2551 | 50 | 6/5/2015 | 122.7 | 5.71 | 4295/3860 | 10.7 | 0.68 | 4.3E-08 |
| 1149/2552 | 50 | 1/11/2015 | 68.5 | 5.71 | 786/724 | 10.3 | 0.65 | 1.2E-07 |
| 1150/2553 | 50 | 21/2/2016 | 50.7 | 5.71 | 1099/1017 | 10.9 | 0.53 | 1.9E-04 |
| 1151/2554 | 50 | 18/6/2016 | 87.6 | 5.71 | 3635/3279 | 11.3 | 0.53 | 1.9E-07 |
| 1152/2555 | 50 | 2/10/2016 | 142.3 | 5.71 | 6937/5992 | 11.3 | 0.52 | 5.0E-04 |
| 1153/2556 | 50 | 20/5/2017 | 61.0 | 5.71 | 2798/2477 | 10.5 | 0.47 | 4.1E-03 |
| 1154/2557 | 50 | 31/7/2017 | 188.8 | 5.71 | 7704/6924 | 11.5 | 0.36 | 9.5E-03 |
| 1155/2558 | 50 | 2/11/2018 | 169.0 | 5.71 | 8955/8055 | 10.5 | 0.42 | 6.5E-03 |
| 1156/2559 | 50 | 25/5/2019 | 31.4 | 5.71 | 1327/1159 | 11.1 | 0.45 | 7.7E-03 |
| 1157/2560 | 51 | 21/11/2013 | 74.5 | 5.67 | 1267/1174 | 11.1 | 0.56 | 4.4E-07 |
| 1158/2561 | 51 | 3/4/2014 | 17.1 | 5.67 | 309/318 | 11.7 | 0.47 | -2.2E-03 |
| 1159/2562 | 51 | 26/4/2014 | 41.3 | 5.67 | 653/744 | 12.7 | 0.41 | -3.5E-03 |
| 1160/2563 | 51 | 19/6/2014 | 61.5 | 5.67 | 1082/966 | 12.5 | 0.46 | -1.3E-03 |
| 1161/2564 | 51 | 5/9/2014 | 23.1 | 5.67 | 464/477 | 11.4 | 0.59 | -6.9E-07 |
| 1162/2565 | 51 | 2/10/2014 | 111.5 | 5.67 | 3310/3101 | 14.2 | 0.59 | -3.2E-07 |
| 1163/2566 | 51 | 25/2/2015 | 48.6 | 5.67 | 1040/968 | 17.6 | 0.54 | -8.0E-08 |
| 1164/2567 | 51 | 6/5/2015 | 122.7 | 5.67 | 1809/1719 | 18.8 | 0.54 | -1.9E-07 |
| 1165/2568 | 51 | 1/11/2015 | 68.5 | 5.67 | 352/333 | 22.4 | 0.55 | -6.8E-07 |
| 1166/2569 | 51 | 21/2/2016 | 50.7 | 5.67 | 353/382 | 26.4 | 0.56 | 1.3E-06 |
| 1167/2570 | 51 | 18/6/2016 | 87.6 | 5.67 | 1166/1066 | 26.0 | 0.56 | -1.2E-06 |
| 1168/2571 | 51 | 2/10/2016 | 142.3 | 5.67 | 1753/1676 | 26.0 | 0.56 | 5.0E-04 |
| 1169/2572 | 51 | 2/11/2018 | 169.0 | 5.67 | 1473/1475 | 23.5 | 0.57 | 1.0E-03 |
| 1170/2573 | 51 | 25/5/2019 | 31.4 | 5.67 | 6/9 | 25.9 | 0.66 | 1.0E-03 |
| 1171/2574 | 52 | 21/11/2013 | 3.8 | 5.63 | 65/48 | 6.9 | 0.86 | -8.7E-07 |
| 1172/2575 | 52 | 10/1/2014 | 4.6 | 5.63 | 101/75 | 11.4 | 0.85 | -1.0E-06 |
| 1173/2576 | 52 | 24/1/2014 | 39.6 | 5.63 | 616/542 | 14.6 | 0.83 | -6.3E-07 |
| 1174/2577 | 52 | 6/3/2014 | 26.4 | 5.63 | 566/464 | 13.1 | 0.79 | 2.6E-03 |
| 1175/2578 | 52 | 3/4/2014 | 17.1 | 5.63 | 424/289 | 13.0 | 0.80 | 3.8E-03 |
| 1176/2579 | 52 | 26/4/2014 | 41.3 | 5.63 | 774/657 | 14.2 | 0.80 | 1.2E-03 |
| 1177/2580 | 52 | 19/6/2014 | 61.5 | 5.63 | 1144/986 | 14.4 | 0.77 | 3.0E-07 |
| 1178/2581 | 52 | 5/9/2014 | 23.1 | 5.63 | 523/449 | 12.9 | 0.83 | 5.4E-07 |
| 1179/2582 | 52 | 2/10/2014 | 111.5 | 5.63 | 4134/3486 | 14.6 | 0.78 | 5.6E-03 |
| 1180/2583 | 52 | 25/2/2015 | 48.6 | 5.63 | 1446/1316 | 15.0 | 0.94 | -6.4E-07 |
| 1181/2584 | 52 | 6/5/2015 | 122.7 | 5.63 | 2466/2072 | 18.2 | 0.99 | 1.4E-07 |
| 1182/2585 | 52 | 1/11/2015 | 68.5 | 5.63 | 431/412 | 22.1 | 0.93 | 1.4E-07 |
| 1183/2586 | 52 | 21/2/2016 | 50.7 | 5.63 | 593/558 | 20.1 | 0.94 | 1.2E-05 |
| 1184/2587 | 52 | 18/6/2016 | 87.6 | 5.63 | 2062/1776 | 22.4 | 0.84 | 2.0E-07 |
| 1185/2588 | 52 | 31/7/2017 | 188.8 | 5.63 | 5916/5029 | 19.3 | 0.76 | 1.0E-03 |
| 1186/2589 | 52 | 2/11/2018 | 169.0 | 5.63 | 4945/4250 | 24.3 | 0.73 | 6.4E-03 |
| 1187/2590 | 52 | 25/5/2019 | 31.4 | 5.63 | 529/481 | 27.8 | 0.79 | 5.6E-03 |
| 1188/2591 | 53 | 21/11/2013 | 2.3 | 5.76 | 83/53 | 8.8 | 0.50 | 1.9E-02 |
| 1189/2592 | 53 | 29/11/2013 | 1.3 | 5.76 | 43/21 | 9.6 | 0.31 | 2.3E-02 |
| 1190/2593 | 53 | 10/1/2014 | 4.6 | 5.76 | 192/92 | 11.1 | 0.32 | 2.2E-02 |
| 1191/2594 | 53 | 24/1/2014 | 39.5 | 5.76 | 1319/839 | 8.7 | 0.53 | 1.9E-02 |
| 1192/2595 | 53 | 6/3/2014 | 26.4 | 5.76 | 1062/683 | 6.0 | 0.69 | 1.7E-02 |

| Partition No. | D. No. | Start date | Dur. [d] | m [g] | Events | $p_0$ [keV] | $p_1$ [keV] | $p_2$ [keV] |
|---|---|---|---|---|---|---|---|---|
| 1193/2596 | 53 | 3/4/2014 | 17.1 | 5.76 | 708/410 | 8.3 | 0.62 | 1.8E-02 |
| 1194/2597 | 53 | 26/4/2014 | 41.8 | 5.76 | 1545/915 | 5.0 | 0.74 | 1.2E-02 |
| 1195/2598 | 53 | 19/6/2014 | 61.5 | 5.76 | 2182/1397 | 0.6 | 0.90 | 6.2E-03 |
| 1196/2599 | 53 | 5/9/2014 | 23.0 | 5.76 | 857/516 | 0.9 | 0.88 | 9.1E-03 |
| 1197/2600 | 53 | 2/10/2014 | 117.6 | 5.76 | 6132/4009 | 1.2 | 0.87 | 1.2E-02 |
| 1198/2601 | 53 | 25/2/2015 | 50.7 | 5.76 | 2160/1418 | 7.1 | 0.80 | 1.5E-02 |
| 1199/2602 | 53 | 6/5/2015 | 143.6 | 5.76 | 4660/3176 | 4.7 | 0.88 | 1.4E-02 |
| 1200/2603 | 53 | 1/11/2015 | 100.8 | 5.76 | 1838/1199 | 1.0 | 0.95 | 1.2E-02 |
| 1201/2604 | 53 | 20/2/2016 | 84.1 | 5.76 | 2037/1298 | 0.5 | 0.77 | 1.4E-02 |
| 1202/2605 | 53 | 18/6/2016 | 90.7 | 5.76 | 4983/3184 | 1.0 | 0.95 | 1.2E-02 |
| 1203/2606 | 53 | 2/10/2016 | 146.9 | 5.76 | 8828/5497 | 6.0 | 0.63 | 1.8E-02 |
| 1204/2607 | 53 | 20/5/2017 | 58.2 | 5.76 | 3425/2089 | 10.0 | 0.34 | 2.1E-02 |
| 1205/2608 | 53 | 31/7/2017 | 186.0 | 5.76 | 9760/6131 | 10.3 | 0.31 | 2.1E-02 |
| 1206/2609 | 53 | 21/7/2018 | 6.4 | 5.76 | 52/26 | 11.3 | 0.15 | 2.1E-02 |
| 1207/2610 | 53 | 2/11/2018 | 170.7 | 5.76 | 9970/6079 | 10.2 | 0.13 | 2.2E-02 |
| 1208/2611 | 53 | 25/5/2019 | 114.0 | 5.76 | 6222/3845 | 11.1 | 0.10 | 2.2E-02 |
| 1209/2612 | 54 | 21/11/2013 | 2.3 | 5.68 | 55/48 | 10.6 | 0.34 | 1.5E-02 |
| 1210/2613 | 54 | 29/11/2013 | 1.3 | 5.68 | 44/19 | 15.4 | 0.00 | 1.8E-02 |
| 1211/2614 | 54 | 10/1/2014 | 4.6 | 5.68 | 137/130 | 9.7 | 0.40 | 2.0E-02 |
| 1212/2615 | 54 | 24/1/2014 | 39.5 | 5.68 | 1039/954 | 4.0 | 0.81 | 2.2E-02 |
| 1213/2616 | 54 | 6/3/2014 | 26.4 | 5.68 | 824/724 | -1.3 | 0.79 | 2.5E-02 |
| 1214/2617 | 54 | 3/4/2014 | 17.1 | 5.68 | 544/491 | -3.3 | 0.79 | 2.4E-02 |
| 1215/2618 | 54 | 26/4/2014 | 41.8 | 5.68 | 1184/1210 | -8.1 | 0.40 | 2.7E-02 |
| 1216/2619 | 54 | 19/6/2014 | 61.5 | 5.68 | 1836/1803 | -0.5 | 0.00 | 3.1E-02 |
| 1217/2620 | 54 | 5/9/2014 | 23.0 | 5.68 | 803/735 | 7.6 | 0.36 | 3.1E-02 |
| 1218/2621 | 54 | 2/10/2014 | 117.6 | 5.68 | 6592/6139 | 0.0 | 0.71 | 3.3E-02 |
| 1219/2622 | 54 | 25/2/2015 | 50.7 | 5.68 | 2717/2656 | 15.6 | 0.52 | 3.1E-02 |
| 1220/2623 | 54 | 6/5/2015 | 143.6 | 5.68 | 5399/5274 | 6.8 | 0.96 | 2.2E-02 |
| 1221/2624 | 54 | 1/11/2015 | 100.8 | 5.68 | 1842/1761 | 5.6 | 0.86 | 1.6E-02 |
| 1222/2625 | 54 | 18/6/2016 | 90.7 | 5.68 | 5957/5711 | 3.2 | 0.81 | 2.4E-02 |
| 1223/2626 | 54 | 2/10/2016 | 146.9 | 5.68 | 10148/9761 | 8.0 | 0.46 | 3.4E-02 |
| 1224/2627 | 54 | 20/5/2017 | 58.2 | 5.68 | 3765/3789 | 9.2 | 0.29 | 2.1E-02 |
| 1225/2628 | 54 | 31/7/2017 | 186.0 | 5.68 | 8729/8510 | 10.8 | 0.28 | 5.8E-03 |
| 1226/2629 | 54 | 21/7/2018 | 6.4 | 5.68 | 61/79 | 11.2 | 0.30 | 4.9E-03 |
| 1227/2630 | 54 | 2/11/2018 | 170.7 | 5.68 | 10973/10862 | 9.9 | 0.32 | 3.9E-03 |
| 1228/2631 | 54 | 25/5/2019 | 114.0 | 5.68 | 6900/6837 | 11.6 | 0.24 | 5.3E-03 |
| 1229/2632 | 55 | 21/11/2013 | 2.3 | 5.88 | 31/28 | 5.8 | 0.33 | 1.8E-02 |
| 1230/2633 | 55 | 29/11/2013 | 1.3 | 5.88 | 22/21 | 11.6 | 0.00 | 2.1E-02 |
| 1231/2634 | 55 | 10/1/2014 | 4.6 | 5.88 | 84/100 | 11.8 | 0.17 | 2.0E-02 |
| 1232/2635 | 55 | 24/1/2014 | 39.5 | 5.88 | 636/589 | 12.0 | 0.34 | 1.9E-02 |
| 1233/2636 | 55 | 6/3/2014 | 26.4 | 5.88 | 483/465 | 12.4 | 0.17 | 1.9E-02 |
| 1234/2637 | 55 | 3/4/2014 | 17.1 | 5.88 | 322/315 | 6.4 | 0.36 | 9.9E-03 |
| 1235/2638 | 55 | 26/4/2014 | 41.8 | 5.88 | 701/704 | 0.0 | 0.72 | 1.7E-06 |
| 1236/2639 | 55 | 19/6/2014 | 61.5 | 5.88 | 1035/974 | 1.9 | 0.67 | 3.4E-03 |
| 1237/2640 | 55 | 5/9/2014 | 23.0 | 5.88 | 512/454 | 5.0 | 0.66 | 1.1E-02 |
| 1238/2641 | 55 | 2/10/2014 | 117.6 | 5.88 | 4252/4016 | 6.1 | 0.58 | 1.5E-02 |
| 1239/2642 | 55 | 25/2/2015 | 50.7 | 5.88 | 1645/1603 | 11.2 | 0.30 | 1.9E-02 |
| 1240/2643 | 55 | 6/5/2015 | 335.1 | 5.88 | 8461/7878 | 11.0 | 0.36 | 1.9E-02 |
| 1241/2644 | 55 | 2/10/2016 | 146.9 | 5.88 | 6191/5963 | 7.4 | 0.53 | 9.9E-03 |
| 1242/2645 | 55 | 20/5/2017 | 58.2 | 5.88 | 2695/2702 | 6.2 | 0.51 | 3.7E-03 |
| 1243/2646 | 55 | 31/7/2017 | 186.0 | 5.88 | 6209/5944 | 10.7 | 0.16 | 9.0E-03 |
| 1244/2647 | 55 | 21/7/2018 | 6.4 | 5.88 | 42/38 | 9.3 | 0.35 | 7.4E-03 |
| 1245/2648 | 55 | 2/11/2018 | 170.7 | 5.88 | 9246/8875 | 9.4 | 0.32 | 7.6E-03 |
| 1246/2649 | 55 | 25/5/2019 | 114.0 | 5.88 | 6200/5991 | 9.3 | 0.33 | 9.1E-03 |
| 1247/2650 | 56 | 21/11/2013 | 2.3 | 5.98 | 49/26 | 0.0 | 0.66 | 1.5E-02 |
| 1248/2651 | 56 | 29/11/2013 | 1.3 | 5.98 | 32/24 | 0.0 | 0.62 | 1.7E-02 |
| 1249/2652 | 56 | 10/1/2014 | 4.6 | 5.98 | 116/101 | 6.4 | 0.37 | 1.9E-02 |
| 1250/2653 | 56 | 24/1/2014 | 39.5 | 5.98 | 804/640 | 12.7 | 0.12 | 2.2E-02 |
| 1251/2654 | 56 | 6/3/2014 | 26.4 | 5.98 | 633/512 | 6.4 | 0.39 | 1.8E-02 |
| 1252/2655 | 56 | 3/4/2014 | 58.9 | 5.98 | 1246/1143 | 0.0 | 0.66 | 1.4E-02 |
| 1253/2656 | 56 | 19/6/2014 | 61.5 | 5.98 | 1321/1042 | 2.7 | 0.69 | 9.2E-03 |
| 1254/2657 | 56 | 5/9/2014 | 23.0 | 5.98 | 640/513 | 5.4 | 0.72 | 4.5E-03 |
| 1255/2658 | 56 | 2/10/2014 | 117.6 | 5.98 | 5944/5084 | -0.8 | 0.63 | 1.1E-02 |
| 1256/2659 | 56 | 25/2/2015 | 194.3 | 5.98 | 6733/5570 | 6.0 | 0.80 | 5.4E-07 |
| 1257/2660 | 56 | 1/11/2015 | 100.8 | 5.98 | 1750/1453 | 9.4 | 0.40 | 1.1E-02 |
| 1258/2661 | 56 | 18/6/2016 | 90.7 | 5.98 | 3655/2996 | 12.7 | 0.00 | 2.1E-02 |
| 1259/2662 | 56 | 31/7/2017 | 186.0 | 5.98 | 7957/6645 | 11.8 | 0.57 | 1.1E-02 |
| 1260/2663 | 56 | 21/7/2018 | 6.4 | 5.98 | 27/12 | 10.7 | 0.44 | 8.5E-03 |
| 1261/2664 | 56 | 2/11/2018 | 170.7 | 5.98 | 6974/5811 | 10.6 | 0.36 | 1.1E-02 |
| 1262/2665 | 56 | 25/5/2019 | 114.0 | 5.98 | 4269/3431 | 11.3 | 0.40 | 1.1E-02 |
| 1263/2666 | 57 | 21/11/2013 | 3.5 | 5.74 | 62/56 | 6.3 | 0.79 | 1.4E-02 |
| 1264/2667 | 57 | 10/1/2014 | 4.6 | 5.74 | 118/93 | 4.2 | 0.94 | 1.8E-02 |

| Partition No. | D. No. | Start date | Dur. [d] | m [g] | Events | $p_0$ [keV] | $p_1$ [keV] | $p_2$ [keV] |
|---|---|---|---|---|---|---|---|---|
| 1265/2668 | 57 | 24/1/2014 | 39.6 | 5.74 | 940/860 | 1.9 | 0.98 | 2.4E-02 |
| 1266/2669 | 57 | 6/3/2014 | 26.1 | 5.74 | 752/598 | 1.7 | 0.95 | 2.3E-02 |
| 1267/2670 | 57 | 3/4/2014 | 16.9 | 5.74 | 461/429 | 1.7 | 1.03 | 1.9E-02 |
| 1268/2671 | 57 | 26/4/2014 | 30.7 | 5.74 | 761/649 | 1.8 | 1.03 | 1.7E-02 |
| 1269/2672 | 57 | 19/6/2014 | 55.3 | 5.74 | 1397/1292 | 1.7 | 0.98 | 1.8E-02 |
| 1270/2673 | 57 | 5/9/2014 | 23.1 | 5.74 | 699/639 | 2.9 | 1.00 | 2.2E-02 |
| 1271/2674 | 57 | 2/10/2014 | 117.5 | 5.74 | 5382/4948 | 6.6 | 0.76 | 2.2E-02 |
| 1272/2675 | 57 | 25/2/2015 | 50.5 | 5.74 | 1474/1430 | 1.5 | 0.96 | 8.1E-03 |
| 1273/2676 | 57 | 6/5/2015 | 143.2 | 5.74 | 3730/3416 | 1.6 | 0.98 | 9.9E-03 |
| 1274/2677 | 57 | 1/11/2015 | 88.8 | 5.74 | 1385/1228 | 1.5 | 0.89 | 2.0E-02 |
| 1275/2678 | 57 | 20/2/2016 | 64.8 | 5.74 | 847/791 | 4.1 | 0.77 | 1.9E-02 |
| 1276/2679 | 57 | 20/6/2016 | 83.5 | 5.74 | 4466/4006 | 1.5 | 0.89 | 2.0E-02 |
| 1277/2680 | 57 | 2/10/2016 | 147.9 | 5.74 | 8693/7662 | 4.9 | 0.76 | 1.9E-02 |
| 1278/2681 | 57 | 20/5/2017 | 60.0 | 5.74 | 1517/988 | 11.6 | 0.58 | 2.0E-02 |
| 1279/2682 | 57 | 31/7/2017 | 177.1 | 5.74 | 1742/1712 | 11.2 | 0.60 | 2.0E-02 |
| 1280/2683 | 57 | 2/11/2018 | 167.4 | 5.74 | 8237/7462 | 14.4 | 0.26 | 2.6E-02 |
| 1281/2684 | 57 | 25/5/2019 | 114.7 | 5.74 | 2607/2754 | 12.4 | 0.34 | 2.2E-02 |
| 1282/2685 | 58 | 21/11/2013 | 2.2 | 5.76 | 58/52 | 12.2 | 0.25 | -6.0E-03 |
| 1283/2686 | 58 | 29/11/2013 | 1.3 | 5.76 | 25/46 | 13.6 | 0.00 | -1.2E-02 |
| 1284/2687 | 58 | 3/4/2014 | 16.9 | 5.76 | 684/694 | 10.5 | 0.53 | -1.4E-03 |
| 1285/2688 | 58 | 26/4/2014 | 30.7 | 5.76 | 1012/1102 | 12.5 | 0.54 | -1.4E-03 |
| 1286/2689 | 58 | 19/6/2014 | 55.3 | 5.76 | 1776/1921 | 13.8 | 0.55 | 2.4E-08 |
| 1287/2690 | 58 | 5/9/2014 | 23.1 | 5.76 | 757/794 | 11.9 | 0.67 | -7.4E-08 |
| 1288/2691 | 58 | 2/10/2014 | 117.5 | 5.76 | 5178/5715 | 9.0 | 0.67 | -2.5E-07 |
| 1289/2692 | 58 | 25/2/2015 | 50.5 | 5.76 | 2086/2292 | 8.0 | 0.56 | -3.2E-07 |
| 1290/2693 | 58 | 6/5/2015 | 143.2 | 5.76 | 4270/4830 | 11.0 | 0.58 | -8.6E-07 |
| 1291/2694 | 58 | 1/11/2015 | 88.8 | 5.76 | 1611/1740 | 14.0 | 0.60 | -1.4E-06 |
| 1292/2695 | 58 | 20/2/2016 | 64.8 | 5.76 | 964/1030 | 11.3 | 0.57 | 2.7E-07 |
| 1293/2696 | 58 | 20/6/2016 | 83.5 | 5.76 | 4444/4745 | 11.6 | 0.51 | 2.4E-03 |
| 1294/2697 | 58 | 2/10/2016 | 147.9 | 5.76 | 7904/8676 | 9.2 | 0.46 | 3.4E-03 |
| 1295/2698 | 58 | 20/5/2017 | 60.0 | 5.76 | 3128/3438 | 8.6 | 0.48 | 2.3E-03 |
| 1296/2699 | 58 | 31/7/2017 | 177.1 | 5.76 | 7990/7901 | 9.5 | 0.42 | 4.5E-03 |
| 1297/2700 | 58 | 21/7/2018 | 4.9 | 5.76 | 32/49 | 10.5 | 0.35 | 7.1E-03 |
| 1298/2701 | 58 | 2/11/2018 | 167.4 | 5.76 | 9720/9909 | 9.4 | 0.34 | 6.9E-03 |
| 1299/2702 | 58 | 25/5/2019 | 114.7 | 5.76 | 6468/6572 | 11.0 | 0.32 | 7.1E-03 |
| 1300/2703 | 59 | 21/11/2013 | 2.2 | 5.69 | 42/27 | 11.5 | 0.57 | -4.0E-03 |
| 1301/2704 | 59 | 29/11/2013 | 45.5 | 5.69 | 954/752 | 12.8 | 0.49 | -8.1E-03 |
| 1302/2705 | 59 | 6/3/2014 | 26.1 | 5.69 | 549/459 | 15.6 | 0.73 | -4.0E-03 |
| 1303/2706 | 59 | 3/4/2014 | 16.9 | 5.69 | 252/196 | 35.3 | 0.48 | 2.1E-02 |
| 1304/2707 | 59 | 26/4/2014 | 30.7 | 5.69 | 37/29 | 40.6 | 0.47 | 2.1E-02 |
| 1305/2708 | 59 | 19/6/2014 | 55.3 | 5.69 | 4/11 | 41.7 | 1.11 | -6.4E-07 |
| 1306/2709 | 59 | 5/9/2014 | 23.1 | 5.69 | 142/161 | 41.2 | 1.24 | -8.0E-07 |
| 1307/2710 | 59 | 2/10/2014 | 117.5 | 5.69 | 2454/2088 | 23.9 | 0.90 | 6.0E-06 |
| 1308/2711 | 59 | 25/2/2015 | 50.5 | 5.69 | 1003/828 | 25.2 | 0.87 | -3.9E-07 |
| 1309/2712 | 59 | 6/5/2015 | 143.2 | 5.69 | 1843/1535 | 20.8 | 1.18 | -4.8E-07 |
| 1310/2713 | 59 | 1/11/2015 | 88.8 | 5.69 | 888/767 | 16.4 | 1.49 | -5.7E-07 |
| 1311/2714 | 59 | 20/2/2016 | 64.8 | 5.69 | 29/19 | 17.3 | 1.30 | -6.2E-08 |
| 1312/2715 | 59 | 20/6/2016 | 83.5 | 5.69 | 3/11 | 34.9 | 1.12 | 8.9E-07 |
| 1313/2716 | 59 | 2/10/2016 | 147.9 | 5.69 | 0/0 | 32.5 | 0.96 | 2.1E-03 |
| 1314/2717 | 59 | 21/7/2018 | 4.9 | 5.69 | 0/1 | 32.5 | 0.80 | 1.6E-02 |
| 1315/2718 | 59 | 2/11/2018 | 167.4 | 5.69 | 3717/3137 | 24.1 | 0.77 | 3.7E-03 |
| 1316/2719 | 59 | 25/5/2019 | 114.7 | 5.69 | 1302/1071 | 28.2 | 0.80 | 1.0E-02 |
| 1317/2720 | 60 | 21/11/2013 | 73.8 | 5.68 | 1514/1073 | 9.4 | 0.60 | 1.5E-02 |
| 1318/2721 | 60 | 3/4/2014 | 16.9 | 5.68 | 337/256 | 10.7 | 0.67 | 1.6E-02 |
| 1319/2722 | 60 | 26/4/2014 | 30.7 | 5.68 | 589/371 | 11.7 | 0.78 | 1.5E-02 |
| 1320/2723 | 60 | 19/6/2014 | 55.3 | 5.68 | 1027/724 | 10.5 | 0.75 | 1.4E-02 |
| 1321/2724 | 60 | 5/9/2014 | 23.1 | 5.68 | 527/411 | 5.2 | 0.87 | 1.0E-02 |
| 1322/2725 | 60 | 2/10/2014 | 117.5 | 5.68 | 3671/2758 | 0.8 | 1.04 | 5.9E-03 |
| 1323/2726 | 60 | 25/2/2015 | 50.5 | 5.68 | 969/731 | 11.5 | 0.66 | 1.0E-02 |
| 1324/2727 | 60 | 6/5/2015 | 143.2 | 5.68 | 2251/1724 | 5.2 | 0.91 | 8.2E-03 |
| 1325/2728 | 60 | 1/11/2015 | 88.8 | 5.68 | 918/664 | 0.8 | 0.85 | 1.3E-02 |
| 1326/2729 | 60 | 20/2/2016 | 64.8 | 5.68 | 596/409 | 6.7 | 0.52 | 1.5E-02 |
| 1327/2730 | 60 | 20/6/2016 | 83.5 | 5.68 | 2654/2063 | 1.0 | 0.83 | 9.8E-03 |
| 1328/2731 | 60 | 2/10/2016 | 147.9 | 5.68 | 7533/5434 | 5.2 | 0.67 | 1.3E-02 |
| 1329/2732 | 60 | 20/5/2017 | 60.0 | 5.68 | 2401/1769 | 8.7 | 0.49 | 1.6E-02 |
| 1330/2733 | 60 | 31/7/2017 | 177.1 | 5.68 | 1391/1134 | 12.1 | 0.40 | 1.8E-02 |
| 1331/2734 | 60 | 21/7/2018 | 4.9 | 5.68 | 16/16 | 9.8 | 0.43 | 1.6E-02 |
| 1332/2735 | 60 | 2/11/2018 | 167.4 | 5.68 | 6531/4495 | 10.1 | 0.27 | 1.8E-02 |
| 1333/2736 | 60 | 25/5/2019 | 114.7 | 5.68 | 1821/1301 | 11.0 | 0.12 | 2.0E-02 |
| 1334/2737 | 61 | 21/11/2013 | 2.5 | 5.71 | 58/41 | 7.8 | 0.77 | 7.8E-03 |
| 1335/2738 | 61 | 29/11/2013 | 1.3 | 5.71 | 37/16 | 7.0 | 0.79 | 8.4E-03 |
| 1336/2739 | 61 | 10/1/2014 | 4.6 | 5.71 | 145/90 | 8.4 | 0.75 | 1.0E-02 |

| Partition No. | D. No. | Start date | Dur. [d] | m [g] | Events | $p_0$ [keV] | $p_1$ [keV] | $p_2$ [keV] |
|---|---|---|---|---|---|---|---|---|
| 1337/2740 | 61 | 24/1/2014 | 39.6 | 5.71 | 1057/747 | 8.1 | 0.74 | 1.2E-02 |
| 1338/2741 | 61 | 6/3/2014 | 26.4 | 5.71 | 797/592 | 6.4 | 0.77 | 1.2E-02 |
| 1339/2742 | 61 | 3/4/2014 | 17.0 | 5.71 | 591/340 | 9.8 | 0.75 | 1.3E-02 |
| 1340/2743 | 61 | 26/4/2014 | 41.3 | 5.71 | 1267/775 | 11.9 | 0.82 | 7.0E-03 |
| 1341/2744 | 61 | 19/6/2014 | 59.0 | 5.71 | 1620/1023 | 8.4 | 0.89 | 3.9E-03 |
| 1342/2745 | 61 | 5/9/2014 | 21.8 | 5.71 | 723/463 | 6.6 | 0.89 | 3.9E-03 |
| 1343/2746 | 61 | 2/10/2014 | 117.5 | 5.71 | 5394/3591 | 3.4 | 0.84 | 5.9E-03 |
| 1344/2747 | 61 | 25/2/2015 | 47.1 | 5.71 | 1505/1004 | 5.2 | 0.84 | 6.1E-07 |
| 1345/2748 | 61 | 6/5/2015 | 140.6 | 5.71 | 3093/2098 | 2.8 | 0.89 | 3.5E-03 |
| 1346/2749 | 61 | 1/11/2015 | 100.8 | 5.71 | 1105/786 | 0.0 | 0.93 | 7.0E-03 |
| 1347/2750 | 61 | 20/2/2016 | 83.3 | 5.71 | 1270/890 | 0.0 | 0.92 | 6.3E-03 |
| 1348/2751 | 61 | 18/6/2016 | 88.7 | 5.71 | 3097/2040 | 0.0 | 0.93 | 7.0E-03 |
| 1349/2752 | 61 | 2/10/2016 | 139.2 | 5.71 | 7820/5112 | 3.1 | 0.82 | 8.2E-03 |
| 1350/2753 | 61 | 20/5/2017 | 59.6 | 5.71 | 3340/2198 | 7.9 | 0.65 | 1.4E-02 |
| 1351/2754 | 61 | 31/7/2017 | 180.5 | 5.71 | 9552/5839 | 9.3 | 0.63 | 1.8E-02 |
| 1352/2755 | 61 | 2/11/2018 | 170.7 | 5.71 | 10052/6825 | 8.2 | 0.61 | 1.3E-02 |
| 1353/2756 | 61 | 25/5/2019 | 114.6 | 5.71 | 6425/4230 | 9.4 | 0.54 | 1.4E-02 |
| 1354/2757 | 62 | 21/11/2013 | 8.4 | 5.67 | 262/299 | 10.3 | 0.70 | 1.8E-03 |
| 1355/2758 | 62 | 24/1/2014 | 39.6 | 5.67 | 1218/1186 | 11.4 | 0.65 | 2.0E-03 |
| 1356/2759 | 62 | 6/3/2014 | 26.4 | 5.67 | 938/916 | 12.2 | 0.58 | 1.1E-03 |
| 1357/2760 | 62 | 3/4/2014 | 17.0 | 5.67 | 591/563 | 11.6 | 0.56 | 2.9E-03 |
| 1358/2761 | 62 | 26/4/2014 | 41.3 | 5.67 | 1285/1328 | 12.3 | 0.55 | 2.9E-03 |
| 1359/2762 | 62 | 19/6/2014 | 59.0 | 5.67 | 1818/1859 | 12.6 | 0.55 | 2.6E-03 |
| 1360/2763 | 62 | 5/9/2014 | 21.8 | 5.67 | 692/690 | 12.1 | 0.60 | 2.6E-03 |
| 1361/2764 | 62 | 2/10/2014 | 117.5 | 5.67 | 4028/3952 | 13.5 | 0.63 | 5.7E-07 |
| 1362/2765 | 62 | 1/11/2015 | 100.8 | 5.67 | 31/54 | 19.6 | 0.64 | 5.0E-08 |
| 1363/2766 | 62 | 20/2/2016 | 83.3 | 5.67 | 24/73 | 17.5 | 0.64 | 1.6E-06 |
| 1364/2767 | 62 | 18/6/2016 | 88.7 | 5.67 | 1912/1957 | 19.6 | 0.64 | 5.0E-08 |
| 1365/2768 | 62 | 2/10/2016 | 139.2 | 5.67 | 5277/5557 | 21.3 | 0.63 | 5.0E-04 |
| 1366/2769 | 62 | 20/5/2017 | 59.6 | 5.67 | 1609/1670 | 20.7 | 0.60 | 1.0E-03 |
| 1367/2770 | 62 | 31/7/2017 | 180.5 | 5.67 | 3480/3747 | 21.1 | 0.61 | 1.0E-03 |
| 1368/2771 | 62 | 2/11/2018 | 170.7 | 5.67 | 6016/6431 | 21.0 | 0.51 | 7.1E-03 |
| 1369/2772 | 62 | 25/5/2019 | 114.6 | 5.67 | 4255/4606 | 23.5 | 0.62 | 6.1E-03 |
| 1370/2773 | 63 | 21/11/2013 | 2.5 | 5.72 | 79/76 | -5.5 | 0.73 | 1.8E-02 |
| 1371/2774 | 63 | 29/11/2013 | 1.3 | 5.72 | 47/49 | 0.8 | 0.89 | 1.4E-02 |
| 1372/2775 | 63 | 10/1/2014 | 4.6 | 5.72 | 196/145 | 0.7 | 0.96 | 9.6E-03 |
| 1373/2776 | 63 | 24/1/2014 | 39.6 | 5.72 | 1393/1246 | 0.8 | 0.96 | 8.1E-03 |
| 1374/2777 | 63 | 6/3/2014 | 26.4 | 5.72 | 1077/899 | 1.0 | 0.90 | 1.1E-02 |
| 1375/2778 | 63 | 3/4/2014 | 17.0 | 5.72 | 727/618 | 1.2 | 0.90 | 1.2E-02 |
| 1376/2779 | 63 | 26/4/2014 | 41.3 | 5.72 | 1668/1391 | 1.1 | 0.96 | 8.5E-03 |
| 1377/2780 | 63 | 19/6/2014 | 59.0 | 5.72 | 2225/2120 | 0.6 | 1.01 | 2.1E-03 |
| 1378/2781 | 63 | 5/9/2014 | 427.8 | 5.72 | 8324/7970 | 0.5 | 1.00 | -1.6E-06 |
| 1379/2782 | 63 | 20/2/2016 | 83.3 | 5.72 | 619/671 | 5.2 | 0.81 | 7.8E-03 |
| 1380/2783 | 63 | 18/6/2016 | 88.7 | 5.72 | 1185/1358 | 0.2 | 0.91 | 8.4E-03 |
| 1381/2784 | 63 | 2/10/2016 | 139.2 | 5.72 | 3204/3214 | 4.3 | 0.79 | 1.6E-02 |
| 1382/2785 | 63 | 2/11/2018 | 170.7 | 5.72 | 5258/5129 | 6.3 | 0.55 | 1.6E-02 |
| 1383/2786 | 63 | 25/5/2019 | 114.6 | 5.72 | 3257/2920 | 7.1 | 0.52 | 1.9E-02 |
| 1384/2787 | 64 | 21/11/2013 | 2.5 | 5.75 | 37/29 | 14.0 | 0.69 | 2.5E-02 |
| 1385/2788 | 64 | 29/11/2013 | 1.3 | 5.75 | 30/25 | 9.0 | 0.76 | 2.4E-02 |
| 1386/2789 | 64 | 10/1/2014 | 4.6 | 5.75 | 141/96 | 10.1 | 0.75 | 2.2E-02 |
| 1387/2790 | 64 | 24/1/2014 | 39.6 | 5.75 | 917/766 | 7.4 | 0.85 | 1.6E-02 |
| 1388/2791 | 64 | 6/3/2014 | 26.4 | 5.75 | 675/539 | 3.6 | 0.96 | 1.3E-02 |
| 1389/2792 | 64 | 3/4/2014 | 17.0 | 5.75 | 458/353 | 7.8 | 0.85 | 1.6E-02 |
| 1390/2793 | 64 | 26/4/2014 | 41.3 | 5.75 | 1020/869 | 22.5 | 1.08 | 1.0E-02 |
| 1391/2794 | 64 | 19/6/2014 | 59.0 | 5.75 | 14/18 | 20.9 | 1.11 | 6.8E-03 |
| 1392/2795 | 64 | 5/9/2014 | 21.8 | 5.75 | 46/53 | 8.7 | 0.82 | 1.4E-02 |
| 1393/2796 | 64 | 2/10/2014 | 117.5 | 5.75 | 3031/2513 | 4.3 | 0.79 | 1.9E-02 |
| 1394/2797 | 64 | 25/2/2015 | 47.1 | 5.75 | 528/465 | 3.9 | 0.92 | 1.8E-02 |
| 1395/2798 | 64 | 6/5/2015 | 140.6 | 5.75 | 1831/1615 | 0.6 | 1.12 | 1.2E-02 |
| 1396/2799 | 64 | 1/11/2015 | 100.8 | 5.75 | 617/550 | 0.9 | 1.17 | 4.0E-03 |
| 1397/2800 | 64 | 20/2/2016 | 83.3 | 5.75 | 763/691 | 9.7 | 0.54 | 1.3E-02 |
| 1398/2801 | 64 | 18/6/2016 | 88.7 | 5.75 | 1702/1495 | 0.5 | 1.09 | 2.1E-03 |
| 1399/2802 | 64 | 2/10/2016 | 139.2 | 5.75 | 2776/2555 | 9.2 | 0.55 | 1.4E-02 |
| 1400/2803 | 64 | 20/5/2017 | 59.6 | 5.75 | 606/556 | 12.9 | 0.40 | 2.4E-02 |
| 1401/2804 | 64 | 31/7/2017 | 180.5 | 5.75 | 2185/1570 | 16.6 | 0.80 | 2.1E-02 |
| 1402/2805 | 64 | 2/11/2018 | 170.7 | 5.75 | 9881/8751 | 6.7 | 0.59 | 2.1E-02 |
| 1403/2806 | 64 | 25/5/2019 | 114.6 | 5.75 | 5058/4290 | 12.0 | 0.72 | 1.9E-02 |